Liquid Lewis acids in catalysis

By

James Michael Hogg, MChem

Presented to the School of Chemistry and Chemical Engineering

The Queen's University of Belfast

in fulfilment

of the requirements

for the degree of

Doctor of Philosophy

The Queen's University of Belfast

January 2017

Acknowledgements

Firstly I would like to thank Dr. Małgorzata Swadźba-Kwaśny, she has mentored me since I started at QUILL as a research technician and she encouraged me to start this PhD. Her confidence in my abilities has helped keep me focused and overcome periods of self-doubt. Thank you for your time, guidance, encouragement and friendship. I hope we will have the opportunity to collaborate again in the future.

I am also grateful for the support and encouragement Prof. Martin Atkins has provided during my thesis. I also appreciated his insights into the world of industrial chemistry which I would have remained largely ignorant about without. Furthermore I am grateful for the funding provided.

I would like to thank Prof. Ken Seddon for the funding and opportunities afforded to me by the QUILL Research Centre, and his excellent music taste. I am sure to this day that a mutual respect for King Crimson was a deciding factor in my being hired as a technician, which led to me starting this PhD.

There are also various people who at times have provided me with valuable suggestions. I would like to thank Dr Leila Moura for helping me understand density and viscosity measurements in greater detail. Dr John Holbrey has also provided many pointers during meetings helping to trim the rough edges of my research for which I thank him. That and the lengthy discussions on seventies progressive rock bands. I would like to thank both Dr Fergal Coleman and Dr Albert Ferrer-Ugalde with whom I had the pleasure to work with on the Petronas sponsored PAO project.

The technical staff at QUILL and Queen's have provided invaluable assistance in many ways. Many thanks to Phillip who helped keep the SimDist GC alive over the years, as well as Suzi, Angela and Lindsey who helped with the use of the various analytical techniques. I would like to thank Richard for not going crazy every time I asked for help difficult NMR experiments of exotic nuclei.

I would also like to thank Fiona, Deborah, Sarah and Sinead for their behind the scenes work. The help with orders, shipments, flights to conferences and many such thankless tasks required to keep things running smoothly is greatly appreciated.

I have also enjoyed a good working relationship with Dr Chrobok and the various students from her lab who have travelled to and fro between Belfast and Gliwice in particular Karolina Matuszek. I hope such collaborations can continue in the future.

As part of this thesis I was privileged to spend 6 weeks at FAU-Erlangen-Nuremberg in Germany under the supervision of Prof Wasserschied and Dr Haumann. I would like to thank them for introducing me to an area of research I would have otherwise not had the opportunity to work on. I would also like to thank Martin Lijewski for taking time to train me on the equipment used and discussing results and planning work and introducing me to the wonders of Franconian beer and cuisine (Schäufele). I would like to thank Vincent, Alex and Nathan for making me feel welcome during my visit.

I have made many personal friendship over the years at QUILL as many people have come and gone over the years. These friendships have made QUB a great place work. In no particular order I would like to thank my comrades Lucy, Mark, Leila, Yoan, Jeni, Sophie, Gosia, Rachel, Fergal, Eoghain, Sonia, John and Albert.

Abstract

Lewis acids are vitally important catalysts utilised in a wide variety of chemical transformations. Main group halides are the archetypal Lewis acid used in industry and whilst being cheap commodity chemicals which high Lewis acidities, they can have significant drawback such as toxicity. In particular for the production of low viscosity polyalphaolefin base oils, BF_3 is used as the catalyst which is a toxic gas requiring specialist high pressure and corrosion resistant equipment.

Chlorometallate ionic liquids have been reported to be potent Lewis acids, due to unsaturated or oligomeric halometallate anions, and academic research has assessed them in a wide variety of applications. There are also reported industrial process which use chloroaluminate ionic liquids as catalysts and/or solvents for transitions metals. Whilst ionic liquids present interesting alternatives to main group halides, their positives are offset by complicated and time consuming cation synthesis, which also drives up the cost of the ionic liquid.

A series of Lewis acidic liquids, based on boron, aluminium, gallium and antimony were synthesised which were produced from "off the shelf chemicals" utilising simple synthetic methodology.

Liquid coordination complexes (LCCs) were recently reported by Abbot, Lui and Swadźba-Kwaśny as consisting of mixed ionic and molecular species. Speciation studies of (LCCs) have so far been mainly limited to oxygen donors. Speciation of LCCs were extended to heavier phosphine chalcogenide donors (*S*- and *Se*-) where it was found that heavier donors push the equilibrium present in LCCs to prefer molecular adducts over ionic species. Heptyl cyanide as a ligand was also found to produce an ionic liquid of the formula $[Al(C_7CN)_6][3(Al_nCl_{3n+1})]$ rather than the expected LCC, which would allow for the synthesis of highly Lewis acidic anions at lower metal chloride content of typically chloroaluminate ionic liquids.

Borenium ionic liquids were synthesised by addition of substituted pyridine ligands to BCl_3 followed by halide extraction with $AlCl_3$. The borenium ionic liquids were found to be exceptionally Lewis acidic, $120 < AN < 180$ as measured on the Gutmann scale, when measured neat. In organic solvents the acidity of $[BCl_2(3pic)][Al_2Cl_7]$ was found to decrease from 170 to 123 which was more comparable to literature examples.

The methodology applied to synthesise borenium ionic liquids was extended to antimony(III), antimony(V) and tin(IV) chlorides. The products of the later two were complicated by redox

reactions and ligand redistribution upon addition of $AlCl_3$. Antimony(III) cations were successfully produced, though were found to be extremely viscous (η > 500 cP at 303 K).

Both LCCs and borenium ionic liquids were applied as catalysts for the carbocationic oligomerisation of 1-decene. Both catalysts demonstrated a greater selectivity to the economically valuable oligomers (C_{30} – C_{50}) than typical chloroaluminate ionic liquids. Scale up reactions (3 L 1-decene) showed that the physical properties of the blended PAO samples were dependent upon the temperature of the reaction and the catalyst used to produce the oligomers. As such there is a careful trade-off between yield, product quality and waste produced which would have to be managed on an industrial scale.

Finally LCCs were also tested as SCILL co-catalysts for the hydrogenation of toluene to methylcyclohexane. The catalyst Ur-$AlCl_3$ χ_{AlCl3} = 0.60 was found to accelerate the reaction, without yielding side products. In comparison to $[C_4C_1im][Al_2Cl_7]$ the LCC was found to be a more potent co-catalyst at higher temperatures (T ≥ 80 °C) but less potent at lower temperatures. Many of the LCCs tested stalled the reaction completely, in particular those with $GaCl_3$.

It has been demonstrated that highly Lewis acidic materials can be made using simple synthetic procedures, utilising cheap commodity chemicals, in a way that does not require lengthy alkylation steps as required for chlorometallate ionic liquids. The Lewis acidity of these liquids has been demonstrated by Guttmann acceptor measurements and by catalytic activity. Both LCCs and borenium ionic liquids were shown to give differing product distributions or rates of reactions to chloroaluminate ionic liquids, suggesting that whilst LCCs and borenium ionic liquids contain highly Lewis acidic species they cannot be considered 1:1 replacements of chloroaluminate ionic liquids.

Table of contents

List of Figures

List of Tables

List of Equations

Abbreviations

2,2,4,6-TMP – 2,2,4,6-tetramethylpyridine

2FPy – 2-Fluoropyridne

2Pic – 2-Methylpyridine (2-picoline)

3FPy – 3-Fluoropyridine

3Pic – 3-Methylpyridine (3-picoline)

4Pic – 4-Methylpyridine (4-picoline)

AcA – Acetamide

AN – Gutmann acceptor number

$[C_0C_0im]$ – Imidazolium cation

$[C_nmim]^+$ – 1-Alkyl-3-methylimidazolium cation

C_7CN – Heptylcyanide

C_n – A hydrocarbon chain consisting of *n* carbon atoms

CAPEX – Capital expenditure

Cat – Catechol, 1,2-dihydroxybenzene

CIA – Chloride ion affinity

$[Cp]^-$ – Cyclopentadiene anion

$[DCA]^-$ – Dicyanamide anion

DCM – Dichloromethane

DMA – *N*,*N*-Dimethylacetamide

DMH - Dimethylhexane

DMSO – Dimethylsulphoxide

Eq – Equivalent

FAB – Fast atom bombardment

FIA – Fluoride ion affinity

FLPs – Frustrated Lewis pairs

HIA – Hydride ion affinity

HSAB – Hard soft acid base

HOMO – Highest occupied molecular orbital

$[Him]^+$ – Protonated imidazolium cation

IL – Ionic liquid

MeCN – Acetonitrile

MIA – Methanide ion affinity

NHC – *N*-Heterocyclic carbene

NMA – *N*-methylacetamide

NMR – Nuclear magnetic resonance

$[NTf_2]^-$ – Bis(trifluoromethylsulfonyl)imide anion

OPEX – Operational expenditure

$[OTf]^-$ – Trifluoromethanesulfonate anion

$P_{222}O$ – Triethylphosphine oxide

$[P_{4444}]^+$ – Tetrabutyl phosphonium cation

$[P_{66614}]^+$ – Trihexyltertradecyl phosphonium cation

P_{888} – Trioctylphosphine

$P_{888}O$ – Trioctylphosphine oxide

$P_{888}S$ – Trioctylphosphine sulphide

PDC – Process Design Center

Ph_3PS – Triphenylphosphine sulphide

Py – Pyridine

RON – Research octane number

SCILL – Solid catalyst with ionic liquid layer

SILP – Supported ionic liquid phase

SimDist – Simulated distillation gas chromatography

SUr – Thiourea

TGA – Thermogravimetric analysis

THF – Tetrahydrofuran

TMP – Trimethylpentene

Ur – Urea

USP – Untied States patent

VFT – Vogel-Fulcher-Tammann

VI – Viscosity index

VN – Viscosity number

LCC – Liquid coordination complex

LUMO – Lowest unoccupied molecular orbital

Mes – Mesitylene (2,4,6-trimethylbenzene)

WIPO – World intellectual property organisation

wt% - Weight per cent

χ_A – Molar fraction of A

Publications arising from this work

Papers

1) J. M. Hogg, F. Coleman, A. Ferrer-Ugalde, M. P. Atkins and M. Swadźba-Kwaśny, Liquid coordination complexes: a new class of Lewis acids as safer alternatives to BF_3 in synthesis of polyalphaolefin, *Green Chem.*, 2015, **17**, 1831. DOI: 10.1039/c4gc02080d (IF – 8.02)
2) S. Coffie, J. M. Hogg, L. Cailler, A. Ferrer-Ugalde, R. W. Murphy, J. D. Holbrey, F. Coleman, and M. Swadźba-Kwaśny, Superacidic Ionic Liquids with Tricoordinate Borenium Cation, *Angew. Chem. Int. Ed*., 2015, **54**, 14970. DOI: 10.1002/anie.201508653 (IF – 11.71)
3) K. Matuszek, A. Chrobok, J. M. Hogg, F. Coleman and M. Swadźba-Kwaśny, Friedel–Crafts alkylation catalysed by $GaCl_3$-based liquid coordination complexes, *Green Chem.*, 2015, **17**, 4255. DOI: 10.1039/c5gc00749f (IF – 8.02)
4) M. Lijewski, J. M. Hogg, M. Swadźba-Kwaśny, P. Wasserscheid and M. Haumann, Coating of Pd/C catalysts with Lewis-acidic ionic liquids and liquid coordination complexes – SCILL induced activity enhancement in arene hydrogenation, *RSC Adv.* 2017, **7**, 27558. DOI: 10.1039/C7RA03295A (IF – 3.289)

Papers to be published

1) Liquid coordination complexes of phosphine chalcogenides, to be submitted to *Inorg. Chem.*, in preparation
2) Inorganic ionic liquids with nitrile ligands: $[M(C_7CN)_6]_3[M_xCl_y]$, to be submitted to *Dalton Trans.*, in preparation
3) Borenium ionic liquid - catalysed synthesis of polyalphaolefins, in preparation, to be submitted to *ACS Sustainable Chem. Eng.*, in preparation
4) Synthesis and characterisation of antimony(III) cation containing ionic liquids, to be submitted to *Dalton Trans.*, in preparation

Patent

1) Oligomerisation Process - WIPO Pat, WO2016005769 A2, 2016

1 Introduction

This chapter contains an introduction to the concept of acidity, from historical views to modern definitions and discusses various approaches to quantifying Lewis acidity. Furthermore, it describes several examples of catalytic applications of liquid Lewis acids, in particular halometallate ionic liquids. The catalytic processes studied in this thesis are introduced at the beginning of relevant chapters.

1.1 Acidity

1.1.1 Historical definitions

The word 'acid' derives from the Latin *acidus* meaning sour, originally referring to acidic liquids such as vinegar. Acids were identified as substances which tasted sour, reacted with chalk in an effervescent manner and turned certain plant dyes, such as litmus, red.[1,2] The term 'alkali' is derived from Arabic and refers to plant ashes, *i.e.* potash. Alchemists and early chemists defined alkali as the counterpoint to acids, in particular that an acid lost its properties upon contact with an alkali. Alkalis were also found to turn litmus blue, have a bitter taste and a "*soapy*" feel.[3]

The thrust of early acid-base research was focused upon finding a unifying acidic principle. For example, Lavoisier proposed oxygen, the name of which is derived from the Greek for 'acid former', as the universal acidic principle.[4] Elements which were highly oxidised were acidic, *e.g.* SO_3, and those that were weakly oxidised were basic, *e.g.* Na_2O. Following this reasoning, Lavoisier inferred that hydrochloric acid must contain oxygen, saying of "*acid of sea salt*" that it "*is composed by the union of oxygen and an acidifiable base*",[4] though other chemists could find no proof of this.[2]

In the first definition approaching a modern view of acidity and basicity, Arrhenius proposed that a compound which resulted in an increase in the concentration of H^+ ions in an aqueous solution was an acid, and conversely, a base resulted in an increase in the concentration of OH^- ions. This definition had the advantage that the conductivity of a solution could be measured, and the correlation between strong acids/bases and high conductivity allowed for the ranking of acids and bases by strength.[3]

Arrhenius's definition was limited, in that it required an acid/base to have ions: H^+ or OH^-, capable of dissociation, even though examples existed where no such dissociation could

occur (*e.g.* BF_3 or NH_3). Secondly, the concept was limited to an aqueous solution. Franklin, working on the chemistry of salts in liquid ammonia, demonstrated similarities between auto-ionisation of ammonia and water.[5,6] This prompted Germann to develop the generalised solvent theory of acids in bases, whereby auto-ionisation of a solvent resulted in a positively charged solvonium and negatively charged solvate species.[7] A substance dissolved in the solvent which increased the solvonium concentration was defined as an acid, and a substance which increased the solvate species concentration was defined as a base.[3] Again, this required dissociation of both acid and solvent molecules into ions, despite many examples where this behaviour was not observed.

In the beginning of the 20th century two theories of acidity were formalised, which constitute the basis of modern understanding of acids and bases, namely Brønsted-Lowry definition[8] and Lewis definition.[9,10]

1.1.2 Lewis acidity

In 1923, Lewis defined an acid as a substance which could accept a lone pair of electrons to complete its octet and a base as a substance which could donate a lone pair to another to complete the second's octet.[9] The modern IUPAC definition of a Lewis acid is"*a molecular entity (and the corresponding chemical species) that is an electron-pair acceptor and therefore able to react with a Lewis base to form a Lewis adduct, by sharing the electron pair furnished by the Lewis base*".[11] The quintessential example of a Lewis acid-base reaction is that between ammonia and boron trifluoride (Figure 1.1-1). The empty orbital on the boron atom can accept donation of the lone pair from the ammonia, forming an adduct where both the boron and nitrogen have filled octets.

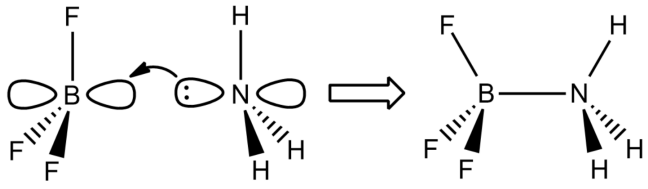

Figure 1.1-1: Reaction between ammonia and boron trifluoride

In addition to such textbook examples, large swathes of chemistry can be viewed as acid-base reactions under this definition. For example, in organometallic chemistry, ligand coordination to a central metal atom can be seen as donating electron density to the central acidic metal atom. Somewhat confusingly, hydrogen bonding may also be considered under

the umbrella of Lewis acid chemistry as a hydrogen bond donor (which is accepting electron density) is an acid and the hydrogen bond acceptor (electron donor) is a base.[1]

In the 1960s, Pearson introduced the empirical principle of hard and soft acids and bases (HSAB).[12] By studying the equilibrium constants of nucleophilic displacement reactions, it was noted that acids could be divided into 2 groups: those which would bind strongly to bases with a high proton affinity, and those which would bind strongly to polarisable or unsaturated bases with a much lower proton affinity. A hard acid/base typically is small, with low polarisability and high charge density, conversely a soft acid/base is larger, has high polarisability and low charge density. These descriptions represent the extreme cases and intermediate behaviour can also occur.[1,3,12] Klopman was able (to a certain degree) to quantify the observed reactivity describe by Pearson's HSAB theory computationally, through frontier molecular orbital (FMO) approach, defining reactions as "*charge controlled*" in the case of hard acid/bases, or "*frontier controlled*" for soft acids/bases.[13] For example Klopman was able to show mathematically why nucleophilic attack on pyridine occurs in the 2-postion for hard nucleophiles, such as $[OH]^-$, whereas soft nucleophiles, *e.g*. $[CN]^-$, preferentially attack in the 4-position. Parr and Pearson later formulated a more rigorous mathematical definition of hardness. Absolute hardness was defined as the second derivative of total ground state electronic energy as a function of the number of electrons in an atom with constant nuclear charge.[14] From this definition they were able to rank the hardness of acids and bases and explain why soft-soft and hard-hard interactions are preferable to hard-soft interactions. However, this calculated parameter does not take into account the state, or environment of the acid/base. More recent developments in computational approaches to Lewis acidity are summarised in a review by Geerlings *et al*.[15]

1.1.3 Quantifying Lewis acidity

Because the strength of a Lewis acid always has to be considered in the context of its reaction with a particular base, in certain reaction environment, there is no 'natural', unambiguous method of quantifying the strength of a Lewis acid, though it can be measured by proxy. Typically, a probe molecule or ion is used, and the interaction between probe and acid is quantified by either computation or physical measurement. In a review of borocations Ingelson discussed the chemical behaviour of boranes and borocations stating "*no absolute scale of borocation Lewis acidity can be provided due to the inherent dependence on the probe Lewis base*".[16] This is exemplified by the fact that $[CatB(NH_3)]^+$ is capable of extracting

fluoride from $[SbF_6]^-$, whereas $B(C_6F_5)_3$ does not but is incapable of extracting hydride from $[B(H)(C_6F_5)_3]^-$.[17]

1.1.3.1 Gutmann acceptor number (AN)

Gutmann measured the donor-acceptor properties of a variety of solvents to order them by nucleophilicity and electrophilicity.[18] The AN of an acid is established from the ^{31}P NMR chemical shift of a solution of triethylphosphine oxide, $P_{222}O$, dissolved in a sample of said acid. The ^{31}P NMR chemical shift is measured at several concentrations of the probe and subsequently extrapolated to infinite dilution. This allows to correct for the effect of concentration and ensures minimum disturbance of equilibria potentially existing in the studied medium. The measured chemical shift is referenced against the ^{31}P NMR chemical shift of $P_{222}O$ in hexane and Equation 1.1-1 is used to calculate the AN value.[19]

$$AN = 2.348 \cdot (\delta(A)_{inf} - \delta(Hexane)_{inf}) \qquad \text{Equation 1.1-1}$$

Trietheylphosphine oxide was selected as a probe molecule for a number of reasons:

- The ^{31}P nucleus is naturally 100 % abundant and has spin ½, providing clear NMR spectra
- The coordinating atom is the oxygen, with the phosphorous atom shielded by three ethyl chains, providing stability to the molecule even in highly acidic environments
- The ethyl chains are sufficiently short to prevent steric hindrance, which could affect the results
- It is strongly donating, so the ^{31}P chemical shift is highly sensitive to its environment
- It is soluble in a wide array of solvents

The scale was arbitrarily defined, based upon the ^{31}P NMR chemical shift of the probe molecule in hexane (AN = 0) and $SbCl_5$ in 1,2-dichloroethane (AN = 100).[19, 20] A larger value indicates greater loss of electron density from the phosphorus atom, and as such a stronger acid. This method has been used widely to measure the acidity of many solvents, Brønsted acids,[21] Lewis acids[22] and ionic liquids.[23–26] However, it is not universally applicable, when Stephan *et al.*[27] attempted to measure the AN value for the dicationic imidazolium-phosphonium salt, $[(SIMes)PFPh_2][B(C_6F_5)_4]_2$, they found that the $P_{222}O$ and the acid underwent fluorine-oxygen exchange (Figure 1.1-2).

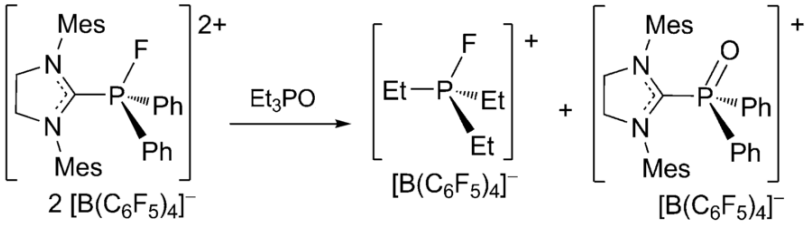

Figure 1.1-2: Reaction of $P_{222}O$ with a dicationic imidazolium-phosphonium salt[27]

Beckett proposed a simplified method for measuring the acceptor number, whereby a fixed concentration of $P_{222}O$ is used and no extrapolation of $\delta^{31}P$ to infinite dilution is made.[28] This approach is useful for molecular acids with well-defined structure. However, for complex systems with dynamic equilibria (*e.g.* chloroaluminate(III) ionic liquids), which may be perturbed by the presence of the probe, extrapolation to infinite dilution ensures the most accurate result.

1.1.3.2 Child's method and other NMR spectroscopic probes

Child *et al.* reported the ^{1}H and ^{13}C NMR spectra of adducts formed between a variety of Lewis acids and α,β-unsaturated aldehyde.[29] The ^{1}H NMR chemical shifts for H_2, H_3 and H_4 protons of croton aldehyde (**Figure 1.1-3 - Left**), recorded for 1:1 adducts, were strongly dependent on the Lewis acid, with the H_3 proton showing the widest range of chemical shift change. This led to suggestion that the change in charge distribution on the aldehydes could be used as a convenient method to rank Lewis acids, which could be used to predict their reactivity with respect to substrates.

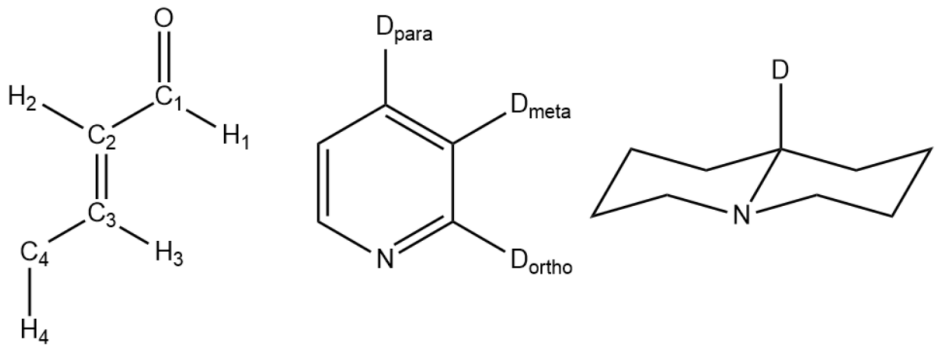

Figure 1.1-3: Left crontonaldehyde with numbering system, middle deuterated pyridine, right deuterated quinolizidine

Hilt *et al.* used the deuterated nitrogen bases, D_5-pyridine and D_1-quinolizidine, to measure the acidity of silyl triflates and metal halides, which correlated with the rates of Diels-Alder reactions.[30,31] Deuterated bases present the advantage of uncomplicated spectra, and do not

have to be used in stoichiometric quantities to obtain concentration-independent chemical shift.[30,31] The rate of Diels-Alder reaction correlated well with the $\Delta\delta D_{para}$ (Figure 1.1-3 - Middle), with the notable exception of Me_3SiOTf.[30] Later, molecular Lewis acids were used to catalyse cycloadditions, the rate of which correlated with ΔδD in quinolizidine (Figure 1.1-3). This measurement was complicated by the appearance of an additional peak in the D NMR spectrum, caused by *cis*/*trans* isomerisation of the probe molecule.[31]

Barron and co-workers used the polycyclic ketone, 9-fluorenone, as a spectroscopic probe for the measurement of the acidity of group 13 metal halides.[32] They recorded the change in the ^{13}C NMR shift for the C_1 carbon, though Child previously reported local anisotropy affecting measurements if the probing nuclei was too close to basic oxygen.[29] The authors compared this measurement to a variety of other measurements which have been used to quantify acidity, and reported poor matchup between ^{13}C NMR, ^{1}H NMR, λ_{max}, XRD and $\nu_{C=O}$, reporting differing trends depending on the measurement used.

1.1.3.3 Ion affinity scales

Calculating the enthalpy of reaction between ions and acids is also used to rank the strength of acids (and bases).[1] Krossing *et al.* calculated ion affinities, notably the fluoride ion affinity (FIA) in the gas phase, according to Equation 1.1-2,[33] This allowed Krossing to rank Lewis acids by their strength according to the enthalpy of reaction. Highly electron-deficient metal centres were found to have the greatest enthalpy of reaction.

$$A_{(g)} + F^-_{(g)} \rightarrow AF^-_{(g)}$$ Equation 1.1-2

Where $\Delta H = -FIA$

Subsequently, a range of hard and soft anion affinities (H^-, Me^-, F^- and Cl^-) for various molecular acids were computed. The order of Lewis acidity was probe-dependent.[34] For example, when comparing two molecular Lewis acids, PF_5 and PCl_5, both were found to have similarly strong affinities for the hard anions Cl^- and F^-. In contrast, PCl_5 was found to be a significantly stronger Lewis acid than PF_5, when H^- and Me^- were used as probes. Similarly, in series of GX_3 (X = F, Cl, Br, I), all acids were of very similar strength with respect to the Cl^- affinity, but acidity increased in the homologue series when measured with H^-, F^- or Me^- probes. Ingleson *et al.* synthesised the compound $[(acridine)BCl_2][AlCl_4]$,[35] which was found to have two highly Lewis acidic centres. The authors measured both hydride and chloride ion affinity of both the boron atom and the C9 carbon, using $AlCl_3$ as a reference. The C9 carbon was found to be more Lewis acidic to hydride than the boron centre but the situation was

reversed when calculating the chloride ion affinity. Ingelson reported HIA for a number of borocations and found that the transfer of hydride anions between acids could only be accurately predicted when there was a large difference in the HIA values.[17]

1.1.3.4 Other methods: *N*-donors as probes

Vibrational spectroscopy was used to investigate Lewis acidity in solids, employing *N*-donor probes, such as pyridine or acetonitrile, typically used in near-stoichiometric quantities with respect to acidic sites. Some of the methods have been adapted to study liquid acids as well. For example, pyridine was used as a probe molecule to study ionic liquids, which then allows for the vibration (Py – H) and (Py – Lewis acid) to be seen at *ca*. 1550 and 1450 cm^{-1} respectively, allowing for distinction between Brønsted and Lewis acidic sites.[36,37] Kou *et al.* report only a 6 cm^{-1} wavenumber difference between $[C_4C_1im]Cl\text{-}AlCl_3$ between basic (χ_{AlCl3} > 0.40) and highly acidic compositions (χ_{AlCl3} > 0.67). Similarly only a small difference is seen between $[C_4C_1im]Cl\text{-}MCl_x$ χ_{MClx} > 0.67 (M = Zn, Cu, Fe or Al), suggesting the method is too insensitive for an accurate ranking of Lewis acidic strength. Moreover, vibrational spectroscopy is characterised by lower sensitivity and much narrower change in signal position, when compared to NMR probes. Again, the use of near-stoichiometric quantities is likely to disturb equilibria in more complex acidic systems.

1.1.4 Brønsted acidity

Brønsted[8] and Lowry,[38] working in parallel, defined an acid as a proton donor and a base as a proton acceptor. This definition has advantages over the theories proposed by Arrhenius, Germann and Franklin, in that Brønsted-Lowry theory allows for acid-base reactions to be defined in all media, though it does not account for the acidity of compounds like BF_3. There is a direct relationship between Lewis and Brønsted acidities. Protons are very hard Lewis acids, therefore Brønsted acids are Lewis acid-base adducts, and the proton transfer is a competition between two Lewis bases for the affinity of a proton (Equation 1.1-3).[2,34,39] An interesting consequent of Brønsted-Lowry theory is that acids and bases are relative;[2] as such sulphuric acid itself is capable of acting as a base to stronger acids, such as disulphuric acid.[39]

$$HA + B \leftrightarrows HB^+ + A^- \qquad \text{Equation 1.1-3}$$

As the defining characteristic of Brønsted acidity is the transfer of a clearly defined entity, H^+, it can be unambiguously quantified by a number of methods. In aqueous solutions, the pH is a measure of the concentration of $[H_3O]^+$ ions (Equation 1.1-5). The pH of a solution depends on both the strength and the concentration of the acid dissolved. As such, an acid's strength

is determined by its dissociation constant, K_a (Equation 1.1-6), though pK_a is more commonly used (Equation 1.1-7) as the values of K_a span many orders of magnitude. In order for Equation 1.1-6 to be true, one must assume that the concentration of water remains constant and that acid concentration is equal to its activity. Consequently, this equation applies only to dilute aqueous solutions.

$$HA_{(aq)} + H_2O_{(l)} \leftrightarrows H_3O^+_{(aq)} + A^-_{(aq)} \qquad \text{Equation 1.1-4}$$

$$pH = -\log_{10}[H_3O]^+ \qquad \text{Equation 1.1-5}$$

$$K_a = [H_3O^+]_{(aq)}\,[A^-]_{(aq)} / [HA]_{(aq)} \qquad \text{Equation 1.1-6}$$

$$pK_a = -\log_{10}K_a \qquad \text{Equation 1.1-7}$$

The strength of Brønsted acids and bases is limited by the solvent levelling effect. As strong Brønsted acids tend to fully dissociate in water and protonate it, the most acidic species present is the hydronium ion, $[H_3O]^+$ (Equation 1.1-4).[2,40] This implies that weak solutions of HCl, $HClO_4$, HBr, HNO_3 *etc.* in water should appear equally acidic, having the same concentration of $[H_3O]^+$. In contrast, if the acid is dissolved in a poor proton acceptor, the equilibrium in Equation 1.1-3 (where the solvent is acting as a base) will be shifted to the left. For example, HCl would not be dissociated in acetic acid, and as such would be a stronger acid than in water, as the protonating agent would be HCl, not $[H_3O]^+$.[2]

With increasing acid concentration, the approximations required for Equation 1.1-6 do not hold and the equation no longer provides an accurate description of the behaviour of the acid.[40] In 1932 Hammett and Deyrup devised a method for measuring the acidity of concentrated and highly acidic compounds.[41] They used "*simple basic indicators*" which underwent a colour change upon protonation (either colourless to coloured or *vice versa*) and measured the change in the light absorption. From this they inferred the degree of protonation of the base. They defined the acidity function, H_0, as:

$$H_0 = -pK_{BH+} - \log_{10}(C_{BH+}/C_B) \qquad \text{Equation 1.1-8}$$

Where:

pK_{BH+} = the acid dissociation constant of the protonated base

C_{BH+} = the concentration of the protonated base

C_B = the concentration of the neutral base

To be deemed suitable, the bases chosen for the measurement of the Hammett function are required to:[41, 40]

- have a distinct measurable colour change upon protonation of the neutral base
- have a molar extinction coefficient such that the colour change can be detected at concentrations low enough that the bases added does not affect the overall acidity of the sample being measured
- be protonated with a single H^+, without any side reactions, decomposition or double protonation during the measurement which would adversely affect results

Using this approach, it was possible to determine the acidities of very concentrated solutions of H_2SO_4 and $HClO_4$, and to correlate the acidity of the medium, as determined by H_0, with reaction rates of various acid-catalysed reactions, a topic which was later reviewed by Long and Paul.[42] Although the validity of some of the bases that were used in these measurements has been discussed,[40, 43] as well as methods of refining the measurement of the pK_{BH+} values of the bases used,[44] the Hammett acidity function continues to be a useful tool in the measurement of highly acidic and non-aqueous systems, for example the acidity of the proton in chloroaluminate(III) ionic liquids.[45]

1.1.5 Superacidity

1.1.5.1 Brønsted superacids

When talking about superacids, it is typically Brønsted superacids that come to mind. A Brønsted super acid is simply defined as an acid with greater strength than pure sulphuric acid (H_0 *ca.* -12),[40] as typically measured by the Hammett function. Although there are examples of molecular Brønsted superacids, such as trifluromethansulphonic acid, H_0 = -13,[46] the strongest Brønsted superacids are adducts of strong Brønsted acids and Lewis acids. The conjugate base of the Brønsted acid reacts with Lewis acid to form an extremely weak conjugate base with a diffuse charge (*i.e.* a softer anion), decreasing the strength of the interaction between the proton (hard cation) and anion.[47] For example, the mixture of fluorosulphuric acid and antimony pentafluoride (Equation 1.1-9) gained the moniker "*Magic acid*"(H_0 = -23) after a paraffin wax candle was dissolved in it.[48]

$$FSO_3H + SbF_5 \rightarrow H[FSO_3SbF_5] \qquad \text{Equation 1.1-9}$$

Olah demonstrated numerous examples of paraffins protonated with superacids to form short-lived non-classical carbocations.[49,50] This can be useful for stabilising unusual species;

for example, mixtures of $HBr/AlBr_3$ and benzene formed a non-classical carbocation, $[C_6H_7]^+$, with a the bromoaluminate anion, $[Al_2Br_7]^-$.[51]

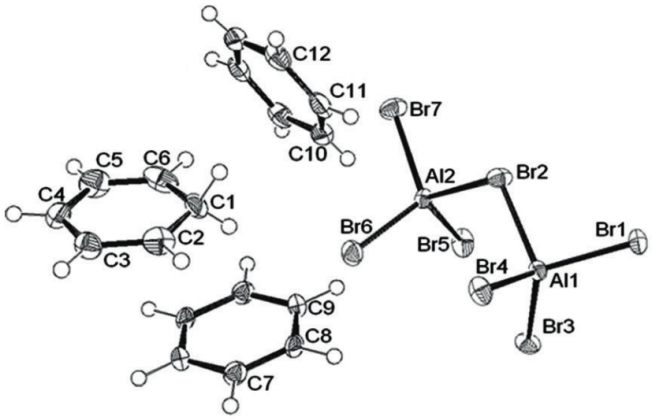

Figure 1.1-4: Crystal structure of $[C_6H_7][Al_2Br_7]$[51]

1.1.5.2 Lewis superacids

As already discussed, the strength of a Lewis acid is defined by the scale being used to measure it (FIA, Gutmann acceptor number, *etc*.). In consequence, the definition of a Lewis super acid is dependent upon that scale. Krossing defined a Lewis superacid according to the FIA scale as "*molecular Lewis acid which are stronger than monomeric SbF_5 in the gas phase*".[33,34] Interestingly, according to Krossing's calculations, $AlBr_3$ is a Lewis superacid in terms of FIA scale, with its FIA value larger than SbF_5 by 17 kJ/mol ± 2. At the same time, it is not superacidic according to the CIA scale, being 15 kJ/mol ± 2 weaker than SbF_5. On the Guttmann acceptor number scale, acids with AN > 100 (*i.e.* that are inducing ^{31}P deshieliding in $P_{2\,2\,2}O$ higher than $SbCl_5$) are considered to be Lewis superacids.[52] Olah suggested that anhydrous $AlCl_3$ should be used as the threshold strength in Lewis superacidity as it was "*the most commonly used Friedal-Crafts acid*".[39] In organic chemistry papers, some Lewis acidic reagents, such as metal triflates, have been described as Lewis superacids without any quantification of the term.[53]

1.2 Liquid Lewis acids

1.2.1 Halides

There is a number of halides of main group elements and transition metals are both liquid and Lewis acidic. They may be used neat as Lewis acidic catalysts, or modified before use. Their main application are carbocationic processes, as summarised in Table 1.2-1.

Table 1.2-1: Examples of liquid Lewis acids used in carbocationic chemistry[54–56]

Catalyst	Core applications
$BF_3{\cdot}OEt_2$	Alkylation, isomerisation, acylation, oligomeristaion/polymerisation
$SnCl_4$	Acylation, alkylation and mild catalyst
$TiCl_4$	Alkylation, acylation, less active than $AlCl_3$
VCl_4	Alkylation and acylation
AsF_5	Alkylation and acylation
AsF_3	Alkylation and acylation
SbF_5	Alkylation and acylation, powerful halogenating agent/oxidant
$SbCl_5$	Alkylation and acylation, powerful halogenating agent/oxidant

Antimony pentafluoride and pentachloride are used as halogenating agents of both organic and inorganic compounds.[55,56] They have also been utilised as strong oxidants.[57] Brønsted superacids produced on mixing anhydrous HF and SbF_5 have been used in alkylations, hydrocarbon rearrangements and other carbocationic chemistry.[58]

Tin tetrachloride readily undergoes scrambling with organotin compounds to form organotin halides (Equation 1.2-1 – Equation 1.1-3)[56,58] which can further be reacted with *sp2* hybridised carbons forming reagents used in the Stille coupling reaction.[59] It is also used as a chelation control agent in asymmetric synthesis.[58]

$$3SnR_4 + SnCl_4 \leftrightarrows 4SnR_3Cl \qquad \text{Equation 1.2-1}$$

$$SnR_4 + SnCl_4 \leftrightarrows 2SnR_2Cl_2 \qquad \text{Equation 1.2-2}$$

$$SnR_4 + 3SnCl_4 \leftrightarrows 4SnRCl_3 \qquad \text{Equation 1.2-3}$$

Titanium tetrachloride has been utilised in aldol condensations,[60] and was used by Natta, in conjunction with $AlEt_3$, as a polymerisation catalyst for propene.[61] Later on, titanocene dichloride derivatives of titanium tetrachloride and methylaluminoxane were researched extensively for small olefin polymerisation.[62]

Liquids containing trimethylsilyl cations are powerful Lewis acids, which are utilised in synthesis, in particular in anion exchange reactions. For example, trimethylsilyl triflate is utilised to in the synthesis of antimony cations, by removing a halide form the antimony and replacing it with the weakly coordinating $[OTf]^-$ anion.[63] The trimethylsilylhalide may be easily removed from the reaction mixture due to its low boiling point.

1.2.2 Halometallate ionic liquids

1.2.2.1 History

The term ionic liquid can be taken quite literally to mean a liquid composed of ions. As such, sodium chloride above *ca.* 800 °C would be considered an ionic liquid. However, since its

popularisation the 1980s, the term has been used to describe salts which melt below the arbitrary temperature of 100 °C and it is often used as a short hand for room temperature ionic liquids, which melt below ambient temperature.

Halometallate ionic liquids,[64,65,66] in particular chloroaluminate(III) ionic liquids, garnered interest mainly due to the desire for new battery designs for the U.S. airforce,[67] as well as the ability to electroplate steel with an inert aluminium layer.[68 69] In the early 1980s Wilkes *et al.* reported mixtures of 1-alkyl-3-methylimidazolium chloride with aluminium(III) chloride which were liquid at 25 °C for certain molar ratios of $AlCl_3$ ($0.40 \leq \chi_{AlCl3} \leq 0.67$). These system inspired much of the development of modern ionic liquids, largely based on imidazolium cations.[70] Even though the focus has largely shifted from halometallate anions to "air- and water-stable" anions, such as $[BF_4]^-$ and $[PF_6]^-$, $[NTf_2]^-$ and $[OTf]^-$ there is sustained strong interest in halometallate ionic liquids for industrial applications, with several major processes reported in the recent years.[71–73]

1.2.2.2 Speciation

Halometallate ionic liquids are synthesised in a one-step addition process of metal halide to an organic halide salt (dialkylimidazolium, tetraalkylammonium or tetraalkylphosphonium are all commonly used cations) – see Figure 1.2-1.

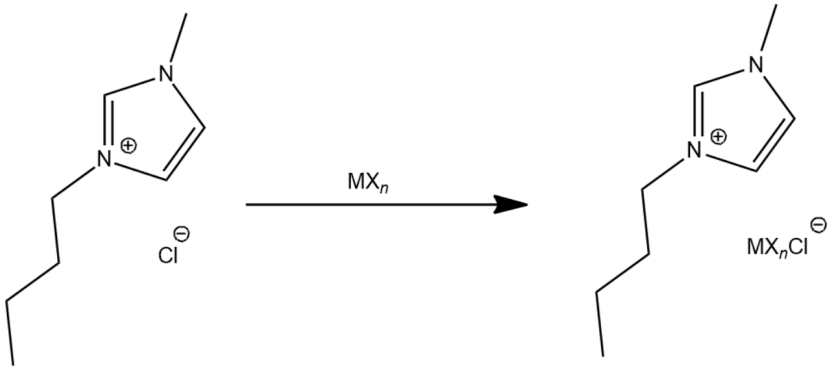

Figure 1.2-1: Addition of metal halide to $[C_4C_1im]Cl$ to form a halometallate ionic liquid as described by Wilkes *et al.*[70]

Crucially, the molar ratio of the reactants, also called composition, can vary within a wide range. Composition of halometallate ionic liquids is typically reported as the molar ratio of metal halide in the overall composition, χ_{MXn}. Speciation of halometallate anions changes with composition, which results in most properties of halometallate anions being composition-dependent.[65] The core techniques for studying speciation will be demonstrated below, with the emphasis on the speciation of chloroaluminate(III) ionic liquids.

An indirect, popular method of studying speciation changes as a function of χ_{MCl_x} is the construction of a phase diagram. For example, Hurley and Wier reported a phase diagram of the mixture of *N*-ethylpyridinium bromide and aluminium chloride (Figure 1.2-2, Left), with two eutectic mixtures (*ca.* 45 °C when χ_{AlCl3} = 0.33 and *ca*. -40 °C when χ_{AlCl3} = 0.67), and a peritectic point (88 °C when χ_{AlCl3} = 0.50).[74] The authors showed that the aluminium existed as a single compound, $[C_2py][AlCl_3Br]$ at the peritectic composition.

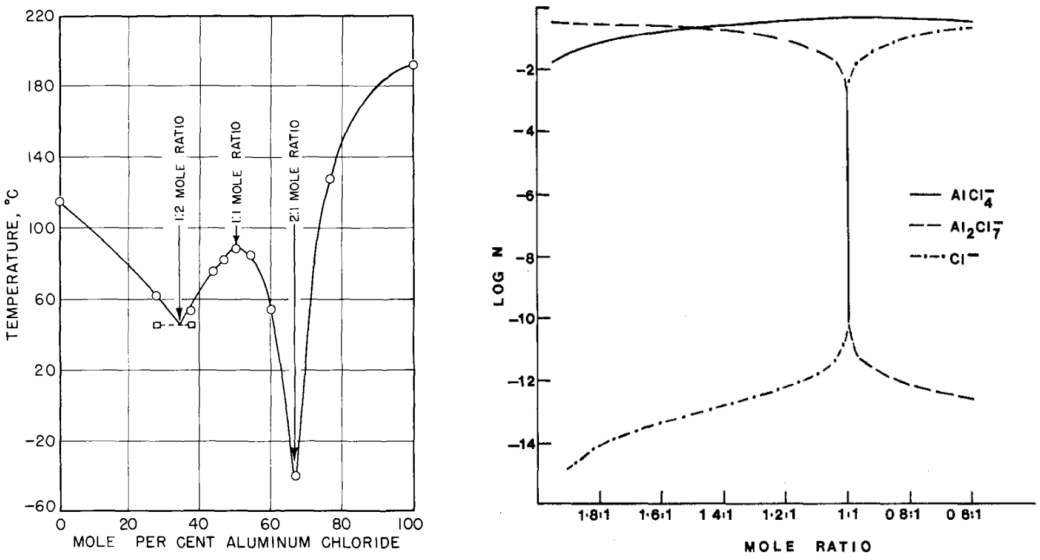

Figure 1.2-2: Phase diagram for 1-ethylpyridinium chloride aluminium(III) chloride (left).[74] Species concentration *vs.* ionic liquid composition for 1-butylpyridinium chloride aluminium(III) chloride (right)[75]

Osteryoung and co-workers studied 1-butylpyridinium chloroaluminate(III) ionic liquids using Raman spectroscopy[76] and electrochemistry.[75,77,78] Based on comparison with high temperature chloroaluminate(III) molten salts (*e.g.* NaCl-$AlCl_3$ mixtures), bands were assigned to the tetrahedral anion $[AlCl_4]^-$ for $\chi_{AlCl3} \leq 0.50$, the dimeric $[Al_2Cl_7]^-$ anion at χ_{AlCl3} = 0.67, and a mixture of the two at intermediate compositions.[76] No free aluminium(III) chloride was detected. Potentiometric titrations were used to measure the equilibrium constants for the same system ($0.33 \leq \chi_{AlCl3} \leq 0.67$), assuming that major equilibria were as shown in Equation 1.2-4 to Equation 1.2-6.[75] The mole fraction of Cl^-, $[AlCl_4]^-$ and $[Al_2Cl_7]^-$ was measured as a function of composition, for $0.38 \leq \chi_{AlCl3} \leq 0.64$ (Figure 1.2-2, Right). At $\chi_{AlCl3} <$ 0.50, the ionic liquid contained a mixture of $[AlCl_4]^-$ and Cl^-, whereas at $\chi_{AlCl3} > 0.50$, a mixture of $[Al_2Cl_7]^-$ and $[AlCl_4]^-$ was detected. Finally, for equimolar composition (χ_{AlCl3} = 0.50) there was a rapid decrease in the concentration of both Cl^- and $[Al_2Cl_7]^-$, which recombined to form $2[AlCl_4]^-$.

$$AlCl_3 + Cl^- \rightleftarrows [AlCl_4]^- \quad \text{Equation 1.2-4}$$

$$AlCl_3 + [AlCl_4]^- \rightleftarrows [Al_2Cl_7]^- \quad \text{Equation 1.2-5}$$

$$2[AlCl_4]^- \rightleftarrows [Al_2Cl_7]^- + Cl^- \quad \text{Equation 1.2-6}$$

$$[Al_nCl_{3n+1}]^- \rightleftarrows [Al_{n-2}Cl_{3n-5}] + Al_2Cl_6 \ (n \geq 3) \quad \text{Equation 1.2-7}$$

Wilkes *et al.* studied 1-alkyl-3-methylimidazolium chloroaluminate(III) ionic liquids using NMR spectroscopy[79,80,81] and physical property measurements, such as viscometry.[82] Importantly, the anion speciation and associated equilibria were found independent of the cation, despite anion-cation interactions, clearly demonstrated by variation in ^{1}H and ^{13}C NMR spectroscopy. The chemical shifts of the H-2 proton and C-2 carbon of the imidazolium ring were heavily dependent upon composition, shifting upfield as strongly coordinating Cl^- was replaced by less coordinating $[AlCl_4]^-$, and then displaying further (albeit milder) deshielding as $[AlCl_4]^-$ was replaced by $[Al_2Cl_7]^-$. Takahashi *et al*. measured ^{27}Al NMR spectra for $[C_2mim]Cl\text{-}AlCl_3$, $0.50 \leq \chi_{AlCl3} \leq 0.67$, over a broad temperature range.[83] The single signal of at *ca.* 103 ppm, arising from the anion, was independent from composition, since $[AlCl_4]^-$ and $[Al_2Cl_7]^-$ both have aluminium in tetrahedral environment, coordinated by four chlorines. In contrast, the line width of the peak was broadening proportional to the increasing concentration of $[Al_2Cl_7]^-$, as the symmetry of the anion decreased from T_d to C_{2v}.

At higher $AlCl_3$ concentrations, $\chi_{AlCl3} > 0.67$, higher oligomers of $[Al_nCl_{3n+1}]^-$ were postulated to exist,[84] though these became less stable as the chain length increased, and disproportionated according to Equation 1.2-7.[85] As such, the highest practical composition available in chloroaluminate(III) ionic liquids is achieved when $\chi_{AlCl3} = 0.67$, with $AlCl_3$ precipitating from $\chi_{AlCl3} > 0.67$ compositions.

Following the studies on chloroaluminate(III) systems, other haloaluminate ionic liquids were investigated, with chlorogallates(III) being the most interesting in the context of this thesis. Gale *et al.* used Raman spectroscopy to study mixtures of $[C_2C_1im]Cl$ and $GaCl_3$, $0.35 \leq \chi_{GaCl3} \leq 0.77$.[86] For neutral and basic composition the Raman data matched the $[GaCl_4]^-$ anion; the presence of $[Ga_2Cl_7]^-$ in the acidic region $0.50 < \chi_{GaCl3} \leq 0.67$ was also confirmed, suggesting equilibria similar to those in chloroaluminates(III) (Equation 1.2-4 - Equation 1.2-6). However, in contrast to chloroaluminate(III) systems, chlorogallate(III) ionic liquids were homogeneous liquids up to $\chi_{GaCl3} = 0.75$. The authors postulated the existence of oligomeric chlorogallate(III) anions, *e.g.* $[Ga_3Cl_{10}]^-$, since free Ga_2Cl_6 could not be detected. In a later EXAFS study, the interatomic distance between two neighbouring gallium atoms was found to be consistent with crystallographically determined Ga···Ga distance in $[Ga_2Cl_7]^-$, with no indication of

molecular Ga_2Cl_6.[87] Finally, Lewis acidity measured in the form of AN for $[C_8C_1im]Cl\text{-}GaCl_3$, was shown to increase above $\chi_{GaCl3} = 0.67$, suggesting a new highly Lewis acidic species, most likely the $[Ga_3Cl_{10}]^-$ anion.[25]

A rather comprehensive list (Figure 1.2-3) of chlorometallate anions, detected by different methods in a wide variety of chlorometallate ionic liquids, was published in a 2014 review by Estager *et al*..[65] These typically show: (i) free chloride and saturated metal chloride anions at low χ_{MClx} values, (ii) at least one χ_{MClx} value where there is no free chloride and a single monomeric chlorometallate anon is present, and (iii) oligomeric chlorometallate anions or coordinationally unsaturated chlorometallate anions at higher χ_{MClx} values. For each system, a maximum is reached where the excess metal chloride precipitates from the liquid. Details of speciation are dependent upon the coordination chemistry of the metal. For example, $ZnCl_2$ forms a compound at $\chi_{ZnCl2} = 0.33$, with the $[ZnCl_4]^{2-}$ anion, in contrast to chloroaluminate(III) ionic liquids, forming $[AlCl_4]^-$ at $\chi_{AlCl3} = 0.50$. On the other hand, in ionic liquids based on $HgCl_2$ and $InCl_3$, acidic oligomeric anions are not formed. Chloroindate(III) ionic liquids form $[InCl_6]^-$ anions, forming a compound at $\chi_{InCl3} = 0.25$, with higher χ_{InCl3} values containing coordinationally unsaturated $[InCl_4]^-$, and possibly $[InCl_5]^{2-}$.[25, 88] It can be seen from these examples that speciation cannot simply be extrapolated to all elements within a given group.

	χ_{MX_x}						
	0.25	0.33	0.50	0.60	0.67	0.75	Analysis methods
Ti(IV)		$[TiCl_6]^{2-}$			$[Ti_2Cl_9]^-$		IR, Raman[129]
Zr(IV)	Cl^-; $[ZrCl_6]^{2-a}$	$[ZrCl_6]^{2-a}$	$[Zr_2Cl_{10}]^{2-a}$		$[Zr_2Cl_9]^{-a}$		DSC,[87] crystallography
Hf(IV)	Cl^-; $[HfCl_6]^{2-a}$	$[HfCl_6]^{2-a}$	$[Hf_2Cl_{10}]^{2-a}$		$[Hf_2Cl_9]^{-a}$		DSC[87]
Nb(V)	Cl^-; $[NbCl_6]^-$		$[NbCl_6]^-$	$[NbCl_6]^-$; Nb_2Cl_{10}			Raman[35]
Mn(II)		$[MnCl_4]^{2-}$	$[MnCl_3]^{-a}$				Raman, IR,[130] EXAFS[131]
Fe(II)		$[FeCl_4]^{2-}$		$[FeCl_4]^{2-}$; $FeCl_2\downarrow$			Raman,[36] XPS[60]
Fe(III)	Cl^-; $[FeCl_4]^-$		$[FeCl_4]^-$	$[FeCl_4]^-$; $[Fe_2Cl_7]^-$	$[FeCl_4]^-$; $[Fe_2Cl_7]^-$; $FeCl_3\downarrow$		Raman,[36] XPS[60]
Co(II)	Cl^-; $[CoCl_4]^{2-}$	$[CoCl_4]^{2-}$	$[CoCl_2(CoCl_4)_2]^{4-}$; $[Co(CoCl_4)_3]^{4-a}$	$[CoCl_2(CoCl_4)_2]^{4-}$; $[Co(CoCl_4)_3]^{4-}$; $CoCl_2\downarrow^a$			UV-VIS[72]
Ni(II)	Cl^-; $[NiCl_4]^{2-}$	$[NiCl_4]^{2-}$	$[NiCl_4]^{2-}$; $NiCl_2\downarrow$				Crystallography,[132] EXAFS[133,134]
Pd(II)		$[PdCl_4]^{2-}$					Crystallography,[100,135] EXAFS[118]
Pt(II)		$[PtCl_4]^{2-}$					Crystallography[99,116]
Cu(I)	Cl^-; $[CuCl_{(2+n)}]^{(1-n)-}$		$[CuCl_2]^-$		$[Cu_2Cl_3]^-$		IR, Raman,[26] viscometry[81]
Cu(II)		$[CuCl_4]^{2-}$	$[Cu_2Cl_6]^{2-a}$				UV-VIS, EXAFS[65,66]
Au(III)	Cl^-; $[AuCl_4]^-$		$[AuCl_4]^-$	$[AuCl_4]^-$; $AuCl_3\downarrow$			Raman, *ab initio*[39]
Zn(II)	Cl^-; $[ZnCl_4]^{2-}$	$[ZnCl_4]^{2-}$	$[Zn_2Cl_6]^{2-}$	$[Zn_2Cl_6]^{2-}$; $[Zn_3Cl_8]^{2-}$	$[Zn_3Cl_8]^{2-}$	$[Zn_4Cl_{10}]^{2-}$	Raman,[27,35]
Cd(II)		$[CdCl_4]^{2-a}$	$[Cd_2Cl_6]^{2-a}$				Crystal structure[136]
Hg(II)		$[HgCl_4]^{2-a}$					Crystal structure[137]
Al(III)	Cl^-; $[AlCl_4]^-$		$[AlCl_4]^-$	$[AlCl_4]^-$; $[Al_2Cl_7]^-$	$[Al_2Cl_7]^-$	$[Al_xCl_y]^-$; $AlCl_3\downarrow$	Raman,[32,33] ^{27}Al NMR,[46]
Ga(III)	Cl^-; $[GaCl_4]^-$		$[GaCl_4]^-$	$[GaCl_4]^-$; $[Ga_2Cl_7]^-$	$[Ga_2Cl_7]^-$	$[Ga_3Cl_{10}]^-$	Raman,[34,138] ^{71}Ga NMR, EXAFS[51]
In(III)	$[InCl_6]^{3-}$	$[InCl_5]^{2-}$	$[InCl_4]^-$	$[InCl_4]^-$; $InCl_3\downarrow$			Raman,[37,38] XPS
Sn(II)	Cl^-; $[SnCl_3]^-$		$[SnCl_3]^-$	$[SnCl_3]^-$; $[Sn_2Cl_5]^-$	$[SnCl_3]^-$; $[Sn_2Cl_5]^-$; $SnCl_2\downarrow$		Raman,[48]
Pb(II)	Cl^-; $[PbCl_4]^{2-}$	$[PbCl_4]^{2-}$	$[PbCl_4]^{2-}$; $[PbCl_3]^-$; $PbCl_2\downarrow$				Raman,[207] Pb NMR[103]

[a] Speciation assumed based on stoichiometry, solid-state studies or indirect techniques, such as DSC.

Figure 1.2-3: Speciation of various halometallate ionic liquids.[65]

1.2.2.3 Acidity

1.2.2.3.1 Lewis acidity

As a rule of the thumb, ionic liquids containing free halide are Lewis basic, those containing only coordinationally saturated anions are weakly Lewis basic, and those with di-, oligonuclear or coordinationally unsaturated anions are considered Lewis acidic.[65]

Gutmann acceptor number is by far the most common approach to quantify Lewis acidity of ionic liquids, with AN values for many chlorometallate systems (Zn^{II}, Sn^{II}, Ga^{III} and In^{III}) correlating well with the speciation. A notable exception are chloroaluminates(III), for AN values of 93 ± 3 were recorded for $[C_8mim]Cl\text{-}AlCl_3$, within the entire studied compositional range ($0.33 \leq \chi_{AlCl3} \leq 0.67$).[25] Similar results were previously found for 1-butylpyridinium chloroaluminate(III) ionic liquids ($0.44 \leq \chi_{AlCl3} \leq 0.67$).[24] It is likely that, due to the high oxophilicity of aluminium, an exchange between Cl^- and $P_{222}O$ has occurred.

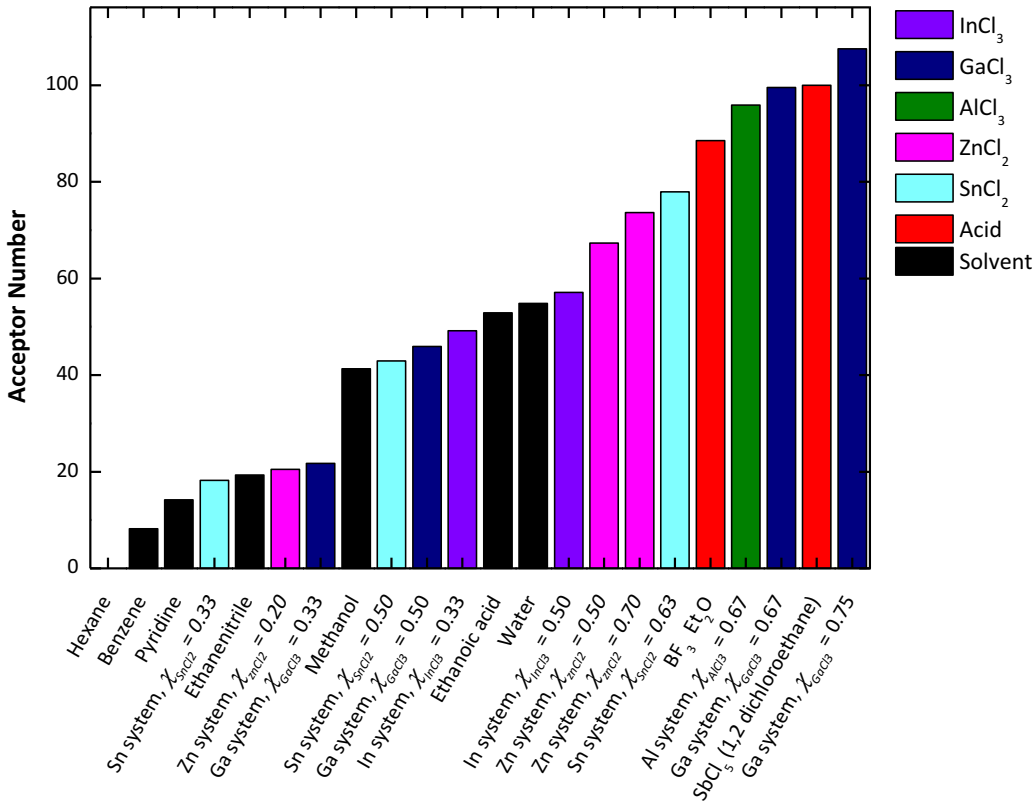

Figure 1.2-4: Acceptor number, as measured by the Guttmann acceptor method, of various halometallate systems, Brønsted acids and solvents where hexane = 0 and $SbCl_5$ = 100[26]

The Lewis acidity of halometallates may derive from coordinationally unsaturated anions, as is the case for chloroindate ionic liquids, but in majority of systems it arises from the splitting

of the oligomeric anion, resulting in a "free" neutral metal chloride and a smaller anion, as exemplified using chloroaluminate(III) anions in Equation 1.2-8.[25]

$$[Al_2Cl_7]^- + B \rightarrow [AlCl_4]^- + [AlCl_3B] \qquad \text{Equation 1.2-8}$$

The latter is the case for all strongly Lewis acidic systems, such as chloroaluminate or chlorogallate ionic liquids (Figure 1.2-4). Therefore, it is important to note that Lewis acidic ionic liquids are as a matter of fact 'latent' Lewis acids, which do not have a free orbital available, but can be considered as adducts of an acid, MCl_3, and a very weak base, $[MCl_4]^-$.

1.2.2.3.2 Brønsted acidity

Halometallate anions do not contain any hydrogen atoms, as such it is obvious that they themselves are not Brønsted acidic. However, following on from the discussion on Brønsted superacidity, arising from adducts of a Lewis acid and a Brønsted acid (Chapter 1.1.5) and the solvent levelling effect (Chapter 1.1.4), it is easy to understand how Lewis acidic ionic liquids can behave as Brønsted superacids. Typically, the source of superacidic protons are protic impurities (*e.g.* water, alcohols) interacting with Lewis acids in ionic liquids, releasing HCl (Equation 1.2-9).[64]

$$[Al_2Cl_7]^- + H_2O \rightarrow [Al_2Cl_6OH]^- + HCl \qquad \text{Equation 1.2-9}$$

Osteryoung *et al.*[89–91] demonstrated that water in chloroaluminate(III) ionic liquids forms hydroxychloroaluminate or oxychloroaluminate species[92] and HCl,[93] depending on the concentration of water and the acidity of the ionic liquid. In basic ionic liquids, HCl is found as $[HCl_2]^-$, $[H_2Cl_3]^-$ or $[H_3Cl_4]^-$, depending on the concentration of HCl in the ionic liquid.[45] In acidic compositions, the HCl was found to be loosely hydrogen-bonded to the anions, $[AlCl_4]^-$ and $[Al_2Cl_7]^-$. As the size of the anion increases, decreased charged density results in weaker hydrogen bonds and therefore greater acidity of the proton, leading to Brønsted superacidic behaviour of HCl in highly Lewis acidic compositions.[45] Crucially, the acidity does not arise from hypothetical species $HAlCl_4$, which was theorised to form as a reaction between HCl and $AlCl_3$, as this compound has been shown by computational modelling to be stable at cryogenic temperatures only.[94] For some applications, these protic impurities may cause unwanted side reactions. Addition of $EtAlCl_2$ was found to remove protic impurities from the melt by formation of ethane and $AlCl_3$ (which proceeds to behave normally in the melt). Excess $EtAlCl_2$ was also found to bind Cl^- anions forming the anion $[EtAlCl_3]^-$ and thus altering

the speciation of the ionic liquid in a similar manner to $AlCl_3$.[95] HCl can also be removed by placing the sample under reduced pressure for an extended period.[91]

1.2.2.4 Halometallate ionic liquids as catalysts

Haloaluminate ionic liquids are often treated as synonymous with Lewis acidic ionic liquids, and have been studied in a plethora of catalytic applications, including several industrial implementations at a multi-ton scale. However, as a matter of fact, most of the studied processes that are described as Lewis acid-catalysed involve Brønsted catalysis, arising from superacidic protons.[96] In general, Lewis acidic ionic liquids are used in catalysis in three ways: as Brønsted acids, as Lewis acids and as solvents/ligand source/co-catalysts stabilising active metal species.

1.2.2.4.1 Brønsted acid catalysis

Many petrochemical processes rely on the use of Brønsted acidic catalysts for reactions proceeding *via* carbocationic mechanisms. For example, the production of refinery alkylates for high octane fuels is catalysed on an industrial scale using either H_2SO_4 or HF.[97] $AlCl_3$ was reported to be too acidic which resulted in side reactions such as cracking.[98] Chauvin reported the use of chloroaluminate ionic liquids as catalysts for isobutane-butene alkylations,[98] which was expanded upon by Jess *et al*.[99–104] The tuneable acidity of the ionic liquid was found to play a crucial role: highly acidic ionic liquids increased cracking side reactions, whilst too low an acidity caused polyalkylations.[98,105] Jess investigated the effect of the addition of protic impurities to the ionic liquid $[C_8mim]Br\text{-}AlCl_3$.[99] The addition of either water or hydrogen sulfonate increased selectivity to the desired trimethylpentanes (which have a high octane number) up to a certain concentration, after which a large increase in polyalkylates was observed. Chen *et al.* reported the addition of aromatic compounds to chloroaluminate(III) ionic liquids, which saw an increase of TMP yield and decrease of unwanted light and heavy ends.[106] The authors suggest an interaction between the Lewis acid and the π system of the aromatic ring supresses side reactions. Liu synthesised $[Et_3NH]Cl\text{-}AlCl_3$ ionic liquid and tested metal halide additives in alkylation;[107] CuCl was found to increase selectivity to TMPs. Interestingly the authors of many papers report no significant formation of conjunct polymers[98,103,105,108] (also known as acid soluble oils) which are a known problem with H_2SO_4 catalysed alkylation.[109] Lui *et al.* however observed solid formation during the alkylation.[110] The solid was found to be a mixture of CuCl and conjunct polymers. The solid formation was accompanied by a drop in catalytic performance, with the post reaction ^{27}Al NMR of the ionic

liquid showing a narrowing of the chloroaluminate anion suggesting a change from $[Al_2Cl_7]^-$ to $[AlCl_4]^-$.

Research described in the above publications underpins the development of several industrial processes. In 2006, PetroChina reported retrofitting a 65,000 tonne/year H_2SO_4 alkylation unit for use with a mixed halometallate ionic liquid (IONIKYLATION process).[72] It was reported that the presence of the composite anion $[AlCl_4CuCl]^-$, as evidenced by a second peak in the ^{27}Al NMR spectrum at *ca.* 97 ppm and FAB-MS, resulted in higher production of TMPs and an increase of the RON of the product.[108] However other authors have proposed contradictory views on the effect of the copper(I) chloride additive. When measuring the acidity by FTIR spectrum of $[Et_3NH]Cl – AlCl_3$ χ_{AlCl3} =0.60 with added salts and pyridine as a probe molecule, Bui *et al.* observed an increase in the peak intensity of the [py-H] stretching frequency relative to the [py-Al] upon the addition of metal salts.[101] Thus the author proposed the release of HCl as shown in Figure 1.2-5. That the peak at *ca.* 97 ppm in the ^{27}Al NMR spectrum is not due to $[AlCl_4CuCl]^-$ would seem to be supported by Lui *et al.* who reported that the peak at could be depleted by vacuum evacuation and restored by addition of HCl gas with the authors stating that species is $[Al_2Cl_6OH]^-$.[111] The plant however was shut after some time due to apparent corrosion issues, chloride contamination of the product and unfavourable economics.

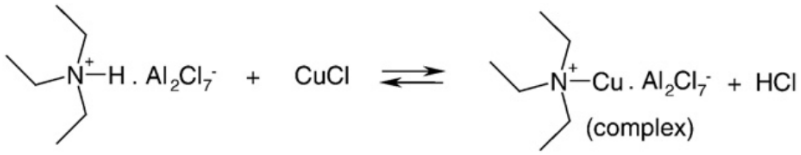

Figure 1.2-5: Propossed formation of HCl leading to Brønsted superacidic catalytic activity in the ionic liquid $[Et_3NH][Al_2Cl_7]$ with added CuCl[101]

Chevron Philips, who have been developing their ISOALKYL ionic liquid alkylation technology over the past 20 years, have committed to converting a 4,500 barrel per day HF alkylation unit with to the ISOALKYL technology and is licencing the process through Honeywell UOP.[112] Plans to retrofit the alkylation unit in Utah, USA are to commence in 2017, pending planning permission.[73] This new technology is set to reduce many of the safety concerns with transporting large volumes of toxic HF[113] as well as catalyst consumption as regeneration of the ionic liquid catalyst can performed onsite. The ionic liquid process also has the advantage of being able to utilise more varied feedstocks than the liquid acid alkylation process and typically gives less conjunct polymers than liquid acid alkylations.[114]

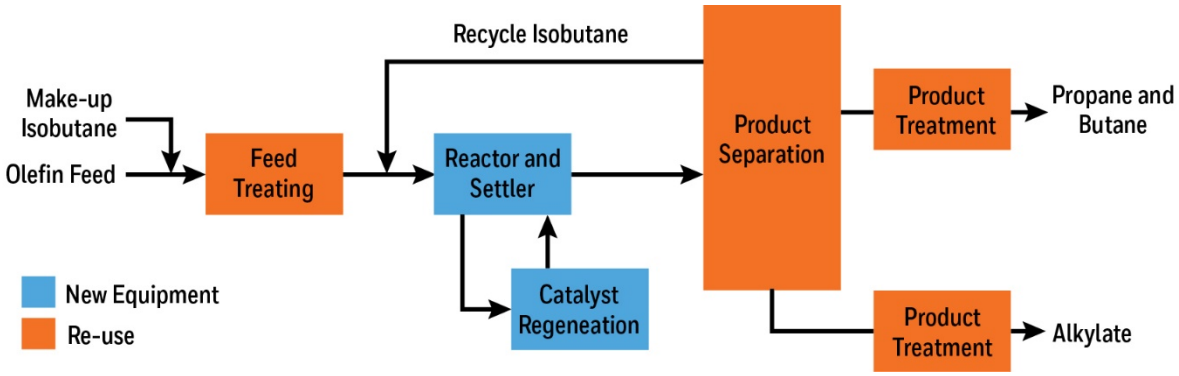

Figure 1.2-6: IONALKYLATION basic plant schematic[114]

Another example of Brønsted acid-catalysed reaction is the Prins condensation of paraformaldehyde and isobutene, which was carried out using tetraalkylammonium and pyrdinium chlorostannate ionic liquids grafted onto a silica support.[115] The cation was covalently tethered to a silica support as the chloride salt. Upon addition of $SnCl_4$ the anion $[SnCl_5]^-$ was formed. Compared to the homogeneous $SnCl_4$, the ionic liquid converted less paraformaldehyde but had a higher selectivity to the desired product, 3-methy-3-buten-1-ol. When both were supported on silica, again lower conversion and higher selectivity were seen, but crucially – significant leaching of tin was seen with the $SnCl_4$ catalyst, whereas none was observed for the immobilised ionic liquids.

Wasserscheid *et al.* used chloroaluminate ionic liquids as catalysts for the alkylation of cumene, both in liquid-liquid bi-phasic systems and as SILP catalysts using the ionic liquid $[C_2C_1im][Al_2Cl_7]$.[116–118] For the supported chloroaluminate ionic liquid they report that pre-treating the support by washing the support with an excess of chloroaluminate in dichloromethane was more effective at removing surface hydroxyl groups from the silica support than calcination. Chemical pre-treatment of the support was shown to be crucial in improving reproducibility and selectivity, as well as reducing leaching of aluminium to the product from 5.8 wt% with the calcined support to 2.0 wt% with the chemically pre-treated support. The time required to reach 80 % conversion with the supported catalyst dropped to approximately $1/6^{th}$ of the time required for the liquid-liquid biphasic reaction (Table 1.2-2). Recycling experiments were performed by decanting the product materials from the reactor and refilling with a new batch of solvent and cumene. Though water was only imperfectly excluded, conversion over 4 runs remained constant (though an increase in ortho substituted cumene was observed).

Table 1.2-2: Distribution of diisopropylbenzene isomers by catalyst used[116]

	Time [min]	Meta	Ortho	Para
Biphasic	23	60	0	40
Calcined SILP (α = 0.2)	4	44	5	51
Chemically treated SILP (α = 0.2 T)	4	57	2	41

1.2.2.4.2 Metal complex stabilisation

In the early 1970s, Parshall discussed the use of ionic liquids as an ideal medium for catalytic reactions, pointing out that their immiscibility with reaction products and their high boiling points allow for removal of product by decantation or distillation respectively. Parshall reported the use of tetraalkylammonium chlorostannate and chlorogermanate ionic liquids as solvents for $PtCl_2$.[119] The solution was found to be active in hydrogenation and carbonylation reactions. It was postulated that the $[SnCl_3]^-$ anion would act as a ligand to the platinum, and complexes such as $[(C_2H_5)_4N]_3[Pt(SnCl_3)]$ were extracted from the ionic liquid. In ionic liquids with a high $[SnCl_3]^-$ concentration, poly-olefins were selectively hydrogenated to mono-olefins, which was explained by the polyolefin and $[SnCl_3]^-$ being more successful at competing for coordination sites on the platinum than the mono-olefin, which prevented further hydrogenation. The ionic liquid was stable under reaction conditions in the absence of oxygen. The products could easily be separated from the reaction mixture, though the system had drawbacks in the high operating temperatures due to the high melting point of the ionic liquids.

Wasserscheid and Waffenschmidt extended this principle utilising syngas for hydroformylation reactions.[120] Two substrates, methyl-3-pentenoate and 1-octene, were hydroformylated utilising a platinum complex dissolved in one of two acidic chlorstannate(II) ionic liquids. Relative rates of isomerisation, hydrogenation and hydroformylation were found to be dependent upon the solvent, temperature and pressure of the reaction.

Chauvin and co-workers developed a process for the dimerisation of short chained olefins, ethane, propene and butenes, to high octane fuels and to precursors of value added petrochemicals. It utilised a ternary ionic liquid $[C_4C_1im]Cl\text{-}AlCl_3\text{-}EtAlCl_2$ as a solvent for nickel complexes.[121] The active nickel species is formed by ligand exchange. Olivier-Bourbigou proposed Equation 1.2-10[122] however, given that pentacoordinate aluminium halide complexes are not known in chloroaluminate(III) ionic liquids[65] and the aluminium species are present in excess Equation 1.2-11 seems more likely. The charged nickel species is effectively

immobilised in the ionic liquid phase and given that the product is poorly soluble in the ionic liquid phase the product can be separated by simple settling and decantation.

$$L_2NiX_2 + [EtAlCl_3]^- \rightarrow [AlCl_3X_2]^- + [L_2EtNi]^+ \qquad X = Cl, Br \qquad \text{Equation 1.2-10}$$

$$L_2NiX_2 + [EtAl_2Cl_6]^- \rightarrow 2[AlCl_3X]^- + [L_2EtNi]^+ \qquad X = Cl, Br \qquad \text{Equation 1.2-11}$$

The composition of the ionic liquid had to be carefully controlled to prevent deactivation of the catalyst.[122] Alkylaluminium(III) chlorides remove protic impurities from the melt, minimising undesired carbocationic processes.[123] Basic anions coordinate to the nickel, therefore an acidic composition was required.[123] Alkyaluminium(III)chloride-containing anions are more basic than chloroaluminate(III) anions and are more soluble in the organic phase, which caused $EtAlCl_2$, and other alkylaluminiums(III) formed by Et^- / Cl^- exchange between anions, being lost to the organic phase.[124] The losses had to be periodically replaced. Nevertheless, the immiscibility of the ionic liquid and product significantly decreased the consumption of nickel and aluminium when compared to the previous homogeneous process.[121,124] This immiscibility between product and ionic liquid retards further reaction of the dimers preventing oligomer formation and increasing selectivity to the desired dimer products.[122] The process was piloted under the name Difasol, and designed to retrofit in the older, homogenous Dimersol plants.[71,122]

Wilkes and Carlin used 1-ethyl-3-methylimidizolium chloroaluminate(III) ionic liquids as a solvent for Cp_2TiCl_2 for the polymerisation of ethane.[125] As with the Difasol process, basic compositions with high concentration of chloride anions lead to coordinationally saturated metal centres, which quenched catalytic activity. Acidic ionic liquids with a small amount of alkylaluminium(III) chloride co-catalysts were catalytically active and, when quenched with methanol, precipitated the polyethene product. The mechanism of action, whereby the titanium loses chloride to the acidic aluminium species, $[Al_2Cl_7]^-$, is the same as seen before with titanium complexes. (Equation 1.2-12).[126] However, a lower rate of polymerisation was reported in comparison to other Cp_2TiCl_2-catalysed polymerisations, most likely due $[AlCl_4]^-$ coordinating to the active complex, $[Cp_2TiR]^+$ (Equation 1.2-13).

$$Cp_2TiCl_2 + [RAlCl_6]- \rightleftarrows [Cp_2TiR]^+ + 2[AlCl_4]- \qquad \text{Equation 1.2-12}$$

$$[Cp_2TiR]^+ + [AlCl_4]- \rightleftarrows [Cp_2TiR(AlCl_4)] \qquad \text{Equation 1.2-13}$$

Raubenheimer *et al*. used neutral $[C_4C_1im][AlCl_4]$ with a small addition of $EtAlCl_2$, creating an acidic ionic liquid (χ_{AlCl3} = 0.52), to oligomerise olefins from C2 to C8, in the absence of protons.[127] Significantly reduced oligomerisation rates were observed with higher oligomers,

unless $TiCl_4$ was added - this yielded atactic polymers of narrow polydispertity and *ca*. C_{40}-C_{120} chain length, depending on feedstock and reaction conditions.

1.2.2.4.3 Lewis acid catalysis

[C_4mim]Cl-$AlCl_3$ (χ_{AlCl3} = 0.67) was used as a Lewis acidic activator of aromatic rings, allowing for the hydrogenation over Pd/C under benign conditions.[128] By addition of 1 equivalent of [C_4mim]Cl-$AlCl_3$ (χ_{AlCl3} = 0.67), the reduction of benzene to cyclohexane was completed at ambient temperature, under 1 bar H_2, in 24 h. Using computational chemistry and NMR spectroscopy to study the reaction mechanism, the ionic liquid was shown to activate the aromatic ring whilst simultaneously stabilising it against unwanted side reactions (see Chapter 4).

Diels-Alder cycloaddition is a popular model reaction to study new Lewis acidic catalysts. Lee studied Diels-Alder reactions in basic and mildly acidic (χ_{AlCl3} = 0.51) chloroaluminate(III) ionic liquids.[129] A marked increase in *endo* selectivity was seen when the ionic liquid changed from basic (5:1 *endo*:*exo*) to slightly acidic (19:1 *endo*:*exo*). However, only 79% conversion was achieved after 72 h. In contrast, Chrobok and co-workers recently used strongly acidic chloroaluminate(III) (χ_{AlCl3} = 0.67) and chlorogallate(III) (χ_{GaCl3} = 0.67 and 0.75) ionic liquids, on a silica support, and achieved 99% conversion within 5 min reaction time with high (typically ≥ 95 %) *endo* selectivity.[130] Abbott *et al.* used less acidic, albeit considerably more water tolerant ionic liquids based on 1:2 mixtures of choline chloride and either $SnCl_2$ and $ZnCl_2$,[131] which typically gave high yields (≥ 85%) and high *endo* selectivity (typically ≥ 92%) though over a greater reaction time than the group 13 ionic liquids. Though when reacting cyclopentadiene and methyl acrylate, Abbott *et al.* report a lower *endo*-selectivity than Chrobok *et al.* (83% *endo* product *vs.* 94% *endo* product). Yin *et al.* expanded on the use of $ZnCl_2$ ionic liquids for Diels-Alder reactions by exploring the reaction of myrcene and acrolein.[132] Increased selectivity to the *para*-substituted product was seen when acidic $ZnCl_2$ ionic liquids were used (χ_{ZnCl2} > 0.33).[26] Conversions were seen to increase with increasing acidity up to (χ_{ZnCl2} > 0.67) above which there was little change. Furthermore both Yin and Abbott report successful recycling of their ionic liquids with Yin reporting unchanged results over 5 runs. Conversely Chrobok saw loss of activity after 4 runs and reported deactivation of the chlorogallate ionic liquids by the 10th run.

Hölderich *et al.* used chlorometallate ionic liquids as Lewis acidic catalysts for acylation of aromatic compounds, using [C_4C_1im]Cl-MCl_3 (χ_{MCl3} = 0.67, M = Al or Fe) and [C_4C_1im]Cl-$SnCl_2$

(χ_{SnCl2} = 0.67).[133] In biphasic liquid phase reactions, both [C_4C_1im]Cl-$AlCl_3$ (χ_{AlCl3} = 0.67) and [C_4C_1im]Cl-$SnCl_2$ (χ_{SnCl2} = 0.67) gave low conversions of the aromatic, but a high selectivity to the monoacylated product. Conversely, [C_4C_1im]Cl-$FeCl_3$ (χ_{MCl3} = 0.67) gave a much higher conversion, but in some cases a lower selectivity was achieved. Interestingly, conversion and selectivity were seen to increase with increasing temperatures with a significant increase of both between 60 and 80 °C. It was explained that HCl produced during the reaction evaporated from the mixture, preventing further reactions of the product and degradation of the catalysts.

1.2.2.5 Drawbacks of halometallate ionic liquids

One of the most cited drawbacks to chloroaluminate ionic liquids (and ionic liquids in general) is the cost, particularly of the cation, which is often a spectator ion only.[134] When compared to commercially available acid catalysts (BF_3, HF, H_2SO_4, $AlCl_3$, *etc*.) the use of ionic liquids must offer tangible benefits in order to offset the increased cost of their use as catalysts and/or solvents.

Like many strong Lewis acids, the chloroaluminate anion $[Al_2Cl_7]^-$ is highly sensitive to water, reacting to form a series of chlorohydroxoaluminate and chlorooxyaluminate species dependent upon the composition of the ionic liquid.[64,96] This not only depletes the concentration of the Lewis acidic anion, but also results in highly Brønsted acidic species, which may or may not be desirable, depending on the application.[65] The cations are typically formed from quaternary ammonium, alkylimidazoles and alkylpyridiniums halide salts, which are hydroscopic, meaning great care must be taken in drying the reagents during prior the synthesis.[90]

1.2.3 Liquid coordination complexes

Recently room temperature liquid mixtures of small organic molecules and aluminium(III) chloride have been reported and their speciation has revealed similarities to chloroaluminate(III) ionic liquids. These mixtures have been dubbed "*liquid coordination complexes*" by Swadźba-Kwaśny and co-workers.[135]

1.2.3.1 Coordination complexes of Lewis acidic metal halides in organic and inorganic chemistry

Lewis acidic reagents are often used as catalysts in organic chemistry. They are typically comprised of a metal halide, which is in most cases is aluminium(III) chloride, mixed with

aprotic organic donors, such as THF, acetonitrile or dimethylformamide. The donor modifies the Lewis acidity of the metal halide. Typically, reactions are performed in solutions, and ratios of metal halide to donor vary in a wide range, which seems to be based on trial-and-error rather than on the coordination chemistry considerations. Speciation and physical properties of neat reagents are not typically characterised, but in isolated cases they have been mentioned to be liquids rather than solids. For example, $AlCl_3$ in aprotic solvents have been used as Lewis acidic catalysts in acylation of benzodioxane.[136,137] Benzodioxane derivatives have Lewis basic oxygen atoms in their structure, and as such would be expected to complex to the $AlCl_3$, retarding reaction rates. The $AlCl_3$–solvent mixtures were found to catalyse the acylation readily under mild conditions. The speciation of the catalytic mixtures was not studied.

In contrast, speciation of metal halides with organic donor molecules, as a function of composition, is often studied by coordination chemists, who, unfortunately, do not tend to link these studies with catalytic applications. For example, aluminium(III) halides combined with small donor molecules have been studied by Deroualt, Cowley and Atwood,[138–144] typically at low loadings of AlX_3 ($\chi_{AlX3} \leq 0.5$, X = Cl, Br). Aluminium(III) chloride was found to form both neutral molecular complexes, such as $AlCl_3$·THF and $AlCl_3$·THF_2, or ionic species, *e.g.* $[Al_2Cl_2THF_4][AlCl_4]$, depending on the concentration and reaction conditions.[138,145,146] In contrast, ionic species formed in acetonitrile by asymmetric cleavage of Al_2X_6 at all concentrations measured.[141–143,147] Interestingly the coordination of the cation was dependent on the concentration of $AlCl_3$, changing from mixed ligand, $[Al_2Br_2(MeCN)_4]^+$ at low aluminium(III) halide concentrations, to $[Al(MeCN)_6]^+$ at high aluminium(III) halide concentrations. Crucially ^{81}Br and ^{35}Cl NMR spectroscopy showed that when $\chi_{AlX3} \leq 0.5$ no free X^- anion was observed in direct contrast to halometallate ionic liquids.[65] A review of group 13 cationic metal complexes by Atwood showed this asymmetric cleavage of the M_2X_6 unit to form ionic species to be commonplace.[148]

1.2.3.2 Coordination complexes of Lewis acidic metal halides in ionic liquid context

1.2.3.2.1 Speciation

Abbott and co-workers explored the use of simple organic bases with $ZnCl_2$ to form "*eutectic based ionic liquids*".[149] The two materials were mixed at various compositions, the eutectic point was found, and subsequently the materials were only studied at that composition. Speciation was studied using FAB mass spectrometry, which showed primarily the existence

of monocharged cations, $[ZnCl(base)_x]^+$ where $1 \leq x \leq 3$, and monocharged anions, $[Zn_xCl_{2x+1}]^-$ where x = 1, 2 or 3. This is however highly dubious, since it has been reported that mass spectrometry can give erroneous results for the speciation of liquid state chlorometallate anions, with chlorozincate(II) systems used as the model example.[65,26] A noticeable quote from Abbotts's paper reads "*While urea forms ambient temperature eutectics with $SnCl_2$ and $FeCl_3$, it does not form with $AlCl_3$.*"[149], a statement which is countered by a subsequent paper from the same group, where 1:1 mixtures of $AlCl_3$ and urea or acetamide were synthesised and are indeed room temperature liquids.[150] Again, using FAB mass spectrometry, the species present were found to consist of cations of the form $[AlCl_2L_x]^+$ where x = 1 or 2 and the anion was found to be $[AlCl_4]^-$ with traces of $[Al_2Cl_7]^-$. The ^{27}Al NMR spectroscopy of the neat liquid AcA-$AlCl_3$ χ_{AlCl3} = 0.50 showed 3 peaks at 101.1, 88.6 and 73.6 ppm, in the ratios 1:2:1, which were assigned $[AlCl_2AcA_2]^+$, $[AlCl_4]^-$ and $[AlCl_2AcA]^+$. There are a number of problems with this assignment. Firstly, as pointed out by Holbrey *et al.*, mass spectrometry can give erroneous results for speciation of the liquid phase. Although assignments for chloroaluminates can match up well with other techniques "*this appears as much a coincidence as a rule*".[65] Secondly, it is known that increasing coordination number for aluminium results in an upfield shift, as seen with $[AlCl_3{\cdot}THF]$ (tertracoordinate, 94 ppm) *vs.* $[AlCl_3{\cdot}THF_2]$ (pentacoordinate, 63 ppm),[145] so it seems unlikely that $[AlCl_2AcA_2]^+$ would correspond to a more downfield signal than $[AlCl_2AcA]^+$. Thirdly, it has been well established that the ^{27}Al NMR chemical shift for chloroaluminate anion is *ca*. 102-103 ppm, without any major deviations from this value.[83,145,151] Finally, in a comprehensive and authoritative review of cationic complexes of Group 13 elements, Atwood reported tricoordinate cationic complexes of aluminium to be rare, requiring both sterically hindering ligands, which urea and acetamide could not be considered, and weakly coordinating anions.[148,152] Interestingly, Abbott and co-workers reported solid suspensions in compositions outside of the $0.50 \leq \chi_{AlCl3} \leq 0.67$ range (neutral to acidic), whereas $ZnCl_2$-based analogues were liquid at lower metal loadings, $\chi_{ZnCl2} \leq 0.28$ (basic composition).[149,150,153]

Coleman *et al*. reported the synthesis of a range of liquid L-MCl_3 systems, within the compositional range $0.50 \leq \chi_{MCl3} \leq 0.75$ (M = Al or Ga), which they named liquid coordination complexes (LCCs).[135] Raman spectroscopy showed that with increasing metal chloride content the anion changed from $[MCl_4]^-$ at χ_{MCl3} = 0.50 to $[M_2Cl_7]^-$ at χ_{MCl3} = 0.60. At χ_{MCl3} = 0.67 no change was seen for aluminium systems (excess of $AlCl_3$ was reported to remain undissolved at this composition) but gallium systems were homogenous liquids, and contained larger anionic oligomers. ^{27}Al and ^{71}Ga NMR spectroscopy was used to investigate

the metal centres. ^{71}Ga NMR spectra proved to be fruitless as the "*signals were too broad to be separated from the baseline*".[135] ^{27}Al NMR spectra (Figure 1.2-7) were much more informative with clear spectra for L-MCl_3 $\chi_{MCl3} = 0.50$, where L = AcA, Ur, SUr, P_{888} and $P_{888}O$ as well as AcA-$AlCl_3$ $\chi_{AlCl3} = 0.60$. All ligands except P_{888} at $\chi_{AlCl3} = 0.50$ show the characteristic sharp peak for the $[AlCl_4]^-$ anion at 102 ± 1 ppm. For AcA-$AlCl_3$ $\chi_{AlCl3} = 0.50$, a good agreement was found between Coleman's and Abbott's papers, with 3 intensive peaks at the same chemical shifts (discrepancies up to 2 ppm between the two papers). Also the 1:2:1 ratio of the 3 peaks was reported in both papers, however Coleman's paper notes a much smaller peak further upfield. In contrast to Abbot and co-workers, Coleman *et al*. assigned chemical shifts to aluminium species in accordance with the previously discussed known coordination chemistry of aluminium (Table 1.2-3).

Table 1.2-3 ^{27}Al NMR chemical shifts for L-$AlCl_3$, $\chi_{AlCl3} = 0.50$.[135]

Ligand	$[AlCl_4]^-$	$[AlCl_3L]$	$[AlCl_2L_2]^+$	$[AlCl_3L_2]$
Ur	102.2	88.8	72.9	53.5
AcA	102.5	90.3	75.1	56.4
$P_{888}O$	103.0	90.4	75.4	70.4
SUr	102.2	109.3	119	65.5

For the system AcA-$AlCl_3$ $\chi_{AlCl3} = 0.60$, the ^{27}Al NMR spectrum shows a broad peak with 2 sharp peaks emerging. The broadening of the aluminium chloride anion peak with increasing aluminium chloride concentration is seen in typical chloroaluminate ionic liquids.[83] As such, this broad peak was suggested to indicate the formation of $[Al_2Cl_7]^-$, with the authors acknowledging the possibility of ligand exchange, in analogy to that seen in the AcA-$AlCl_3$ $\chi_{AlCl3} = 0.50$ system, and suggest the equilibria show in Figure 1.2-8.

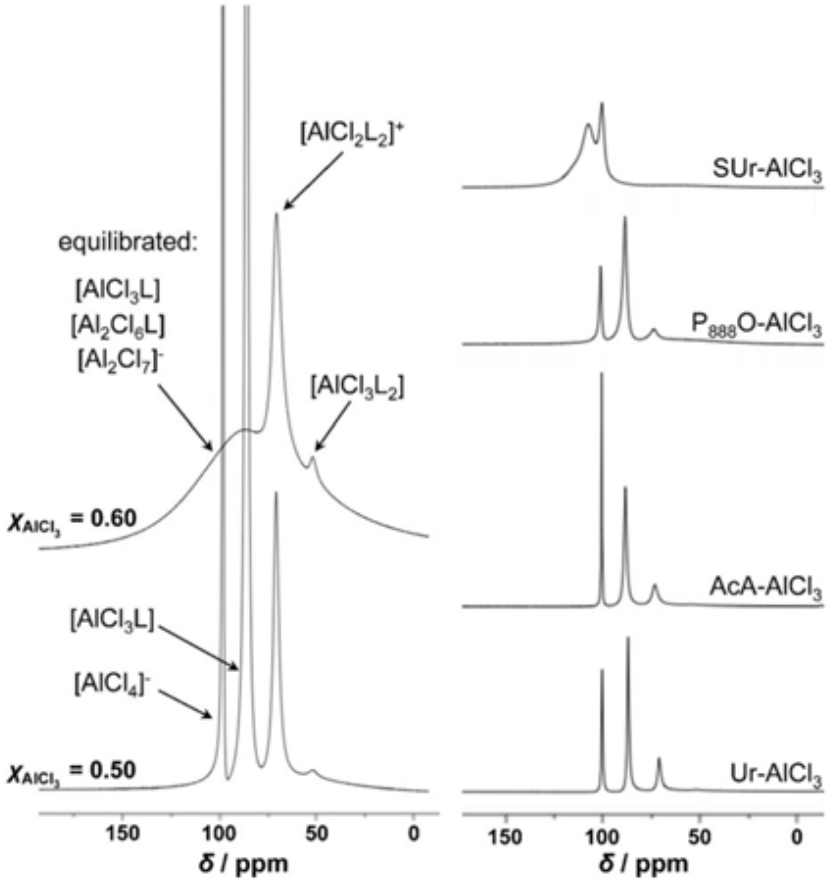

Figure 1.2-7 ^{27}Al NMR spectra of the AcA-$AlCl_3$ system, χ_{AlCl3} = 0.50 and 0.60 (left), and L-$AlCl_3$ χ_{AlCl3} = 0.50 (right).[135]

χ_{MCl3}	
	$2MCl_3 + 2L$
	↓
0.50	$[MCl_2L_2][MCl_4] \rightleftharpoons 2[MCl_3L]$
	↓ + MCl_3
0.60	$[MCl_2L_2][M_2Cl_7] \rightleftharpoons [MCl_3L] + [M_2Cl_6L]$
	↓ + MCl_3
0.67	$[MCl_2L_2][M_3Cl_{10}] \rightleftharpoons 2[M_2Cl_6L]$

Figure 1.2-8: The equilibria present in LCC systems as a function of χ_{MCl3}.[135]

The presence of oligomeric anions suggested that LCCs would be potent Lewis acids. Coleman *et al.* used the Gutmann acceptor number approach (Chapter 1.1.3.1) to quantify the Lewis acidity of selected LCCs.[135] For DMA-$GaCl_3$ χ_{GaCl3} = 0.60, AN = 103 was measured. For DMA-$AlCl_3$ χ_{AlCl3} = 0.60, multiple peaks were seen in the ^{31}P NMR spectrum, corresponding to AN =

96 - 103. For comparison, the ionic liquids $[C_8mim]Cl\text{-}GaCl_3$ $\chi_{GaCl3} = 0.60$ and $[C_8C_1im]Cl\text{-}AlCl_3$ $\chi_{AlCl3} = 0.60$ had AN values of 95 and 93, respectively.[25]

Liu *et al.* studied $AlCl_3$ mixtures with acetamide, *N*-methylacetamide and *N*,*N*-dimethylacetamide, which all have the potential to act as *O*-donors and *N*-donors, using a combination of ^{27}Al NMR, UV-Vis and vibrational spectroscopies.[154]. For the sake of comparison, mixtures of $AlCl_3$ with acetone (*O*-donor) and propylamine (*N*-donor), were also studied. It has been demonstrated that acetamide coordinated exclusively through the oxygen atom, showing no IR absorption related to Al-N vibrations, nor evidence of charge transfer from N to Al in its UV-Vis spectrum. Conversely, methylated acetamides showed evidence of small contribution from Al-N vibrations in IR, decreased change in the vibrational frequency of C=O, and charge transfer for both Al-N and Al-O, which the authors suggest is due to bidentate coordination through both nitrogen and oxygen. From ^{27}Al NMR spectroscopy (in DCM solution), LCCs containing methylated acetamides had a higher proportion of $[AlCl_4]^-$ than acetamide - which the authors interpreted as the formation of $[AlCl_2(\eta^2\text{-}L)]^+$ in the former case, shifting equilibrium in **Equation 1.2-14** to the right. This corroborates with Raman data, indicating the presence of $[AlCl_4]^-$ at higher χ_{AlCl3} values for compositions with methylated acetamides, but not for compositions with AcA.

$$[AlCl_3L] + [Al_2Cl_7]^- \leftrightarrows [AlCl_2(\eta^2\text{-}L)]^+ + 2[AlCl_4]^- \qquad \textbf{Equation 1.2-14}$$

Dai and co-workers studied mixtures of 4-propylpyridne and $AlCl_3$, which are liquid at $0.52 \leq \chi_{AlCl3} \leq 0.60$. They were described to contain $[AlCl_4]^-$ and $[AlCl_2(4\text{-proylpyridine})_2]^+$ for compositions $\chi_{AlCl3} = 0.50$ (assigned by NMR spectroscopy) and $\chi_{AlCl3} = 0.52$ (assigned by mass spectrometry).[155] At $\chi_{AlCl3} = 0.52$ no $[Al_2Cl_7]^-$ was observed by mass spectrometry, though the significant broadening of the peaks in the ^{27}Al NMR spectrum at $\chi_{AlCl3} = 0.57$ would suggest the presence of dimeric species. The same group reported mixtures of dipropyl sulphide with $AlCl_3$, though with a maximum aluminium content of $\chi_{AlCl3} = 0.51$.[156] The authors use only mass spectrometry to determine the speciation, reporting $[AlCl_4]^-$ and $[AlCl_2(\text{dipropyl sulphide})_2]^+$ to be present at $\chi_{AlCl3} = 0.51$.

Endres and co-workers worked with mixtures of 1-butylpyrolidine and $AlCl_3$, in the compositional range of $0.43 \leq \chi_{MCl3} \leq 0.56$, with liquid compositions forming between $0.47 \leq \chi_{AlCl3} \leq 0.55$. Interestingly, the ^{27}Al NMR spectrum at $\chi_{MCl3} = 0.50$ was remarkably similar to that of the mixture of 4-propylpyridine and $AlCl_3$.[155] Upon increasing the χ_{AlCl3} value, the peaks broaden, which could be indicative of the presence of dimeric species. Using IR spectroscopy,

the authors excluded the presence of $[Al_2Cl_7]^-$, noting the absence of peaks which are detected in 2:1 mixtures of 1-butylpyrolidionium chloride and aluminium(III) chloride.

1.2.3.2.2 Applications

Liu *et al.* reported the use of these mixtures for isobutene alkylation producing high octane fuels.[157] They reported a comparison of the performance of $AlCl_3$ combined with formamide, acetamide, *N*-methylacetamide or *N,N*-dimethlyacetiamde, and a chloroaluminate(III) ionic liquid, $[HN_{222}]Cl\text{-}AlCl_3$. LCCs (here called ionic liquid analogues) typically gave higher selectivity to the desired C_8 fraction, with a higher trimethylpentane (TMP) to dimethylhexane (DMH) ratio than the benchmark ionic liquid at the same molar ratio (χ_{AlCl3} = 0.60), which resulted in higher research octane number (RON). The LCC composition (χ_{AlCl3} value) could be modified to further increase the selectivity to C_8, and to increase the TMP:DMH ratio by a factor of 2.5. As with the PetroChina process, the addition of CuCl further increased RON. By controlling the reaction conditions, the alkylate produced reached a very high RON = 98.40.

The author of this thesis contributed to the publication by Matuszek *et al*., reporting on Friedel-Crafts alkylation of benzene with 1-decene by $GaCl_3$-based LCCs.[158] LCCs with high χ_{GaCl3} values were found catalyse the reaction more rapidly than those with lower χ_{GaCl3} values. At 1 mol % loading, Ur-$GaCl_3$ χ_{GaCl3} = 0.75 gave complete conversion of 1-decene in 2 min, compared to Ur-$GaCl_3$ χ_{GaCl3} = 0.60, which gave incomplete conversion after 50 min. Both catalysts had a similar selectivity to the monoalkylated product and the desired 2-phenyldecane. Compared to $[C_2C_1im][Ga_2Cl_7]$, LCCs with the same primary anion, *i.e*. those at χ_{GaCl3} = 0.60 composition, typically gave higher reaction rates and selectivities, although with lower overall conversions.[158]

Aside from catalytic applications, LCCs based on $AlCl_3$ have been of increasing interest for electrochemists, predominantly Dai and co-workers used them for the electrodeposition of aluminium.[155,156,159] Furthermore, Endres and co-workers electrodeposited aluminium from mixtures of 1-butylpyrolidine and $AlCl_3$.[159]

1.3 Motivation for this work

As discussed in the introduction, homogenous acid catalysts are of key industrial importance - and are relatively cheap bulk chemicals, well-known since the 19th century. However, they also pose numerous issues, of increasing importance in the modern age. BF_3 and HF are highly

volatile and toxic, resulting in increased CAPEX and OPEX of catalytic processes. Tests in the Nevada desert in 1986, during which *ca.* 4500 litres of HF was released in a 2 minute period, showed that lethal concentrations were detected as far as 8 km from the release site.[113] Other acids, such as H_2SO_4 or $AlCl_3$, are used in stoichiometric or near-stoichiometric quantities, producing significant amounts of waste, which must be neutralised prior to disposal - and again, disposal of large volumes of waste leads to increased OPEX.[160] Whilst solid catalysts such as zeolites are noted for being used in a wide variety of aspects of the chemical industry and offering many of the advantages of ionic liquids, they themselves have problems with activity, selectivity and catalyst deactivation.[161,162]

Ionic liquids are noted for their low vapour pressure and as such remove one of the key methods of personal harm (volatility). They also offer easy phase separation of catalyst and hydrocarbon products, reducing costs associated with loss of catalyst and product purification. The most often quoted disadvantage of ionic liquids - their price - could be overcome by developing liquid Lewis acids of characteristics similar to ionic liquids, but without costly spectator cation - which was the aim of this work. The focus was on the development of low-cost alternative to chloroaluminate(III) ionic liquids, produced from off-the-shelf chemicals to be economically competitive, whilst retaining equal (or superior) characteristics in terms of high Lewis acidity and tunability of physical properties. There were two parallel strands to this work: fundamental studies on the synthesis and speciation of liquid Lewis acids, and their application in industrially relevant catalytic processes, in particular to oligomerisation of linear alphaolefins (synthesis of lubricant base oils).

2 Synthesis and characterisation of liquid Lewis acids

In this chapter, the synthesis and characterisation of four groups of liquid Lewis acids are discussed. Liquid coordination complexes based on Group 13 metals (Al and Ga) were studied as less expensive and tuneable alternatives to the corresponding chlorometallate ionic liquids. Borenium ionic liquids were developed for their potential Lewis superacidic properties, combined with relatively low price and high tunability, which also makes them attractive for industrial applications. Two smaller projects, on ionic liquids based on cationic complexes of antimony(III) and tin(IV), respectively, were initiated to expand the synthetic principle used for borenium ionic systems to other Lewis acidic main group halides.

2.1 Liquid coordination complexes

LCCs have been developed within the last decade, mainly for use in the electrochemical deposition of aluminium.[135,155,156,159,163] Limited physical property data were gathered by Abbott[150] and Swadźba-Kwaśny[135] groups. In this work, a wide range of liquid coordination complexes for catalytic applications were synthesised and characterised. Speciation studies were carried out to understand how catalyst choice might affect reactions. Physical properties data were required for the engineers involved in industrially-sponsored catalytic projects, to develop techno-economical models. They have also proven to have interesting relationship with speciation.

2.1.1 Experimental

2.1.1.1 Materials and methods

All experiments were performed in a glovebox (MBraun labmaster dp, <0.3 ppm of H_2O and O_2) or using standard argon Schlenk techniques. All glassware was dried overnight in an oven (*ca.* 100 °C) before use.

Aluminium(III) chloride (99.999%) and gallium(III) chloride (99.999 %) were purchased in sealed ampules, under argon from Alfa Aesar. Sulphur (99.95 %), selenium (99.95 %), urea (99.5 %), thiourea (99 %), triphenylphosphine sulphide (99 %) and acetamide (99 %) were purchased from Sigma Aldrich and were all dried under reduced pressure (80 °C, < 1 mbar, 48 h) before use. Trioctylphosphine oxide (99.5 %) was provided by Cytec and dried as described above. Dimethylacetamide (99.8 %, anhydrous, Sigma Aldrich) was distilled from calcium hydride and stored over activated 3 Å molecular sieves. Triocytlphospine (99.5 %) was provided by Cytec and used as received. 2,2,4,6-Tetramethylpiperidine (provided by

Evonik) trioctylamine (99 %, Sigma Aldrich) and heptylcyanide (99.5 %, Sigma Aldrich) were all dried over 3 Å molecular sieves. Triethylphosphine oxide (99 %, Sigma Aldrich) was used as received.

2.1.1.2 Spectroscopy

Multinuclear NMR was used throughout this body of work. All NMR spectra were recorded on either a Bruker Avance DPX 400 MHz, or a Bruker Avance DPX 600 MHz spectrometer. The frequency of the measurements are summarised below (Table 2.1-1).

Table 2.1-1: Summary of the frequency of measurements used for each spectrometer

Nuclei	Bruker Avance DPX 400 Frequency of Measurement (MHz)	Bruker Avance DPX 600 Frequency of Measurement (MHz)
^{1}H	400	600
^{13}C	100	150
^{19}F	376	-
^{27}Al	104	156
^{31}P	162	243
^{77}Se	-	114
^{119}Sn	-	224

Samples which were liquid at room temperature were recorded using DMSO capillaries as an external deuterium lock to prevent the solvent affecting the equilibria present in the sample.

Infrared spectra were measured using a PerkinElmer Spectrum-100 FTIR spectrometer with ATR attachment, with a total range of 7800 to 370 cm^{-1}, with a resolution of 0.5 cm^{-1}. Air-sensitive samples were loaded into a vial in the glovebox and sealed with parafilm. Then, the vial was removed from the glovebox and transferred to the IR spectrometer. The vial was inverted and placed over the crystal of the ATR attachment, allowing for the liquid sample to flow onto the crystal, protecting the sample from contact with air.

Raman spectra were measured using a PerkinElmer Raman station 400F spectrometer, with a 785 nm focused laser beam. As samples were often air sensitive, the quartz cuvette was loaded in the glovebox and sealed using parafilm. If the sample was volatile (*e.g.* $SbCl_5$) a layer of inert hydrocarbon was added on top of the sample to prevent exposure. Samples were typically run for a total of 100 scans with 2 s exposure each.

2.1.1.3 Ligand synthesis

Trioctylphosphine sulphide and trioctylphosphine selenide were synthesised by the reaction of equimolar amounts of elemental sulphur/selenium powder and trioctylphosphine. Elemental sulphur/selenium (0.7961 g, 24.83 mmol/ 1.7562 g, 22.24 mmol) was added slowly

in 0.2 g aliquots to trioctylphosphine (9.2039 g, 24.83 mmol/ 8.2438 g, 22.24 mmol), with rapid stirring (500 rpm) allowing for the heat from the exothermic reaction to dissipate until the flask was cool to touch, and then the mixture was left to react overnight (60 °C, 500 rpm, 12 h). Subsequently, reaction mixtures were filtered to give clear, colourless liquids in quantitative yields, and traces of the solid element (<1% of the initial loading). Purity was analysed by ^{31}P NMR spectroscopy.

P_{888}S: ^{31}P-NMR (243 MHz, DMSO capillary) δ (ppm): 44.91 (1P, s, P=S)
P_{888}Se: ^{31}P-NMR: (243 MHz, DMSO capillary) δ (ppm): 36.41 (1P, d, P=Se, $^{1}J_{P\text{-}Se}$ 678 Hz), 48.35 (1P, s, P=O)

2.1.1.4 LCC synthesis

The typically procedure for LCC synthesis is as follows: the donor ligand was weighed out into a sample vial containing a PTFE-coated magnetic stirrer bar. Subsequently, metal chloride was added in small batches (0.1 g). After every addition, the reactants were vigorously mixed (500 rpm), typically heat was evolved. Before more metal chloride was added the sample vial was allowed to cool to touch. . Upon completion of the addition, the resulting liquid was stirred overnight and, if required, heated (up to *ca.* 100 °C) until no solid remained (0.5 -24 h). Products were analysed by ^{1}H, ^{13}C, ^{31}P, ^{27}Al, ^{71}Ga or ^{77}Se NMR spectroscopy, where appropriate. See appendix for detailed synthesis of each LCC reported.

2.1.1.5 Physical properties measurements

Density was measured using a U-shaped oscillating tube Anton Paar DMA 4500 density meter. The density meter was capable of holding a constant temperature, ± 0.01 °C, and measured density to an accuracy of ± 0.0001 g cm^{-3}. The density meter was calibrated using *n*-octane, triple distilled water and bromobenzene.

Viscosity was measured using an Anton Paar AMVn automated rolling ball viscometer. The rolling ball viscometer was capable of measuring time to a resolution of 0.001 s with an accuracy of 0.002 s. Viscosity could be measured within the range of 0.3 – 20000 mPa s, with a repeatability <0.1% and reproducibility of <0.5%. Temperature was measured with a resolution of 0.01 °C and accuracy of <0.05 °C. The rolling ball viscometer was calibrated using Anton Paar viscosity and density calibration oils APN 26, APN 100 and APN 415, which were obtained from an ISO-17025 certified laboratory.

2.1.1.6 Thermogaravametric analysis

All measurements were carried out using a TA Instruments Q50 thermogravimetric analyser. The platinum pans were cleansed with fire before use. The experiments were carried out under a flow of dry nitrogen flow (20 cm^3 min^{-1}). In the glove box, a gas-tight syringe was loaded with the LCC sample, and removed from the glovebox. A TGA pan was w prefilled with dry hexane; the tip of the needle was immersed in hexane, and the LCC sample was placed under protective layer of hexane. Subsequently, the sample loaded in the TGA machine and held at 60 °C until the mass loss stabilised. Then, the temperature was ramped to 500 °C at 5 °C min^{-1}.

2.1.1.7 Guttmann acceptor number measurements

Three samples of each LCC (*ca.* 1 g) were weighed out accurately into samples vials. Triethylphosphine oxide was weighed accurately into each sample (*ca.* 1, 2 and 3 wt %). ^{31}P NMR spectra were measured as stated in Chapter 2.1.1.2. The chemical shifts were used to extrapolate the chemical shift of an infinitely dilute solution, from which the acceptor number was calculated according to Equation 1.1-1.

2.1.2 Results and discussion

2.1.2.1 Synthesis of Group 13 LCCs

LCC were synthesised using a number of ligands, with a wide range of *O*-, *S*-, *Se*-, *N*- and *P*-donors, combined with either of the two Group 13 metal chlorides: $AlCl_3$ or $GaCl_3$. The combinations of metal chloride and ligand, along with the physical state of the product at room temperature, are listed in Table 2.1-2. Oxygen donors included in the study were: acetamide (AcA), dimethyl acetamide (DMA), urea (Ur) and trioctylphosphine oxide ($P_{888}O$). Sulphur donors used were thiourea (SUr), triphenylphosphine sulphide (Ph_3PS) and trioctylphosphine sulphide ($P_{888}S$). *N*-donors were: heptyl cyanide (C_7CN), 2,2,4,6-tetramethylpiperidine (2,2,4,6-TMP) and trioctylamine (N_{888}). Trioctylphosphine (P_{888}) was the only phosphorous donor the study and trioctylphosphine selenide ($P_{888}Se$) was the only selenium donor used. Many of these LCCs were newly synthesised, with the exception of those reported by Abbott, Swadźba-Kwaśny and Lui (selected combinations of $AlCl_3$ and $GaCl_3$ with AcA, Ur, SUr, P_{888}, $P_{888}O$, NMA and DMA).

Most reactions were highly exothermic, rapid processes, particularly for hard donors, which required slow addition of the metal chloride. In some cases, external heat was required to

bring the reaction to completion. Typically, a clear liquid was obtained, with the colour depending on the ligand. Urea, and thiourea gave colourless liquids (though if urea and $AlCl_3$ were reacted rapidly, a coloured product was seen, as described by Abbott *et al.*, likely due to thermal decomposition of the organic molecule).[150] Acetamide gave a lightly coloured liquid. DMA, P_{888}, and $P_{888}O$ all gave yellow to brown liquids. Colour was also found to be dependent on χ_{MCl3} value. DMA reacted with $GaCl_3$ was a brown-yellow liquid at $\chi_{GaCl3} > 0.50$, but for $\chi_{GaCl3} = 0.50$ it was a purple liquid, which solidified over the course of a few weeks (unfortunately, attempts to grow a single crystal were unsuccessful to date). Reaction rates were clearly dependent on both the metal and the ligand. Oxygen has a high affinity to Group 13 metals. The reaction of urea and aluminium chloride was rapid (< 1 h) and very exothermic, requiring very slow addition of the $AlCl_3$ to the urea, with little or no external heat to drive the reaction to completion. The sulphur analogue, SUr, reacted very slowly (> 3 h) and required continuous heating. Trioctylphosphine oxide reacting with gallium chloride gave a yellow liquid from two white powders within seconds. Interestingly, even though the chlorogallate anion is highly water sensitive, the $P_{888}O$-$GaCl_3$ systems were biphasic with water, taking several days without external agitation to react. The reaction of $AlCl_3$ with triphenylphosphine sulphide took several hours to complete. The two white powders when mixed and heated, slowly collapsed into a liquid like a poorly made *soufflé*.

Gallium-containing LCCs were found to be liquid in the compositional range $0.50 \leq \chi_{GaCl3} \leq 0.75$ regardless of ligand, in contrast to aluminium ones, which were typically liquid when $0.50 \leq \chi_{AlCl3} \leq 0.60$, and even this liquidus range was not obtained for every ligand. As the χ_{MCl3} value increases, the anion changes from monomeric $[MCl_4]^-$ at $\chi_{MCl3} = 0.50$, through dimeric $[M_2Cl_7]^-$ at $\chi_{MCl3} = 0.60$, to trimeric $[M_3Cl_{10}]^-$, at $\chi_{MCl3} = 0.67$ (**Figure 1.2-8**) and even larger units are conceivable.[135] Aluminium is not known to form homogenous ionic liquids with anions larger than dimeric $[Al_2Cl_7]^-$ (**Equation 1.2-7**), with excess $AlCl_3$ precipitating from more concentrated solutions.[65] Similarly, excess aluminium chloride was observed to precipitate from the majority of LCCs above $\chi_{AlCl3} = 0.60$, consistent with the literature.[135]

Some ligand-metal chloride combinations were solid at room temperature but melted at temperatures approaching *ca*. 150 °C. Aluminium-containing systems were more often solid, or contained a precipitate, than their gallium-based counterparts. 2,2,4,6-TMP reacted with $AlCl_3$ to yield a high-melting brown solid, whereas 2,2,4,6-TMP-$GaCl_3$ gave a light yellow liquid. Triphenylphosphine sulphide combined with either $AlCl_3$ or $GaCl_3$ formed a crystalline solid at room temperature. Octane nitrile gave yellow liquids with both $AlCl_3$ and $GaCl_3$,

although in the former case, a large amount of precipitate was formed for χ_{AlCl3} = 0.60. Trioctylamine and $AlCl_3$ mixtures contained precipitate at all synthesised χ_{AlCl3} values.

Table 2.1-2: Group 13 LCCs synthesised during the course of this work

Metal Chloride	Ligand	χ_{MCl3}	Physical State	Firstly Reported
$AlCl_3$	AcA	0.60	Liquid	[150]
	DMA	0.60	Liquid	[135]
	Ur	0.50	Liquid	[150]
		0.60	Liquid	[135]
	SUr	0.50	Liquid	[135]
		0.60	Liquid	[135]
	N_{888}	0.50	Liquid + Solid	This Work
	P_{888}	0.50	Liquid	[135]
		0.60	Liquid	[135]
	$P_{222}O$	0.50	Solid	This Work
		0.60	Liquid	This Work
	$P_{888}O$	0.50	Liquid	[135]
		0.60	Liquid	[135]
	$P_{888}S$	0.50	Liquid	This Work
		0.60	Liquid	This Work
	$P_{888}Se$	0.50	Liquid	This Work
		0.60	Liquid	This Work
	C_7CN	0.50	Liquid	This Work
	C_7CN	0.60	Liquid + Solid	This Work
	PPh_3S	0.60	Solid	This Work
	2,2,4,6-TMP	0.60	Solid	This Work
$GaCl_3$	AcA	0.67	Liquid	[135]
	DMA	0.50	Solid	[135]
		0.60	Liquid	[135]
		0.67	Liquid	[135]
		0.75	Liquid	[135]
	Ur	0.60	Liquid	[135]
		0.67	Liquid	[135]
		0.75	Liquid	[135]
	SUr	0.67	Liquid	[135]
	P_{888}	0.67	Liquid	[135]
	$P_{888}O$	0.50	Liquid	[135]
		0.60	Liquid	[135]
		0.67	Liquid	[135]
		0.75	Liquid	[135]
	C_7CN	0.50	Liquid	This Work
		0.60	Liquid	This Work
		0.67	Liquid	This Work
		0.75	Liquid	This Work

2.1.2.2 Multinuclear NMR spectroscopy considerations

All NMR spectra were recorded using neat LCCs and an external DMSO lock. As LCCs consist of equilibrated species, it was crucial not to perturb the equilibria (*e.g.* by the use of solvent) for the most accurate identification of present complexes. This does however have the disadvantage of significant line broadening due to higher viscosities of tested samples.

Whilst ^{1}H and ^{13}C NMR spectroscopies are useful for the identification of organic molecules, their use in this work was very limited. Typically, the ^{1}H and ^{13}C NMR spectra of ligand and LCC were very similar (Figure 2.1-1), aside from a downfield shift of some signals, confirming coordination of a ligand to the metal centre. Furthermore, for P_{888} and $P_{888}X$ (X = O, S, Se), a significant broadening of ^{1}H signals was observed, likely due to viscosity increase. Aside from confirming that the ligand was coordinated, little could be inferred about the speciation of the LCC as a whole. Despite firm literature evidence for the presence of multiple ligand-containing species, for example $[MCl_2L_2]^+$ and $[MCl_3L]$, they were indistinguishable by either ^{1}H or ^{13}C NMR spectroscopy. Even for simple ligands, such as urea (Figure 2.1-1 – Right), the ^{13}C spectra did not provide information of great use for speciation studies. As such, NMR studies of these nuclei were not used for routine analysis of the products.

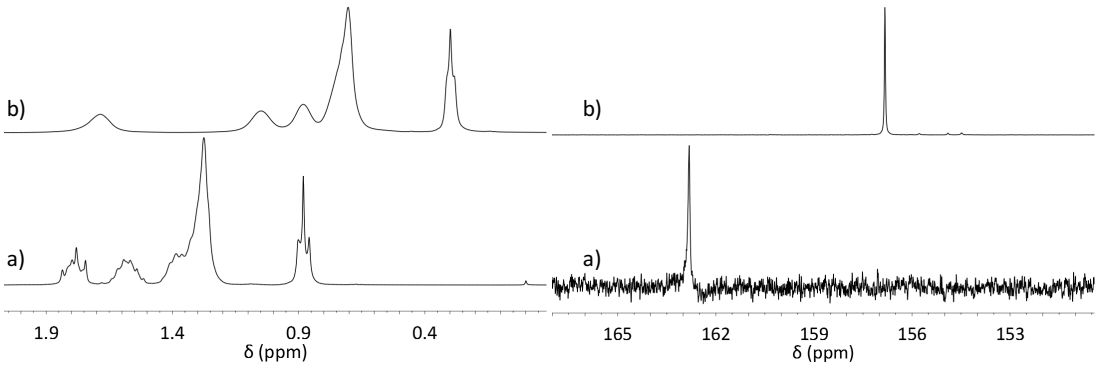

Figure 2.1-1: Left: ^{1}H NMR spectra of a) $P_{888}Se$ and b) $P_{888}Se$-$AlCl_3$ χ_{AlCl3} = 0.60. Right: ^{13}C NMR spectra of a) urea (D_2O solution) and b) Ur-$AlCl_3$ χ_{AlCl3} = 0.60

Although gallium has two NMR-active nuclei, ^{69}Ga and ^{71}Ga, both are quadrapolar and yield broad lines in their spectra.[151] For those LCCs which were acidic ($\chi_{GaCl3} \geq 0.60$) no peaks were distinguishable from the baseline, which is consistent with the previously reported literature.[87,135] As such, this spectroscopy was not found to be useful.

To study LCCs' speciation, the nuclei of choice are those that are directly partake in the coordination, or are readily affected by their environment, and can distinguish between different coordination modes. The ^{27}Al nucleus is 100% abundant and reasonably receptive (20% relative to ^{1}H),[145,151] though the high spin (5/2) can lead to line broadening. ^{27}Al NMR spectroscopy has been widely used for characterisation of chloroaluminate ionic liquids and LCCs, as stated in Chapter 1.2.[83,135,154] The ^{31}P nucleus is highly receptive, has a wide range of chemical shift values which vary with even small changes to its environment, is 100% abundant and is spin 1/2. As such, it provides valuable information on speciation. For ligands that contain selenium as the coordinating atom, ^{77}Se is spin 1/2 and can provide information

on the local environment. NMR spectroscopy of these three nuclei revealed most information about the speciation of synthesised products.

2.1.2.3 Previously-reported LCCs

Some LCCs prepared for catalytic studies in this work were previously synthesised by Coleman *et al.* and Abbott *et al.*, and characterised by Raman and NMR spectroscopies.[135,149] LCCs with *O*-donors were found to have a common pattern in their ^{27}Al NMR spectra at χ_{AlCl3} = 0.50. Namely, three peaks at *ca.* 103, 90 and 75 ppm were seen for $P_{888}O$, Ur, and AcA ligands (in neat LCCs). When using AcA, NMA and DMA as ligands, Liu *et al.* saw this pattern persevered up to χ_{AlCl3} = 0.61 (in DCM solution), with broadening of the peaks indicating the presence of increasing quantities of dimeric aluminium species. Still, 3 distinct peaks were observable. For $AlCl_3$-AcA χ_{AlCl3} = 0.60, measured as neat liquid, Coleman *et al*. observed significant broadening of the peaks centred at *ca.* 92 ppm, indicating dimeric species. SUr and P_{888} ligands were reported by Coleman *et al.* to result in a downfield shift in their ^{27}Al NMR spectra (in agreement with earlier literature reports). Peaks greater than *ca.* 103 ppm were assigned to the species $[AlCl_2L_2]$ and $AlCl_3L$.

All ^{27}Al NMR spectra, measured for neat LCCs reported in the literature, corresponded with these described patterns.

2.1.2.4 Phosphine chalcogenides LCCs

2.1.2.4.1 Ligand synthesis

Trioctylphosphine sulphide and selenide were synthesised from trioctylphosphine by the addition of sulphur and selenium, respectively. Their purity was confirmed by ^{31}P NMR spectroscopy (Figure 2.1-2). Samples were studied neat (with a DMSO capillary), except for solid $P_{888}O$, which was recorded as a $CDCl_3$ solution. Interestingly, the phosphine oxide and sulphide were found to have very similar chemical shifts (all chemical shifts are summarised in Table 2.1-8 at the end of this section).

The starting trioctylphosphine contained a small amount of trioctylphosphine oxide (7% by integration of the corresponding ^{31}P signals), which is also visible in the sample of $P_{888}Se$. The presence of small amount of $P_{888}O$ resulted in small amount of Se left unreacted (< 1% as measured by the mass of selenium filtered after the reaction). The ^{1}J (^{31}P – ^{77}Se) (Hz) coupling constant for $P_{888}Se$ was 678 Hz (Table 2.1-5), which is in reasonable agreement for that

reported for $P_{111}Se$ (684 Hz).[151] The same level of oxide impurity can be assumed for the phosphine sulphide product, although the oxide signal is obscured by the $P_{888}S$ peak.

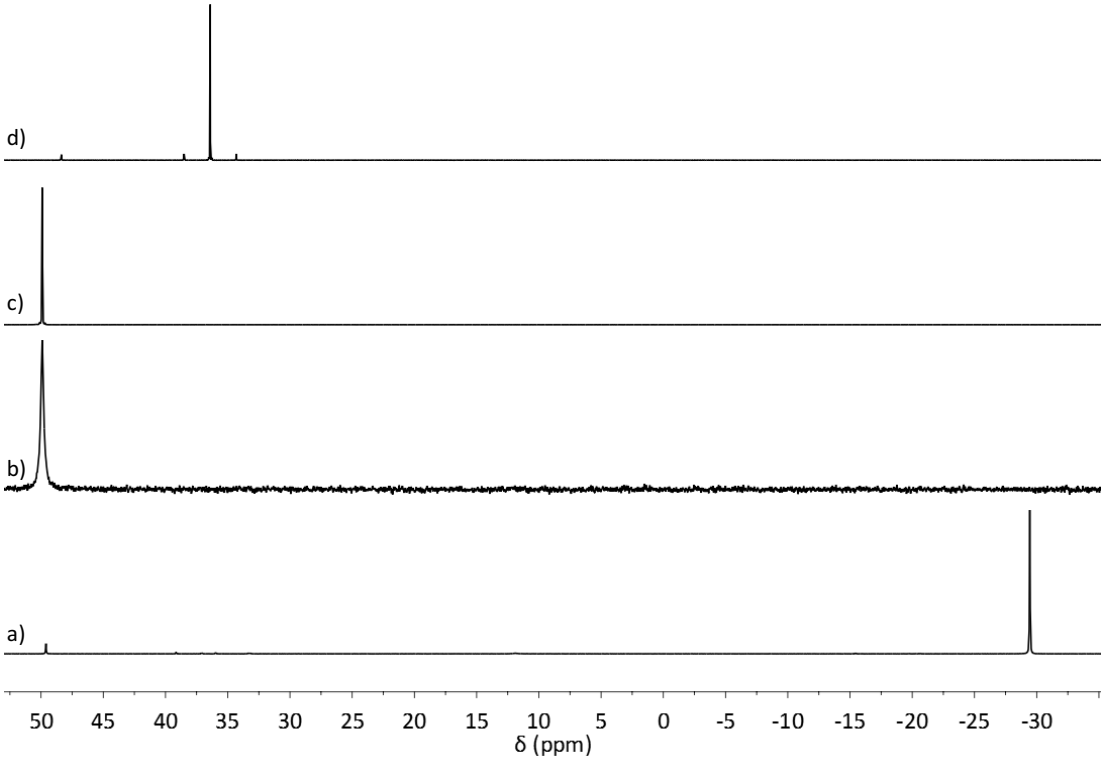

Figure 2.1-2: ^{31}P NMR spectra of a) P_{888}, b) $P_{888}O$ ($CDCl_3$) c) $P_{888}S$, and d) $P_{888}Se$

Table 2.1-3: ^{31}P NMR chemical shifts of phosphine and phosphine chalcogenide ligands

Ligand	δ ^{31}P (ppm)
Trioctylphosphine (P_{888})	-29.44
Trioctylphosphine Oxide ($P_{888}O$)	49.91
Trioctylphosphine Sulphide ($P_{888}S$)	49.91
Trioctylphosphine Selenide ($P_{888}Se$)	36.41

2.1.2.4.2 Speciation of the $P_{222}O$-$AlCl_3$ system

As stated in Chapter 1.1.2, triethylphosphine oxide is used as a probe molecule for measuring the Lewis acidity by the Gutmman acceptor method, so it was instrumental to have NMR spectra of neat $AlCl_3$-$P_{222}O$ χ_{AlCl3} = 0.50 and 0.60 systems for comparison. Since $AlCl_3$-$P_{222}O$ χ_{AlCl3} = 0.50 was solid at room temperature, NMR spectra for the $AlCl_3$-$P_{222}O$ systems were recorded at 55 and 80 °C. Although, in principle, the temperature increase will alter the ratio of the equilibrated species, they should still be the same species as present at room temperature, which offers a useful guide for interpreting Guttmann acceptor number results (Chapter 2.1.1.7).

At 55 °C the ^{27}Al NMR spectrum (Figure 2.1-3-a) of $AlCl_3$-$P_{222}O$ χ_{AlCl3} = 0.50 had 3 distinct peaks at 103.06, 89.91 and 75.06 ppm (ratio 2:5:2) which were assigned to $[AlCl_4]^-$, $[AlCl_3(P_{222}O)]$ and $[AlCl_2(P_{222}O)]^+$, respectively, as they are in good agreement with data for $P_{888}O$-$AlCl_3$ χ_{AlCl3} = 0.50, both measured by Coleman *et al.*[135] and in this work (Table 2.1-8). At 80 °C, the ^{27}Al NMR signals for $AlCl_3(P_{222}O)$ and $[Al_2Cl_2(P_{222}O)_2]^+$ merge, and split again upon cooling to 55 °C (Table 2.1-8). The $[AlCl_4]^-$ peak is also seen to broaden slightly. This behaviour was observed by Coleman *et al*. and would reinforce their view that LCCs consist of species in rapid equilibrium.

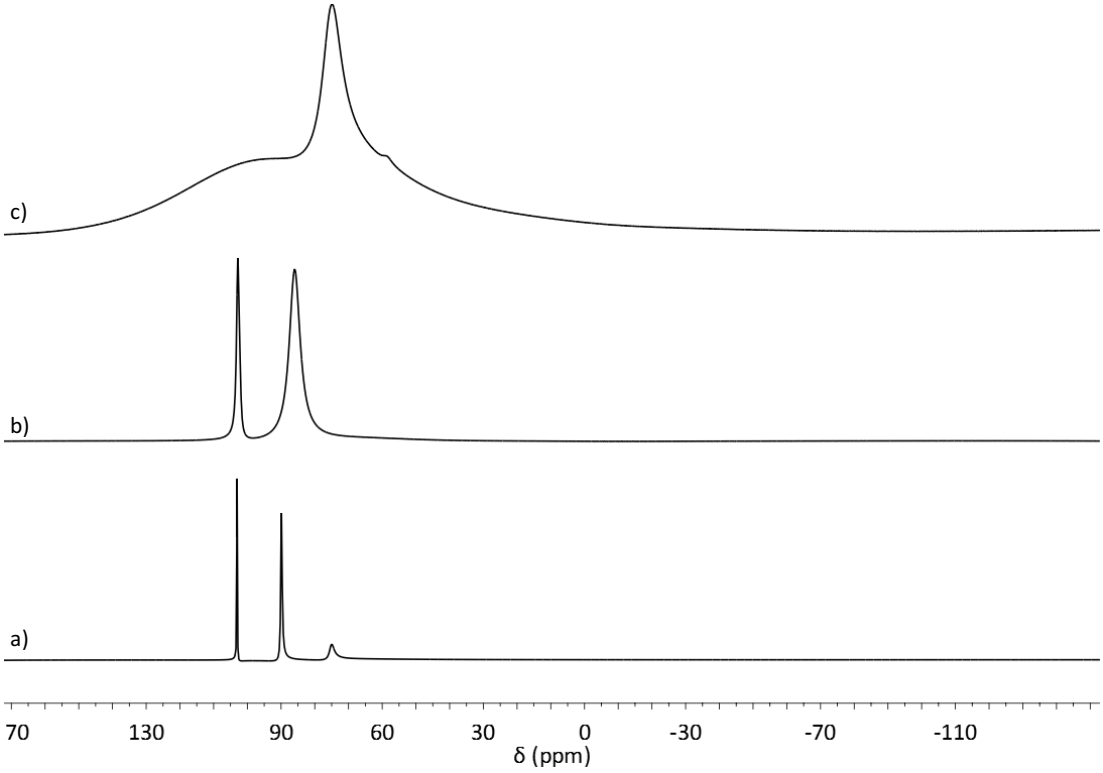

Figure 2.1-3: ^{27}Al NMR spectra of a) $P_{222}O$-$AlCl_3$ χ_{AlCl3} = 0.50 (55 °C) b) $P_{222}O$-$AlCl_3$ χ_{AlCl3} = 0.50 (80 °C) c) $P_{222}O$-$AlCl_3$ χ_{AlCl3} = 0.60

The ^{31}P NMR spectra at 55 °C of $AlCl_3$-$P_{222}O$ χ_{AlCl3} = 0.50 (Figure 2.1-4-a) showed 2 peaks at 80.37 and 82.28 ppm which were assigned to $[AlCl_3(P_{222}O)]$ and $[AlCl_2(P_{222}O)_2]^+$, respectively. Whilst similar to the ^{31}P NMR spectrum of $AlCl_3$-$P_{888}O$ χ_{AlCl3} = 0.50, the peaks were shifted downfield by *ca.* 5 ppm (Table 2.1-8). Again, upon heating to 80 °C, the peaks were seen to merge and split again upon cooling suggesting species in temperature-dependant equilibrium (Figure 2.1-4-b).

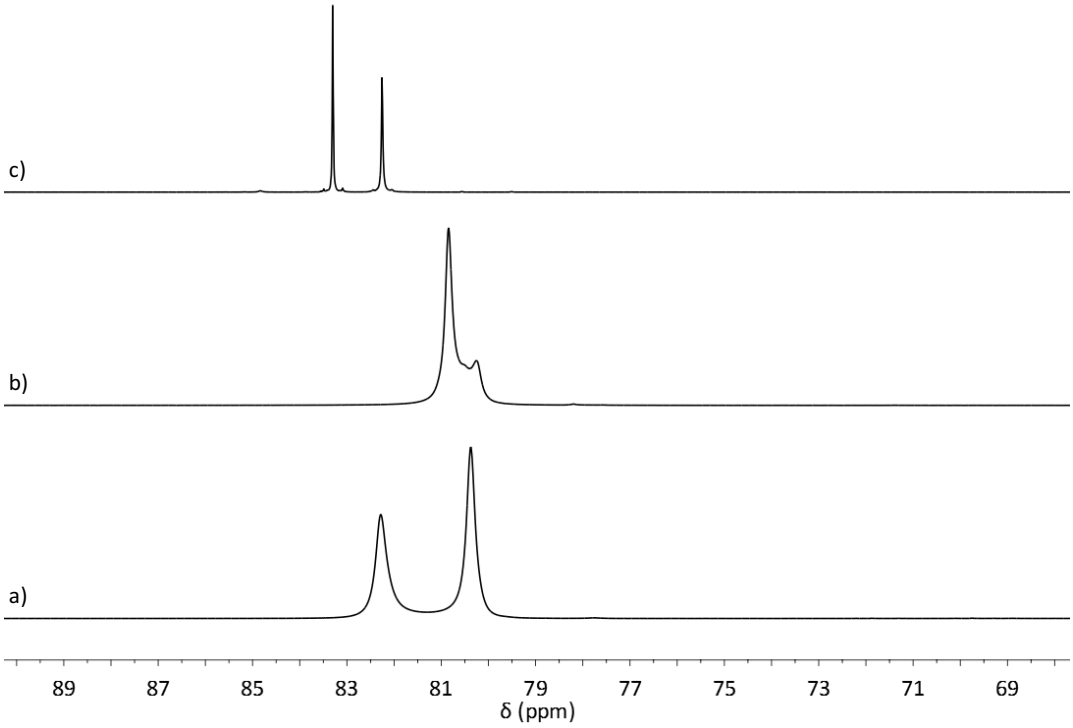

Figure 2.1-4: ^{31}P NMR spectra of a) $P_{222}O$-$AlCl_3$ χ_{AlCl3} = 0.50 (55 °C) b) $P_{222}O$-$AlCl_3$ χ_{AlCl3} = 0.50 (80 °C) c) $P_{222}O$-AlC_3 χ_{AlCl3} = 0.60

The ^{27}Al NMR spectrum of $P_{222}O$-$AlCl_3$ χ_{AlCl3} = 0.60 (Figure 2.1-3-c) was very similar to that recorded by Coleman *et al.* for DMA-$AlCl_3$ χ_{AlCl3} = 0.60[135] and $P_{888}O$-$AlCl_3$ χ_{AlCl3} = 0.60 (Figure 2.1-15-a). A broad feature is seen, indicative of dimeric aluminium species, with a sharp peak emerging at 74.01 ppm, which is assigned to $[AlCl_2(P_{222}O)_2]^+$. In the ^{31}P NMR spectrum of $P_{222}O$-$AlCl_3$ χ_{AlCl3} = 0.60, there were 2 peaks present (82.25 and 83.30 ppm, 1:1 ratio) assigned to $[AlCl_2(P_{222}O)_2]^+$ and $[Al_2Cl_6(P_{888}O)]$, respectively. Again these are downfield of the peaks seen in the ^{31}P NMR spectrum of $P_{888}O$-$AlCl_3$ χ_{AlCl3} = 0.60 by *ca.* 5 ppm.

As was expected, the speciation of $P_{222}O$-$AlCl_3$ mixtures is very similar to that of $P_{888}O$-$AlCl_3$ mixtures, with a slight discrepancy at higher χ_{AlCl3} values. Crucially, the ^{31}P NMR signals in both $P_{222}O$-$AlCl_3$ χ_{AlCl3} = 0.50 and 0.60, were seen to be significantly and consistently downfield, by *ca.* 5ppm, from the corresponding signals in $P_{888}O$-$AlCl_3$ χ_{AlCl3} = 0.50 and 0.60, which will allow for distinguishing between these peaks in Gutmann acceptor number measurements.

2.1.2.4.3 Speciation of phosphine chalcogenide LCCs at χ_{AlCl3} = 0.50

^{27}Al NMR spectra of the three $P_{888}E$-$AlCl_3$ χ_{AlCl3} = 0.50 systems are compared in Figure 2.1-5. As stated in Chapter 2.1.2.4.2, the spectrum corresponding to $P_{888}O$-$AlCl_3$ χ_{AlCl3} = 0.50 (Figure 2.1-5-a), features three signals at 103.81, 90.59, and 75.57 ppm, and is in a very good agreement

with the spectrum reported for the same system by Coleman *et al.*[135] These peaks were assigned to $[AlCl_4]^-$, $[AlCl_3P_{888}O]$, and $[AlCl_2(P_{888}O)_2]^+$, respectively.

The spectra recorded for $P_{888}S$-$AlCl_3$ χ_{AlCl3} = 0.50 (Figure 2.1-5-b) and $P_{888}Se$-$AlCl_3$ χ_{AlCl3} = 0.50 (Figure 2.1-5-c), were significantly different from the phosphine oxide counterpart, and nearly identical with each other. Both contained wide non-Lorentzian signals at *ca*. 103 ppm, accompanied by very broad features around 65 ppm.

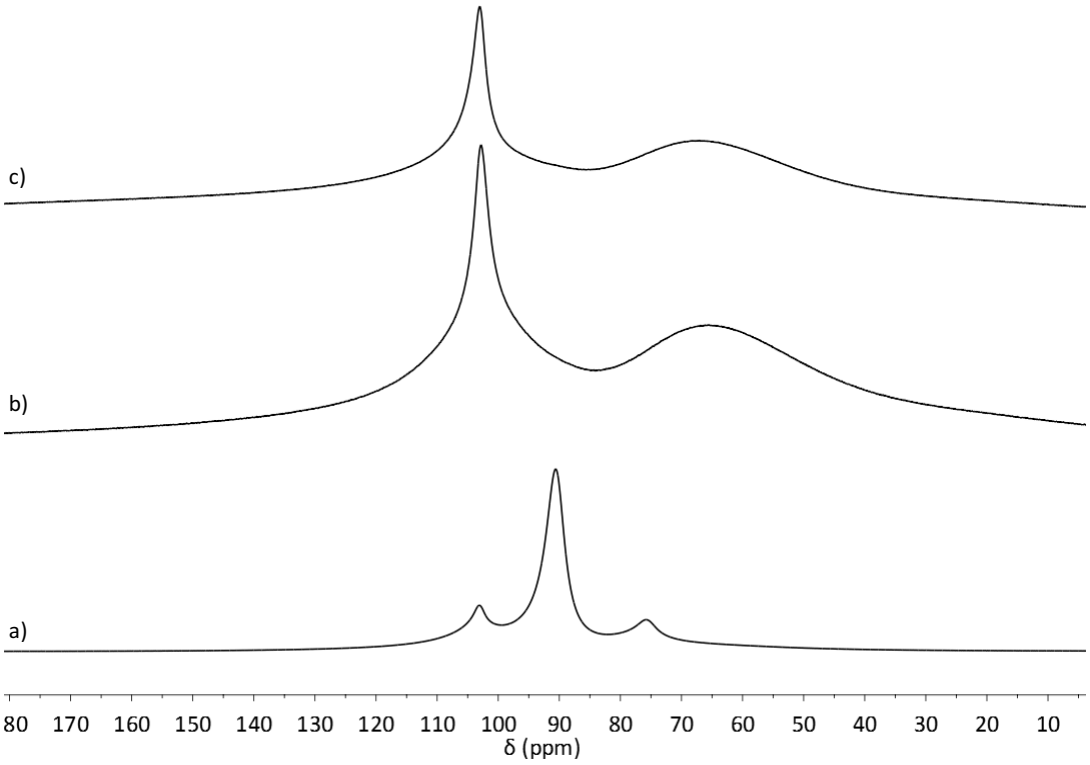

Figure 2.1-5: ^{27}Al NMR spectra of a) $P_{888}O$-$AlCl_3$ χ_{AlCl3} = 0.50, b) $P_{888}S$-$AlCl_3$ χ_{AlCl3} = 0.50, c) $P_{888}Se$-$AlCl_3$ χ_{AlCl3} = 0.50

The broad feature could indicate the presence of pentacoordinate species,[148] which seems unlikely, considering equimolar quantities of ligand and $AlCl_3$. An alternative explanation for a similar system was proposed by Dai and co-workers, who reported a ^{27}Al NMR peak at *ca*. 69 ppm and assigned it as coming from the NMR probe.[155] It was more prominent for higher $AlCl_3$ content in their 4-propylpyridine-$AlCl_3$ mixtures.

To confirm that the signal originates from the probe, ^{27}Al NMR spectrum of a blank (DMSO capillary, no aluminium compounds) was recorded. The blank ^{27}Al spectrum featured a broad signal at *ca*. 67 ppm. By superimposing this spectrum upon the other ^{27}Al NMR spectra it appears that this peak is of a similar magnitude to those seen for of $P_{888}S$-$AlCl_3$ χ_{AlCl3} = 0.50 and of $P_{888}Se$-$AlCl_3$ χ_{AlCl3} = 0.50 (Figure 2.1-6).

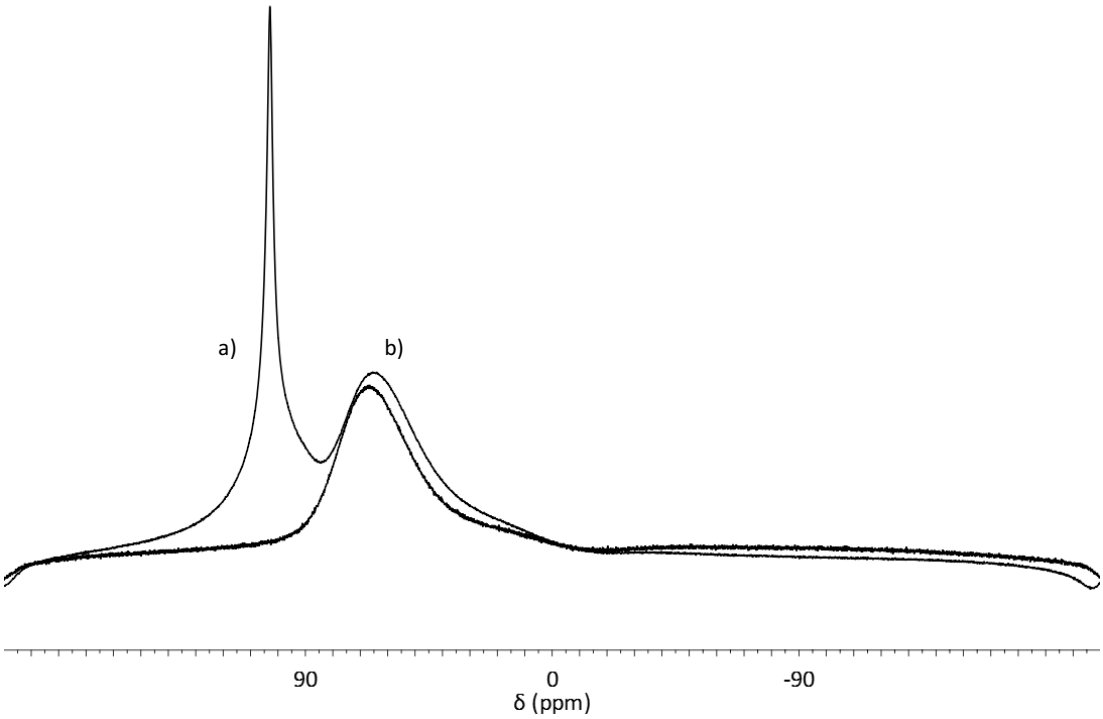

Figure 2.1-6: Representative example of magnitude of background relative to sample, overlay of a) $P_{888}Se$-$AlCl_3$ χ_{AlCl3} = 0.50, and b) blank

The signal for $[AlCl_3(P_{888}E)]$, where E = S or Se, should be expected around 110 ppm,[164] but such feature was not observed and the background was very prominent(Figure 2.1-5-b and c), which leads to three key conclusions for the interpretation of these spectra. Firstly, as the signal from $[AlCl_4]^-$ is sharp and readily distinguishable from the baseline, its low intensity compared the broad background peak indicates $[AlCl_4]^-$ must be present in very low concentrations. Following from this, low concentration of anions implies equally low cation concentration. Finally, the lack of other signal in the ^{27}Al NMR spectrum indicate the majority of Al species are in low symmetry environments and their peaks must be so broad as to be indistinguishable from the baseline.

No ^{27}Al NMR data for phosphine sulphide adducts with $AlCl_3$ were found in the literature. However, the similarity between $P_{888}O$ and other oxygen donors used by Coleman *et al.*[135] suggest that the ^{27}Al NMR chemical shift values of $P_{888}S$-$AlCl_3$ mixtures would be similar to other sulphur donors. The signal at δ ^{27}Al = 103.04 ppm (Table 2.1-8, Figure 2.1-5-b) appears to be a sharp peak emerging from a broader feature, which would suggest at least two species present. Thioether-$AlCl_3$ adducts, studied in CH_2Cl_2 solution, were reported to form $[AlCl_3(Me_2S)]$ and $[AlCl_3(Me_2S)_2]$ complexes, with chemical shifts in the ^{27}Al NMR spectrum at 111.6 and 73.8 ppm, respectively.[164] Despite reporting some mixtures being "*an oil at room temperature",* such as $[AlCl_3(Me_2S)]$, Reid and co-workers did not report a sharp peak at *ca.*

103 ppm, associated with $[AlCl_4]^-$. Coleman *et al.* reported $[AlCl_3(SUr)]$ at 109 ppm. For dimethyl selenoether adducts of $AlCl_3$, Reid and co-workers detected only one peak in the ^{27}Al NMR spectrum, at 110.5 ppm, assigned to $[AlCl_3(Me_2Se)]$.[164] No pentacoordinate species, $[AlCl_3(Me_2Se)_2]$, was observed - even with a large excess of Me_2Se. Reid postulated that this was due to the small size of the aluminium atom comparative to that of selenium.

Comparing the peak width of the $[AlCl_4]^-$ anion in the samples Ur-$AlCl_3$, $P_{222}O$-$AlCl_3$, $P_{888}O$-$AlCl_3$, $P_{888}S$-$AlCl_3$ and $P_{888}Se$-$AlCl_3$ χ_{AlCl3} = 0.50 (Table 2.1-4), one can see that in all LCC samples this is significantly broader than the reported literature values: by one order of magnitude compared to chloroaluminate(III) ionic liquids, and two orders of magnitude compared to $CDCl_3$ solution.[83,164] This broadening in Ur-$AlCl_3$ χ_{AlCl3} = 0.50 and $P_{888}O$-$AlCl_3$ χ_{AlCl3} = 0.50 samples was attributed to the exchange between species in equilibrium.[135] In the $P_{888}E$-$AlCl_3$ χ_{AlCl3} = 0.50 (E=S, Se) samples, even wider signals are found at *ca*. 103 ppm (Table 2.1-4), no doubt in part due to their relatively high viscosity values (Table 2.1-14). Reid and co-workers reported the peak width at half-height ($\delta\nu_{1/2}$) of the molecular adduct $[AlCl_3(Me_2Se)]$ in solution to be 310 Hz, compared to 5 Hz measured for the $[AlCl_4]^-$ signal. It is not unreasonable to assume that, in LCCs, the less symmetrical species $[AlCl_3(P_{888}E)]$ should also produce significantly broader peaks than the observed $[AlCl_4]^-$ anion peak. In this case the peak would appear to be so broad as to be indistinguishable from the baseline.[164]

Table 2.1-4: Half height peak width of the $[AlCl_4]^-$ anion

Compound	$[AlCl_4]^-$ $\delta\nu_{1/2}$ (Hz)
$[C_2C_1im][AlCl_4]$[83]	23
$[AlCl_2\{MeS(CH_2)_2SMe\}_2][AlCl_4]$ ($CDCl_3$ solution)[164]	5
Ur-$AlCl_3$ χ_{AlCl3} = 0.50	158
$P_{888}O$-$AlCl_3$ χ_{AlCl3} = 0.50	356
$P_{888}S$-$AlCl_3$ χ_{AlCl3} = 0.50	890
$P_{888}Se$-$AlCl_3$ χ_{AlCl3} = 0.50	825

^{31}P NMR spectra of the three $P_{888}E$-$AlCl_3$ χ_{AlCl3} = 0.50 systems are compared in Figure 2.1-7. In all three cases, there are two sets of signals in the ^{31}P NMR spectra. The more shielded ones correspond to a neutral adduct species, $[AlCl_3(P_{888}E)]$, with the considerably smaller, relatively deshielded peaks corresponding to the charged species, $[AlCl_2(P_{888}E)_2]^+$. In the ^{31}P NMR spectrum of $P_{888}O$-$AlCl_3$ χ_{AlCl3} = 0.50 (Figure 2.1-7-a), there is a considerable proportion of charged species *vs*. neutral ones (integration ratio 1:2). This is in agreement with the corresponding ^{27}Al NMR spectra, reported by Coleman *et al.*[165] For $P_{888}S$-$AlCl_3$ χ_{AlCl3} = 0.50 (Figure 2.1-7-b), the contribution of the upfield signal is much smaller (integration ratio 1:12). The ^{31}P NMR spectrum of $P_{888}Se$-$AlCl_3$ χ_{AlCl3} = 0.50 (Figure 2.1-7-c) features a singlet at 44.41 ppm, accompanied by satellites arising from ^{77}Se coupling ($^1J_{P\text{-}Se}$ = 473 Hz), with only trace

downfield peak (and a trace feature from $P_{888}O$ impurity). The corresponding ^{77}Se NMR shows a doublet environment (Figure 2.1-8-a, Table 2.1-5, δ ^{77}Se = -239.47 ppm, $^{1}J_{P\text{-}Se}$ = 486 Hz) and a trace relatively deshielded peak (δ ^{77}Se = -213.93 ppm) in a similar fashion to the ^{31}P NMR spectrum. This positively confirms that the molecular adduct is preferred over the charged species for complexes with phosphine sulphide and selenide.

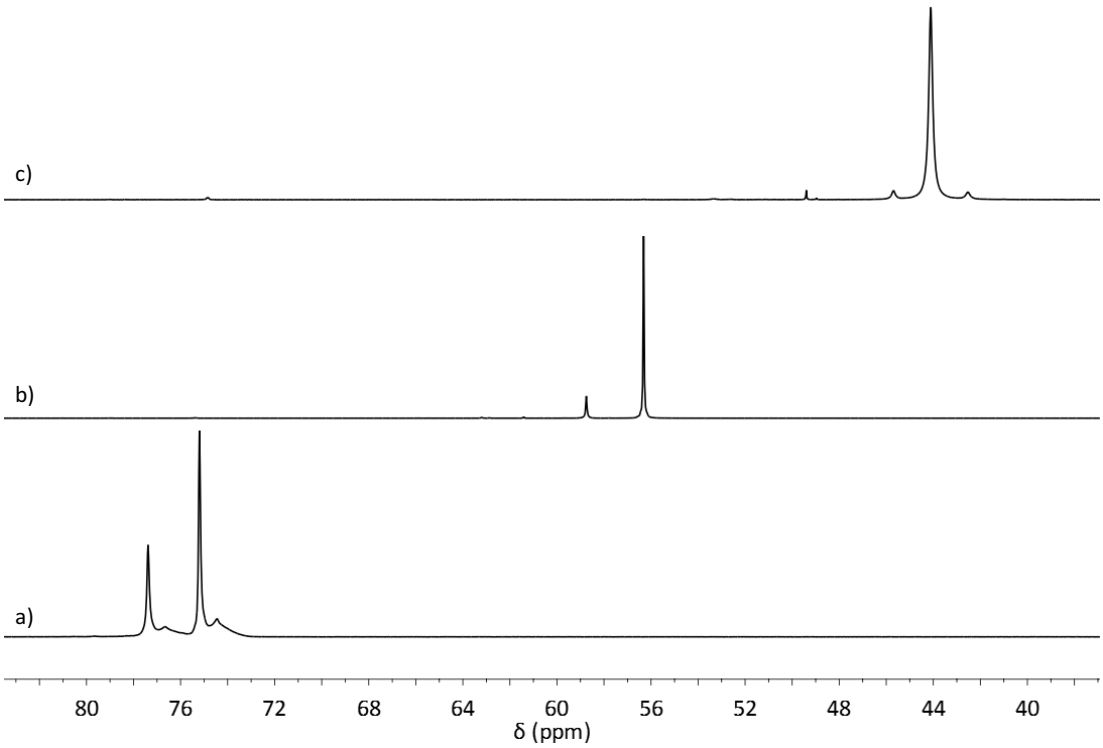

Figure 2.1-7: ^{31}P NMR spectra of a) $P_{888}O$-$AlCl_3$ χ_{AlCl3} = 0.50, b) $P_{888}S$-$AlCl_3$ χ_{AlCl3} = 0.50, c) $P_{888}Se$-$AlCl_3$ χ_{AlCl3} = 0.50

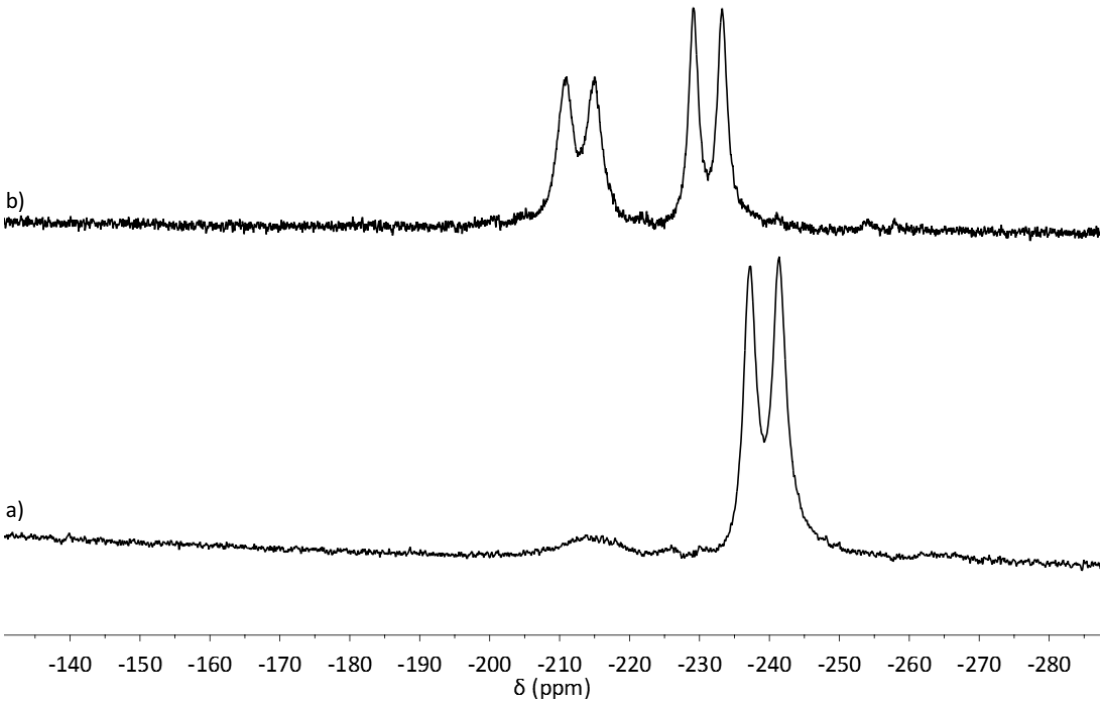

Figure 2.1-8: ^{77}Se NMR spectra for a) $P_{888}Se$ χ_{AlCl3} = 0.50, b) $P_{888}Se$ χ_{AlCl3} = 0.60

Furthermore, the coupling constant between ^{31}P and ^{77}Se is seen to decrease by *ca.* 206 Hz upon complexation of the ligand to $AlCl_3$ (Table 2.1-5). This is consistent with the decrease in coupling constant seen by Burford *et al.* upon complexation of Ph_3PSe to $AlCl_3$.[166]

Table 2.1-5: Chemical shift and coupling data for major peaks in trioctylphosphine selenide compounds.

LCCs	δ ^{31}P (ppm)	^{1}J (^{31}*P* – ^{77}Se) (Hz)	δ ^{77}Se (ppm)	^{1}J (^{31}P – ^{77}*Se*) (Hz)
$P_{888}Se$	36.41	678.25	-388.57	709.68
$P_{888}Se$-$AlCl_3$ χ_{AlCl3} = 0.50	45.30	472.67	-239.47	486.47
	-	-	-213.93	-
$P_{888}Se$-$AlCl_3$ χ_{AlCl3} = 0.60	47.69	-	-231.21	469.31
	47.19	-	-213.00	454.43

For both chloroaluminate ionic liquids[76] and LCCs[135] Raman spectroscopy has been used to determine the presence of chloroaluminate anions. In particular, the $[AlCl_4]^-$ anion can be readily identified by a sharp peak at *ca.* 350 cm^{-1} and the $[Al_2Cl_7]^-$ anion by a sharp peak at *ca.* 310 cm^{-1}. For both $P_{888}S$-$AlCl_3$ and $P_{888}Se$-$AlCl_3$ χ_{AlCl3} = 0.50 (Figure 2.1-9) the Raman spectra feature the sharpest peaks at *ca*. 285 and 400 cm^{-1}, which do not correspond to chloroaluminate anion vibrations.[76] Reid reported both $[AlCl_3(Me_2S)]$ and $[AlCl_3(Me_2Se)]$ as both having Raman peaks at *ca.* 400 cm^{-1} suggesting that the peaks observed here are due to the molecular complex.[164] The very weak absorption at 350 cm^{-1}, suggests minimal presence of $[AlCl_4]^-$, which is consistent with the ^{31}P and ^{27}Al NMR spectra.

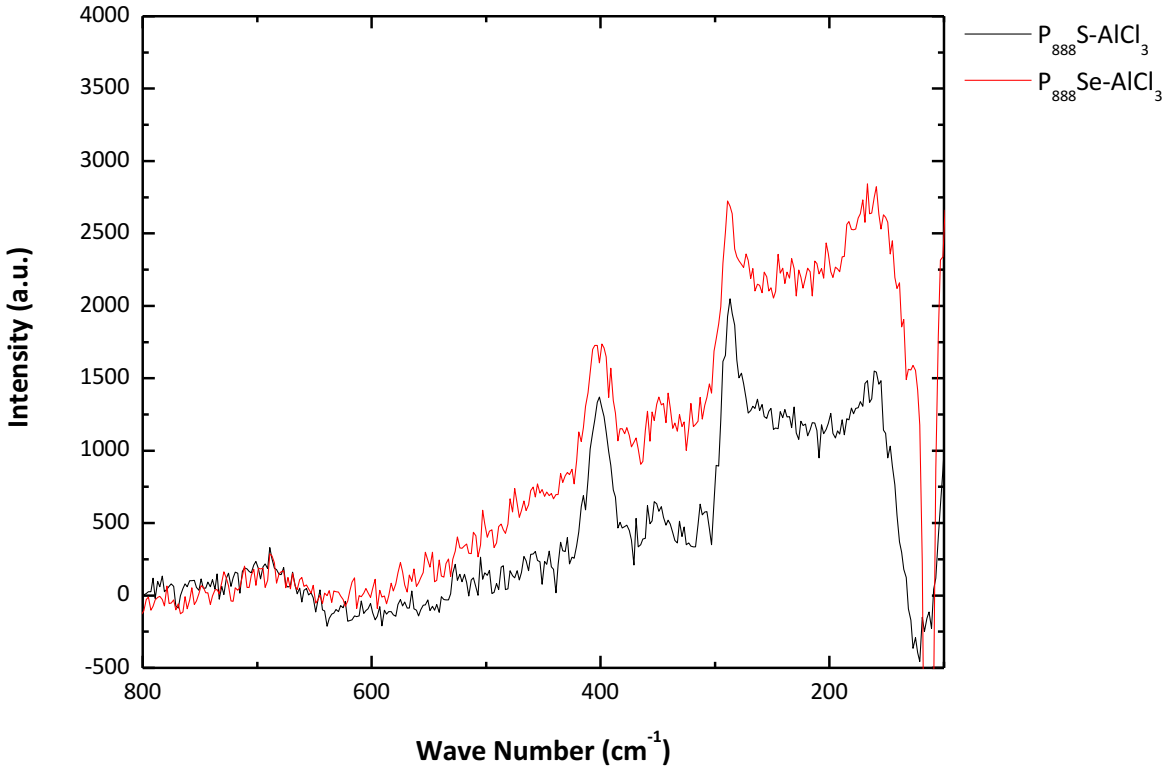

Figure 2.1-9: Raman spectroscopy of $P_{888}S\text{-}AlCl_3$ and $P_{888}Se\text{-}AlCl_3$ χ_{AlCl3} = 0.50

Two major factors appear to promote the formation of charged $[MX_2L_2][MX_4]$ complexes: the presence of the dimeric unit, 'M_2X_6', that can be split in asymmetric manner, and the donor strength of L, with strong donor favouring the formation of a salt. Both aspects are elaborated below.

Aluminium chloride is accepted to exist as a dimer in the liquid and solution phase. As such the incoming ligand must react with the dimeric species, likely producing the intermediate shown in Figure 2.1-10.

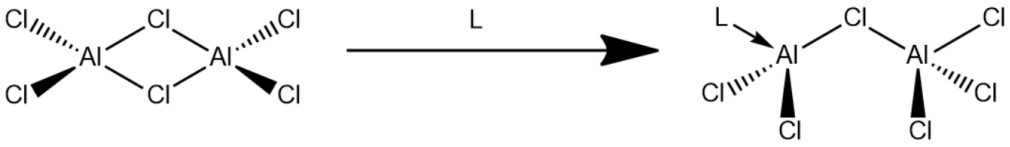

Figure 2.1-10: Proposed reaction of Al_2Cl_6 dimer with L forming the intermediate L-$AlCl_2$-(μCl)-$AlCl_3$

Such an intermediate has not been reported for $AlCl_3$. However the reaction of other dimeric species of the type M_2X_6 (M = B, Ga, X = H, Cl, Br, I) with bases have been studied. Shore studied the reaction of borane and ammonia in THF solutions.[167] Diborane in THF dissociates to the adduct BH_3-THF. This adduct when reacted with NH_3 forms two products, the adduct

BH_3NH_3 and the ionic species $[BH_2NH_3][BH_4]$ as the major and minor products respectively. The reaction was followed by ^{11}B NMR from which the following reaction mechanism was proposed (Figure 2.1-11).

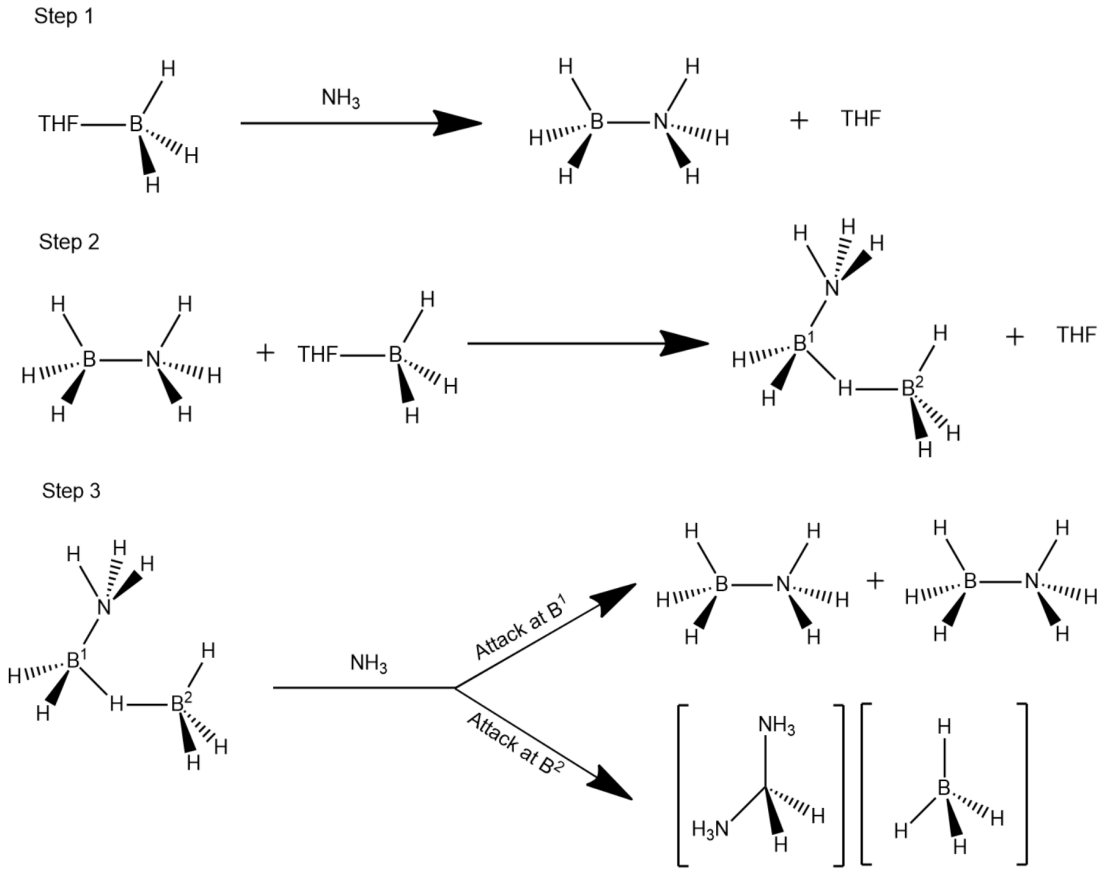

Figure 2.1-11: Shore's proposed mechanism for BH_3.THF reaction with NH_3

The selectivity to either product depended on the reaction conditions. For example, rapid addition of excess NH_3 prevented formation of the ionic product, by rapidly depleting the concentration of BH_3·THF and thus preventing the formation of the intermediate dimeric species NH_3-BH_2(μ-H)BH_3. This indicated that the dimeric intermediate is essential for the formation of the ionic product. Computational analysis revealed that the energy barrier to form $[(NH_3)_2BH_2][BH_4]$ was larger than that calculated to form NH_3BH_3. The presence of dihydrogen bonds (an interaction between two oppositely partially charged hydrogen atoms, *e.g.* N-$H^{\delta+}\cdots H^{\delta-}$B) lowered the energy cost to form charged species, whereas the energy of the neutral adduct was independent of dihydrogen bonding. Hence, stabilisation of the charges formed was found to be another essential requirement for ionic species formation.

Corroborating results were reported for the reaction of $AlCl_3$ with two or more moles of THF. Derouault[138] and Atwood[144] both reported the formation of the ionic product, $[AlCl_2THF_4][AlCl_4]$, whereas Cowley formed the molecular species, $[AlCl_3THF_2]$.[140] Neat $AlCl_3$ was used in the former case, and $(Me_2N)_3SiCl{\cdot}AlCl_3$ for the latter. Using $(Me_2N)_3SiCl{\cdot}AlCl_3$ as the starting material eliminated the presence of the dimer, preventing the formation of the ionic product.

With regards to the donor strength of the ligand, Gandon *et al.*[168] studied three *N*-heterocyclic carbenes (Figure 2.1-12) as adducts with GaX_3 (X = Cl, Br and I), and reported that the product was a salt or a molecular adduct, depending on the strength of the base used. DiMe-IMD formed molecular adducts with $GaCl_3$. Conversely diMe-MDI formed ionic species with GaX_3 (X = Cl, Br and I). Finally $IBioxMe_4$ was found to form the ionic product with $GaCl_3$ and molecular products with $GaBr_3$ or GaI_3.

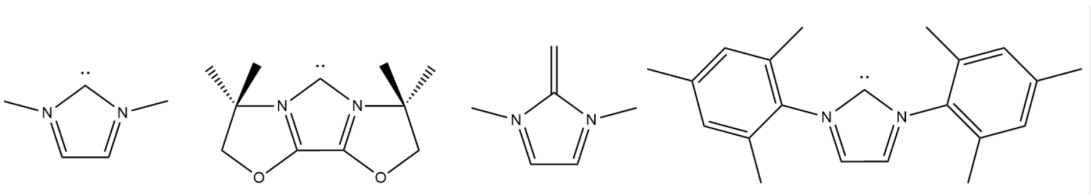

Figure 2.1-12: Structures of *N*-heterocyclic carbenes left to right, diMe-IMD, $IBioxMe_4$, diMe-MDI and diMes-IMD

Two of carbene bases used, diMe-IMD and $IBioxMe_4$, had similar Tolman electronic parameters and were similar to diMes-IMD, suggesting all three bases have similar donating strength.[169] For rhodium complexs,[170] diMes-IMD caused a smaller change in the CO vibration than the diMe-DMI suggesting the latter is a stronger donor (see Table 2.1-6). As di-Mes-IMD was of a similar strength to diMe-IMD and $IBioxMe_4$ this would suggest that diMe-DMI is a stronger base than both diMe-IMD and $IBioxMe_4$. This vibrational data correlated with computed Ga^1-Cl bond lengths and thus, by extension, Ga^1-Cl bond strengths. Furthermore, Gandon *et al*. report the ranking of unoccupied molecular orbitals for the diMe-IMD and diMes-IMD L-$GaCl_2$-(μCl)-$GaCl_3$ complexes. When diMe-IMD was used as the donor, the lowest orbital with a strong coefficient at a gallium atom is the LUMO +1 which was centred at Ga^2 (Figure 2.1-13). The LUMO when diMe-DMI was the donor was centred at Ga^1 (Figure 2.1-13), suggesting in this case, a second ligand will attack at Ga^1. It would seem then that the strength of the donor directly determines whether ionic or molecular species are formed. The anion in both ionic species is closely associated with the imidazolium ring, thus may be

partially stabilised by hydrogen bonding. Furthermore $GaBr_3$ and GaI_3 formed adducts with the $IBioxMe_4$ due to Bent's rule.

Table 2.1-6: Summary of CO vibrations correlated with Ga^1-Cl bond lengths (please note the gallium number here reversed here compared to ref 167 to fit with the numbering in ref 166)

NHC	CO vibration $NiCO_3L$[169] (cm^{-1})	CO vibration $RhClCO_2L$[170] (cm^{-1})	Ga^1-Cl Bond Length[168] (Å)
diMe-IMD	2054.1	-	2.336
$IBioxMe_4$	2049.5	-	2.341
diMes-IMD	2050.5	2006	-
diMe-DMI	-	1966	2.371

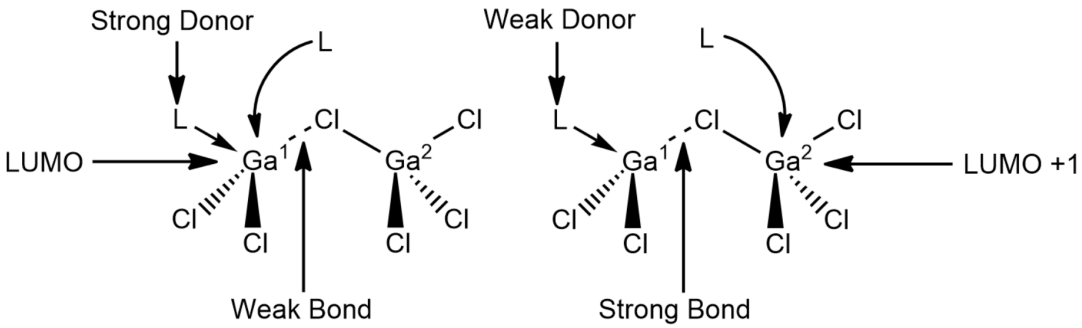

Figure 2.1-13: Pictorial representation of Ga^1-Cl bond strength as a function of L donor strength in L-$GaCl_2$-(μCl)-$GaCl_3$

The donicity of phosphine chalcogenides have been measured by a variety of measurements. However as discussed in Chapter 1.1 no scale is universal, as such two scales for phosphine chalcogenide donors are presented here. Firstly, the basicity of phosphine chalcogenides to the hydrogen bond donor 4-fluorophenol,[1] as represented by the equilibrium constant and Gibbs free energy of formation Δ G° of Equation 2.1-1. The second is the basicity of phosphine chalcogenides to the halogen bond donor di-iodine,[1] of which the equilibrium constant K_c of Equation 2.1-2 has been reported.

$$4F\text{-}C_6H_4OH + B \leftrightarrows 4F\text{-}C_6H_4OH\cdots B \qquad \text{Equation 2.1-1}$$

$$I_2 + B \leftrightarrows I_2\cdots B \qquad \text{Equation 2.1-2}$$

Table 2.1-7: Summary of donicity data for phosphine chalcogenides all measured in CCl_4[1]

Phosphine Chalcogenide	pK_{BHX}	Δ G° (kJ mol^1)	K_c
$P_{888}O$	3.59	- 20.49	-
PPh_3O	3.16	-18.04	-
$P_{888}S$	1.54	-8.79	-
PPh_3S	1.00	-5.71	-
PPh_3Se	0.94	-5.37	-
$P_{222}O$	-	-	108
$P_{222}S$	-	-	1450
$P_{222}Se$	-	-	18000

As can been seen from Table 2.1-7 phosphine oxides are better hydrogen bond acceptors than their heavier phosphine chalcogenide analogues. Conversely, triethylphosphine selenide is a better halogen bond acceptor than its lighter phosphine chalcogenide analogues, as such one would expect $P_{888}O$ to be the strongest donor to $AlCl_3$ which is itself a hard Lewis acid.

However, $P_{888}O$ when reacted with $AlCl_3$ forms both ionic and molecular species. There does not appear to be any computational data regarding this phenomenon and given that the equilibrium between these two products appears to be rapid,[135] it must be assumed that both products are of a relatively equal thermodynamic stability with a small energy barrier between the two.Speciation of phosphine chalcogenide LCCs at χ_{AlCl3} = 0.60

2.1.2.4.4 Speciation of phosphine chalcogenide LCCs at χ_{AlCl3} = 0.60

Compared to equimolar compositions, significant broadening of the ^{27}Al NMR spectrum was observed for all $P_{888}E$-$AlCl_3$ χ_{AlCl3} = 0.60 systems; therefore, little could be deduced from these spectra (Figure 2.1-14). The ^{27}Al NMR spectrum of $P_{888}O$-$AlCl_3$ showed a broad feature with a sharper peak emerging at 74 ppm, in a similar fashion to that reported by Coleman *et. al.*[135] The spectra for the other two analogues are - again - similar to each other, but different from $P_{888}O$-$AlCl_3$, χ_{AlCl3} = 0.60. In all three cases the background feature at *ca*. 65 ppm can be seen: as a shoulder for $P_{888}O$-$AlCl_3$, χ_{AlCl3} = 0.60, and as the dominant feature for the two others. The only recognisable signals deriving from the samples are broad bands at 103 ppm for $P_{888}S$-$AlCl_3$, χ_{AlCl3} = 0.60, and at 102 ppm for $P_{888}Se$-$AlCl_3$, χ_{AlCl3} = 0.60. This indicates that most of the signal from the sample is actually lost in the baseline. In the absence of significant viscosity increase (Chapter 2.1.2.7), this suggests lower symmetry species and/or dynamic exchange between species.

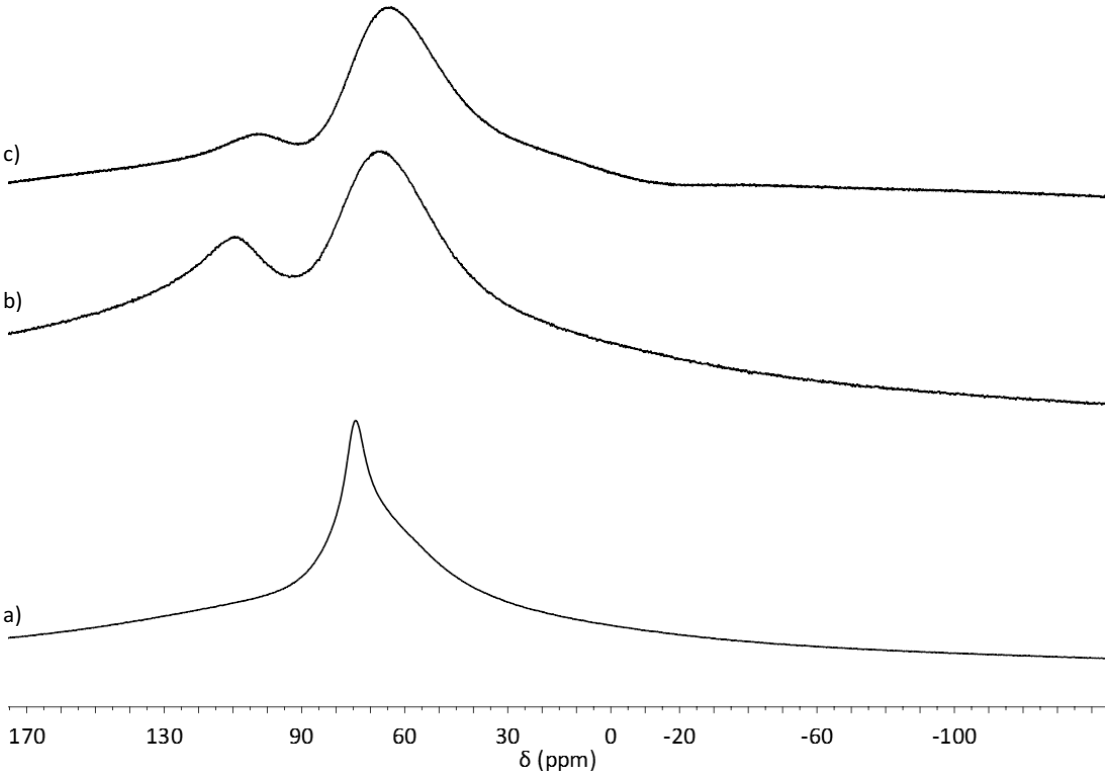

Figure 2.1-14: ^{27}Al NMR spectra of a) $P_{888}O$-$AlCl_3$ χ_{AlCl3} = 0.60, b) $P_{888}S$-$AlCl_3$ χ_{AlCl3} = 0.60, c) $P_{888}Se$-$AlCl_3$ χ_{AlCl3} = 0.60

^{31}P NMR spectra of the χ_{AlCl3} = 0.60 compositions (Figure 2.1-15) were much more informative. The spectrum measured for $P_{888}O$-$AlCl_3$ χ_{AlCl3} = 0.60 (Figure 2.1-15-a) reveals three distinct ^{31}P environments (76.6, 77.4 and 78.1 ppm) - one more than in the neutral composition (75.2 and 77.4 ppm). In addition to monomeric neutral, $[AlCl_3(P_{888}O)]$ and cationic $[AlCl_2(P_{888}O)_2]^+$ species, the third one was detected, with more deshielded phosphorus. As suggested by Coleman *et al.*,[135] this can be assigned to the neutral dimer, $[Al_2Cl_6L]$. The most thermodynamically stable is the symmetric structure with bridging phosphine oxide ligand,[171] which explains deshielding of this peak. Relative proportion of the three species, $[Al_2Cl_6(P_{888}O)]$:$[AlCl_3(P_{888}O)]$:$[AlCl_2(P_{888}O)_2]$, by integration of ^{31}P NMR signals, is: 6:7:2.

The ^{31}P NMR spectrum of $P_{888}S$-$AlCl_3$ χ_{AlCl3} = 0.60 (Figure 2.1-15-b) features two signals (57.0 and 58.6 ppm), shifted slightly downfield from those seen for $P_{888}S$-$AlCl_3$, χ_{AlCl3} = 0.50 (56.3 and 58.7 ppm). In contrast to the neutral system, the acidic composition contains both species in non-negligible quantities (3:2 signal ratio). In the ^{31}P NMR spectrum of $P_{888}Se$-$AlCl_3$ χ_{AlCl3} = 0.60 (Figure 2.1-15-c) there is one broad feature, but it's asymmetry can arguably be interpreted as two signals of similar intensity, at approximate chemical shifts of 47.2 and 47.6 ppm. Unfortunately, this overlap obscured the ^{77}Se satellites and prevented determination of the coupling constants from this spectrum.

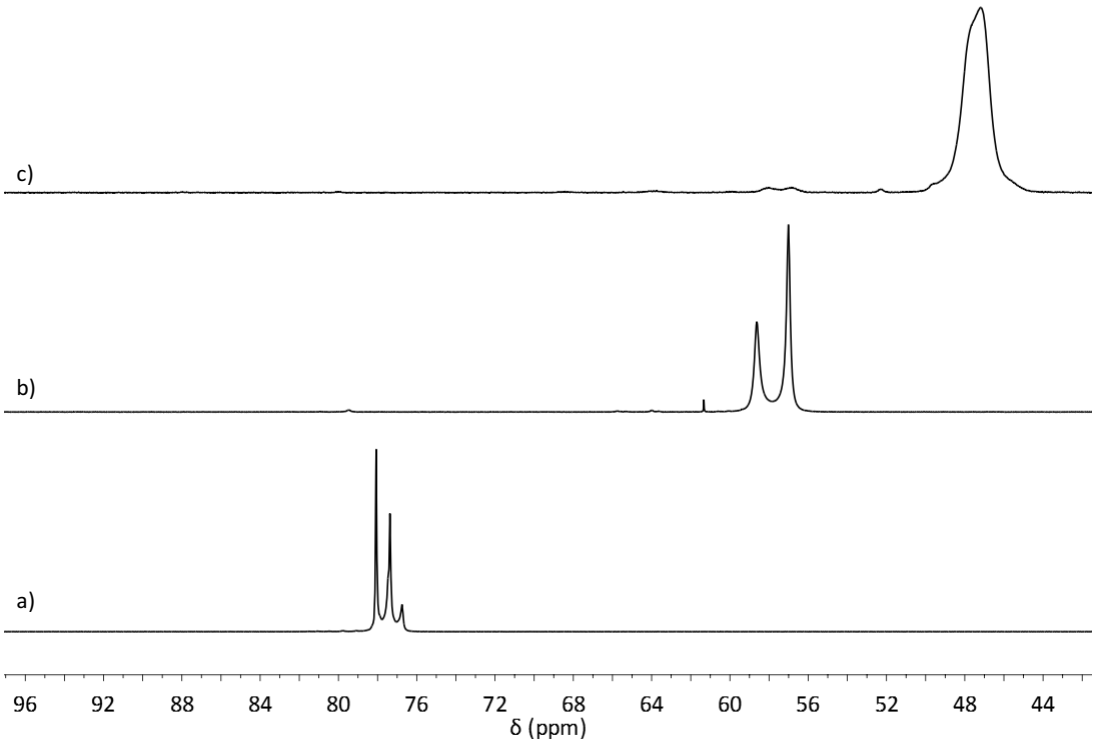

Figure 2.1-15: ^{31}P NMR spectra of a) $P_{888}O$-$AlCl_3$ χ_{AlCl3} = 0.60, b) $P_{888}S$-$AlCl_3$ χ_{AlCl3} = 0.60, c) $P_{888}Se$-$AlCl_3$ χ_{AlCl3} = 0.60

To aid further interpretation, Raman spectroscopy would be invaluable. Unfortunately, the $P_{888}E$-$AlCl_3$ χ_{AlCl3} = 0.60 mixtures produced spectra of very poor quality, and as such peaks could not be accurately discriminated from the background. However, additional information was gained from ^{77}Se NMR spectroscopy (Figure 2.1-8). The spectrum of $P_{888}Se$-$AlCl_3$ χ_{AlCl3} = 0.60 (Figure 2.1-8-b) revealed two doublets (-231.2 and -213.0 ppm, ratio 1:1) both of which had a slightly smaller coupling constant than for $P_{888}Se$-$AlCl_3$ χ_{AlCl3} = 0.50. Together with ^{31}P NMR spectroscopy, this shows that there are two distinct species in $P_{888}Se$-$AlCl_3$ χ_{AlCl3} = 0.60, a neutral adduct and another one, whereby both ^{31}P and ^{77}Se are more deshielded. Taking into consideration the low concentration of aluminium chloride anions (Figure 2.1-14-c), and deshielding of both ^{31}P and ^{77}Se nuclei, this is most likely $[Al_2Cl_6(P_{888}Se)]$. By analogy, the corresponding speciation is assumed for the $P_{888}S$-$AlCl_3$ χ_{AlCl3} = 0.60 system. Slight difference in chemical shifts as a function of composition is most likely due to changes in the acidity of medium.

2.1.2.4.5 Summary and conclusions of phosphine chalcogenide-$AlCl_3$ speciation studies

A summary of the assigned ^{31}P and ^{27}Al NMR spectra peaks are presented in Table 2.1-8. As was expected, $P_{222}O$ as a ligand behaved near identically to $P_{888}O$. $P_{222}O$-$AlCl_3$ χ_{AlCl3} = 0.50 and 0.60 were shown to consist of equilibrated cation, anionic and neutral species. Crucially the

^{31}P NMR spectra showed a consistent downfield shift of peaks compared to $P_{888}O$-$AlCl_3$ χ_{AlCl3} = 0.50 or 0.60, which will allow for identification of peaks belonging to $P_{222}O$-$AlCl_3$ complexes for the measurement of Gutmann Acceptor numbers (Chapter 2.1.1.7).

Table 2.1-8 ^{31}P and ^{27}Al NMR peaks for phosphine chalcogenide LCCs

LCC	$[AlCl_4]^-$/ $[Al_2Cl_7]^-$	$[AlCl_3L]$	$[AlCl_2L_2]^+$	$[Al_2Cl_6L]$
		δ ^{31}P		
$P_{222}O$ χ_{AlCl3} = 0.50 (55 °C)	-	80.37	82.28	-
$P_{222}O$ χ_{AlCl3} = 0.50 (80 °C)	-	80.25	80.85	-
$P_{222}O$ χ_{AlCl3} = 0.60	-	-	82.25	83.30
$P_{888}O$ χ_{AlCl3} = 0.50	-	75.20	77.38	-
$P_{888}O$ χ_{AlCl3} = 0.60	-	76.57	77.37	78.07
$P_{888}S$ χ_{AlCl3} = 0.50	-	56.31	58.75	-
$P_{888}S$ χ_{AlCl3} = 0.60	-	58.63	-	57.01
$P_{888}Se$ χ_{AlCl3} = 0.50	-	45.30	49.40	
$P_{888}Se$ χ_{AlCl3} = 0.60	-	47.23	-	47.57
		δ ^{27}Al		
$P_{222}O$ χ_{AlCl3} = 0.50 (55 °C)	103.06	89.91	75.06	-
$P_{222}O$ χ_{AlCl3} = 0.50 (80 °C)	102.83	85.96	85.96	-
$P_{222}O$ χ_{AlCl3} = 0.60	100.10	-	74.06	-
$P_{888}O$ χ_{AlCl3} = 0.50	103.81	90.59	75.57	-
$P_{888}O$ χ_{AlCl3} = 0.60	95.77	-	74.01	95.77
$P_{888}S$ χ_{AlCl3} = 0.50	103.04	-	-	-
$P_{888}S$ χ_{AlCl3} = 0.60	102.65	-	-	-
$P_{888}Se$ χ_{AlCl3} = 0.50	103.25		-	-
$P_{888}Se$ χ_{AlCl3} = 0.60	102.45	-	-	-

In contrast to the $P_{888}O$ systems, the $P_{888}E$ (E = S, Se) systems contained predominantly neutral species (molecular adducts), with decreasing content of the ionic species as heavier chalcogenide donors are used.

For further confirmation of the proposed speciation, it would be of interest to measure the electrical conductivities of the $P_{888}E$-$AlCl_3$ χ_{AlCl3} = 0.50 and 0.60 (E = O, S, Se) LCCs, and present the results on a Walden plot. The Walden plot is based on Equation 2.1-3, which states that the values of conductivity and viscosity are inversely related.[172]

$$\Lambda\eta = k$$ Equation 2.1-3

Where:

Λ = the conductivity of the sample
η = the viscosity of the sample
k = a constant

As such, a plot of the logarithmic values of viscosity *vs*. conductivity would yield a measure of the concentration of ionic species in the medium. Those which lie closest to KCl solution plot would have a higher degree of ionicity. From the NMR results, particularly Figure 2.1-7, one would expect increasing deviation from the behaviour of the KCl solution, as the molecular weight of chalcogenide increases.

It may also be of interest to perform the ^{27}Al NMR studies in concentrated solutions and/or at higher temperatures, rather than studying neat LCCs at ambient temperatures, as lowering the viscosity may provide better peak resolution.

2.1.2.5 *N*-Donor LCCs

Two *N*-donors were used for the synthesis of LCCs: trioctylamine (N_{888}) and heptylcyanide (C_7CN); in contrast to observations made for *O*-donors by Coleman *et al*., these two *N*-donors gave very different results in terms of LCC formation.

There are several recent publications, whereby amine donor-$AlCl_3$ liquid combinations are used in electrochemistry (Chapter 1.2.3). They tend to have a narrower liquidus range in terms of χ_{AlCl3} values compared to oxygen donors; typically they are liquid up to χ_{AlCl3} = 0.56.[155,159] N_{888}-$AlCl_3$ χ_{AlCl3} = 0.50 contained solid precipitate and was filtered before spectroscopic analysis.

Amine-$AlCl_3$ adducts are reported to give ^{27}Al NMR signals shifted downfield from the $[AlCl_4]^-$ anion.[155,159] In the spectrum of N_{888}-$AlCl_3$ χ_{AlCl3} = 0.50, the tetracoordinate chloroaluminate anion is readily visible at 103.60 ppm, in addition to the background peak (Figure 2.1-16-a, Table 2.1-9). However, little else is identifiable from the ^{27}Al NMR spectrum, indicating that most signal is lost in the baseline. Trioctylamine also lacks any easy to determine features such as IR active bonds that would aid speciation. Similarity to the spectra seen for P_{888}S-$AlCl_3$ and P_{888}Se-$AlCl_3$ (Figure 2.1-5, Table 2.1-9) points towards tentative suggestion that a mix of molecular adduct and charged species is present, with a preference for the former.

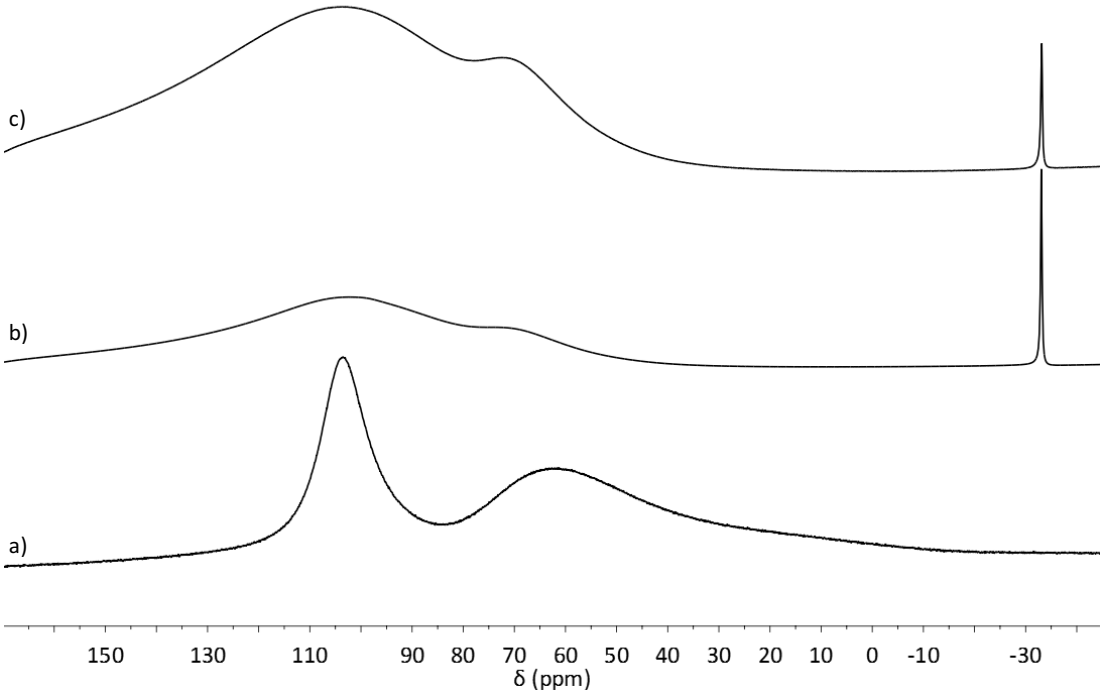

Figure 2.1-16: ^{27}Al NMR spectra for a) N_{888}-$AlCl_3$ χ_{AlCl3} = 0.50 b) C_7CN-$AlCl_3$ χ_{AlCl3} = 0.50 c) C_7CN-$AlCl_3$ χ_{AlCl3} = 0.60

Table 2.1-9: ^{27}Al NMR peaks for *N*-Donor LCCs

LCC	$[AlCl_4]^-$ /$[Al_2Cl_7]^-$	$AlCl_3L$	$[AlCl_2L_2]^+$	$AlCl_3L_2$	$[Al(L)_6]^{3+}$
N_{888}-$AlCl_3$ χ_{AlCl3} = 0.50	103.60	-	-	-	-
C_7CN-$AlCl_3$ χ_{AlCl3} = 0.50	101.94	-	-	-	- 33.08
C_7CN-$AlCl_3$ χ_{AlCl3} = 0.60	103.50	-	-	-	-33.15

Heptylcyanide as a ligand gave unique results, unlike any other ligand used in this study. The ^{27}Al NMR spectrum of C_7CN-$AlCl_3$ χ_{AlCl3} = 0.50 (Figure 2.1-16-b) features a broad peak at 101.9 ppm (in addition to the probe background), suggesting the presence of the dimeric anion $[Al_2Cl_7]^-$ - even though the composition is nominally 'neutral'. The spectrum of C_7CN-$AlCl_3$ χ_{AlCl3} = 0.60 (Figure 2.1-16-c, Table 2.1-9) was virtually identical, with a very broad peak at 103.60 ppm. Furthermore, both spectra show a sharp signal at 33 ppm, corresponding to the hexacoordinate region of the ^{27}Al NMR spectrum, correlating with the $[Al(MeCN)_6]^{3+}$ peak, as reported by Dalibart and co-workers.[143] With increasing $AlCl_3$ content, the area of the anion peak increases relative to the cation peak. Whilst broad, the anion peaks do appear to be symmetrical (aside from the background peak) and do not appear to exhibit any shoulder around 108 ppm which would indicate tetracoordinate aluminium(III) chloride species with a nitrogen donor.[155,159]

Inferred and Raman spectroscopies were recorded for the heptylcyanide LCCs. The IR data (Table 2.1-10) show a strong red-shift in the C≡N vibration of coordinated heptylcyanide, with

nearly identical shifted for the two compositions. This is consistent with the ^{27}Al NMR spectra showing the presence of the $[Al(C_7CN)_6]^{3+}$ cation in both compositions.

Table 2.1-10: IR data of the C≡N bond in octanenitrile-$AlCl_3$ LCCs

Complex / IL	Complex ν / cm^{-1}	Δν / cm^{-1} (a)
C_7CN χ_{AlCl3} = 0.00	2246.6	N/A
C_7CN-$AlCl_3$ χ_{AlCl3} = 0.50	2307.44	60.84
C_7CN-$AlCl_3$ χ_{AlCl3} = 0.60	2306.75	60.15
(a) Δ ν = ν (complex) – ν (ligand)		

Two peaks are observed in the Raman spectrum of neat C_7CN, at 375 and 300 cm^{-1}. C_7CN-$AlCl_3$ χ_{AlCl3} = 0.50 has major peaks at 347 and 190 cm^{-1}, which is consistent with $[AlCl_4]^-$. Takahashi and co-workers showed that even small amount of the dimeric species could result in significant line broadening of the chloroaluminate anion peak in the ^{27}Al NMR. Thus it can be said at χ_{AlCl3} = 0.50 it would appear that a mix of $[AlCl_4]^-$ and $[Al_2Cl_7]^-$. C_7CN-$AlCl_3$ χ_{AlCl3} = 0.60 shows peaks at 346.78 and 315.35 cm^{-1} which are attributable to $[AlCl_4]^-$ and $[Al_2Cl_7]^-$, respectively. As such, from the ^{27}Al NMR spectra and Raman spectra, it can be deduced that a mix of chloroaluminate anions are present.

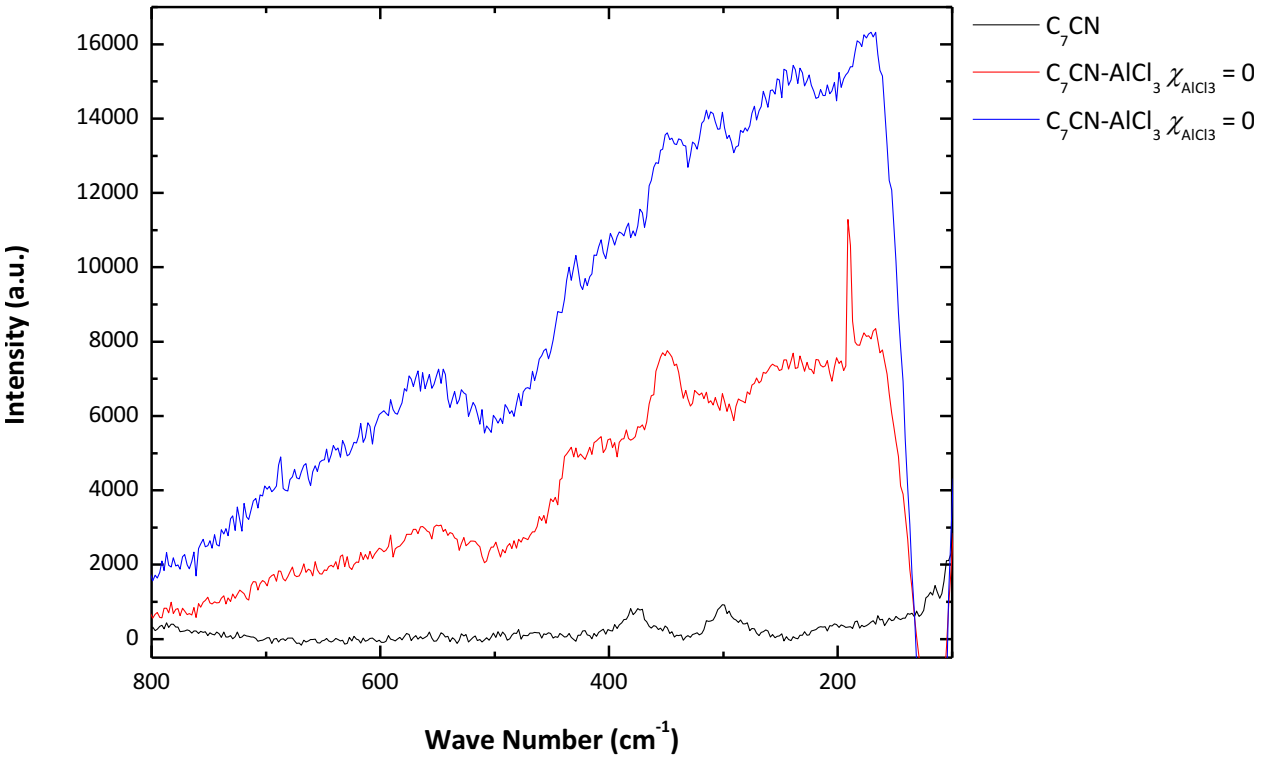

Figure 2.1-17: Raman spectra of C_7CN and C_7CN-$AlCl_3$ χ_{AlCl3} = 0.50 and 0.60

Given that the only observed cation is $[Al(C_7CN)_6]^{3+}$, and no neutral species were detected, one can consider the stoichiometry of the reaction. Although Dalibart and co-workers did

report the existence of less charged cations at very low $AlCl_3$ content ($\chi_{AlCl3} \leq 0.18$), [143,147] the proportion of $[Al(MeCN)_6]^{3+}$ to other cations increased with increasing χ_{AlCl3} values. Assuming this trend to continue until all cations are $[Al(C_7CN)_6]^{3+}$, as observed in this study, one would expect the liquidus range to span $0.33 \leq \chi_{AlCl3} \leq 0.54$, as justified by Equation 2.1-4 - Equation 2.1-6, assuming no neutral species are formed.

$$3AlCl_3 + 6C_7CN \rightarrow [Al(C_7CN)_6]^{3+} + 3[AlCl_4]^- \quad (\chi_{AlCl3} = 0.33) \qquad \text{Equation 2.1-4}$$

$$6AlCl_3 + 6C_7CN \rightarrow [Al(C_7CN)_6]^{3+} + 2[Al_2Cl_7]^- + [AlCl_4]^- \quad (\chi_{AlCl3} = 0.50) \qquad \text{Equation 2.1-5}$$

$$7AlCl_3 + 6C_7CN \rightarrow [Al(C_7CN)_6]^{3+} + 3[Al_2Cl_7]^- \quad (\chi_{AlCl3} = 0.54) \qquad \text{Equation 2.1-6}$$

In conclusion, mixtures of $AlCl_3$ and heptylcyanide form ionic materials that fulfil the definition of room temperature ionic liquids. Simplicity of synthesis and low viscosity make them interesting for both electrochemical and catalytic applications. It would be useful to further develop this rather unique family of ionic liquids, for example by further NMR studies. The ^{27}Al NMR spectra of C_7CN-$AlCl_3$ with a range of $AlCl_3$ loadings ($0.18 \leq \chi_{AlCl3} < 0.60$) would allow to validate Equation 2.1-4 – Equation 2.1-6. Variable temperature ^{27}Al NMR of neat liquids or solutions of C_7CN-$AlCl_3$ mixtures may result in better resolved spectra, which could reveal signals here obscured by the broad peak at *ca.* 103 ppm. The scope could be broadened by other salts of aluminium, for example $Al(OTf)_3$, and possibly another metal halides, in particular $GaCl_3$.

2.1.2.6 Density measurements of LCCs

Densities were measured for a range of $AlCl_3$-LCCs with $\chi_{AlCl3} = 0.60$, and $GaCl_3$-LCCs with $\chi_{GaCl3} = 0.67$, each with a variety of ligands. Several of the $GaCl_3$-based LCCs were also studied as a function of χ_{GaCl3}. All densities were studied as a function of temperature (298 - 343 K).

It is commonly accepted in physical chemistry that density measurements using vibrating u-bend density meters require correction values due to the viscosity of the medium being measured.[173,174] Equation 2.1-7 denotes how errors in density measurements are related to the viscosity of the medium being measured.

$$\Delta\rho/\rho = (-0.5 + 0.45 \cdot \eta^{0.5}) \cdot 10^{-4} \qquad \text{Equation 2.1-7}$$

Where:

$\Delta\rho$ = the difference between the measured density and the true density
ρ = the measured density of the sample

η = viscosity of sample

However, Comuñas and co-workers report that the validity of Equation 2.1-7 is limited to the range 15 – 100 cP.[175] With increasing viscosity, the value of $\Delta\rho$ asymptotically approached a maximum of $5 \cdot 10^{-4}$ cP.[175] Furthermore, Rooney *et al.* suggested that a standard error of ± 0.1% may be assumed for density measurements by vibrating u-bend density meters.[176] As such, the corrections were applied to only those LCCs for which for Equation 2.1-7 was valid within the entire measured range. As Equation 2.1-7 is only valid in the range 15 – 100 cP, calculated error ranges from $1.2 \cdot 10^{-4}$ to $4.0 \cdot 10^{-4}$ g cm^{-1}.

For all measured LCCs, linear density *vs*. temperature relationships were found, typically with very good correlations ($R^2 > 0.99$), as shown in Figure 2.1-18 and Figure 2.1-19, and summarised in

Table 2.1-11. This is in agreement with earlier reports on ionic liquids, halometallate[177] and non-halometallate alike.[178,179]

Density of LCCs is, to a certain extent, inversely proportional to the bulkiness of the ligand: smaller ligands, such as Ur, produce denser LCCs than C_7CN, which again is less dense than LCCs based on the P_{888} and $P_{888}O$ ligands (Figure 2.1-18 and Figure 2.1-19). $AlCl_3$ complexes were in general less dense than their $GaCl_3$ counterparts due to the higher density of $GaCl_3$ over $AlCl_3$. In contrast, changing the oxygen atom for a sulphur atom (Ur to SUr) only marginally increased the density of the complex. Each sulphur atom has roughly double the mass of an oxygen atom but does not radically alter the size of the donor molecule. In short, density is related to the proportion of heavier atoms in each sample, the size of the ligand and the content of metal chloride of the sample.

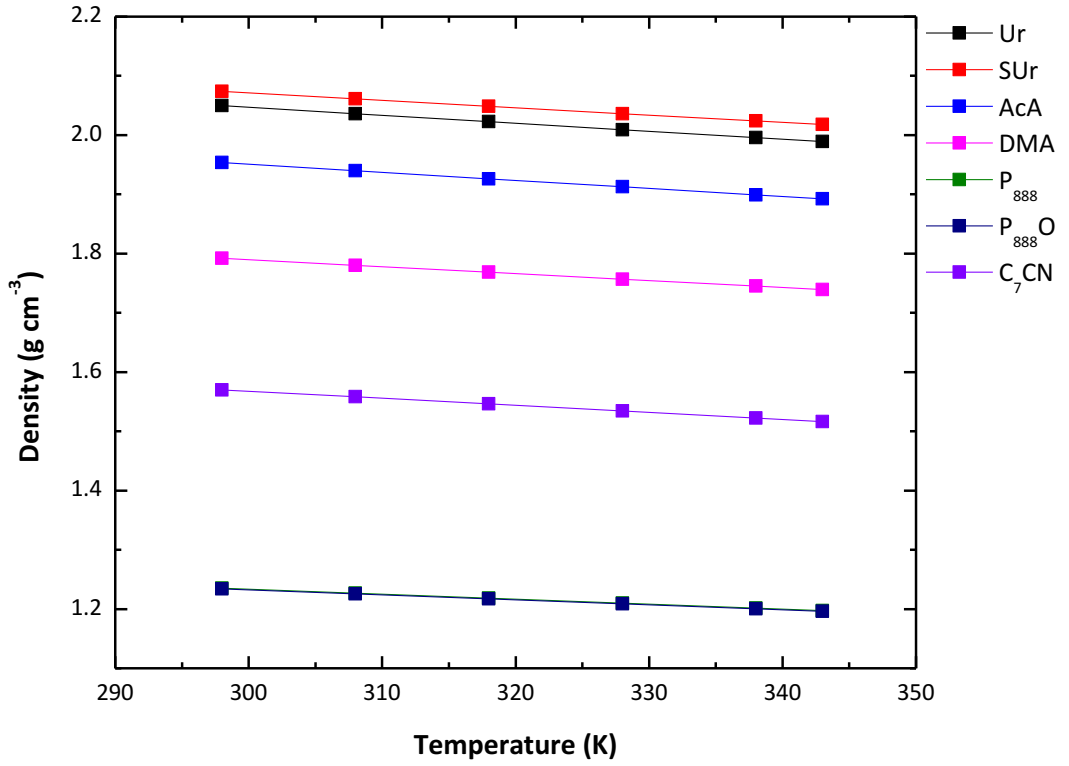

Figure 2.1-18: Density of L-$GaCl_3$ where χ_{GaCl3} = 0.67 as a function of temperature

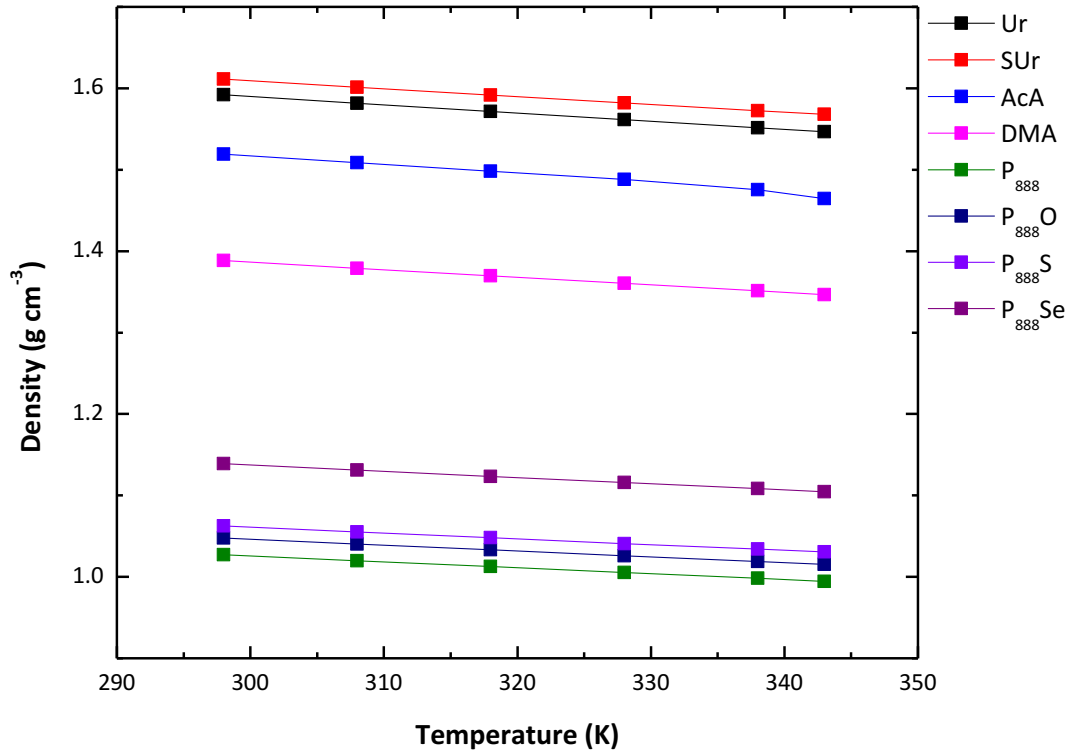

Figure 2.1-19: Density of L-$AlCl_3$ where χ_{AlCl3} = 0.60 as a function of temperature

Table 2.1-11: Density of LCCs in the temperature range 298 – 343 K with linear fitting parameters

Ligand	298 K	308 K	318 K	328 K	338 K	343 K	Y	C	R^2
				χ_{AlCl3} = 0.60					
Ur	1.5920	1.5816	1.5714	1.5614	1.5516	1.5468	-0.0010	1.8910	1.00
SUr	1.6111	1.6013	1.5916	1.5820	1.5726	1.5679	-0.0010	1.8969	1.00
AcA	1.5192	1.5087	1.4983	1.4879	1.4756	1.4647	-0.0012	1.8683	0.98
DMA	1.3883	1.3789	1.3698	1.3604	1.3513	1.3467	-0.0009	1.6639	1.00
P_{888}	1.0271	1.0198	1.0126	1.0054	0.9982	0.9945	-0.0007	1.2604	1.00
$P_{888}O$	1.0475	1.0403	1.0331	1.0260	1.0189	1.0154	-0.0007	1.2424	1.00
$P_{888}S$	1.0626	1.0553	1.0480	1.0409	1.0340	1.0305	-0.0007	1.2156	1.00
$P_{888}Se$	1.1388	1.1311	1.1234	1.1159	1.1084	1.1046	-0.0008	1.1577	1.00
				χ_{GaCl3} = 0.67					
Ur	2.0500	2.0362	2.0226	2.0092	1.9959	1.9893	-0.0013	2.4516	1.00
SUr	2.0738	2.0611	2.0485	2.0362	2.0239	2.0179	-0.0012	2.4442	1.00
AcA	1.9536	1.9397	1.9261	1.9126	1.8992	1.8926	-0.0014	2.3569	1.00
DMA	1.7923	1.7802	1.7687	1.7569	1.7451	1.7393	-0.0012	2.1427	1.00
P_{888}	1.2350	1.2265	1.2181	1.2098	1.2015	1.1973	-0.0012	1.9240	1.00
$P_{888}O$	1.2337	1.2254	1.2171	1.2088	1.2001	1.1964	-0.0008	1.4821	1.00
C_7CN	1.5700	1.5581	1.5462	1.5343	1.5226	1.5165	-0.0008	1.4839	1.00

As expected, a relationship between composition and density is also seen. The density decreased with the decrease in χ_{MCl3} value for all ligands measured (Figure 2.1-20, Table 2.1-12), in agreement with earlier reported on chloroaluminate ionic liquids.[82] When Ur and $P_{888}O$ are used as ligands, there appears to be an approximately linear relationship between composition and density. However, there is a noticeable deviation from this trend in the DMA-$GaCl_3$ composition *vs*. density plot. DMA was shown to coordinate to $AlCl_3$ by both oxygen and nitrogen ligands, and degree of each ligation mode was composition dependant,

which is further complicating the speciation of these LCCs.[154] It is likely that density would be affected by a change in coordination mode.

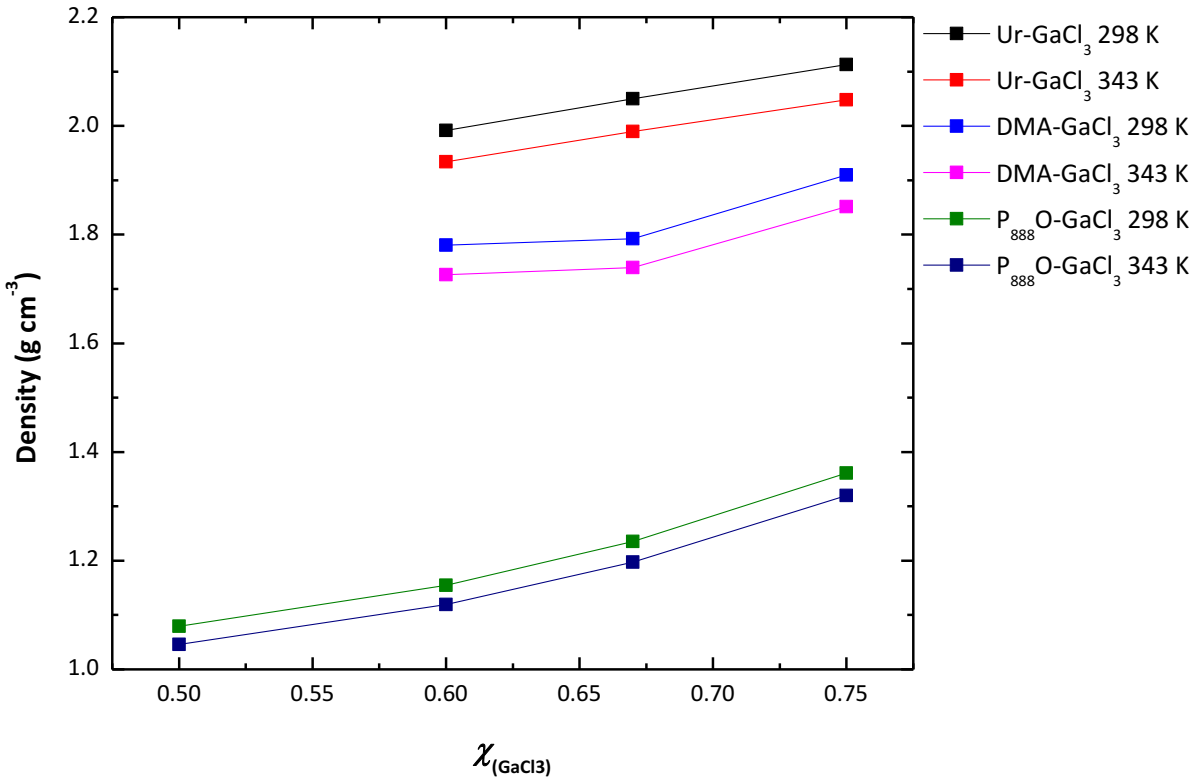

Figure 2.1-20: Density of L-$GaCl_3$ where 0.50 ≤ χ_{GaCl3} ≤ 0.75 for the temperatures 298 and 343 K

Table 2.1-12: Density of L-MCl_3 where 0.50 ≤ χ_{MCl3} ≤ 0.75 in the temperatures range 298 – 343 K with linear fitting parameters

χ_{MCl3}	298 K	308 K	318 K	328 K	338 K	343 K	Y	C	R^2
				$P_{888}S$ – $AlCl_3$					
0.50	1.0156	1.0085	1.0017	0.9950	0.9885	0.9853	-0.0007	1.2156	1.00
0.60	1.0626	1.0553	1.0480	1.0409	1.0340	1.0305	-0.0007	1.2751	1.00
				$P_{888}Se$ – $AlCl_3$					
0.50	1.0934	1.0858	1.0782	1.0707	1.0633	1.0595	-0.0008	1.1121	1.00
0.60	1.1388	1.1311	1.1234	1.1159	1.1084	1.1046	-0.0008	1.1577	1.00
				$P_{888}O$ – $GaCl_3$					
0.50	1.0796	1.0715	1.0638	1.0563	1.0492	1.0458	-0.0007	1.3026	1.00
0.60	1.1544	1.1466	1.1387	1.1308	1.1230	1.1191	-0.0008	1.3884	1.00
0.67	1.2350	1.2265	1.2181	1.2098	1.2015	1.1973	-0.0008	1.4839	1.00
0.75	1.3610	1.3518	1.3429	1.3334	1.3242	1.3195	-0.0009	1.6362	1.00
				Ur – $GaCl_3$					
0.60	1.9915	1.9779	1.9648	1.9524	1.9403	1.9342	-0.0013	2.3687	1.00
0.67	2.0500	2.0362	2.0226	2.0092	1.9959	1.9893	-0.0013	2.4516	1.00
0.75	2.1131	2.0983	2.0837	2.0693	2.0551	2.0480	-0.0013	2.5437	1.00
				DMA – $GaCl_3$					
0.60	1.7803	1.7681	1.75603	1.7441	1.7323	1.7260	-0.0012	2.1386	1.00
0.67	1.7923	1.7802	1.7687	1.7569	1.7451	1.7393	-0.0012	2.1427	1.00
0.75	1.9098	1.8965	1.8835	1.8705	1.8576	1.8512	-0.0013	2.2975	1.00

2.1.2.7 Viscosity measurements of LCCs

In parallel with the density studies, viscosities were measured for $AlCl_3$ -LCCs with χ_{AlCl3} = 0.60, and $GaCl_3$-LCCs with χ_{GaCl3} = 0.67, each with a variety of ligands. Several of the $GaCl_3$-based LCCs were also studied as a function of χ_{GaCl3}.

Dynamic viscosities were recorded using a falling ball viscometer, which is particularly well suited for water sensitive liquids, such as LCCs. The use of a sealed tube, pre-loaded in a glovebox, prevents reaction of the material with atmospheric moisture.

Viscosities were measured over a temperature range from 298 - 343 K, and the temperature-viscosity profile was fitted to a Vogel-Fulcher-Tammann (VFT) equation (Equation 2.1-8).

$$\log \eta = A + B / (T - T_0) \qquad \text{Equation 2.1-8}$$

Where:
η = viscosity,
A, B = fitting parameters,
T_0 = ideal glass transition temperature,
T = temperature

The VFT equation was used, as it has been demonstrated to produce a better fit to the viscosity data of fragile materials (as defined by Angell),[174] such as ionic liquids, than an Arrhenius model.[179,180] Whilst T_0 can be taken to mean the ideal glass transition temperature, the A and B fitting parameters have no direct physical meaning.

The viscosity data and VFT fitting parameters are listed in Table 2.1-13 for $AlCl_3$-LCCs with χ_{AlCl3} = 0.60, and $GaCl_3$-LCCs with χ_{GaCl3} = 0.67, and in Table 2.1-14 for $GaCl_3$ LCCs studied as a function of χ_{GaCl3}.

Table 2.1-13: Viscosity of LCCs in the temperature range 298 – 343 K and VFT fitting parameters

Ligand	298 K	308 K	318 K	328 K	338 K	343 K	A	B	T_0
				χ_{AlCl3} = 0.60					
Ur	88.09	54.90	37.00	26.44	19.67	17.37	-11.89	2095	75.16
SUr	388.0	209.2	142.5	95.16	66.13	56.78	-11.31	2096	94.28
AcA	110.7	66.97	43.87	30.51	22.18	19.19	-12.00	2095	82.46
DMA	82.31	50.87	33.81	23.82	17.59	15.34	-12.21	2095	81.09
P_{888}	116.5	71.35	45.99	31.15	22.046	18.85	-12.31	2096	91.31
$P_{888}O$	170.6	105.5	68.48	46.81	33.15	28.22	-11.84	2096	89.65
$P_{888}S$	334.8	193.3	120.0	77.75	52.28	44.12	-11.88	2097	103.3
$P_{888}Se$	420.9	248.3	145.6	93.86	62.81	51.60	-11.86	2097	107.4
				χ_{GaCl3} = 0.67					
Ur	75.20	46.95	31.88	22.99	17.42	15.43	-12.04	2095	74.86
SUr	-	194.9	112.10	70.89	48.20	40.56	-11.96	2093	104.0
AcA	75.65	46.89	31.46	22.44	16.01	14.55	-12.24	2095	79.87
DMA	89.19	54.85	36.28	25.56	18.85	16.41	-12.15	2095	81.58
P_{888}	-	143.48	89.86	59.12	40.89	34.44	-11.90	2096	97.15
$P_{888}O$	139.9	88.44	59.04	41.10	29.77	25.71	-11.72	2095	82.70
C_7CN	46.86	30.22	20.90	15.60	11.78	10.40	-12.096	2094	64.51

Table 2.1-14: Viscosity of L-MCl_3 where 0.50 ≤ χ_{MCl3} ≤ 0.75 in the temperature range 298 and 343 K and VFT fitting parameters

χ_{MCl3}	298 K	308 K	318 K	328 K	338 K	343 K	A	B	T_0
				$P_{888}S$-$AlCl_3$					
0.50	395.8	220.7	132.1	83.12	54.75	45.39	-12.13	2096	110.7
0.60	334.8	193.3	120.0	77.75	52.28	44.12	-11.88	2097	103.3
				$P_{888}Se$-$AlCl_3$					
0.50	453.1	254.4	147.7	93.37	61.40	50.64	-12.08	2097	112.3
0.60	420.9	248.3	145.6	93.86	62.81	51.60	-11.86	2097	107.4
				$P_{888}O$ – $GaCl_3$					
0.50	161.6	97.84	62.98	42.21	29.67	25.24	-12.07	2096	93.17
0.60	150.8	93.64	61.36	42.16	30.03	25.73	-11.87	2096	87.55
0.67	139.9	88.44	59.04	41.11	29.77	25.71	-11.71	2095	82.70
0.75	132.8	83.19	55.25	38.49	28.06	24.25	-11.76	2095	82.22
				Ur – $GaCl_3$					
0.60	101.6	59.18	38.12	26.48	19.43	16.92	-12.22	2096	85.07
0.67	75.20	46.95	31.88	22.99	17.42	15.43	-12.03	2094	74.86
0.75	63.40	41.00	28.55	20.91	15.91	13.92	-11.82	2094	65.42
				DMA – $GaCl_3$					
0.60	104.26	60.98	38.96	26.77	19.39	16.87	-12.40	2096	89.87
0.67	89.19	54.85	36.28	25.56	18.85	16.41	-12.15	2095	81.58
0.75	77.52	47.93	32.16	22.94	17.18	15.07	-12.29	2095	82.15

The LCCs measured had a viscosity in the range of 46.86 - 453.1 cP, which is within the viscosity range typical for low- to medium-viscosity ionic liquids. At 298 K, the LCCs $GaCl_3$-SUr and $GaCl_3$-P_{888} χ_{GaCl3} = 0.67 were too viscous to measure. From Figure 2.1-21 and Figure 2.1-22 it can be seen that LCCs with bulkier ligands (those with long alkyl chains) typically have a higher viscosity than those with smaller ligands. For example, comparing the $GaCl_3$-LCCs with *O*-donors at 308 K, it can be observed that Ur, DMA and AcA-$GaCl_3$ χ_{GaCl3} = 0.67 had viscosities of 47.0, 46.9 and 54.9 cP, respectively, which are significantly lower compared to $P_{888}O$ χ_{GaCl3} = 0.67 (88.4 cP). This trend was also seen for $AlCl_3$-χ_{AlCl3} = 0.60 LCCs. The long alkyl chain on the phosphine oxide increases van der Waals interaction between species present in the liquid, thus increasing resistance to flow. Following this reasoning, also C_7CN-$GaCl_3$ χ_{GaCl3} =

0.67 should be expected to have a higher viscosity than Ur, AcA and DMA-$GaCl_3$ χ_{GaCl3} = 0.67; however, its viscosity at 308 K was only 30.2 cP. This lower viscosity may be due to difference in speciation between this completely ionic system and the partially ionic LCCs (see Chapter 2.1.2.5). Chlorogallate anions in C_7CN-$GaCl_3$ χ_{GaCl3} = 0.67 are likely to be present as larger oligomers compared to other LCCs at the same χ_{GaCl3} value, and it has been shown that LCCs (Figure 2.1-24) and ionic liquids[82] with larger oligomeric anions have lower viscosity.

The influence of the donor atom can be elucidated by comparing SUr and Ur-$AlCl_3$ χ_{AlCl3} = 0.60, as well as $P_{888}O$, $P_{888}S$ and $P_{888}Se$-$AlCl_3$ χ_{AlCl3} = 0.60 (Figure 2.1-21). In contrast to density, it is clear that the donating atom can have a large effect on the viscosity of the LCCs. At 298 K, SUr-$AlCl_3$ χ_{AlCl3} = 0.60 has a viscosity of 388.0 cP *vs.* 88.1 cP for Ur-$AlCl_3$ χ_{AlCl3} = 0.60. $P_{888}S$-$AlCl_3$ and $P_{888}Se$-$AlCl_3$ χ_{AlCl3} = 0.60 both have a considerably higher viscosity (334.8 and 420.9 cP, respectively) than $P_{888}O$-$AlCl_3$ χ_{AlCl3} = 0.60 (170.6 cP). As discussed in Chapter 2.1.2.4, the speciation of the LCCs varies strongly with change in the donor atom, which is reflected in this large difference in viscosity.

Comparing the $GaCl_3$-LCCs and $AlCl_3$-LCCs where χ_{MCl3} = 0.60 for the ligands Ur, $P_{888}O$ and DMA (Table 2.1-13), there does not appear to be a simple correlation between metal and viscosity - again, in contrast to density studies. For Ur and $P_{888}O$ the aluminium samples are more viscous, but for DMA - gallium is more viscous.

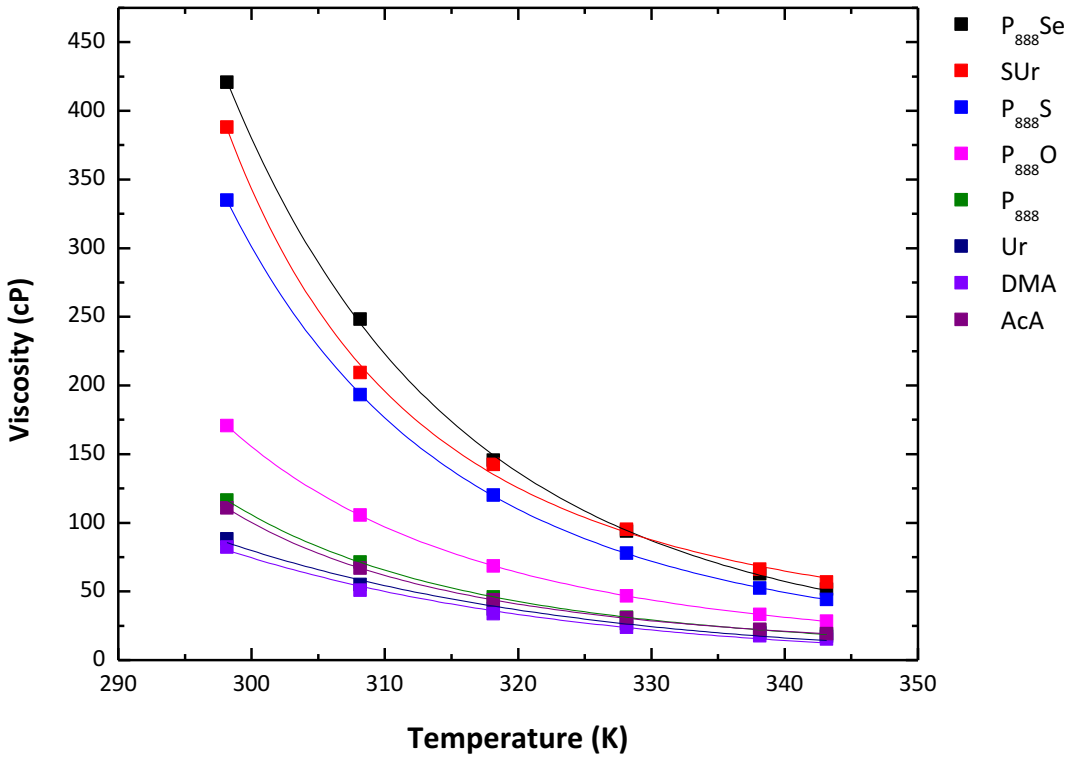

Figure 2.1-21: Viscosity of L-$AlCl_3$ χ_{AlCl3} = 0.60 in the temperature range 298 – 343 K with fitted VFT curve

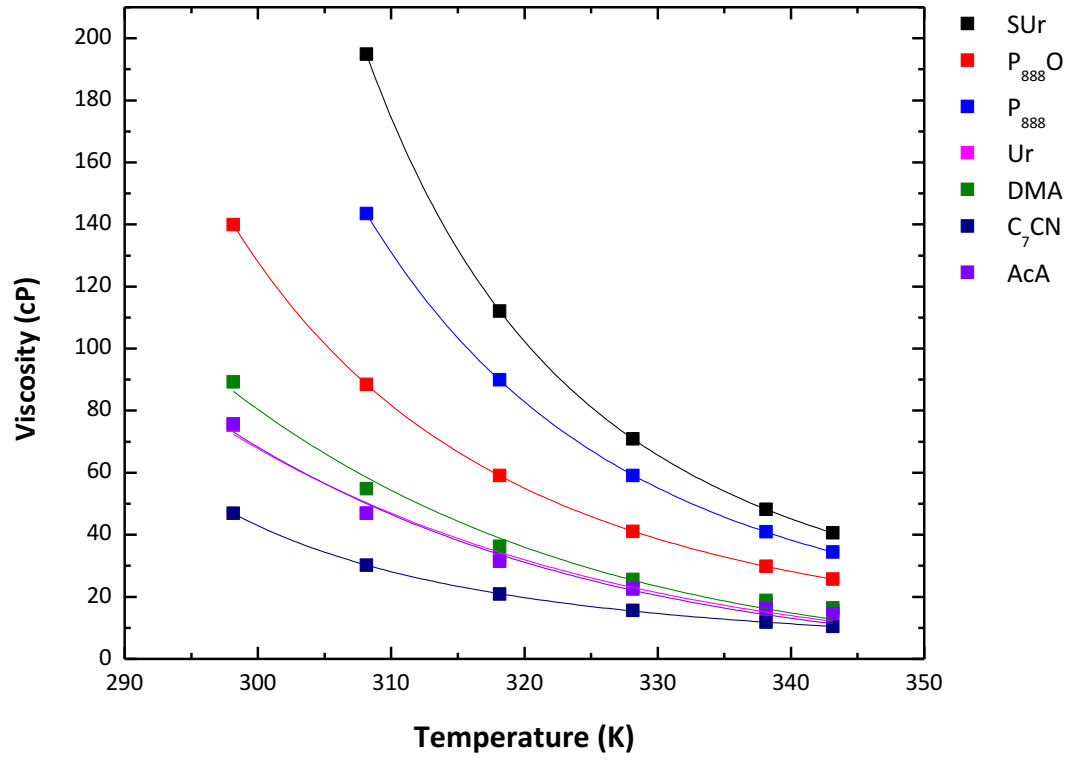

Figure 2.1-22: Viscosity of L-$GaCl_3$ χ_{GaCl3} = 0.67 in the temperature range 298 – 343 K with fitted VFT curve

$GaCl_3$-LCCs with the ligands $P_{888}O$, Ur and DMA, with varying χ_{GaCl3} values, were measured to study the effect of composition upon viscosity (Figure 2.1-23 and Figure 2.1-24). All LCCs

measured had increasing viscosities with decreasing χ_{MCl3} values, which is analogous to the properties of chloroaluminate ionic liquids.[82] As the χ_{MCl3} value of LCCs decreases, the dominant anion changes from the oligomeric, diffusely charged $[M_3X_{10}]^-$ species (found only in $GaCl_3$-LCCs at high χ_{GaCl3} values), to $[M_2X_7]^-$ at *ca*. χ_{MCl3} = 0.60, to the monomeric $[MX_4]^-$ at neutral compositions (χ_{MX3} = 0.50). The oligomeric anions have more diffuse charges, and weaker interaction with the counter cation, which results in lower viscosities.

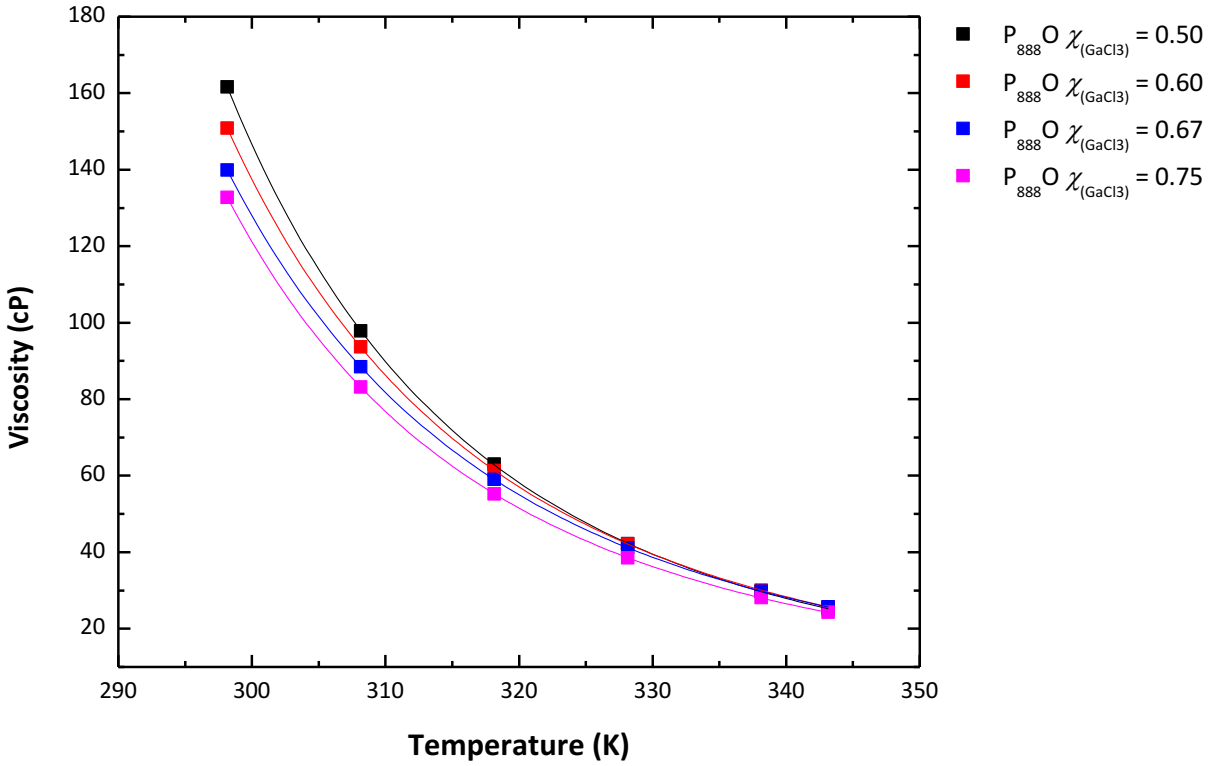

Figure 2.1-23: Viscosity of $P_{888}O$-$GaCl_3$ 0.50 ≤ χ_{GaCl3} ≤ 0.75 in the temperature range 298 – 343 K with fitted VFT curve

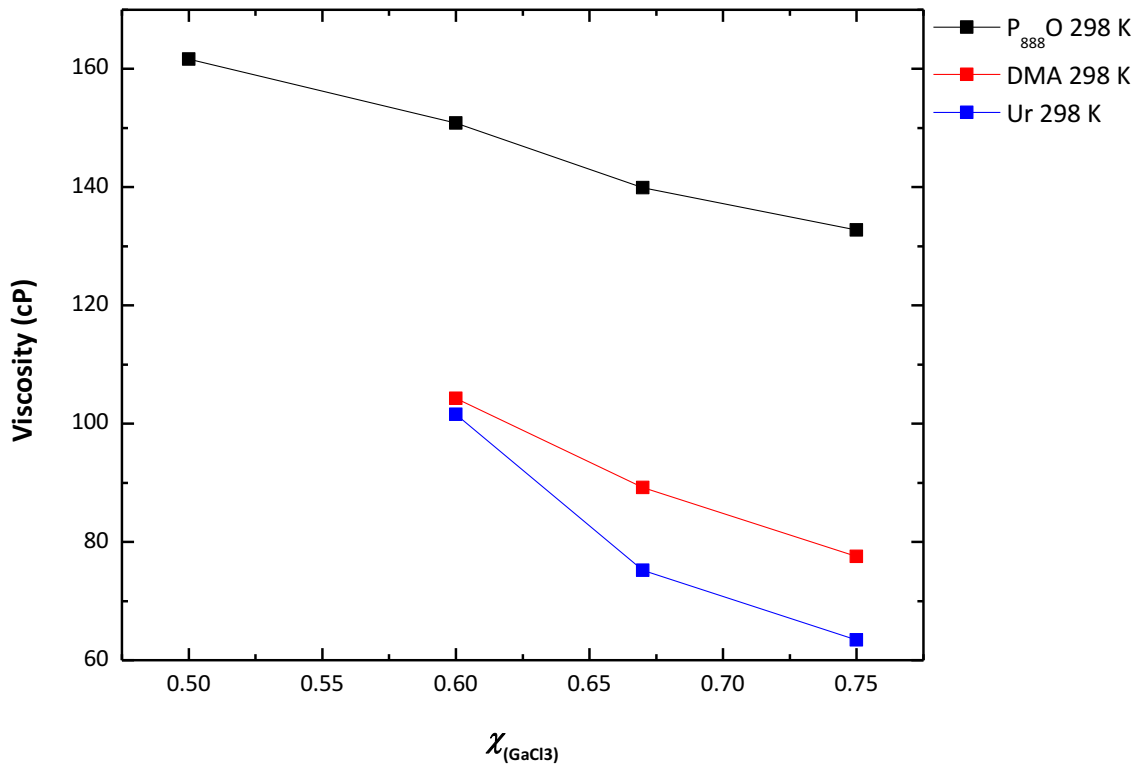

Figure 2.1-24: Viscosity of L-$GaCl_3$ as a function of composition, for $0.50 \leq \chi_{GaCl3} \leq 0.75$ at 298 K

In conclusion, it appears that viscosity is directly related to speciation of LCCs, in addition to other factors, such as the presence of long alkyl chains. Crucially, the shift towards ionic structure lowers the viscosity, whereas the shift towards the molecular structure increases it. As such, the fully ionic C_7CN-$AlCl_3$ system has unexpectedly low viscosity. In contrast, the two systems that comprise mainly neutral adducts, $P_{888}S$-$AlCl_3$ and $P_{888}Se$-$AlCl_3$, had much higher viscosity than their partially ionic homologue, $P_{888}O$-$AlCl_3$. Furthermore, LCCs containing oligomeric anions with diffuse charge are, as a rule of the thumb, less viscous than their analogues with monomeric $[MCl_4]^-$ anions.

2.1.2.8 Thermogravimetric analysis (TGA)

As part of a collaborative effort with the Wasserscheid group (Friedrich-Alexander-Universität Erlangen-Nürnberg, Germany) LCCs were considered as supported catalysts for gas phase refinery alkylations and as co-catalysts for the hydrogenation of aromatics (see Chapter 5). For this, their thermal stability needed to be assessed. Swadźba-Kwaśny and co-workers reported thermal decomposition temperatures for $GaCl_3$-LCCs, but noted that $AlCl_3$-LCCs hydrolysed during sample preparation, preventing meaningful thermogravimetric analysis. A method for measuring the TGA of highly reactive materials was successfully developed and used in this work.

2.1.2.8.1 Method development

The high reactivity of aluminium LCCs to atmospheric moisture presented a challenge for TGA measurements. Following a standard TGA procedure, the LCCs would hydrolyse in the pan before the sample had been loaded into the machine, as reported by Swadźba-Kwaśny and co-workers.[135] To prevent exposure to atmospheric moisture, LCCs were loaded into a gas-tight micro syringe in the glovebox, then taken out, and the tip of the needle was submerged in a TGA pan pre-filled with hexane. The LCC was placed in the pan under protective layer of hexane, and loaded into TGA apparatus. Hexane was evaporated off in the TGA machine, under a stream of dry nitrogen gas, at 60 °C, prior to implementing temperature ramp. To accommodate the variable mass of hexane added, all masses were normalised against the mass of the contents of the pan after the isothermal step.

The temperature of 60 °C was selected to ensure fast evaporation of hexane, but without it boiling (b.p. 68 °C). The time of isothermal curing, however, was subject of optimisation. Without the isothermal step (sample was ramped to 500 °C at 5 °C min^{-1} from ambient temperature) the resulting TGA plots showed a large drop in mass below 100 °C (Figure 2.1-25). It was unknown whether this occurred due to evaporation of hexane dissolved in the LCC, or degradation of the LCCs, or the combination of both.

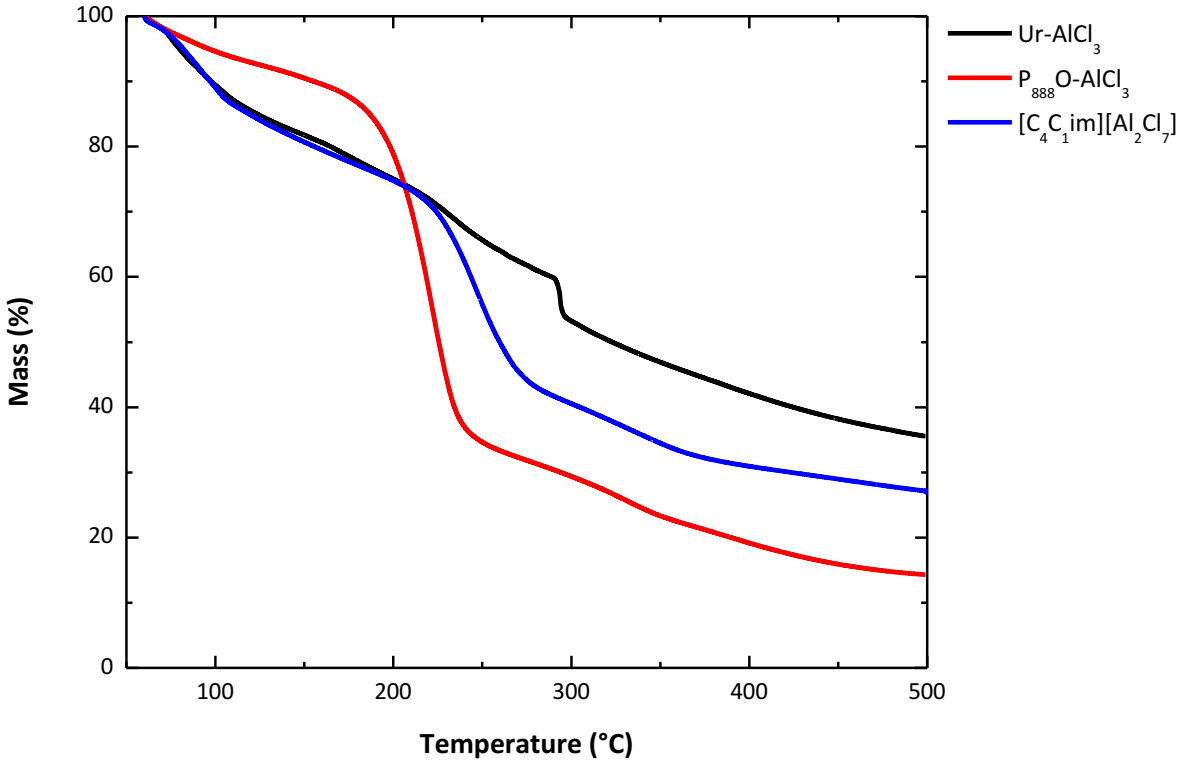

Figure 2.1-25: TGA plots (mass loss as a function of temperature) of LCCs (χ_{AlCl3} = 0.60) and [C_4C_1im] [Al_2Cl_7], with no curing period (ramp to 500 °C, 5 °C min^{-1})

To address this conundrum, a sample of $P_{888}O$-$AlCl_3$ χ_{AlCl3} = 0.60 was cured at 60 °C for 12 h. Over this 12 h period, the sample lost 7.5% of mass in the first 4 h, then 0.6% and 0.3% of mass in the next two 4 h periods, respectively. As the mass loss appears to asymptotically approach a value, it can be assumed that the majority of the hexane has evaporated and that any remaining hexane is of a sufficiently small quantity to have an inconsequential effect on the results. Consequently, the 4 h curing period was adopted. This stabilisation of the mass loss was shown to be repeatable over many runs (Figure 2.1-26). Samples cured at 60 °C for 4 h before ramping to 500 °C showed a smaller mass loss at temperatures < 100 °C (Figure 2.1-27) than those which were not cured (Figure 2.1-25).

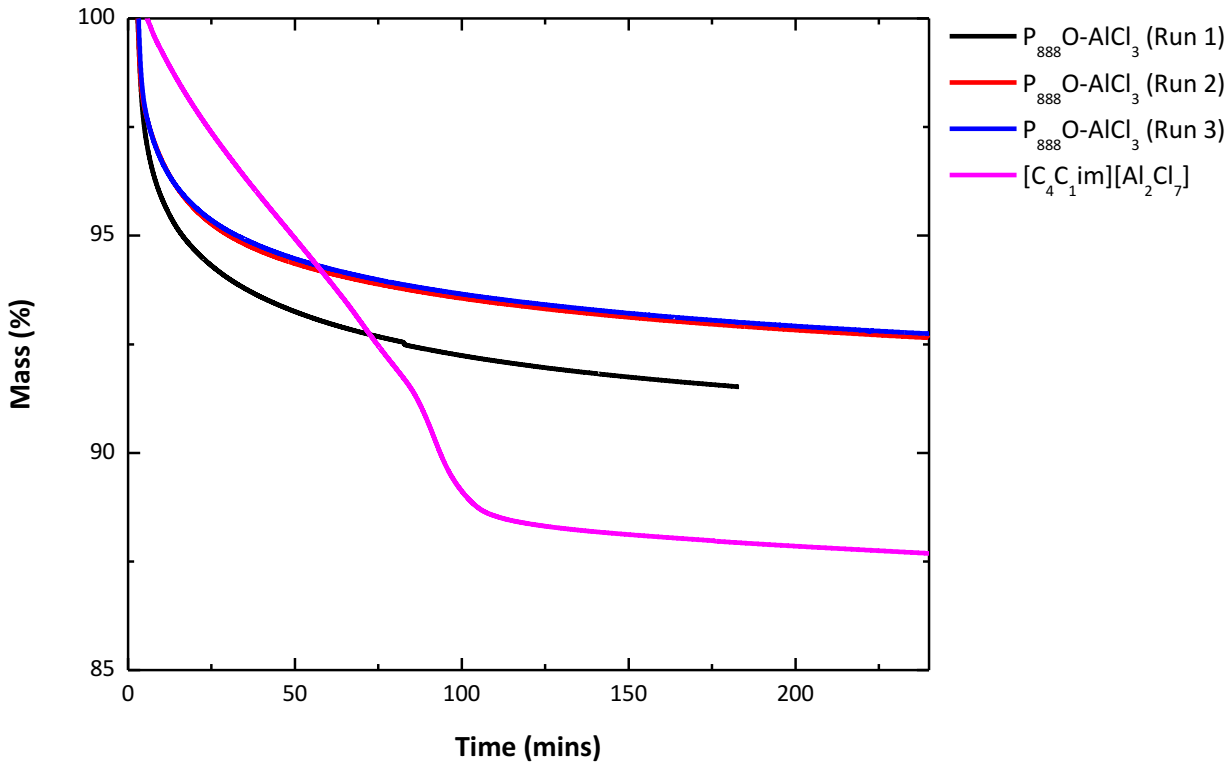

Figure 2.1-26: TGA plots (mass loss as a function of time) of three isothermal curing runs (60 °C) for $P_{888}O$-$AlCl_3$ χ_{AlCl3} = 0.60 and one curing run for $[C_4C_1im][Al_2Cl_7]$

2.1.2.8.2 TGA results for selected L-$AlCl_3$ LCCs

Comparing data recorded here for the L-$AlCl_3$ χ_{AlCl3} = 0.60 systems (Figure 2.1-27) to the TGA samples reported by Coleman *et al.* for analogous L-$GaCl_3$ systems,[135] the mass loss profile for the LCCs based on both $P_{888}O$ and Ur ligands is similar. At lower temperatures (80 °C – 150 °C), a slow steady mass loss was detected, followed by a rapid onset of mass loss, signifying rapid decomposition. However, whereas in $AlCl_3$-LCCs the $P_{888}O$ ligand gave samples of higher thermal stability, in L-$GaCl_3$ systems urea-containing samples had a higher decomposition temperature.

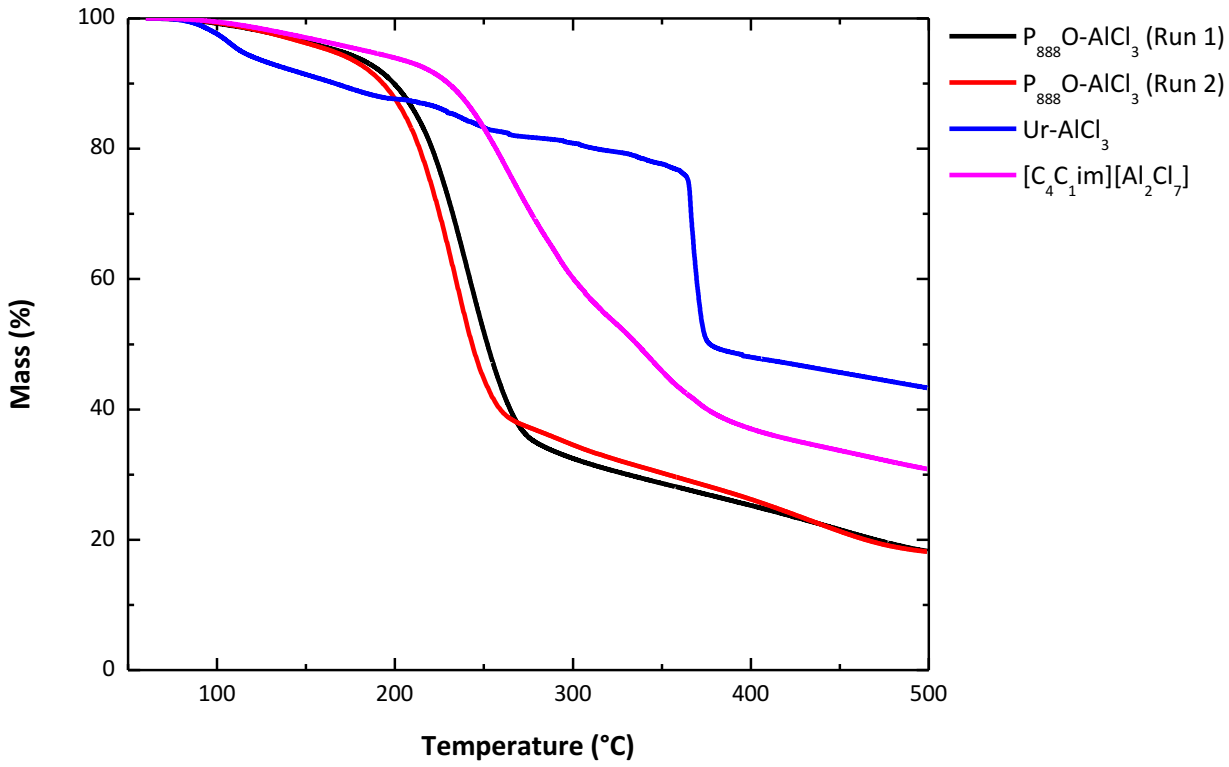

Figure 2.1-27: TGA plots (mass loss as a function of temperature) of LCCs (χ_{AlCl3} = 0.60) and $[C_4C_1im][Al_2Cl_7]$, ramp to 500 °C at 5 °C min^{-1} after curing (60 °C, 4 h)

For $P_{888}O$-$GaCl_3$ LCCs, the largest mass loss was seen to occur above 280 °C, whereas for Ur-$GaCl_3$ systems the decomposition temperature was 230 °C.[135] The decomposition temperatures for $P_{888}O$-$AlCl_3$ and Ur-$AlCl_3$, studied here, were 191 and 364 °C, respectively (Table 2.1-15). The onset of mass loss for the $P_{888}O$ samples coincide with the sublimation temperature of $AlCl_3$.[181] However $AlCl_3$ only makes up 34% of the mass of $P_{888}O$-$AlCl_3$ χ_{AlCl3} = 0.60, and because *ca.* 60% of the mass was lost between 190 and 300 °C, there must be an accompanying decomposition of the $P_{888}O$ ligand (b.p. > 400 °C). Urea is known to degrade thermally above its melting point. Urea makes up 23% by mass of the LCC Ur-$AlCl_3$ χ_{AlCl3} = 0.60, which is comparable to the mass lost (25 %) before the rapid change in the rate of mass loss at 364 °C. However, it is unlikely that no $AlCl_3$ would be lost until 364 °C. Compared to the TGA of 4-propylpyridine-$AlCl_3$[155] and 1-butylpyrolidine-$AlCl_3$,[159] it might appear that the LCCs measured here are slightly less stable than the both former (5% mass loss > 200 °C, T_d 250 °C) and the later (5% mass loss > 220 °C, T_d 270 °C). However, in the literature examples quadruple the heating rate (20 °C s^{-1}) was used, making comparison difficult, as it is well known that such high heating rates give falsely high thermal decomposition temperatures.[182]

Table 2.1-15: TGA data for L-$AlCl_3$ χ_{AlCl3} = 0.60 and $[C_4C_1][Al_2Cl_7]$

L-$GaCl_3$ χ_{GaCl3} = 0.60	$P_{888}O$ Run 1	$P_{888}O$ Run 2	Ur-$AlCl_3$	$[C_4C_1][Al_2Cl_7]$
5 % mass loss (°C)	169	164	113	184
T_d (˚C)	198	191	364	235

In conclusion, the thermal stability of LCCs reported here was found to be rather low, rendering them unsuitable for non-sacrificial applications above 80 °C. On the other hand, from this work and literature it was demonstrated that thermal stability was strongly dependent on both metal halide and ligand, so it is likely that more stable systems could be designed. In addition, one should be careful when considering T_d values reported in the literature, which may not reflect the actual thermal stability upon prolonged exposure.[182]

2.1.2.9 Guttmann AN measurements

2.1.2.9.1 Method development

As stated in Chapter 1.1.2, Lewis acidity is typically measured by using a donor molecule, which can be investigated by a spectroscopic or computational technique. To measure the Lewis acidity of LCCs, the Guttmann acceptor method was used, where $P_{222}O$ is used as a ^{31}P NMR probe. Typically, in every measured sample, there is a single ^{31}P NMR signal originating from the probe - this had been true for all Brønsted acids and ionic liquids reported to date, including halometallate ionic liquids. The acceptor number measurements for LCCs were complicated by the fact that $P_{222}O$ was acting as the third ligand in the system, in addition to the chloride anions and the neutral donor, further complicating the equilibria and potentially inducing the formation of multiple probe-bearing species. In some cases, such as ^{31}P NMR spectra of Ur-$GaCl_3$ χ_{GaCl} = 0.60 and Ur-$AlCl_3$ χ_{AlCl3} = 0.60 (Figure 2.1-28), only one major peak was found, though due to the broadness of the signal other peaks may be obscured - or such broad peaks may indicate a dynamic equilibrium. In contrast, in ^{31}P NMR spectra of AcA-$GaCl_3$ χ_{GaCl3} = 0.67 and $AlCl_3$-AcA χ_{AlCl3} = 0.60, (Figure 2.1-29), there are several species present, which indicates that $P_{222}O$ is present in a number of coordination environments. Since this is unusual for Gutmann acceptor number measurements and there are no established procedures to treat such data. In this work, a number of approaches were considered.

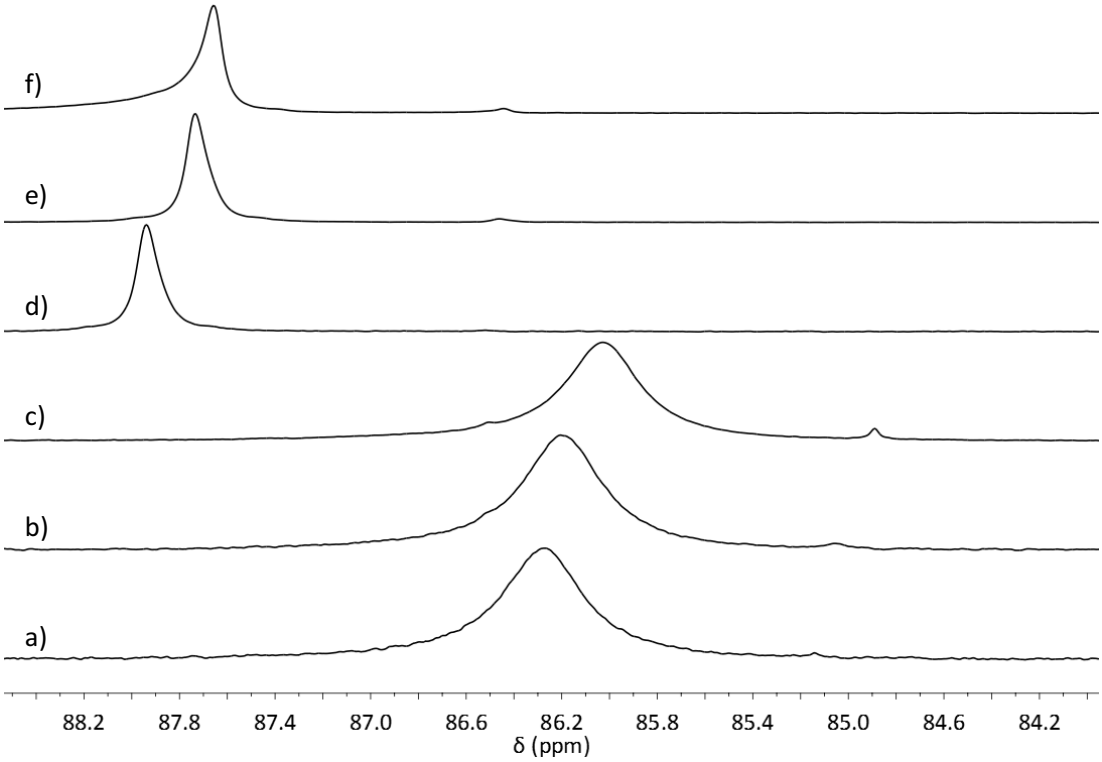

Figure 2.1-28: ^{31}P NMR spectra of Ur-$AlCl_3$ χ_{AlCl3} = 0.60 with $P_{222}O$ at a) 1 wt%, b) 2 wt%, c) 3 wt% and Ur-$GaCl_3$ χ_{GaCl3} = 0.60 with $P_{222}O$ at d) 1 wt%, e) 2 wt%, f) 3 wt%

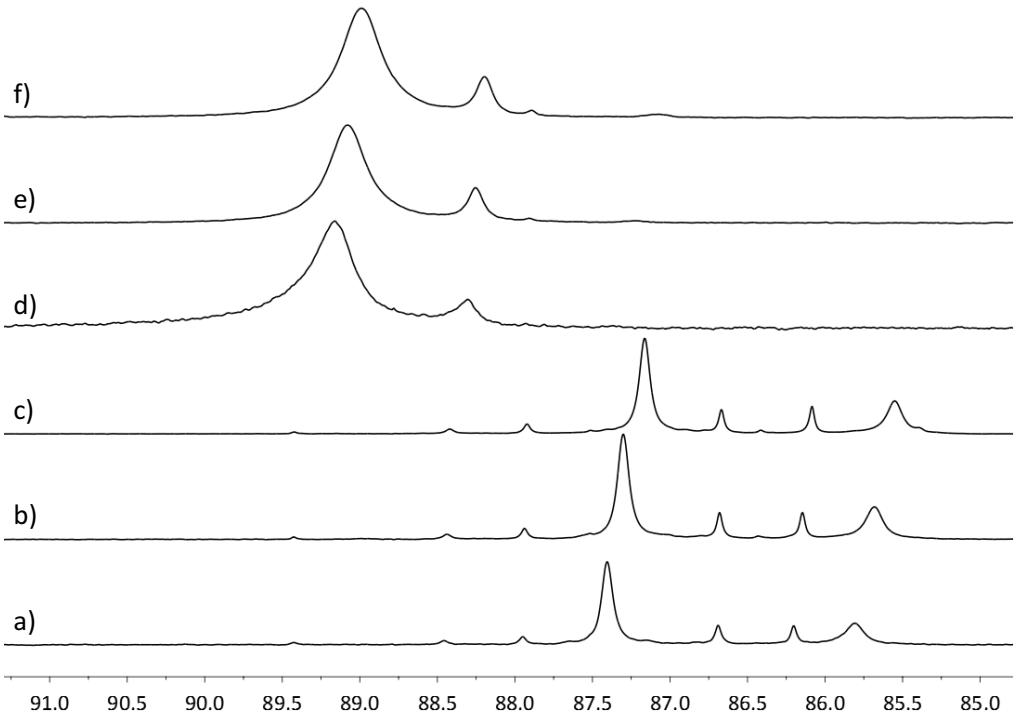

Figure 2.1-29: ^{31}P NMR spectra of AcA-$AlCl_3$ χ_{AlCl3} = 0.60 with $P_{222}O$ at a) 1 wt%, b) 2 wt% c) 3 wt%, and AcA-$GaCl_3$ χ_{GaCl3} = 0.60 with $P_{222}O$ at d) 1 wt%, e) 2 wt%, f) 3 wt%

In LCCs, there are many species in equilibria, of which dimeric aluminium species are expected to be Lewis acidic - and each such species will give different AN value. Since there is a chance that a reactant would interact with a given acidic species depending upon its concentration, it was firstly envisaged that a weighted average of the peaks could be used to determine an average acidity of an LCC. However, inaccuracies would arise owing to fact that the ^{31}P NMR signals are not quantitative, so ratio of different species cannot accurately be derived from their integration.

The most deshielded signal was considered, as this signal would signify the most acidic entity in the entire system. However, the most downfield signals were in some cases of low intensity, so the strongest Lewis acid would be indeed present at a very low concentration - making the reported AN value not representative of the actual catalytic potential.

Finally, it was observed that most spectra did feature a dominant peak, in addition to several smaller signals (Figure 2.1-28). Although 31P NMR signals cannot be directly integrated, it was rather obvious that the largest peak would correspond to the most prominent Lewis acid, therefore it was taken to be the measure of acidity. In addition, to signify that multiple peaks were present, a range of ^{31}P NMR signals recorded for the probe in each case was also quoted in this work.

Considering that $P_{888}O$ is structurally similar to the probe molecule, it was plausible that in the ^{31}P NMR spectrum the $P_{888}O$ peaks could obscure the smaller $P_{222}O$ signals. This was addressed through comparative ^{31}P NMR spectroscopic studies of LCCs based on $P_{888}O$ and $P_{222}O$ (Chapter 2.1.2.4). Comparison of $P_{222}O$-$AlCl_3$ χ_{AlCl3} = 0.60 and $P_{888}O$-$AlCl_3$ χ_{AlCl3} = 0.60 showed that ^{31}P NMR peaks were shifted downfield by *ca.* 5 ppm for the former, which allowed for identification of the $P_{222}O$ peaks, even in structurally similar $P_{888}O$-MCl_3 systems.

2.1.2.9.2 AN values measured for LCCs

Table 2.1-16 shows the AN values of the largest peak observed in the ^{31}P NMR spectrum. In addition, a range of acceptor numbers was calculated, based on all peaks that could be identified as belonging to $P_{222}O$, and were seen in each of the three $P_{222}O$-LCC solutions (1, 2 and 3 wt%). The chlorometallate ionic liquids, $[C_8C_1im]Cl$-MCl_3, with the same MCl_3 loading as studied LCCs, as well as those with the same dominant anion, are listed for comparison (see Chapter 1.2, Figure 1.2-3 and Figure 1.2-8 for relevant speciation discussion).

Table 2.1-16: Acceptor number data for LCCs

IL / LCCs	δ $^{31}P_{inf}$ (largest peak)	AN (largest peak)	AN range
	$AlCl_3$		
$[C_8C_1im]Cl\text{-}AlCl_3\ \chi_{AlCl3}$ = 0.60 [25]	39.74	93.3	-
$[C_8C_1im]$ Cl-$AlCl_3\ \chi_{AlCl3}$ = 0.67 [25]	40.86	96.0	-
$P_{888}O\text{-}AlCl_3\ \chi_{AlCl3}$ = 0.60	40.22	94.4	94.4 – 102.1
Ur-$AlCl_3\ \chi_{AlCl3}$ = 0.60	43.41	101.9	101.9 – 107.8
P_{888}-$AlCl_3\ \chi_{AlCl3}$ = 0.60	43.50	102.1	97.6 – 104.5
SUr-$AlCl_3\ \chi_{AlCl3}$ = 0.60	43.82	102.9	102.9 – 107.5
AcA-$AlCl_3\ \chi_{AlCl3}$ = 0.60	44.56	104.6	100.9 – 109.1
	$GaCl_3$		
$[C_8C_1im]Cl\text{-}GaCl_3\ \chi_{GaCl3}$ = 0.67 [25]	42.36	99.54	
$[C_8C_1im]$ Cl-$GaCl_3\ \chi_{GaCl3}$ = 0.75 [25]	45.77	107.5	-
P_{888}-$GaCl_3\ \chi_{GaCl3}$ = 0.67	44.53	104.6	93.3 – 104.6
$P_{888}O\text{-}GaCl_3\ \chi_{GaCl3}$ = 0.67	44.73	105.0	-
SUr-$GaCl_3\ \chi_{GaCl3}$ = 0.67	45.91	107.8	-
$C_7CN\text{-}GaCl_3\ \chi_{GaCl3}$ = 0.67	45.93	107.8	107.6 – 107.8
Ur-$GaCl_3\ \chi_{GaCl3}$ = 0.67	46.11	108.3	-
AcA-$GaCl_3\ \chi_{GaCl3}$ = 0.67	46.26	108.6	106.5 – 108.6

The acceptor numbers associated with the dominate peaks measured for LCCs were slightly higher compared to the corresponding chlorometallate ionic liquids of the same χ_{MCl3} value, and of a comparable or very slightly higher value as those with the same main anion (Table 2.1-16).

As discussed in Chapter 1.2, LCCs form oligomeric anions at lower χ_{MCl3} values than chlorometallate ionic liquids (contrast Figure 1.2-3 and Figure 1.2-8). Thus, when comparing the variation of the acceptor number with χ_{GaCl3} of the typical chloroaluminate, $[C_8C_1]Cl\text{-}GaCl_3$, and a LCCs (Table 2.1-17, Figure 2.1-30), it is unsurprising that at the same $GaCl_3$ loading LCCs would typically have a higher acidity. Interestingly, Figure 2.1-30 shows a convergence of AN values at high $GaCl_3$ loading (χ_{GaCl3} = 0.75), suggesting that there is little difference between the acidity of $[Ga_3Cl_{10}]^-$, the main anion of $GaCl_3$ ionic liquids at χ_{GaCl3} = 0.75, and $[Ga_4Cl_{13}]^-$, which is expected to be the main anion of $GaCl_3$-LCCs at χ_{GaCl3} = 0.75.

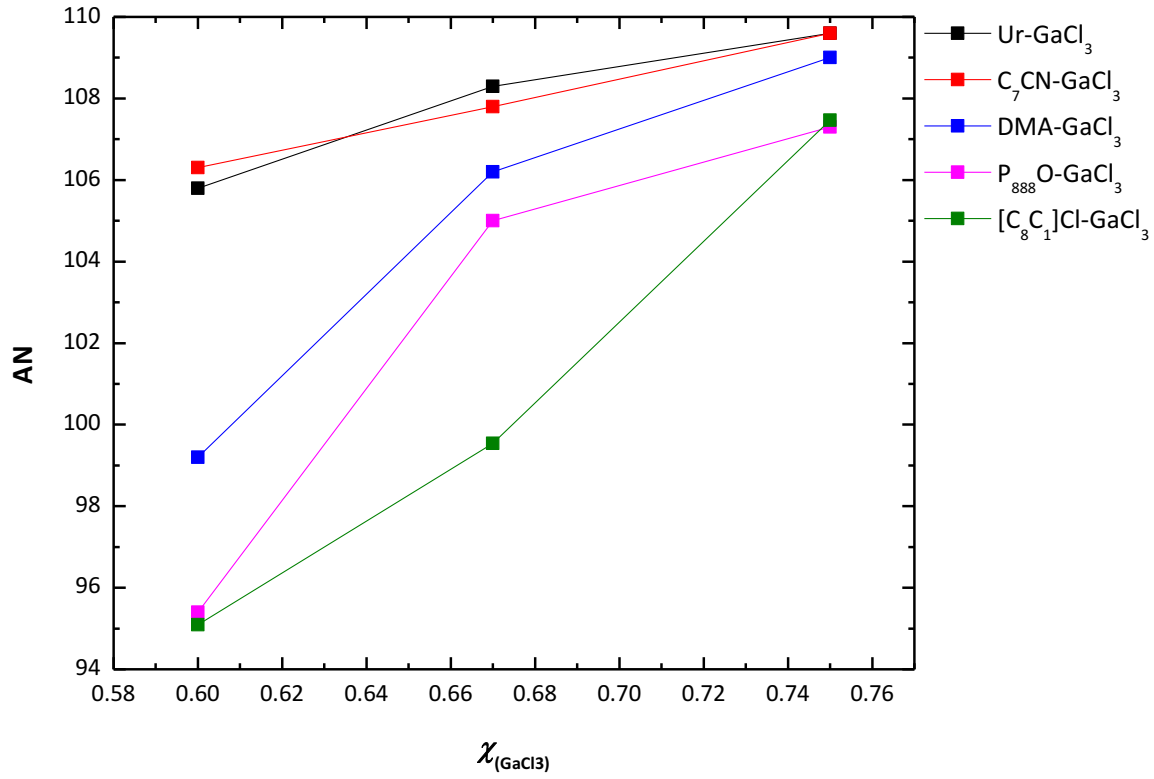

Figure 2.1-30: Acceptor numbers of L-$GaCl_3$ 0.50 ≤ χ_{GaCl3} ≤ 0.75 with $[C_8C_1im]Cl$-$GaCl_3$ for comparrision[25]

Table 2.1-17: Acceptor numbers of L-$GaCl_3$ 0.50 ≤ χ_{GaCl3} ≤ 0.75 with $[C_8C_1im]Cl$-$GaCl_3$ for comparrision[25]

Lewis acid	χ_{GaCl3}	$\delta\ ^{31}P_{inf}$ (largest peak)	AN (largest peak)
$[C_8C_1im]Cl$-$GaCl_3$[25]	0.60	40.50	95.09
	0.67	42.36	99.54
	0.75	45.77	107.47
Ur-$GaCl_3$	0.60	45.08	105.8
	0.67	46.11	108.3
	0.75	46.67	109.6
$P_{888}O$-$GaCl_3$	0.60	40.63	95.4
	0.67	44.73	105.0
	0.75	45.71	107.3
C_7CN-$GaCl_3$	0.60	45.26	106.3
	0.67	45.93	107.8
	0.75	46.68	109.6
DMA-$GaCl_3$	0.60	42.25	99.2
	0.67	45.25	106.2
	0.75	46.43	109.0

From AN values gathered here, LCCs with a wide variety of ligands and χ_{MCl3} values can be considered on the borderline - or above the threshold - for Lewis superacidity on the Gutmann scale.[18] These high AN values are comparable to those of chlorometallate ionic liquids, which have already found wide uses as acid catalysts (Chapter 1.2.2.4). As such, just from this physical chemistry study, they can be anticipated to be potent acid catalysts. This

was indeed demonstrated by this author and co-workers in Friedel-Crafts alkylation of benzene,[158] and in further catalytic applications, discussed in Chapter 3 – Chapter 4.

2.1.3 Conclusions

A series of LCCs were synthesised, some new to the literature, and characterised, both in terms of physical properties and by spectroscopic methods. The work presented here has shown that LCCs have similarities to chlorometallate ionic liquids, including the presence of oligomeric chlorometallate anions χ_{MCl3}, and that have potential as Lewis acid catalysts. LCCs can be synthesised by a simple procedure from cheap bulk chemicals (e.g. $AlCl_3$ and Urea) making them less expensive and easier to synthesise than analogous chloroaluminate ionic liquids. This gives LCCs a competitive edge when looking to apply them to industrial catalytic processes.

The series $P_{888}E$ (E = *O, S, Se*) was investigated by spectroscopic methods. All the ligands formed mobile liquids with $AlCl_3$, at both χ_{AlCl3} = 0.50 and 0.60. As the donor atom was replaced with heavier chalcogenides, the molecular adduct, $[AlCl_3(P_{888}E)]$, was preferred over the ionic products, $[AlCl_2L_2][AlCl_4]$. The densities and viscosities of both $AlCl_3$- and $GaCl_3$-LCCs were measured. The densities were found to vary linearly with temperature, much like in ionic liquids. The viscosities were found to be lower for LCCs with urea type ligands over the trioctylphosphine family of ligands. Much like chloroaluminate ionic liquids, the viscosity was seen to decrease with increasing χ_{MCl3}, due to the change in halometallate anion. The donor atom was also seen to have a large effect on the viscosity: with heavier donor atoms, *i.e.* S and Se, resulting in much larger viscosities than oxygen donors, due to the difference in speciation.

C_7CN-MCl_3 presented an interesting case, which would warrant further investigation. The ligand in this case displaced all chloride from the aluminium cation, forming $[Al(C_7CN)_6]^{3+}$, with the ^{27}Al NMR spectrum showing a mix of halometallate anions and no neutral species. Thus this combination of donor and $AlCl_3$ forms an ionic liquid, not an LCC. By considering the stoichiometry of the reaction, the neutral point of this ionic liquid would be predicted to be at χ_{AlCl3} = 0.33, meaning highly acidic catalysts could be made at much lower metal chloride loadings than those reported for chloroaluminate ionic liquids with organic cations (*i.e.* having neutral point at χ_{AlCl3} = 0.50). The low viscosity of the ionic C_7CN-MCl_3 family may be counterintuitive, as one would expect Coulombic forces to increase, not to decrease viscosity. Similarly the high viscosity measured for predominantly molecular $P_{888}E$-MCl_3 (E =

S, Se) compared to low viscosity of $P_{888}O\text{-}MCl_3$ is unexpected as one would expect the ionic species to be more viscous.

The thermal stability of $P_{888}O\text{-}AlCl_3$ and Ur-$AlCl_3$, χ_{AlCl3} = 0.60 were measured to assess their suitability for high temperature applications. Firstly, a method for preventing exposure to atmospheric moisture was developed, to allow TGA of the highly reactive LCCs to be measured. Thermal stabilities were found to be low, with significant mass loss occurring by 113 and 160 °C for Ur-$AlCl_3$ and $P_{888}O\text{-}AlCl_3$, χ_{AlCl3} = 0.60, meaning that for high temperature applications, LCCs could not be used as recyclable catalysts.

The acidity of LCCs was measured by the Gutmann acceptor method. The interpretation of these results were complicated by the appearance of many signals in the spectra, which was not reported for previously studied systems.[25] This multitude of signals was interpreted as deriving from many acidic species present. The optimum way to report the results was resolved: the AN was calculated for the largest ^{31}P NMR peak, as well as the entire range of ^{31}P NMR chemical shifts, and both values were reported. LCCs typically had a higher acidity than chlorometallate ionic liquids of the same composition (χ_{MCl3}), and a comparable AN to chlorometallate ionic liquids with the same dominant anion. High Lewis acidities, bordering on Lewis superacidity, combined with low synthetic cost, bear the promise of a wide variety of catalytic applications.

2.2 Borenium ionic liquids

Within the last decade, main group catalysis has been gaining increasing interest, as complementary to transition metal catalysis and Brønsted acid catalysis.[183] There has been a growing interest in boron based Lewis acids as catalysts, with cationic boron species emerging as highly active Lewis acid catalysts.[16,184] Research in our group has been focussed on incorporating main group cationic Lewis acids into ionic liquids; amongst others, a new class of Lewis superacidic ionic liquids based on borenium cations have been developed.[52] In this chapter, the synthesis and characterisation of a range of borenium ionic liquids is outlined, and their use as catalysts for oligomerisation of olefins is demonstrated in Chapter 3.3.

2.2.1 Literature review

2.2.1.1 Boron Lewis acids

Boron trifluoride is a molecular Lewis acid, used on the industrial scale as a Lewis acidic catalyst (Table 1.2-1, Chapter 3.1.3). Its Lewis acidity is derived from the empty *p*-orbital situated on the boron atom. The strength of the Lewis acidity of boron halides is dependent on the substituents and increases in the order $BF_3 < BCl_3 < BBr_3 < BI_3$.[58] This increase in acidity is due to decreasing π donation from the lone pair on the halogen to the empty p-orbital on the boron. This results in a decrease of electron density on the boron atom, increasing the acidity. Similarly in boranes, the Lewis acidity depends upon the ligands and their composition. For example in the triarylborane series $Mes_2BC_6H_4$-4-X (X = F, H, Me), the Lewis acidity was found to decrease in the order F > H > Me.[22] Lewis acidity is also affected by steric hindrance. With both tris(trifluorophenyl)borane and tris(difluorophenyl)borane the Lewis acidity was decreased when both ortho positions on the phenyl ring were occupied by fluorine atoms, as opposed to 1 fluorine and 1 hydrogen atom (Figure 2.2-1).[22]

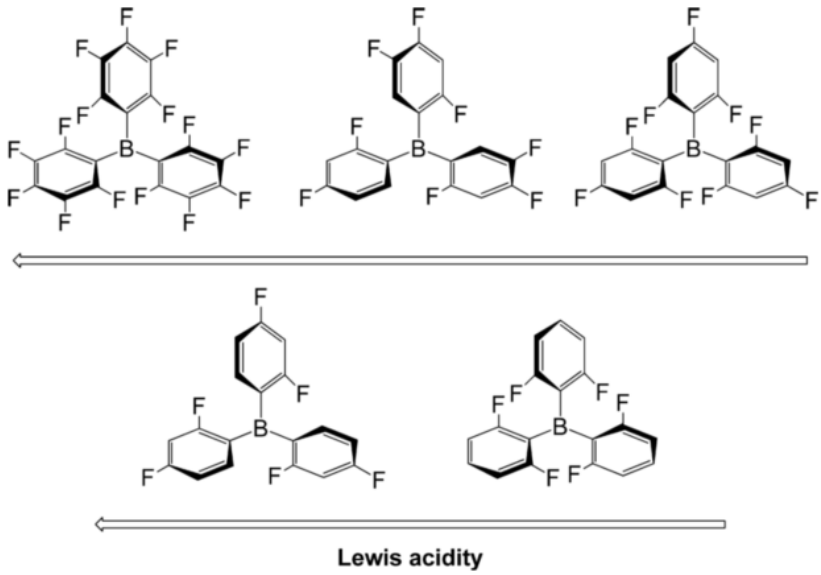

Figure 2.2-1: Lewis acidity of fluoro-substituted triaraylboranes[22]

The electron deficiency, and therefore Lewis acidity, on the boron atom can be increased by introduction of a formal positive charge. There are three types of boron cation (Figure 2.2-2). Borinium cations have two substituents and are extremely reactive, requiring orbital overlap and bulky ligands to stabilise the subvalent boron cation.[185] Borenium ions are tricoordinate, highly Lewis acidic, with two covalent and one dative bond. Finally, boronium cations are tetracoordinate with two covalent and two dative bonds.[184]

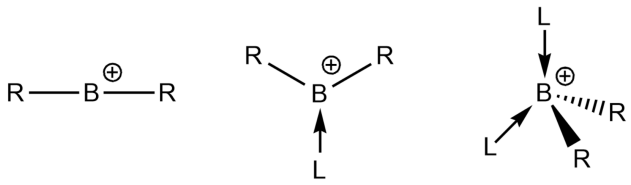

Figure 2.2-2: Left to right, structural representation of borinium, borenium and boronium cations

These charged boron species have been reviewed by Nöth[186] and by Piers,[184] with emphasis on synthesis, structure and spectroscopic properties, by Ingelson who reviewed fundamental properties and applications,[16] and by Vedejs,[187] who looked at boron cation chemistry from an organic perspective. Borenium cations are of most interest for Lewis acidity, owing to the balance between high Lewis acidity, ease of synthesis and relative stability (in moisture-free conditions).

2.2.1.2 Synthesis of borenium cations

The most common synthetic route to borenium cations is the hydride/halide abstraction from a tetracoordinate, charge-neutral boron adduct. In 1970 Ryschkewitsch reported the first synthesis of a borenium cation, $[BCl_2(4pic)]^+$, by mixing $AlCl_3$ and $[BCl_3(4pic)]$ in DCM (Equation 2.2-1).[188] A significant change in the ^{11}B NMR spectrum was seen: from a sharp signal in the starting material to a very broad downfield shift, indicative of tricoordinate boron.[151] The authors noted that a 1:2 mixture of $[BCl_3(4pic)]$ and $AlCl_3$ was a mobile liquid at room temperature, but as research on room-temperature ionic liquids was then in its infancy, this observation did not attract any attention. Another adduct, $[BCl_3(NMe_3)]$, was found to only partially react with $AlCl_3$ (Equation 2.2-2). The authors attributed this to the lack of the aryl π system, which would stabilise the positive charge on the borenium cation. Extraction of a halide to form the cationic boron has also been achieved using $SbCl_5$ as the extracting agent.

$$[BCl_3(4pic)] + 2AlCl_3 \rightarrow [BCl_2(4pic)][Al_2Cl_7] \qquad \text{Equation 2.2-1}$$

$$[BCl_3(NMe_3)] + 2AlCl_3 \rightleftharpoons [BCl_2(NMe_3)][Al_2Cl_7] \qquad \text{Equation 2.2-2}$$

Diphenylboronchloride was reacted with pyridine and pyridine-*N*-oxide forming a tetracoordinate species, which upon addition of $SbCl_5$ formed the tricoordinate cation with the $[SbCl_6]^-$ counterion.[189]

$$[BPh_2LCl] + SbCl_5 \rightarrow [BPh_2L][SbCl_6] \qquad \text{Equation 2.2-3}$$

L = pyridine, pyridine-*N*-oxide

Finally, trimethylsilyltriflate has also been used to generate borenium cations by halide extraction. The $[Me_3Si]^+$ cation was used to remove fluorine from bis(trimesityl)boron fluoride in the presence of a substituted pyridine to give the triaryl boron cation with the triflate anion.[190]

$$[BMes_2LCl] + Me_3SiOTf \rightarrow [BMes_2L][OTf] + Me_3SiF$$ Equation 2.2-4

L = 4-picoline, *N,N*-dimethylpyridin-4-amine

Borenium ions may also be formed by nucleophilic displacement of a ligand from the boron by a neutral ligand. Nöth *et al.* reported using a variety of bases (L = Et_3N, py or 2,6-dimethylpyridine) to attempt to displace an anion from R_2BX, where R = nBu, Ph or N,N'-dimethylethyldiamine and X = Cl^- or $[OTf]^-$.[191] Here, the leaving group and steric repulsion between the potential ligands was found to be of importance (Table 2.2-1). When NEt_3 was used, a tertracoordinate species was formed, but when using 2,6-dimethylpyridine displacement of the triflate anion to form the cationic borenium species was favoured. Chloride was a less favourable leaving group than triflate, only being displaced when the boron substituents had greater steric hindrance.

Table 2.2-1: Summary of Noth's results showing whether tetracoordinate adducts or tricordinate borenium cations formation is favoured.[191]

BR_2X	NEt_3	Pyridine	2,6-Lutidine
$B(n\text{-}Bu)_2Cl$	Tetracoordinate	Tetracoordinate	Tetracoordinate
$B(n\text{-}Bu)_2OTf$	Tetracoordinate	Tetracoordinate	Tricoordinate
BPh_2Cl	Tetracoordinate	Tetracoordinate	Mix
BPh_2OTf	Tetracoordinate	Mix	Tricoordinate
B(MeNEtNMe)Cl	-	Tricoordinate	Tricoordinate
B(MeNEtNMe)OTf	-	Tricoordinate	Tricoordinate

Another alternative method to hydride/halide abstraction is treating a compound with an N-B bond with a strong acid. For example, Corey *et al.* utilised chiral oxazaborolidines which when reacted with triflic acid were protonated at the nitrogen atom. Two species were found to be in equilibrium with each other, a tetracoordinate boron species, with the triflate anion coordinating to boron atom, and a borenium ion with the triflate as a distinct anion (Figure 2.2-3).[192] When the triflic acid was replaced with bistriflimidic acid a similar reaction was seen again with both a tetracoordinate boron species and borenium ion in equilibrium with each other.[193] The fact that both $[OTf]^-$ and $[NTf_2]^-$, which are typically regarded as weakly coordinating anions,[152] coordinate to these borenium ions shows their high acidity.

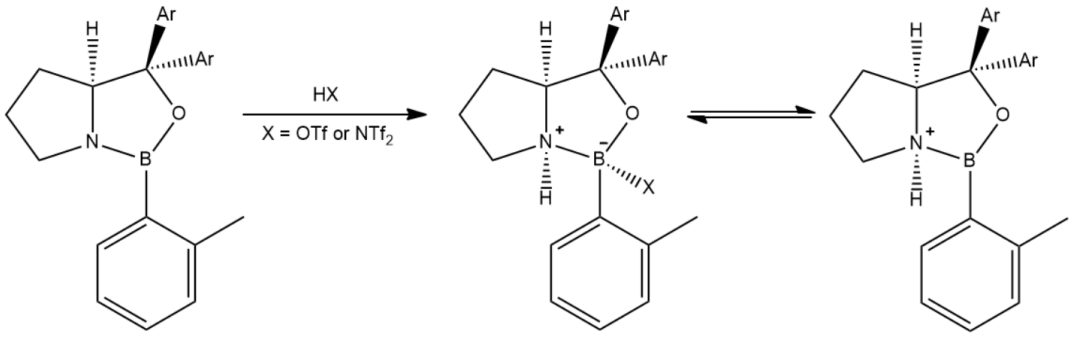

Figure 2.2-3: Formation of borenium ions by addition of a strong acid to a oxazaborolidine[193]

2.2.1.3 Borenium cations as Lewis acidic catalysts

Boron trifluoride has been used extensively in the industry, for the synthesis of polyalphaolefins (Chapter 3.1.3) and as a catalyst in a wide variety of Friedel Crafts alkylations and acylations.[58,194] Although borenium cations are generally stronger Lewis acids,[17,34] they are structurally more complicated, and thus more expensive. They are also only recent additions to the catalytic portfolio, therefore their uses are typically on the laboratory scale. Corey *et al.* used their chiral oxazaborolidine adducts with strong Brønsted acids (Figure 2.2-3), as catalysts for Diels Alder cycloaddition, obtaining high enantioselectivity even for highly electron-deficient dieneophiles.[193] Importantly, no catalytic activity was seen with the starting chiral oxazaborolidines, and when methanesulfonic acid was used in place of triflic acid, a significant decrease in conversion was seen.[192] Methanesulfonic acid being a weaker acid (and thus having a stronger conjugate base) than trifilic acid, induced shift of the equilibrium in Figure 2.2-3 to the left, effectively decreasing the concentration of the catalytically active, tricoordinate species.

Borenium ions have also been used as the acid component of frustrated Lewis pairs (FLPs). FLPs are acid-base combinations which cannot form a typical acid-base adduct due to sterically hindering substituents.[195] The typical examples of FLPs are made up of hindered phosphines, such as $P(tBu)_3$ or $P(Mes)_3$, with electron-deficient boranes, such as $B(C_6F_5)_3$.[196] Through availability of HOMO on the base and LUMO on the acid, FLPs mimic the catalytic behaviour of transition metals, and can for example reversibly bind small molecules, for example, H_2[197] or CO_2.[198] Notably, the strength of the acid was found to be import in the heterolytic splitting of H_2. When tris(pentaflurophenyl)borane was mixed with $P(tBu)_3$ in the presence of hydrogen, the salt $[HP(tBu)_3][HB(C_6F_5)_3]$ rapidly formed (Equation 2.2-5), however using triphenylborane as the acid only resulted in a low yield of the corresponding salt, $[HP(tBu)_3][HBPh_3]$.[196]

$$P(tBu)_3 + B(C_6F_5) + H_2 \rightarrow [HP(tBu)_3][HB(C_6F_5)_3]$$ Equation 2.2-5

Borenium ions make for a good alternative to tris(pentafluorophenyl)borane due to their variable (and by extension tuneable) hydride ion affinity.[17] Stephan *et al.* utilised borenium ions in the reduction of imines with a borenium ion, which tolerated other functional groups. They proposed that the imine itself acted as the base in the frustrated Lewis pair (Figure 2.2-4).

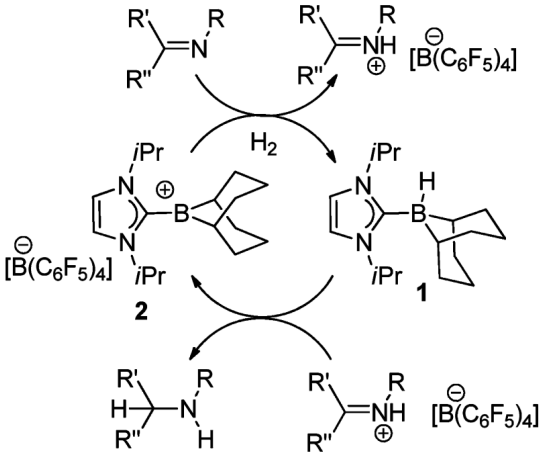

Figure 2.2-4: Imine reduction utilising borenium ion FLP as a catalysts[199]

2.2.1.4 Borenium cations in ionic liquids

Considering the structures of borenium salts, it appears obvious that some of them could be expected to form ionic liquids, considering the prevalence of non-coordinating anions and charge-dispersed cations. However, until recently they have never been researched in this context, with the first borenium ionic liquids reported by our group in 2015.[52]

2.2.2 Experimental

2.2.2.1 Materials and Methods

All reactions were performed in a glovebox (MBraun labmaster dp, <0.3 ppm of H_2O and O_2) or using standard Schlenk techniques with a vacuum and an argon line. All glassware was dried overnight (*ca.* 100 °C) before use.

Boron trichloride solution in heptanes (1 M) was purchased from Sigma Aldrich and used as received. Pyridine, 2-methylpyridine, 3-methylpyridine, and 4-methylpyridine (all 99 %), were all purchased from Sigma Aldrich, distilled and then dried over 3 Å molecular sieves and stored under argon atmosphere before use. 2-Fluoropyridine, 3-fluoropyrinde and

pentafluoropyridine (all 99 %) were purchased from Fluorochem, dried over 3 Å molecular sieves and stored under argon atmosphere before use.

2.2.2.2 Synthesis of borenium ionic liquids

To form the adduct, BCl_3 (1 M solution in heptanes, 20 ml, 20 mmol 1 mol eq) was transferred to a round bottom flask under argon atmosphere and cooled (-20 or -78 °C). The solution was further diluted in an equal volume of dried inert solvent (hexane or DCM, 20 ml). The pyridine base (18 mmol, 0.9 mol eq.) was added dropwise to the solution over a period of 5 min, and the mixture was stirred for 1 h. A white precipitate formed which was isolated by removal of volatiles under reduced pressure (12 h, 50 °C, 10^{-2} mbar) before being transferred to the glovebox.

To form the ionic liquid, the adduct was weighed into a sample vial, to which $AlCl_3$ (2 mol eq) was added in small portions. The two solids were stirred thoroughly before further addition of each small portion of $AlCl_3$. Upon completion of the addition, the mixture was heated and stirred (60 °C, 1 - 24 h) until a homogeneous liquid was obtained.

All adducts and ionic liquids were analysed by ^{1}H, ^{11}B, ^{13}C and, where applicable, ^{19}F and ^{27}Al NMR spectroscopy.

2.2.3 Results and discussion

2.2.3.1 Adduct synthesis

Table 2.2-2 summarises the results of the adduct synthesis, originally carried out at -78 °C. The products were typically white or off-white powders. Pentafluoropyridine did not react with boron trichloride at -78 °C to form an adduct, so the reaction temperature was increased to room temperature. Irrespective of the reaction temperature, only a small oxidised/hydrolysed boron residue remained after application of a vacuum. The adducts of pyridine, 3-picoline and 4-picoine with BCl_3 were relatively air stable and could be recrystallised from DCM/hexane in without the need for an inert atmosphere, whereas the adducts of BCl_3 with 2-picoline, 2-fluoropyridine and 3-fluoropyridine all decomposed whilst their DCM solutions were exposed to air. As such they were not recrystallised before use. Thus the stability of the complex to atmospheric moisture has been shown to be dependent on both steric and electronic effects.

Upon receiving input from the industrial partner involved in catalytic applications of borenium ionic liquids, the synthetic procedure for two complexes of particular interest: [BCl_3(py)] and [BCl_3(4pic)], was altered to use conditions available in industrial processes. The temperature raised from -78 °C to -20 °C as cryogenic temperatures are not readily available in industry, and the solvent was changed from DCM to hexane as the use of chlorinated solvents is increasingly discouraged by legislation and green chemistry principles.[200] This was found to have no detrimental effect on the purity of either complex.

Table 2.2-2: Physical appearance of BCl_3–pyridine adducts and subsequent ionic liquids

Pyridine Used	Adduct	Addition of $2AlCl_3$	Addition of $2GaCl_3$
Pyridine	White Powder	Homogenous Liquid	Homogenous Liquid
2-Picoline (2 Methylpyridine)	White Powder	Homogenous Liquid	Homogenous Liquid
3-Picoline (3 Methylpyridine)	White Powder	Homogenous Liquid	Homogenous Liquid
4-Picoline (4 Methylpyridine)	White Powder	Homogenous Liquid	Homogenous Liquid
2-Fluoropyridine	White Powder	Liquid + Precipitate	Homogenous Liquid
3-Fluoropyridine	White Powder	Liquid + Precipitate	Homogenous Liquid
Pentafluoropyridine	No Reaction Observed	n/a	n/a

The ^{1}H spectra of free bases (L) and corresponding [BCl_3L] adducts (Figure 2.2-5 and Figure 2.2-6, respectively) show a large shift downfield in the ^{1}H NMR spectra for all bases used, indicative of electron density being withdrawn from the ring by complexation. For all but two adducts, complexed ligands appear to be in one electronic environment, most likely corresponding to [BCl_3L]. The mixture of 2-picoline and BCl_3 showed 2 sets of environments, which were integrated and shown to be present in a 1:1 ratio (Figure 2.2-6-b). Both sets of signals were consistent with the expected pattern for the 2-picoline structure and shifted upfield with respect to the free base, which suggests two different boron adducts being formed. The ^{1}H NMR spectrum of [BCl_3(2Fpy)] is of a poor quality in terms of signal resolution, but the peaks integration is in agreement with 2Fpy. In contrast, the mixture of 3-fluoropyridine and BCl_3 saw extra signals which did not correlate to the free base and may correlate to undesired side reactions of the ligand (Figure 2.2-6-f).

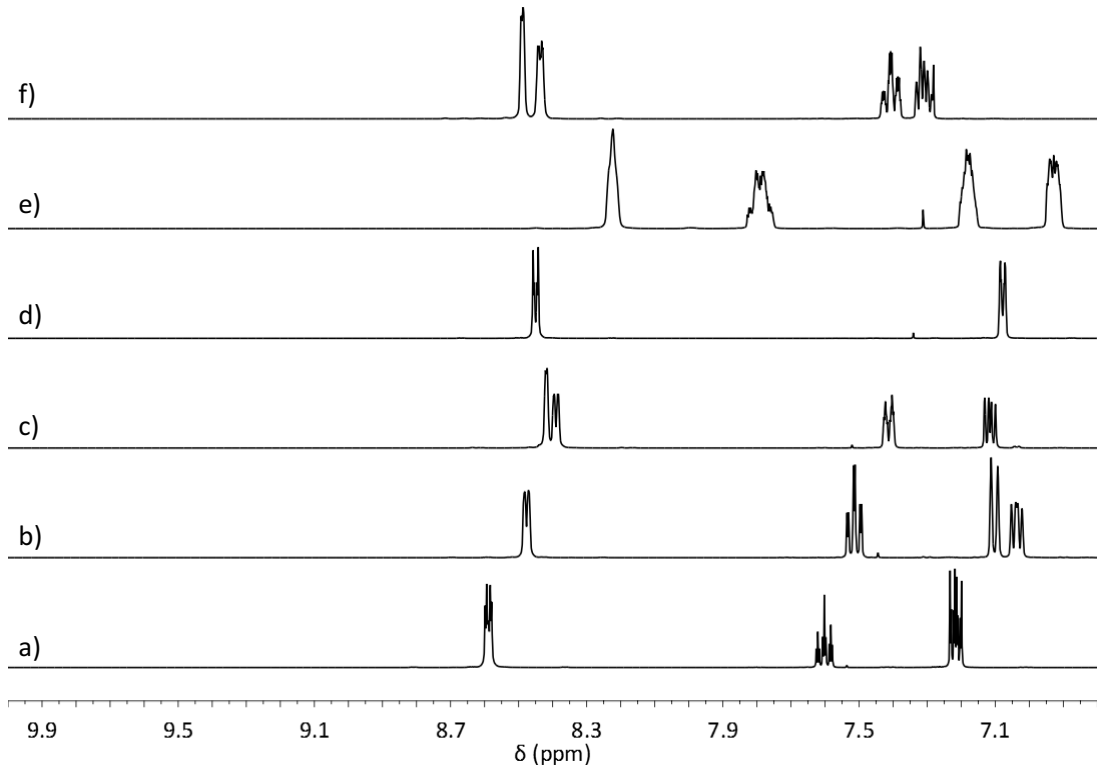

Figure 2.2-5: ^{1}H NMR spectra of a) pyridine, b) 2-picoline, c) 3-picoline, d) 4-picoline, e) 2-fluoropyridine, f) 3-fluoropyridine ($CDCl_3$)

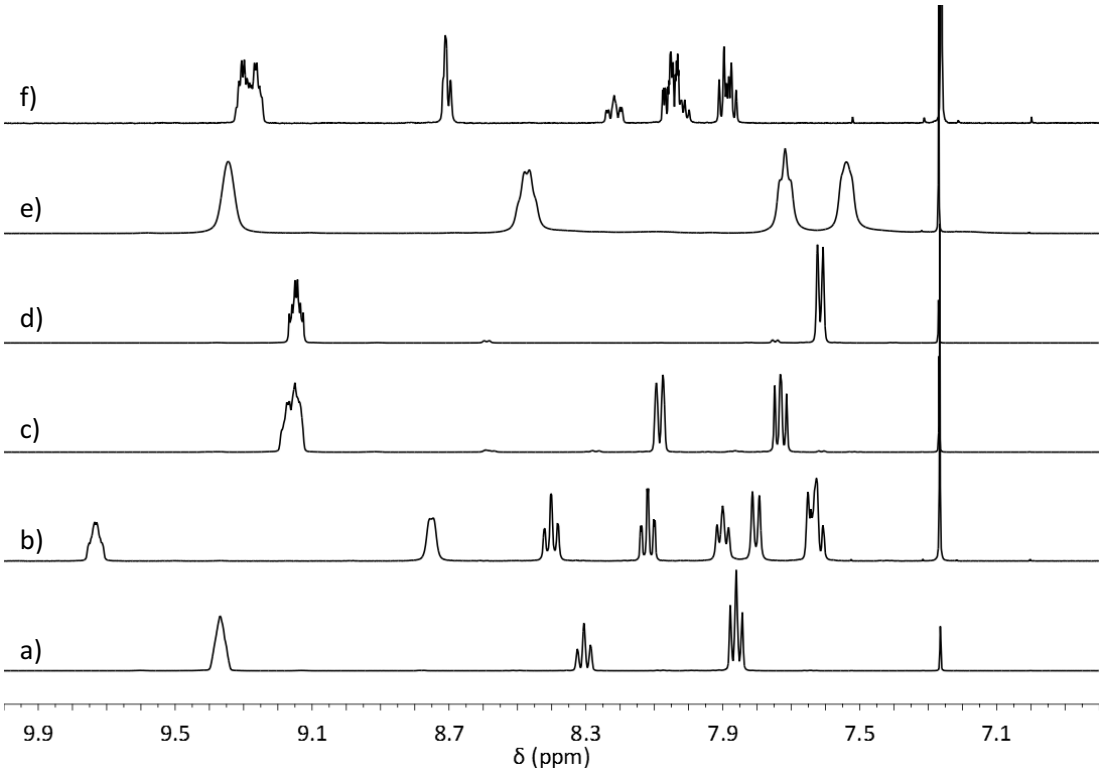

Figure 2.2-6: ^{1}H NMR spectra ($CDCl_3$) of [BCl_3L] adducts, where L is: a) pyridine, b) 2-picoline, c) 3-picoline, d) 4-picoline, e) 2-fluoropyridine, f) 3-fluoropyridine

For all synthesised adducts, the ^{11}B NMR spectra (Figure 2.2-7) feature signals within the range of 7 - 9 ppm, which correspond to tetra coordinate boron compounds,[145] significantly upfield from the ^{11}B NMR chemical shift for BCl_3 (47 ppm, measured in $CDCl_3$). A single peak was found for each adduct, with the exception of [BCl_3 (2pic)], which contained two signals (Figure 2.2-7-b). This is in agreement with the ^{1}H NMR spectrum of [BCl_3(2pic)] (Figure 2.2-6-b), which also shows two environments in the ratio 1:1, and could be indicative of a mix of neutral adduct and salt (Equation 2.2-6). However this would necessitate three ^{11}B environments. The peak at 8.65 ppm is noticeably less symmetrical than the peaks of other adducts (Figure 2.2-7), which could indicate an equilibrated species. Though ^{11}B NMR integrations are not exact, the ratio of the two peaks is roughly 2:1. As such (Equation 2.2-6) would appear to be the best explanation for the data.

$$2\ 2pic + 2BCl_3 \longrightarrow 2[BCl_3(2pic)] \rightleftarrows [BCl_2(2pic)_2][BCl_4] \qquad \text{Equation 2.2-6}$$

Disproportionation of the [BCl_3(2pic)] adduct was not considered a disadvantage; it was possible that the adduct will react with a metal chloride to form an ionic liquid.

Despite products of ligand decomposition being visible in the ^{1}H NMR spectrum (Figure 2.2-6-f), the ^{11}B NMR spectrum of the 3-fluoropyridine and BCl_3 adduct showed a single environment (Figure 2.2-7-f), with no indication of fluoride abstraction by the boron centre, which would result in ligand scrambling.[201]

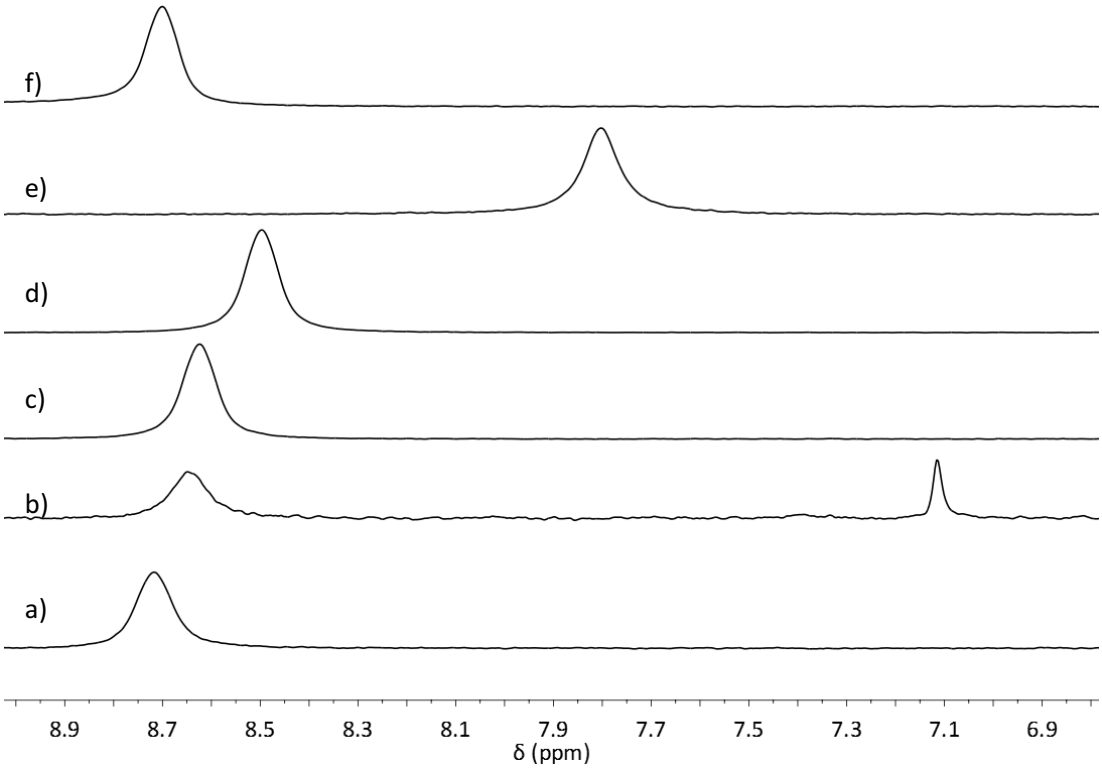

Figure 2.2-7: ^{11}B NMR spectra ($CDCl_3$) of [BCl_3L] adducts, where L is: a) pyridine, b) 2-picoline, c) 3-picoline, d) 4-picoline, e) 2-fluoropyridine, f) 3-fluoropyridine

The ^{19}F NMR spectra of both 2Fpy and 3Fpy (Figure 2.2-8-a) feature a singlet, which for 2Fpy becomes deshielded upon complexation (Figure 2.2-8-b), correlating well with the formation of the adduct, [BCl_3(2Fpy)]. In contrast, the spectrum of 3Fpy and BCl_3 adduct contains two major peaks (Figure 2.2-8-d), which in combination with unassigned signals in the ^{1}H NMR spectrum (Figure 2.2-5-f) indicate a rearrangement/decomposition of the ligand. It is unlikely to be a direct C-F bond activation as there was no evidence of mixed boron halides in either ^{11}B or ^{19}F NMR spectra,[202] and such activation by main group Lewis acids tend to be selective for C-F sp^3 hybridised carbons.[203]

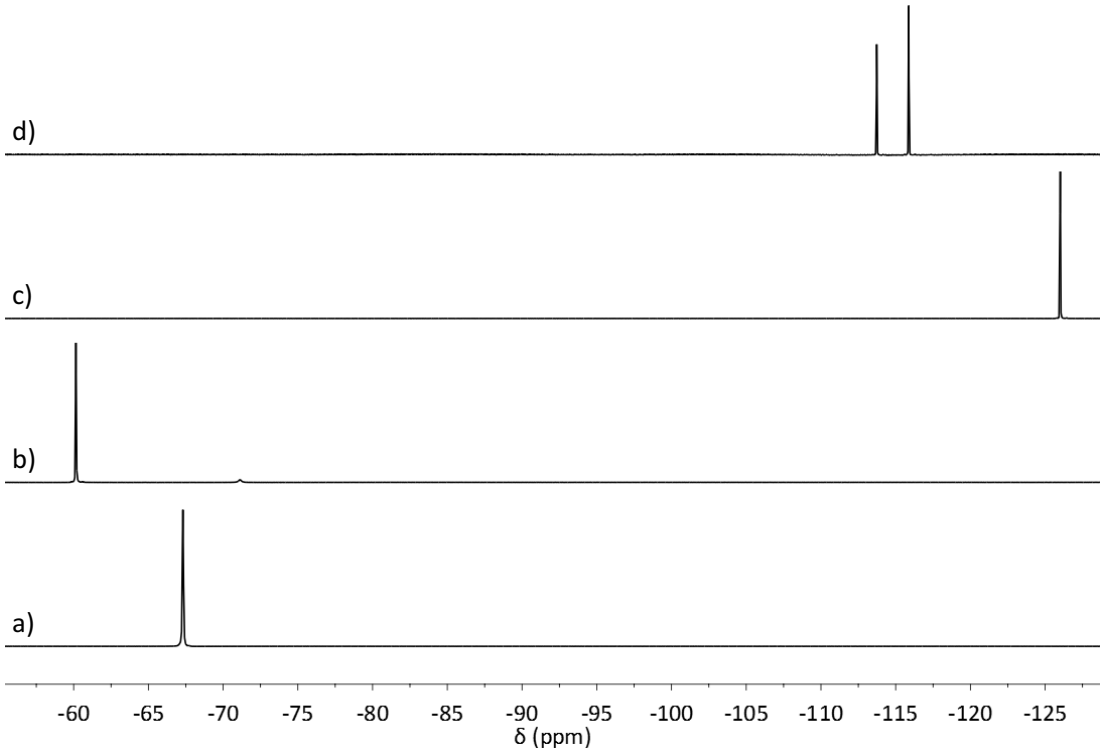

Figure 2.2-8: ^{19}F NMR spectra of fluorinated pyridine compounds: a) 2Fpy, b) [BCl_3(2Fpy)], c) (3Fpy)], d) [BCl_3(3Fpy)]

2.2.3.2 Ionic liquid synthesis

As the ionic liquids synthesised here were applied in the oligomerisation of 1-decene (Chapter 3.3), it was deemed preferential that the catalysts were liquid for ease of manipulation under oxygen and water free conditions. Therefore two moles of metal chloride were reacted per mol of boron adduct in the synthesis of all ionic liquids as some 1:1 combinations have crystals structures reported.[204] All the non-fluoropyridine-BCl_3 adducts reacted rapidly with two equivalents of $AlCl_3$ to form liquids. Adducts with fluorinated pyridines had significant amounts of precipitate present, even when lower $AlCl_3$ loadings were tried. These precipitations were filtered before spectroscopic analysis of the liquid part. All adducts, irrespective of ligand, reacted with two equivalents of $GaCl_3$ to give low viscosity liquids.

The ^{1}H NMR spectra of the neat ionic liquids of the general formula [BCl_2L][Al_2Cl_7] and [BCl_2L][Ga_2Cl_7] are compared in Figure 2.2-9 and Figure 2.2-10, respectively. All spectra for the ionic liquids without fluorinated ligands show a single set of signals with the appropriate integrations and expected splitting patterns. There are also sets of minor peaks of very low intensity, visible in both the aromatic and methyl regions, which also display the splitting

patterns associated with the ligand. These could be associated with ligand scrambling (Figure 2.2-15) or the reaction of borenium ion with adventitious water.

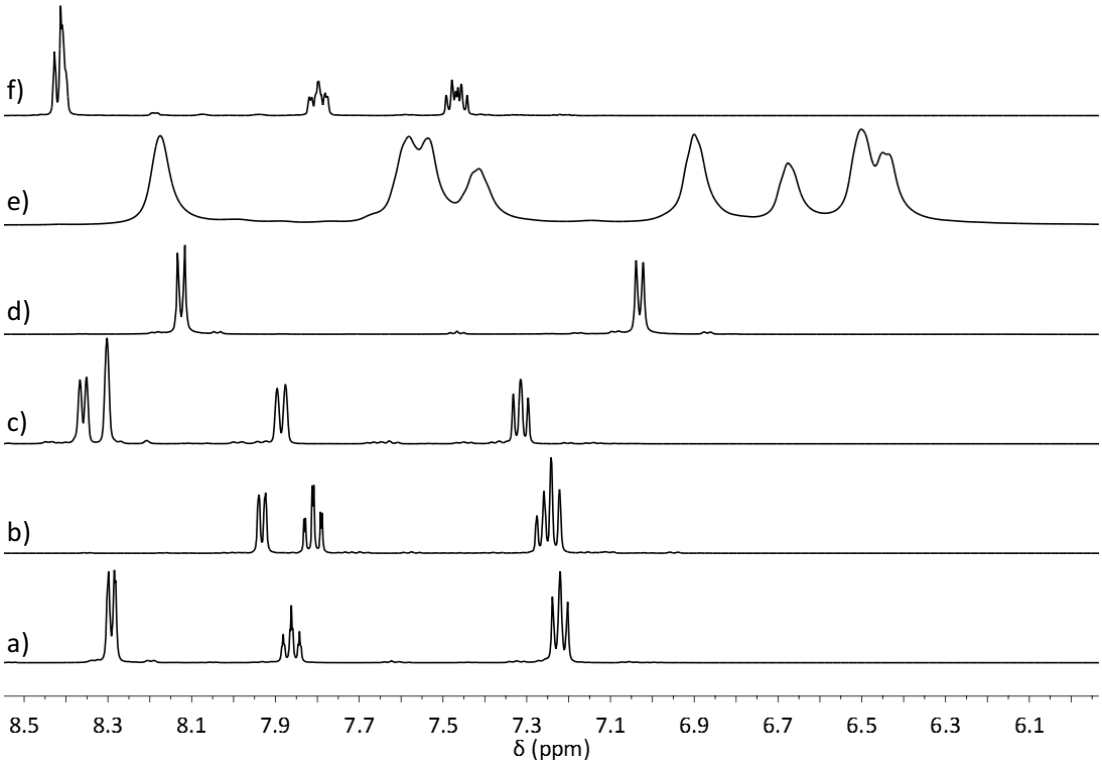

Figure 2.2-9: ^{1}H NMR spectra $[BCl_2L][Al_2Cl_7]$ where L is: a) pyridine, b) 2-picoline, c) 3-picoline, d) 4-picoline, e) 2-fluoropyridine, f) 3-fluoropyridine (DMSO Capillary)

Spectra of ionic liquids with fluorinated ligands were more problematic. It must be remembered that both chloroaluminate liquids contained precipitate, which was filtered off prior to NMR studies, therefore the NMR spectra do not represent stoichiometric compositions. $[BCl_2(3Fpy)][M_2Cl_7]$ features only one set of signals, that correspond almost entirely to the ligand rearrangement product (Figure 2.2-9-f and Figure 2.2-10-e), which was partially formed upon reaction of 3Fpy with BCl_3, indicating that decomposition/rearrangement process was completed when the adduct is reacted with MCl_3.

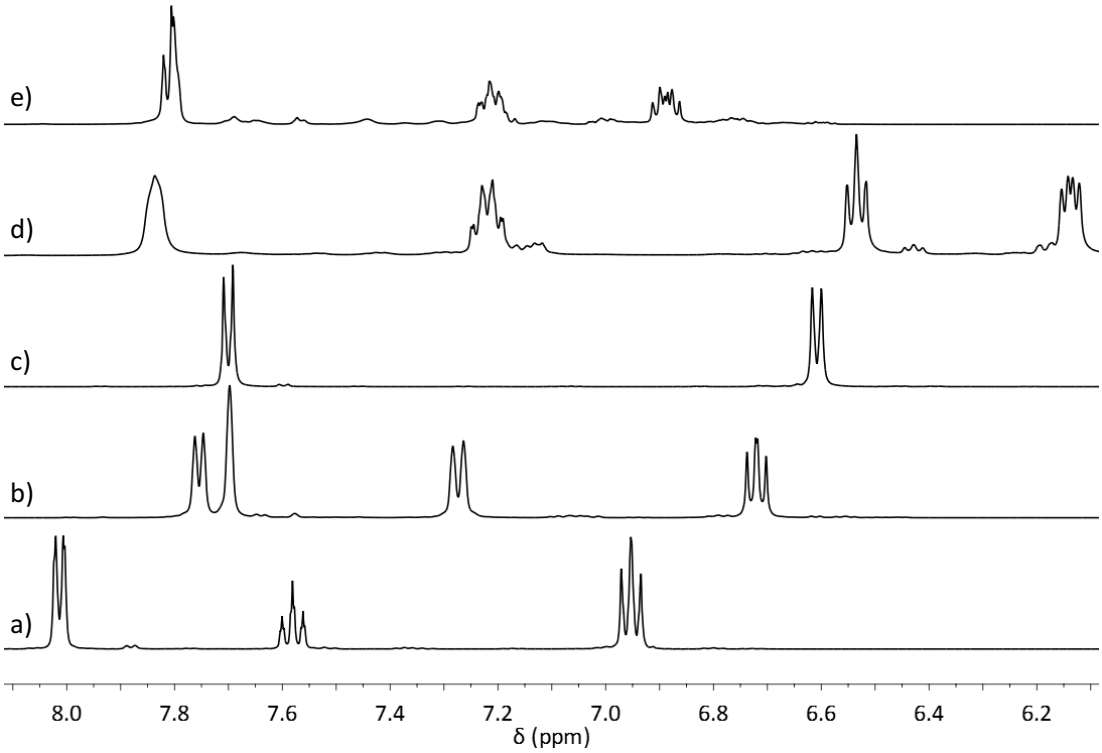

Figure 2.2-10: ^{1}H NMR spectra $[BCl_2L][Ga_2Cl_7]$ where L is: a) pyridine, b) 3-picoline, c) 4-picoline, d) 2-fluoropyridine, e) 3-fluoropyridine (DMSO Capillary)

The ^{1}H NMR spectra $[BCl_2(2Fpy)][M_2Cl_7]$ (Figure 2.2-9-e and Figure 2.2-10-d) feature very broad signals with very poorly resolved multiplets - in particular in the case of chloroaluminate ionic liquids. Since neat ionic liquids are studied, and their viscosity is similar to the other studied systems, the broadness of the signals cannot arise from either high viscosities of tested samples, or from solubility issues. Furthermore, both spectra feature additional set of signals, which are minor and better resolved for $[BCl_2(2Fpy)][Ga_2Cl_7]$ (Figure 2.2-10-d), but almost as prominent as the main signals for $[BCl_2(2Fpy)][Al_2Cl_7]$ (Figure 2.2-9-e).

Solid residues from the BCl_3(*n*Fpy)-$AlCl_3$ mixtures were dissolved in $CDCl_3$ and analysed by multinuclear NMR spectroscopy. ^{1}H NMR spectra of the precipitates filtered from the chloroaluminate systems (Figure 2.2-11) reveal complex mixtures of aromatic compounds. The ^{19}F NMR spectra also showed a number of unidentifiable peaks, with ^{11}B and ^{27}Al NMR spectra indicating only tetracoordinate species present, though due to the poor solubility of the solid, the ^{27}Al spectra are mostly dominated by the probe peak. The peaks are slightly shifted from the downfield from the expected chemical shift for $[AlCl_4]^-$ indicating some degree of ligand transfer to the $AlCl_3$.

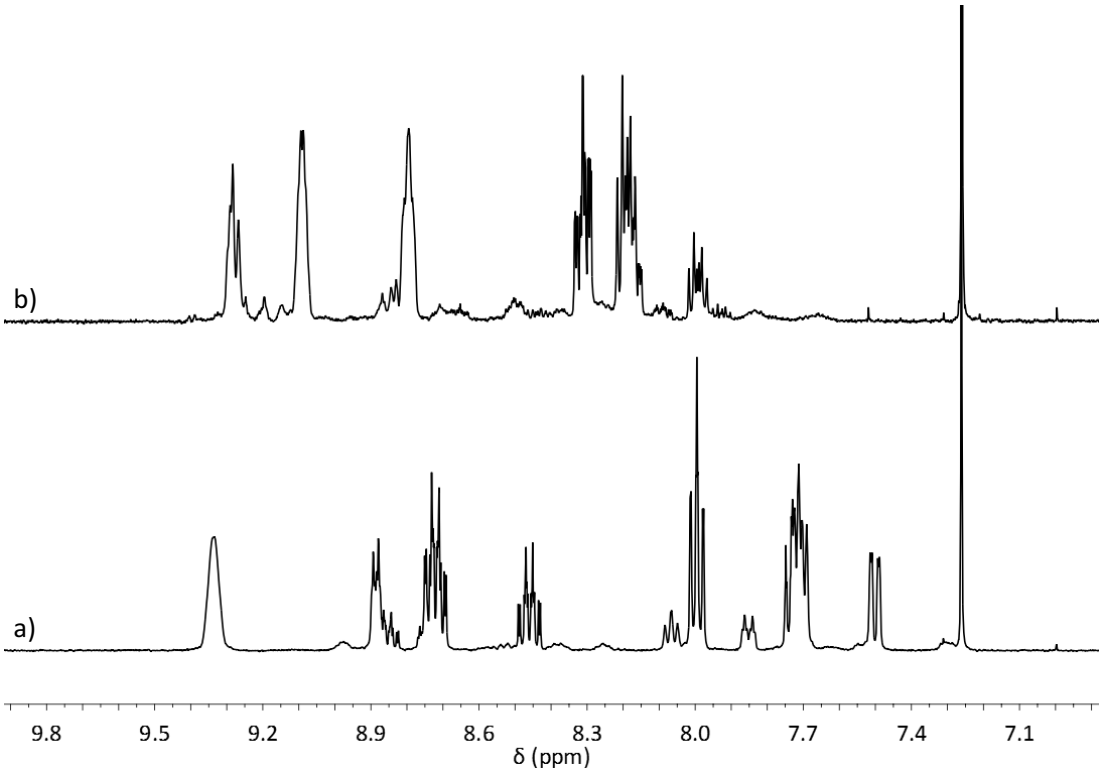

Figure 2.2-11: ^{1}H NMR spectra of a) $[BCl_2(2Fpy)][Al_2Cl_7]$ and b) $[BCl_2(2Fpy)][Ga_2Cl_7]$

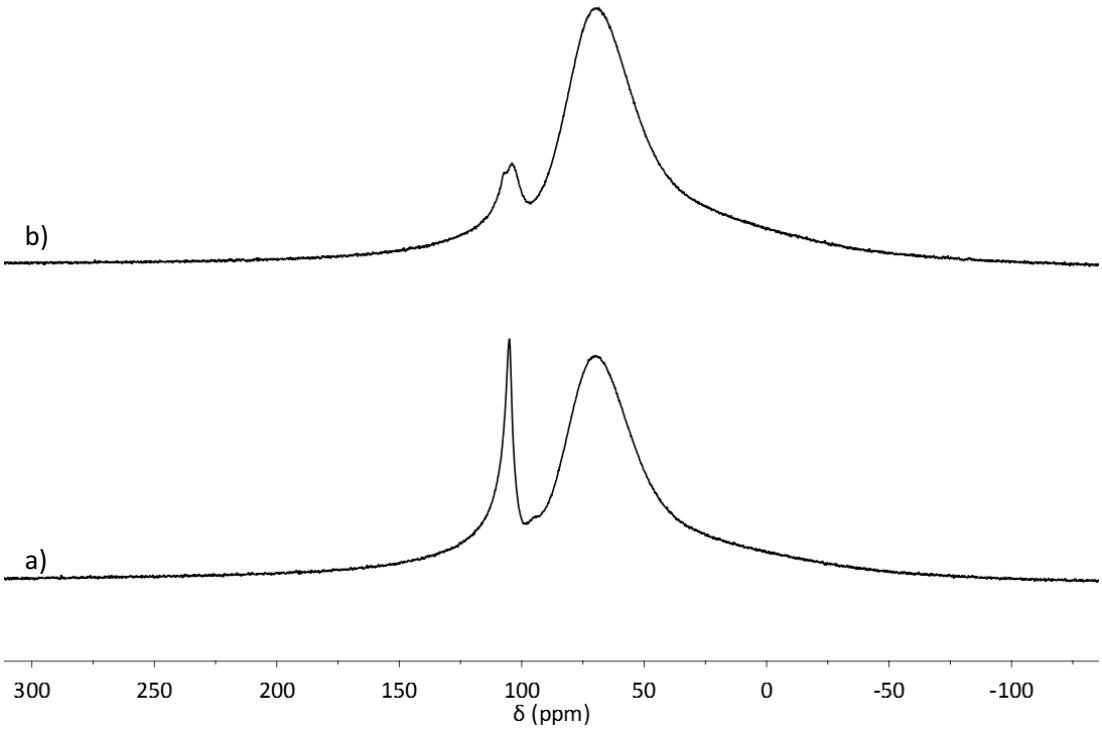

Figure 2.2-12: ^{27}Al NMR spectra of a) $[BCl_2(2Fpy)][Al_2Cl_7]$ and b) $[BCl_2(2Fpy)][Ga_2Cl_7]$

The ^{11}B NMR spectra of neat ionic liquids of a general formula $[BCl_2L][Al_2Cl_7]$ and $[BCl_2L][Ga_2Cl_7]$ are compared in Figure 2.2-13 and Figure 2.2-14, respectively. In most cases, the dominant peaks are found in the region of 30-50 ppm, corresponding to tricoordinate boron

compounds.[145] Typically, dichloroborenium ions are characterised by broad downfield peak,[186] due to lower symmetry and higher deshielding, compared to tetracoordinate adducts. In addition, in some spectra, there is a sharper signal emerging from the broad feature, at *ca.* 47 ppm, which is most clearly illustrated by the system $[BCl_2(3Fpy)][Ga_2Cl_7]$ (Figure 2.2-14-e).

In contrast, ^{11}B NMR spectra of $[BCl_2(2Fpy)][Al_2Cl_7]$ (Figure 2.2-13-e) and $[BCl_2(2Fpy)][Ga_2Cl_7]$ (Figure 2.2-14-d) show no formation of the borenium cation, and only a weak narrow signal at 47 ppm was found in the later. Boron is present as a tetracoordinate species, although the peak is slightly upfield compared to the adduct.

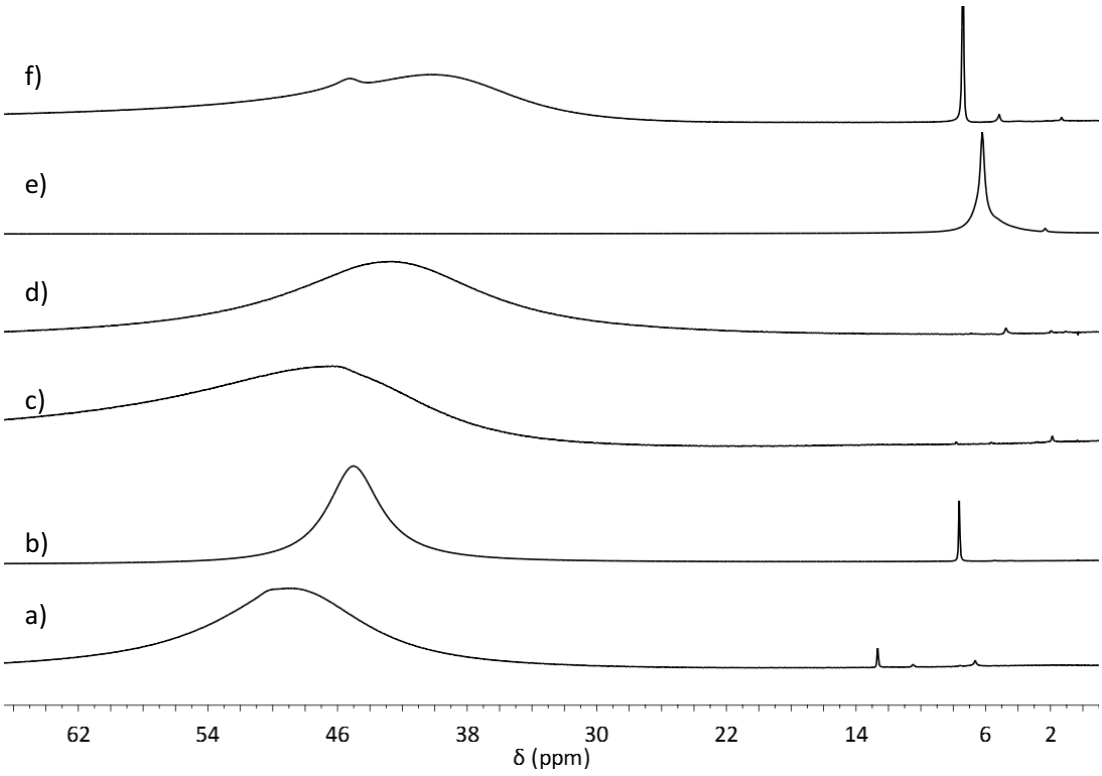

Figure 2.2-13: ^{11}B NMR spectra of $[BCl_2L][Al_2Cl_7]$ where L is: a) pyridine, b) 2-picoline, c) 3-picoline, d) 4-picoline, e) 2-fluoropyridine, f) 3-fluoropyridine (DMSO Capillary)

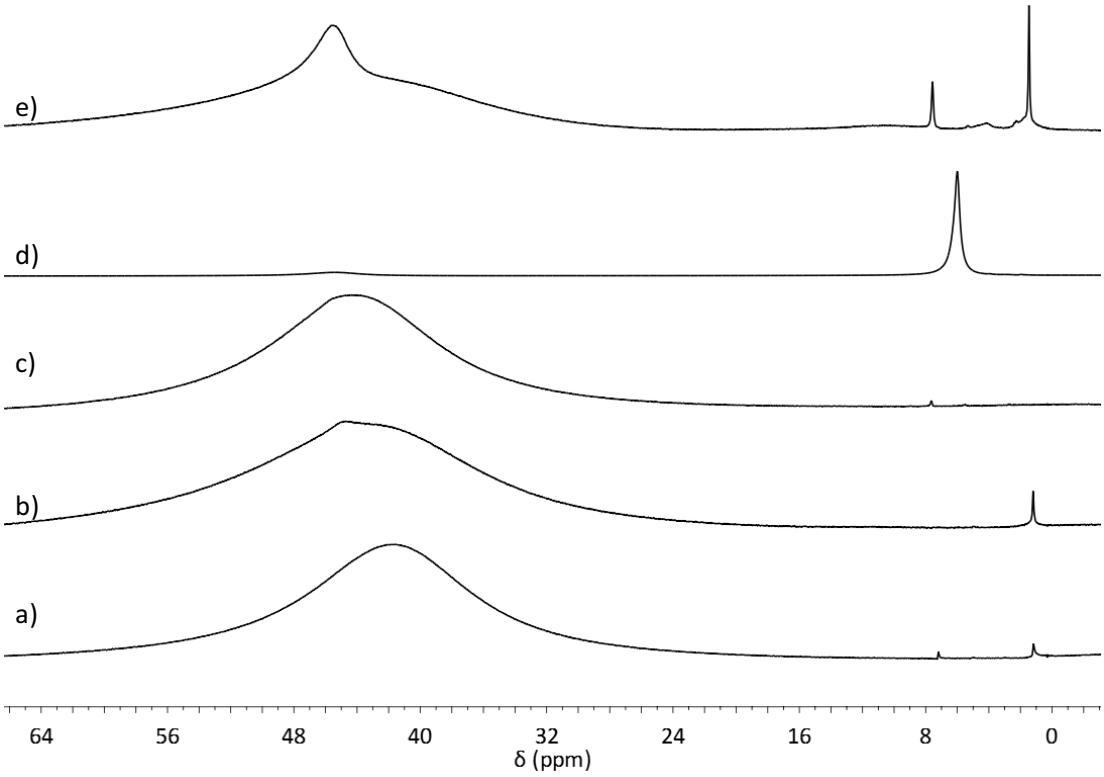

Figure 2.2-14: ^{11}B NMR spectra of $[BCl_2L][Ga_2Cl_7]$ where L is: a) pyridine, b) 3-picoline, c) 4-picoline, d) 2-fluoropyridine, e) 3-fluoropyridine (DMSO Capillary)

It has been reported that ligand scrambling is a common occurrence upon addition of a halide extracting agent to a tetracoordinate boron adduct (Figure 2.2-14).[186,191] The sharpness of the 47 ppm peak in the ^{11}B NMR spectra appears at the same chemical shift irrespective of other components of the system (metal, *N*-donor), therefore, it is most likely originating from BCl_3.

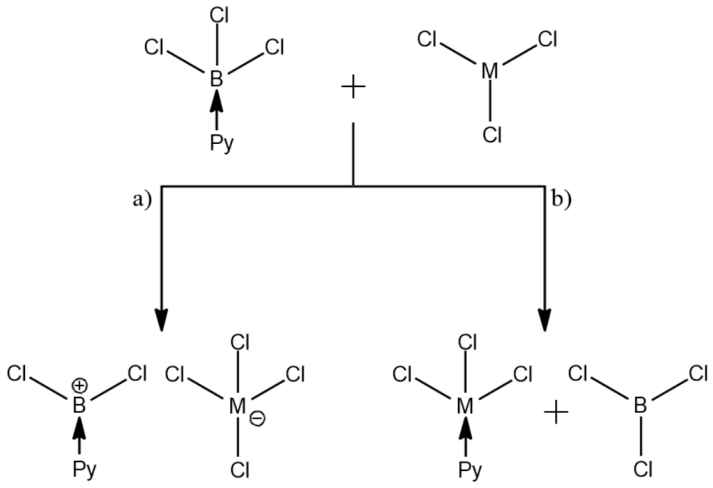

Figure 2.2-15 Possible reaction pathways for the addition of a halide extracting agent to tetracoordinate boron adducts

The preferred reaction pathway depends on the lability of pyridine *vs*. the chloride, which in turn is determined by the sigma donation from the pyridine to the boron. As the fluorine atom has a high electronegativity it will decrease the strength of the electron donation to the boron, and thus makes pathway Figure 2.2-15-b more competitive against pathway Figure 2.2-15-a. The final (thermodynamic) speciation depends also upon the relative affinity of the two competing Lewis acids for the donor. It appears that the stronger preference for the pathway Figure 2.2-14-b, leading to ligand transfer to MCl_3 and generation of BCl_3, is found in combination of fluorinated ligand and $GaCl_3$ as halide abstracting agent - *viz*. the ^{11}B NMR spectrum of $[BCl_2(3Fpy)][Ga_2Cl_7]$ (Figure 2.2-14-e).

To additionally confirm this assignment, vacuum was applied to a sample of $[BCl_2(3Fpy)][Ga_2Cl_7]$ (50 °C, < 1 mbar, 24 h). Evaporation of a gas was seen immediately upon the application of vacuum. Subsequently, ^{11}B NMR spectrum of the sample was recorded (Figure 2.2-16). The peak associated with BCl_3 had completely diminished, with some sharp peaks visible in the tetracoordinate region.

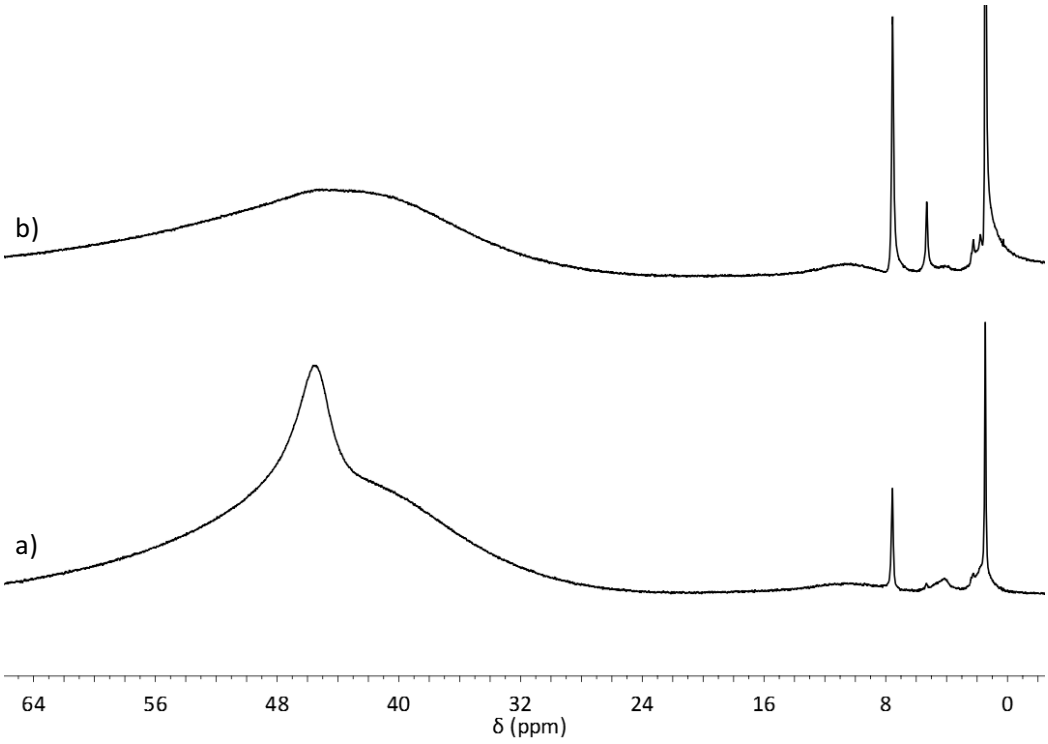

Figure 2.2-16: ^{11}B NMR spectrum of $[BCl_2(3Fpy)][Ga_2Cl_7]$ a) before and b) after application of a vacuum

The ^{27}Al NMR spectra for the non-fluorinated compounds and $[BCl_2(3FPy)][Al_2Cl_7]$ (Figure 2.2-17-a-d and e) show broad signals centred around *ca.* 103 ppm, which is indicative of the dimeric anion $[Al_2Cl_7]^-$. The peaks are less than perfectly Lorenztian, with a shoulder around *ca.* 70 ppm, originating from the NMR probe (see Chapter 2.1.2.4.3, Figure 2.1-6). In the spectrum

of $[BCl_2(2Fpy)][Al_2Cl_7]$ (Figure 2.2-17-e), the signal due to the chloroaluminate anion is significantly more broad and the probe peak is also more prominent (due to the broadness, and thus lower intensity, of the main signal). This indicates ligand transfer and equilibria even more complex than in other systems.

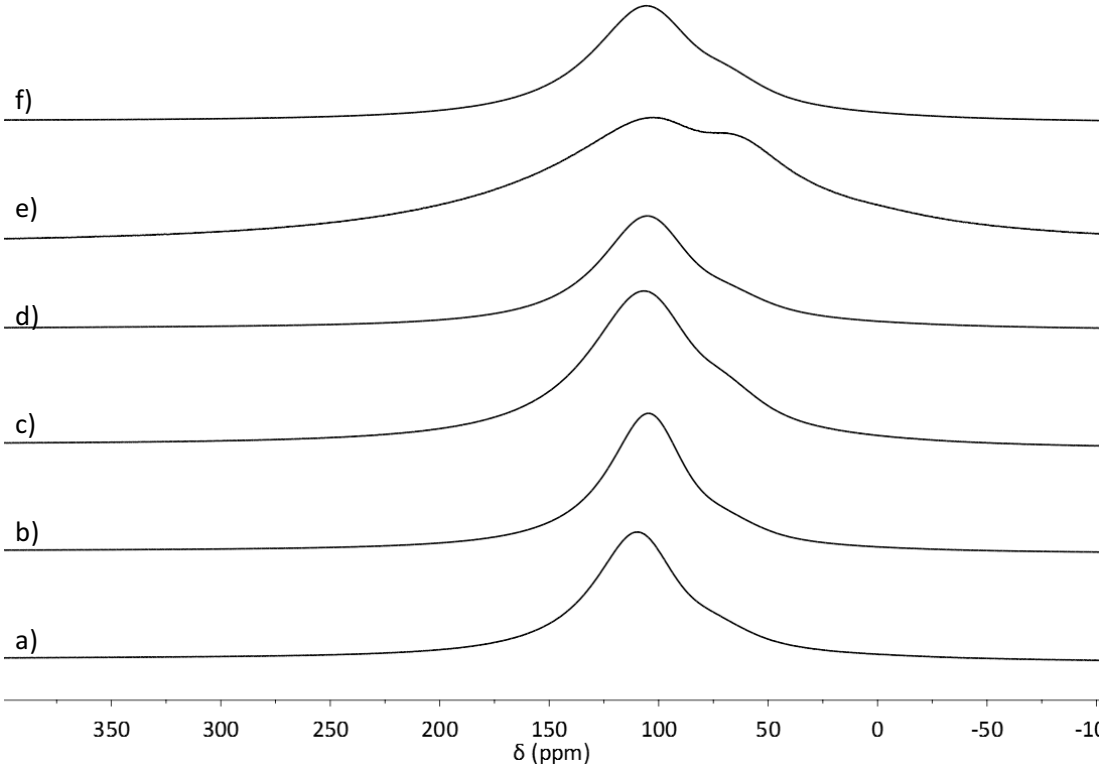

Figure 2.2-17: ^{27}Al NMR spectra of $[BCl_2L][Al_2Cl_7]$ where L is: a) pyridine, b) 2-picoline, c) 3-picoline, d) 4-picoline, e) 2-fluoropyridine, f) 3-fluoropyridine (DMSO Capillary)

The ^{19}F NMR spectra of the BCl_3(*n*Fpy)-MCl_3 mixtures are displayed in Figure 2.2-18. For $[BCl_2(2Fpy)][Al_2Cl_7]$ and $[BCl_2(2Fpy)][Ga_2Cl_7]$ there are 2 signals present with the second signal being significantly smaller for the later liquid (Figure 2.2-18-a and b). This is consistent with the patterns seen in the ^{1}H spectrum of the liquids (Figure 2.2-9-e and Figure 2.2-10-d) where the impurities were considerably smaller for $[BCl_2(2Fpy)][Ga_2Cl_7]$, reinforcing the view that ligand scrambling has taken place.

$[BCl_2(3Fpy)][Al_2Cl_7]$ and $[BCl_2(3Fpy)][Ga_2Cl_7]$ show a main signal at -110.17 and -111.28 ppm respectively, and minor impurities in their ^{19}F NMR spectra (Figure 2.2-18-c and d). The chemical shift is similar to the downfield shift in the ^{19}F NMR spectrum of $[BCl_3(3Fpy)]$ (Figure 2.2-8-d), which reinforces the view that the ligand is rearranging. The smaller impurities peaks are consistent with the ratios seen between the main peak and impurities in the ^{1}H NMR spectra of the liquids (Figure 2.2-9-f and Figure 2.2-10-e) with a higher proportion being seen in both spectra for $[BCl_2(3Fpy)][Ga_2Cl_7]$.

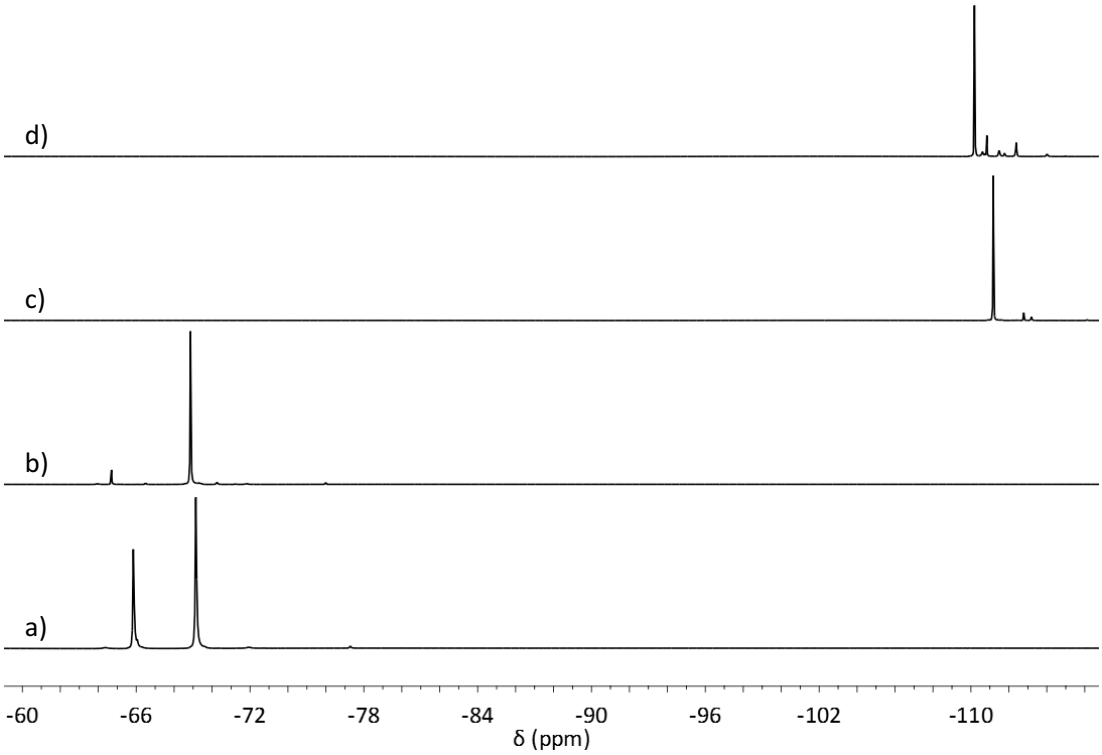

Figure 2.2-18: ^{19}F NMR spectra of fluorinated pyridine compounds: a) $[BCl_2(2Fpy)][Al_2Cl_7]$, b) $[BCl_2(2Fpy)][Ga_2Cl_7]$, c) $[BCl_2(3Fpy)][Al_2Cl_7]$, d) $[BCl_2(3Fpy)][Ga_2Cl_7]$

Table 2.2-3 summaries the main peaks in the ^{11}B and ^{27}Al NMR spectra of adducts and ionic liquids discussed in this section. In most cases these peaks are attributed to three species: $[BCl_3L]$, $[BCl_2L]^+$ and $[Al_2Cl_7]^-$. Additional peaks in the NMR spectra of the 2pic-BCl_3 mixture were attributed to the equilibrium described in Equation 2.2-6. The fluoropyridines were found to be unsuitable as donors for the synthesis of borenium ionic liquids, due to solid side-products precipitating, and ligand decomposition.

Table 2.2-3: ^{11}B and $^{27}AlCl_3$ chemical shifts for pyridine-boron trichloride adducts ($CDCl_3$) and borenium ionic liquids synthesised (neat, DMSO capillary)

Ligand	$[BCl_2(L)]$ $\delta^{11}B$ (ppm)	$[BCl_2(L)][Al_2Cl_7]$ $\delta^{11}B$ (ppm)	$[BCl_2(L)][Al_2Cl_7]$ $\delta^{27}Al$ (ppm)	$[BCl_2(L)][Ga_2Cl_7]$ $\delta^{11}B$ (ppm)
py	8.72	48.79	106.43	41.85
2pic	8.65, 7.11	45.00	104.89	-
3pic	8.62	45.67	106.30	44.69, 43.10
4pic	8.50	44.41	102.59	42.55
2Fpy	7.80	6.21	103.75, 65.38	45.36, 6.00
3Fpy	8.70	45.27, 40.39, 7.40	103.72	45.63, 42.85, 7.57

2.2.3.3 Gutmann AN measurements

Guttmann acceptor numbers were measured for borenium ionic of interest for further catalytic studies and industrial implementation, namely $[BCl_2(py)][Al_2Cl_7]$ and $[BCl_2(3pic)][Al_2Cl_7]$. For the sake of academic interest, also analogues with $[Ga_2Cl_7]^-$ and

$[Ga_3Cl_{10}]^-$ anions were studied, although their prices would be prohibitive in terms of large-scale application.

Two major peaks were observed in the ^{31}P NMR spectra (Figure 2.2-19). The upfield peak was assigned to $P_{222}O$ adduct with the chlorometallate counter anion, with AN values in good agreement with the literature for chloroaluminate ionic liquids.[24, 25] The downfield shift was assigned to $P_{222}O$ adduct with a borenium cation. Interestingly, the peak associated with $[Al_2Cl_7]^-$ anion was larger than that that associated with the $[BCl_2L]^+$ peak (Figure 2.2-19), despite the higher Lewis acidity of the later. To check whether this was thermodynamic distribution, or whether it was kinetic, samples of $[BCl_2(3pic)][Al_2Cl_7]$ with 1, 2 and 3 wt% $P_{222}O$ were measured again, after a fortnight. The ^{31}P NMR peak associated with $[BCl_2L]^+$ increased at the expense of the peak associated with $[Al_2Cl_7]^-$ suggesting that the original peak distribution was a kinetic phenomenon, and that the thermodynamically preferred product is $[BCl_2L(P_{222}O)]^+$.

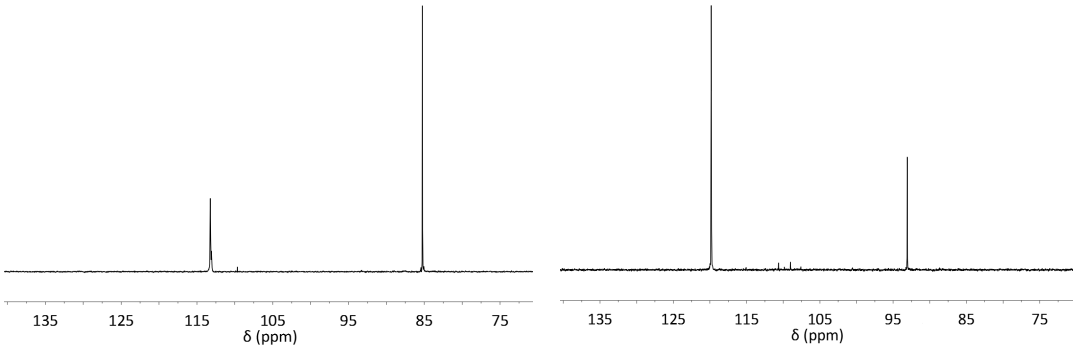

Figure 2.2-19: Typical spectra for Gutmann acceptor measurements. Left: $[BCl_2(3pic)][Al_2Cl_7]$, 1wt% $P_{222}O$, right: $[BCl_2(3pic)][Ga_3Cl_{10}]$ 1wt% $P_{222}O$

The AN values for the $[BCl_2L]^+$ cations were found to be exceptionally high (Table 2.2-4), typically in the range 130 - 185, depending on the degree of interaction of the borenium cation with counteranion. For example, the AN value of 133.70 was recorded for $[BCl_2(py)][Ga_2Cl_7]$, but a much higher value AN of 180.40 was recorded for $[BCl_2(py)][Ga_3Cl_{10}]$. Similarly, AN values of 134.75 and 181.59 were measured $[BCl_2(3pic)][Ga_2Cl_7]$ and $[BCl_2(3pic)][Ga_3Cl_{10}]$, respectively. Intermediate AN values of 161.97 and 169.68 were recorded for $[BCl_2(py)][Al_2Cl_7]$ and $[BCl_2\ 3pic][Al_2Cl_7]$, respectively. This suggests that the strength of cation-anion interaction decreased in order: $[Ga_2Cl_7]^- > [Al_2Cl_7]^- > [Ga_3Cl_{10}]^-$.

Table 2.2-4: Acceptor number values of selected borenium ionic liquids

Ionic liquid	Solvent	$\delta^{31}P$ $[BCl_2L]^+$	AN $[BCl_2L]^+$	$\delta^{31}P$ $[M_nCl_{3n+1}]^-$	AN $[M_nCl_{3n+1}]^-$
$[BCl_2(py)][Al_2Cl_7]$	-	109.56	161.97	85.32	99.76
$[BCl_2py][Ga_2Cl_7]$	-	99.89	133.70	93.33	118.22
$[BCl_2py][Ga_3Cl_{10}]$	-	119.16	180.40	93.33	118.23
$[BCl_2 3pic][Al_2Cl_7]$	-	113.24	169.68	85.25	99.53
$[BCl_2 3pic][Ga_2Cl_7]$	-	99.64	134.57	93.09	117.65
$[BCl_2 3pic][Ga_3Cl_{10}]$	-	119.82	181.59	93.08	117.63
$[BCl_2 3pic][Al_2Cl_7]$	MeCN	95.96	124.45	85.24	99.88
$[BCl_2 3pic][Al_2Cl_7]$	DCM	94.86	122.46	84.37	97.71

The AN values were found to be significantly higher than others reported in the literature for borenium cations. As literature examples of borenium cations are typically solids, acceptor numbers were recorded in solution. As such acceptor number measurements were also performed on solutions of borenium ionic liquids - to find out whether the presence of the solvent affects the effective Lewis acidity of the cation. When toluene was used as a solvent for $[BCl_2(3pic)][Al_2Cl_7]$, a significant colouration of the solution occurred, and eventually a second liquid phase-separated from the solution. In contrast, DCM and MeCN dissolved the ionic liquid with no evidence of side reactions. The AN values measured for these solutions were considerably lower than those found for the neat ionic liquid (122.46 and 124.45 for DCM and MeCN solutions, respectively). ^{11}B NMR spectra of solutions were also recorded. In DCM, the borenium peak narrowed and shifted upfield a little, but was still consistent with a tricoordinate borenium cation (42.57 ppm for the DCM solution *vs*. 45.67 ppm for neat ionic liquid). As expected from coordinating ability of acetonitrile, in MeCN only tetracoordinate species were present. Nevertheless, a relatively high acceptor number indicates lability of MeCN as a ligand, suggesting the presence of "*masked borenium cations*".[16,205] In conclusion from this experiment, it was shown that ionic liquid environment is crucial for retaining exceptionally high AN values.

2.2.4 Conclusions

The borenium ionic liquids presented here, of a general formula $[BCl_2L][M_2Cl_7]$, are extremely strong Lewis superacids, which gives them much potential as catalysts. They were also produced from bulk chemicals (pyridine, $AlCl_3$, BCl_3) in a simple process, which was altered to remove the use of chlorinated solvents and extremely low temperatures, making their synthesis industrially viable. Where L was a non-fluorinated pyridine, the borenium ionic liquids were shown to form as the main product, with only small amounts of BCl_3 indicated

by the deviations from symmetrical shape in ^{11}B and ^{27}Al NMR peaks. These results were further corroborated by the work of colleagues and published in *Angew. Chem. Int. Ed*.[52]

Fluorinated pyridines proved to be unsuitable as ligands for the synthesis of borenium ionic liquids. The adduct between pentafluoropyridine and boron trichloride did not form at all, whereas adducts and 'ionic liquids' made using 2-fluoropyridine and 3-fluoropyridine contained significant amount of impurities, suggesting possible activation of the C-F bond, which is known to occur in the presence of strong acids.[206]

Gutmann acceptor number measurements showed that the borenium ionic liquids to be extremely potent Lewis acids with acceptor numbers in the range of AN = 130 – 180, depending on the anion used, with the Lewis acidity of the borenium cation increasing in the following order: $[Ga_2Cl_7]^-$ < $[Al_2Cl_7]^-$ < $[Ga_3Cl_{10}]^-$. For borenium ionic liquid measured in solvents (DCM, MeCN), lower AN values were measured, comparable to the literature values for solid borenium cations in solution. It has been explicitly demonstrated that ionic liquid environment is crucial for retaining exceptionally high AN values.

The borenium ionic liquids present here rely on the use of chlorometallate anions, which themselves can also be highly Lewis acidic and may affect catalysis. It may be of further interest to see if these anions can be replaced with other non-coordinating non-Lewis acidic anions. A number of such anions exist[152] (*e.g.* OTf, NTf_2), but their price, as well as high degree of fluorination, make them prohibitive for industrial use, both for economic and regulatory reasons.

2.3 Stibenium(III) ionic liquids

In addition to the two core groups of Lewis acidic liquids developed, discussed in Chapter 2.1 and Chapter 2.2, some exploratory research has been carried out into potential liquid Lewis acids based on main group elements other than those found in Group 13. Some recent reports on the chemistry of antimony(III) and antimony(V), mainly the work of Burford and co-workers, suggested that it would lend itself to the preparation of Lewis acidic cations. The synthetic approach adopted followed that described for borenium ionic liquids (Chapter 2.2), with the formation of $[SbCl_xL]$ adduct, followed by a halide abstraction to form an ionic liquid with antimony-based cation.

2.3.1 Literature review

Antimony has access to many oxidation states of with +3 and +5 are the most common. There are literature examples of cations of both oxidation states. Burford and co-workers synthesised the cationic antimony complex $[Sb^{V}Ph_4][OTf]$[207] and the dicationic complex $[Sb^{V}Ph_3][OTf]_2$[208] by addition of Ag[OTf] to $Sb^{V}Ph_4Br$ and $Sb^{V}Ph_3Cl_2$ respectively, which were reacted with a variety of ligands. From the solid state structures the cation anion interaction was found to be dependent upon the ligands used to displace the triflate. Phosphine oxide ligands formed pentacoordinate cationic species with limited interaction with the anion. Conversely both mono and bidentate *N*- donor ligands formed a hexacoordinate cationic species with a closely associated triflate anion. The authors attribute this to the steric requirements of the differing ligands. Phosphine ligands were found to reduce the antimony complex according to Equation 2.3-1.

$$[Sb^{V}Ph_3(OTf)_2] + 2PR_3 \rightarrow [R_3P\text{-}PR_3][OTf]_2 + SbPh_3 \quad \text{Equation 2.3-1}$$
R = Me, nPr

Singhal and co-workers synthesised cationic antimony(V) complexes of the general formula $[(Sb^{V}(C_6F_5)_2L_3][X_3]$ where L = DMSO, 2,3 or 4-pyridine, triphenylarsine oxide, or DMF and X = $[BF_4]^-$ or $[BPh_4]^-$. The complexes were reported to be stable under oxygen and moisture free conditions. The molar conductivity was measured and matched well with literature values of 1:3 electrolytes suggesting no short contacts between the cation and anion and thus a vacant coordination site on the Lewis acid.

Gabbai and co-workers reported the synthesis of an antimony (V) cation of the formula $[SbPh_3Ar]^+$ where Ar = = 9-phenanthryl, 1-pyrenyl or 3-peryleny. The latter two were stable in water and were successfully used a fluoride ion sensors. The cation saw an marked increase in its fluorescence when a fluoride anion was bonded, allowing detection down to ppm level and below in H_2O/DMSO (9:1) solutions.[209]

Antimony(III) chloride is known to react with typical ionic liquid precursors (*i.e*. nitrogen-containing heterocycles) to form stibine(III) anions. Such chemistry is typically carried out in concentrated hydrochloric acid solutions. Jacobson reported the reaction of pyridine and antimony(III) chloride, in a concentrated HCl solution, where $[PyH][SbCl_4]$ was precipitated from the post-reaction mixture.[210] It was shown that, instead of monomeric or oligomeric anions, antimony(III) chloride formed a polymeric network with two bridging chlorides between each antimony atom,[211] which naturally led to the formation of crystalline materials, rather than ionic liquids. Similar results have been reported by Bujak for the

reaction of imidazole with $SbCl_3$ in a 1 : 2 ratio, in concentrated hydrochloric acid, resulting in the formation of [Him][$SbCl_4$].[212] In both cases, the geometry of the chlorines surrounding the central antimony atom was reported to be near-octahedral, with Bujak's paper reporting a "*zig-zag*" structure (Figure 2.3-1).

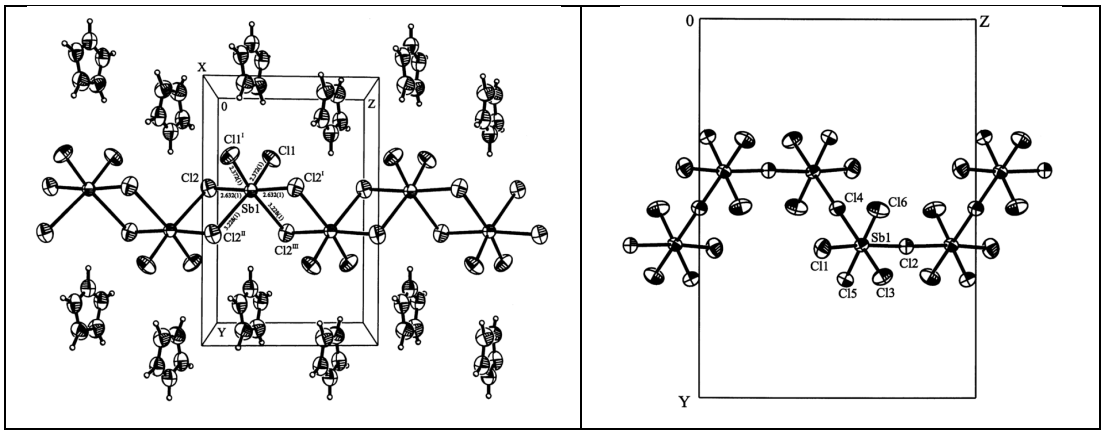

Figure 2.3-1: Crystal structure of [Him]][$SbCl_4$] (left) and [Him]$_2$[$SbCl_5$] (right) showing polymeric network of antimony ions[212]

Bujak *et al.* reported that, by varying the ratio of $SbCl_3$ to the amine, different anions could be formed. At a 7:1 molar ratio of imidazole reacted with $SbCl_3$ to form [Him]$_2$[$SbCl_5$]. Again, an extended polymeric lattice of antimony anions was seen, but only one chloride was bridging between two antimony ions. The cation volume is another factor governing anionic speciation in the solid state: when [C_4C_1im]Cl was reacted with $SbCl_3$, at χ_{SbCl3} = 0.33, discrete $[SbCl_5]^{2-}$ anions were reported, each surrounded by six $[C_4C_1im]^+$ cations.[213]

Reid *et al.* reacted antimony(III) chloride with bidentate phosphine and arsine ligands, which led to the formation of discrete neutral dimers, with two bridging chlorine atoms..[214] Adducts of antimony(III) halide with tricylclohexylphosphine chalcogenide were synthesised by Burford *et al*.[215] Products were dependent on reactant ratio: when the Ph_3PE (E = O, S) was reacted with $SbCl_3$ at χ_{SbCl3} = 0.50, dimeric units were formed, whereas at χ_{SbCl3} = 0.33, monomeric units were seen.

Seemingly from the literature, it is strongly favourable for antimony(III) to share chlorine atoms with its neighbours, resulting in highly crystalline, relatively chemically stable compounds, thus precluding the formation of vacant sites required for Lewis acidity. Nevertheless, Burford and co-workers[216,217] reported quite recently on the synthesis and chemistry of phosphine-coordinated antimony(III) chloride cations, in which chloride ions can

be readily extracted by aluminium(III) chloride or trimethylsilyl triflate to yield antimony(III) cations (Figure 2.3-2).

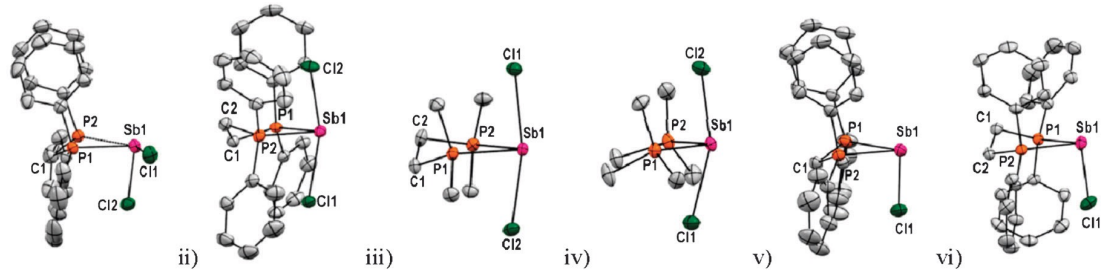

Figure 2.3-2: Crystal structures of cationic Sb(III)-phosphine adducts, with $[AlCl_4]^-$ (i, ii, v), $[CF_3SO_3]^-$ (iii, iv) or $[Al_2Cl_7]^-$ (vi) as the counteranion[216]

Even more recently, it was reported that catenation reactions can readily occur when phosphorous and antimony are directly bonded.[217] Nevertheless, analogies with the synthesis of borenium ionic liquids suggested that it is worthwhile to explore the possibility of synthesising ionic liquids with such Sb(III) cations.

2.3.2 Experimental

2.3.2.1 Materials and methods

All preparations were performed in a glovebox (MBraun labmaster dp, <0.3 ppm of H_2O and O_2) or using standard Schlenk techniques with a vacuum and an argon line. All glassware was dried overnight (*ca.* 100 °C) before use.

Antimony(V) pentachloride (99%), antimony(III) chloride (99.99%) and trimethylsily-trifluromethanesulfonate (99%) were purchased from Sigma Aldrich and used as received.

2.3.2.2 Synthesis of ionic liquids with antimony(V) cations

Antimony(V) chloride (1 g, 3.34 mmol, 1 mol eq.) was weighed out in the glovebox into a pre-dried airtight syringe and transferred, by dropwise addition over 10 mins, to an argon-purged round-bottomed flask containing DCM (20 ml) and the ligand (3 mmol, 0.9 mol eq). The reaction was stirred for 1 h before removal of the solvent under reduced pressure and the resulting liquid was stored in the glovebox. To the resulting liquid, $AlCl_3$ (0.40 g, 3 mmol, 0.9 mol eq.) was added in small aliquots of 0.1 g. All products were analysed by ^1H and ^{31}P NMR.

2.3.2.3 Synthesis of ionic liquids with antimony(III) cations

For the ionic liquids with the chloroaluminate anions, antimony trichloride (0.3828 g, 1.68 mmol, 1 mol eq.) was weighed out in the glovebox into a glass vial and the desired ligand was added (3.36 mmol, 2 mol eq.). The reaction was stirred for overnight yielding a viscous liquid. To the resulting liquid, $AlCl_3$ (0.2240 g, 1.68 mmol, 1 mol eq. or 0.4480 g, 3.36 mmol, 2 mol eq.) was added in small aliquots, and allowed to stir until complete dissolution of the $AlCl_3$ was achieved.

For the ionic liquids with the triflate anion, antimony trichloride (0.3828 g, 1.68 mmol, 1 mol eq.) was dissolved in DCM (20 ml) to which the desired ligand (3.36 mmol, 2 mol eq.) was added. The reaction was stirred for 1 h before the dropwise addition of trimethylsilyl trifluoromethanesulfonate (0.3730 g, 1.68 mmol, 1 mol eq.) over 20 mins. The reaction was stirred for a further 2 h before the volatiles were removed under reduced pressure (60 °C, < 1 mbar, 12 h). The resulting liquid was transferred to the glovebox for storage.

For the large scale preparation of $[SbCl_2(P_{888}O)_2][OTf]$, the reaction did not go to completion using above conditions. As such trimethylsilyl trifluoromethanesulfonate (1.816 g, 8.17 mmol) was combined with $SbCl_3$ (1.86 g, 8.17 mmol) in DCM (30 ml), which were left to react for 5 h, before $P_{888}O$ in DCM was added dropwise (6.32 g, 16.34 mmol in 20 ml). Following extremely slow addition (5 h), the volatiles were removed under reduced pressure (60 °C, < 1 mbar, 12 h). The resulting liquid was transferred to the glovebox for storage. All products were analysed by ^{1}H, and ^{31}P NMR spectroscopy and where appropriate ^{13}C and ^{27}Al NMR and FT-IR spectroscopy also.

2.3.3 Results and discussion

2.3.3.1 Ionic liquids with antimony (V) cations

2.3.3.1.1 Synthesis and analysis of $P_{888}E$-$SbCl_5$ adducts

The first synthetic strategy was following on from that adopted from the synthesis of LCCs: in a glovebox, neat $SbCl_5$ (which is liquid at room temperature) was reacted with neat ligands, which were added slowly, in small portions. This resulted in dark coloured liquids with black particulates. More successful synthesis were carried out in dry dichloromethane, on a Schlenk line, with slow addition of $SbCl_5$ to a ligand solution.

In order to obtain liquids, rather than solids, three ligands with long alkyl chains were screened: P_{888}, $P_{888}O$ and $P_{888}S$, following a successful approach used for LCC design. All products formed liquids of varying appearance: P_{888}-$SbCl_5$ - light yellow liquid, $P_{888}O$-$SbCl_5$ - golden liquid, and $P_{888}S$-$SbCl_5$ - dark liquid with yellow precipitate.

^{1}H and ^{13}C NMR spectra of the products were not very informative, aside from expected downfield shifts in some signals, indicating complexation of the ligand by the antimony centre. ^{31}P NMR spectroscopy, in contrast, was the main source of structural information, in some instances supported with FT-IR spectroscopy.

^{31}P NMR of both the starting materials and the complexes are compared in Figure 2.3-3. For the ease of comparison, all ^{31}P NMR shifts are tabulated in Table 2.1-3. For all ligands, a large downfield shift at the phosphorous centre is seen upon complexation, indicative of loss of electron density on the phosphorous atom.

Among the three products, elucidating the speciation of $SbCl_5$-$P_{888}O$ adduct was the simplest task. The difference in ^{31}P NMR chemical shift between free $P_{888}O$ ligand (Figure 2.3-3-c) and the $SbCl_5$-$P_{888}O$ adduct (Figure 2.3-3-d) was $\Delta\delta$ = 30.95 ppm, consistent with other previously reported phosphine oxide antimony pentachloride complexes.[218] This corroborates with red-shift in the vibrational frequency of the P=O bond, from 1144.9 cm^{-1} in neat $P_{888}O$ to 1030.0 cm^{-1} in $SbCl_5$-$P_{888}O$. The magnitude of the red-shift, $\Delta\nu_{P=O}$ = 114.9 cm^{-1}, was comparable to that reported previously for the $[SbCl_5(P_{111}O)]$ complex.[218] This suggests that the $[SbCl_5(P_{888}O)]$ complex was formed readily and without side reactions.

The ^{31}P NMR signal from the mixture of $SbCl_5$ and P_{888} (Figure 2.3-3-b) shows a very large downfield shift compared to the free ligand (Figure 2.3-3-a), $\Delta\delta$ = 134.23 ppm, well beyond that expected for a complexed phosphine (-50 – 20 ppm).[145] A plausible explanation was found by looking into the reactivity of $Sn^{IV}X_4$ and phosphines, where redox chemistry occurred, resulting in the formation of $[R_3P^{V}X][Sn^{II}X_3]$.[219] The formation of cations such as $[Ph_3PI]^+$ and $[Ph_3PBr]^+$ resulted in significant upfield shift in ^{31}P NMR shifts, as seen here. It is plausible that $SbCl_5$ could be reduced in a similar fashion, as reductive catenation of antimony(III)-phosphine complexes is known in the literature.[217] The ^{31}P NMR signal at ppm (Figure 2.3-3-b) indeed matches the chemical shift for $[P_{888}Cl]^+$, which when synthesised[220] had a signal at 103.95 ppm. There are also two trace peaks at 67.75 and 11.10 ppm. The former is likely a phosphine oxide impurity, present in the P_{888} starting material. The latter is in the region for phosphine coordination compounds and most likely represents a trace of the unstable

[$SbCl_5(P_{888})$] complex. In conclusion, the reaction of $SbCl_5$ and P_{888} proceeds following Equation 2.3-2, yielding as a matter of fact a chloroantimonate(III) ionic liquid.

$$Sb^{V}Cl_5 + P^{III}{}_{888} \longrightarrow [Sb^{V}Cl_5(P^{III}{}_{888})] \longrightarrow [P^{V}{}_{888}Cl][Sb^{III}Cl_4] \qquad \text{Equation 2.3-2}$$

The product of a reaction of $P_{888}S$ and $SbCl_5$ was a liquid with a yellow precipitate. The ^{31}P NMR spectrum of the liquid was remarkably similar to that of the trioctylphosphine reaction with $SbCl_5$ (compare Figure 2.3-3-b and Figure 2.3-3-f), suggesting reduction of the ligand, and subsequent oxidation to $[P_{888}Cl]^+$. Elemental analysis of the liquid revealed 0.44% of sulphur, compared to 51.80% sulphur in the solid, confirming this hypothesis. Interestingly, Reid and co-workers did not report this occurring for the complex [$SbCl_5(Ph_3PS)$], but they did see selenium precipitate from Ph_3PSe-$SbCl_5$ mixtures.[218]

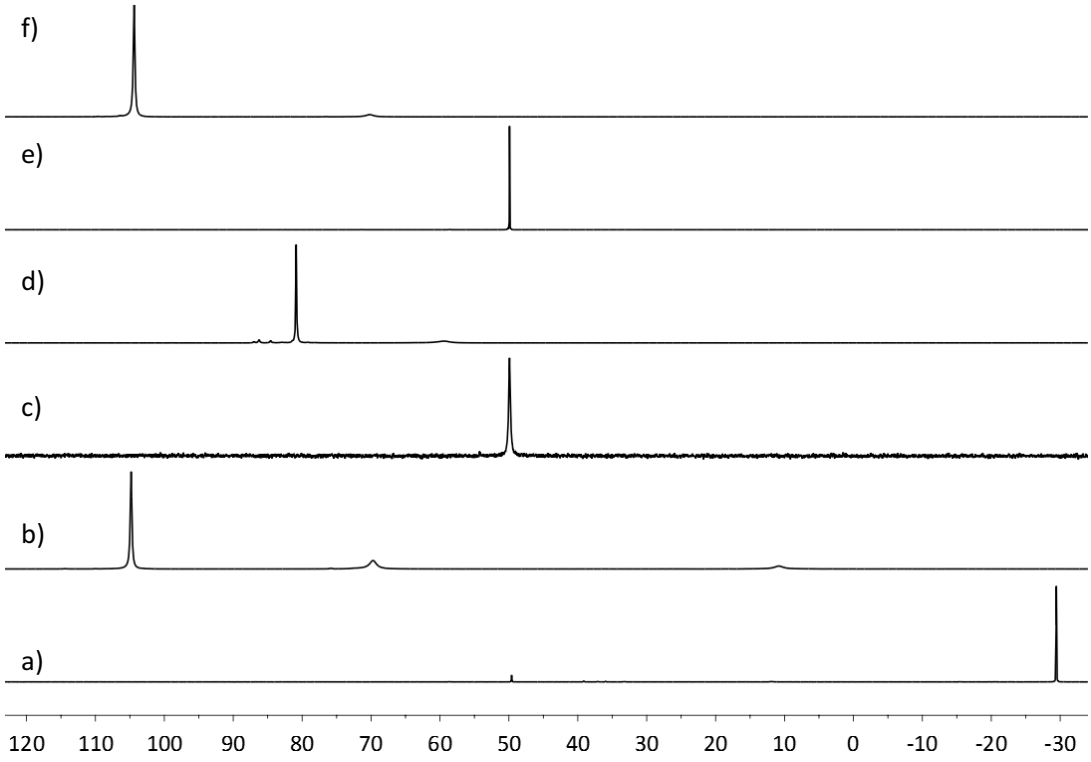

Figure 2.3-3: ^{31}P NMR spectra of a) P_{888}, b) $SbCl_5$-P_{888} , c) $P_{888}O$, d) [$SbCl_5(P_{888}O)$], e) $P_{888}S$, f) $SbCl_5$-$P_{888}S$

Table 2.3-1: ^{31}P NMR data for antimony(V)-phosphine mixtures

Compound	δ ^{31}P / ppm	$\Delta\delta$ ^{31}P / ppm[(a)]
$SbCl_5$-P_{888}	104.82	134.23
[$SbCl_5(P_{888}O)$]	80.86	30.95
$SbCl_5$-$P_{888}S$	104.38	54.47

(a) $\Delta\delta\,^{31}P = \delta\,^{31}P$ (complex) - $\delta\,^{31}P$ (ligand) referenced to the appropriate solvent

In conclusion, out of three studied ligands, the only stable adduct was formed from $SbCl_5$ reacting with trioctylphosphine oxide. This adduct was used for the next synthetic step.

2.3.3.1.2 Synthesis and analysis of $P_{888}E$-$SbCl_5$-$AlCl_3$ ionic liquid

The adduct [$SbCl_5(P_{888}O)$] was reacted with 1 mol eq. of $AlCl_3$. This resulted in vigorous bubbling and simultaneous production of a hard black solid, which was not readily soluble in any available NMR solvents. This suggests that $SbCl_5$ was reduced to antimony black and/or that the organic portion of the complex was carbonised.

In conclusion, the only ionic liquid produced in this part of work was, unexpectedly, [$P_{888}Cl$][$SbCl_4$]. The ionic phosphorous [PR_3Cl]Cl was previously shown to be a part of a catalytic cycle to substitute alcohol functionality with chloride functionality.[220]

2.3.3.2 Ionic liquids with antimony (III) cations

2.3.3.2.1 Synthesis and analysis of $P_{888}E$-$SbCl_3$ adducts

Antimony(III) trichloride reacted with trioctylphosphine, trioctylphosphine oxide and trioctylphosphine sulphide, at χ_{SbCl3} = 0.33, to give a bright yellow liquid, a colourless liquid, and a yellow viscous liquid, respectively. Again, ^{1}H and ^{13}C NMR spectra of the products were not very informative. Each ligand and adduct was analysed by ^{31}P NMR spectroscopy to reveal a downfield shift upon complexation with $SbCl_3$ (Table 2.3-2). FT-IR spectra were recorded for phosphine chalcogenides $P_{888}E$ (E = O, S) and for their adducts with $SbCl_3$. Stretching frequencies of the relevant P=E bonds are listed in Table 2.3-3.

Table 2.3-2: ^{31}P NMR chemical shifts recorded for the phosphine chalcogenide ligands, their adducts with $SbCl_3$ and ionic liquids

Compound	δ ^{31}P / ppm	$\Delta\delta$ ^{31}P / ppm[(a)]	Solvent
P_{888}	-29.41		
$[SbCl_3(P_{888})_2]$	-3.05	26.39	-
$[SbCl_2(P_{888})_2][AlCl_4]$	25.84	55.29	-
$[SbCl_3(P_{888})_2]$-$2AlCl_3$	31.35, 28.27, -24.21	-	-
$[SbCl_3(P_{888})_2][OTf]$	21.01	50.46	-
$P_{888}O$	49.91	-	$CDCl_3$
$[SbCl_3(P_{888}O)_2]$	58.67	8.76	-
$[SbCl_3(P_{888}O)_2][OTf]$	73.99	24.08	-
$P_{888}S$	49.91	-	-
$P_{888}S$	48.65	-	DCM
$[SbCl_3(P_{888}S)]$	53.93	4.02	-
$[SbCl_3(P_{888}S)]$	52.34	3.69	DCM
$[SbCl_3(P_{888}S)_2]$	50.42	0.51	-
$[SbCl_3(P_{888}S)_2]$	48.64	-0.01	DCM
$[SbCl_2(P_{888}S)_2][AlCl_4]$	56.29	6.38	-
$[SbCl_3(P_{888}S)_2]$-$2AlCl_3$	56.67, 63.06, 64.49	-	-
$[SbCl_3(P_{888}S)_2][OTf]$	55.04	5.13	-

(a) $\Delta\ \delta\ ^{31}P = \delta\ ^{31}P$ (complex) - $\delta\ ^{31}P$ (ligand) referenced to the appropriate solvent

The chemical shifts recorded for [$SbCl_3(P_{888})_2$] at -3.05 ppm (Figure 2.3-4-b) and [$SbCl_3(P_{888}O)_2$] at 58.67 ppm (Figure 2.3-6-b) were in reasonable agreement with literature values for the

corresponding adducts.[63,215] Freshly synthesised $[SbCl_3(P_{888})_2]$ did not contain any significant proportion of $[P_{888}Cl]^+$, in its ^{31}P NMR spectrum (Figure 2.3-4-b),[217] though when the sample was kept in the glovebox over the course of a fortnight, a highly deshielded peak associated with $[P_{888}Cl]^+$ was seen at *ca.* 103 ppm. Trioctylphosphine oxide also showed no significant impurities in its ^{31}P NMR spectrum (Figure 2.3-6-b). The stretching frequency of the P=O bond (Table 2.3-3) was found to be red-shifted by $\Delta\nu_{P=O}$ = 76 cm^{-1}, which indicates complexation of the ligand. In conclusion, both $[SbCl_3(P_{888})_2]$ and $[SbCl_3(P_{888}O)_2]$ were successfully synthesised.

Table 2.3-3: FT-IR stretching frequencies of the P=E bond in chalcogenide ligands, their adducts with $SbCl_3$ and ionic liquids

Compound	ν / cm^{-1}	$\Delta\nu$ / cm^{-1} (a)	Solvent
$P_{888}O$	1144.95	-	-
$[SbCl_3(P_{888}O)_2]$	1069.03	-75.92	-
$[SbCl_2(P_{888}O)_2][OTf]$	1043.67	-101.28	-
$P_{888}S$	599.36	-	-
$P_{888}S$	593.28	-	DCM
$[SbCl_3(P_{888}S)]$	563.56	-35.8	-
$[SbCl_3(P_{888}S)]$	566.49	-26.79	DCM
$[SbCl_3(P_{888}S)_2]$	571.94	-27.42	-
$[SbCl_3(P_{888}S)_2]$	569.51	-23.77	DCM
$[SbCl_2(P_{888}S)_2][AlCl_4]$	547.90	-51.46	-
$[SbCl_2(P_{888}S)_2][OTf]$	547.47	-51.89	-

(a) Δ ν = ν (complex) – ν (ligand) referenced to the appropriate solvent

The ^{31}P NMR spectrum of $[SbCl_3(P_{888}S)_2]$ was deshielded by only 0.51 ppm compared to the free ligand (Figure 2.3-8, Table 2.3-2). A similarly small shift was seen when the monophosphine sulphide complex, $[SbCl_3(Cy_3P)]$, was synthesised,[215] where the ^{31}P NMR spectrum of the complex was measured as a $CDCl_3$ solution. The authors suggested this was due to an equilibrium between the unreacted acid and base on one side, and the complex on the other, with the former being preferential in solution. The crystal structure and solid state IR spectrum confirmed the atom connectivity (*i.e.* P=S→Sb) in the solid state.[215] In this work, the complex $[SbCl_3(P_{888}S)_2]$ was studied by NMR spectroscopy as a neat liquid. Furthermore, viscosity of the $[SbCl_3(P_{888}S)_2]$ adduct was significantly higher than that of $P_{888}S$, suggesting a reaction has occurred. Rather than suggesting a dynamic equilibrium, it is postulated that the phosphorus atom is simply less affected by the change of electron density on the sulphur, due to the atoms being closer in electronegativity values, than phosphorous and oxygen are. In addition, sulphur is a weaker donor than oxygen, as evidenced by the trans Sb-Cl bond lengths measured by Burford.[215] *Ergo* it loses less electron density to antimony, and thus less electron density is drawn from the phosphorous. Hence the phosphine sulphide shows a much smaller shift compared to the phosphine oxide upon complexation.

To investigate this conundrum, complexes of two different stoichiometries: $[SbCl_3(P_{888}S)]$ and $[SbCl_3(P_{888}S)_2]$, were synthesised and studied spectroscopically as $CDCl_3$ solutions, in addition to neat liquids (Table 2.3-3). In all complexes measured, with the exception of $[SbCl_3(P_{888}S)_2]$ in DCM, a small deshielding of the ^{31}P nucleus was noted, $\Delta\delta$ = 0.51 to 6.38 ppm (Table 2.3-2), compared to free ligand in the appropriate solvent. This suggested that the acid-base adduct is favoured. $[SbCl_3(P_{888}S)_2]$ in DCM exhibited the same ^{31}P NMR chemical shift as free $P_{888}S$ in DCM. Considering small or non-existent chemical shift differences upon complexation, results from ^{31}P NMR spectroscopy were not conclusive. In contrast, comparing stretching frequencies for P=S bonds of free ligands and adducts, both in solution and neat, revealed a consistent red-shift upon complexation, $\Delta\nu_{P=S}$ = 23.77 to 35.80 cm^{-1}. This is in agreement with results reported by Burford and co-workers for similar adducts.[215] It was thus established that the complexation did occur, despite negligibly small change in ^{31}P NMR chemical shift.

2.3.3.2.2 Synthesis and analysis of ionic liquids

In order to synthesise ionic liquids with cationic $[SbCl_2L_2]^+$ cations, neat complexes were reacted with halide abstracting agents: one or two mole equivalents of $AlCl_3$, or one mole equivalent of Me_3SiOTf. The final products of the reactions were typically liquids of a similar appearance to the adduct, with a more intense colour. The product isolated from $[SbCl_3(P_{888})_2]$ reactions with 1 mol eq. of $AlCl_3$ or Me_3SiOTf were bright yellow liquids, and the product 2 mol eq. of $AlCl_3$ was a dull yellow/brown colour. With $AlCl_3$ the $[SbCl_3(P_{888}O)_2]$ complex became tinged with a yellow brown colour. The product from the reaction of $[SbCl_3(P_{888}O)_2]$ and Me_3SiOTf was a colourless clear liquid, however upon scaling up the reaction to a 10 g synthesis, the liquid left after removing the volatiles was found to be slightly cloudy and a significant impurity peak was seen in the ^{31}P NMR spectrum δ ^{31}P = 86.63 ppm which is comparable to the chemical shifts of the complexes $[Me_3Si(OPMe_3)][OTf]$ and $[Me_3Si(OPCy_3)][OTf]$.[221] As such the reaction conditions were changed as describe in Chapter 2.3.2, yielding a clear colourless liquid. The reaction of $[SbCl_3(P_{888}S)_2]$ with either 1 or 2 mole eq. of $AlCl_3$ resulted in the formation of a viscous dull yellow liquid.

^{31}P NMR spectra of P_{888}, $[SbCl_3(P_{888})_2]$, and of the three products of halide abstraction, are compared in Figure 2.3-4. The P_{888}-$AlCl_3$ χ_{AlCl3} = 0.50 LCC is also shown for comparison. The corresponding ^{27}Al NMR spectra of $[SbCl_3(P_{888})_2]$-$AlCl_3$, $[SbCl_3(P_{888})_2]$-$2AlCl_3$, and P_{888}-$AlCl_3$ χ_{AlCl3} = 0.50 LCC, are presented in Figure 2.3-5.

The ^{31}P NMR spectrum of the $[SbCl_3(P_{888})_2]$-$AlCl_3$ adduct has one clear singlet at 26.18 ppm (Figure 2.3-4-d), assigned to the cation $[SbCl_2(P_{888})_2]^+$, and the corresponding ^{27}Al NMR spectrum shows a narrow peak at 102.62 ppm (Figure 2.3-5-b), assigned to $[AlCl_4]^-$. This confirms that the ionic liquid, $[SbCl_2(P_{888})_2][AlCl_4]$, has been formed. However, there is a trace of the signal associated with $[P_{888}Cl]^+$ visible in the ^{31}P NMR spectrum at *ca.* 103 ppm, suggesting this liquid may not be redox stable over time. When exposed to heat the liquid darkened noticeably. The ^{31}P NMR spectrum of the heated sample showed a main signal at *ca.* 103 ppm, which indicates oxidation of the phosphorous, and thus reduction of the antimony (Figure 2.3-11).

The ^{31}P NMR spectrum of the $[SbCl_3(P_{888})_2]$-$2AlCl_3$ mixture features four signals (Figure 2.3-4-e): a low-intensity broad doublet at *ca*. -24.06 ppm, and three sharp signals at 28.75, 31.36 and 100.32 ppm, which integrate to 1.8:1.6:2.6:1 respectively. The broad upfield peak at -24 ppm is of a similar chemical shift as the signal in LCC P_{888}-$AlCl_3$ χ_{AlCl3} = 0.50 (Figure 2.3-4-c). Also Reid and co-workers found signals in this area of ^{31}P NMR spectrum for a variety of phosphine ligands coordinated to $AlCl_3$ complexes.[222] In contrast, phosphorus coordinated to antimony is reported to give more downfield chemical shifts.[63,216] Therefore, the signal at -24.06 ppm originates from the partial transfer of P_{888} to aluminium(III) chloride. This is supported by the corresponding ^{27}Al NMR spectrum (Figure 2.3-5-c) which shows three broad peaks at 108.84 ppm, corresponding to $AlCl_3$ with a phosphine ligand, 102.34 ppm, indicative of chloroaluminate(III) anion, and 67.99 ppm, originating from the probe (artefact, see Chapter 2.1.2.4). Broadness of the signals is indicative of chloroaluminate(III) dimers, $[Al_2Cl_6(P_{888})]$ and $[Al_2Cl_7]^-$. This matches assignments by Coleman *et al.* for P_{888}-$AlCl_3$ χ_{AlCl3} = 0.50,[135] and correlates with the P_{888}-$AlCl_3$ χ_{AlCl3} = 0.50 spectrum shown here for comparison (Figure 2.3-5-a). The ^{31}P NMR peaks at 28.75 and 31.36 ppm (Figure 2.3-4-e) are likely to originate from the species $[SbCl_2P_{888}]^+$ and $[SbCl_2(P_{888})_2]^+$, respectively, possibly in a dynamic equilibrium. Finally, the ^{31}P NMR signal at 103 ppm is attributed to $[P_{888}Cl]^+$. In conclusion, the $[SbCl_3(P_{888})_2]$-$2AlCl_3$ adduct formed a complex mixture of species; in addition to expected cation, $[SbCl_2(P_{888})_2)]^+$, and anion, $[Al_2Cl_7]^-$, there is also evidence of ligand scrambling between the metal chlorides.

The ^{31}P NMR spectrum of $[SbCl_2(P_{888})_2][OTf]$ (Figure 2.3-4-f) contained a singlet at 21.04 ppm, and a trace signal at 12.82 ppm (integrates to 0.19 of the main peak). In the corresponding ^{19}F NMR spectrum there is a singlet at -78.86 ppm, corresponding to $[OTf]^-$ anion.[217] Similarly, the ^{13}C NMR features a quartet associated with the triflate anion at 119.75 ppm, but does not show the peak associated with the Me_3SiCl at *ca.* 3 ppm. All this spectroscopic evidence

is consistent with the formation of an ionic liquid, $[SbCl_2(P_{888})_2][OTf]$. The most obvious candidate for the impurity peak in the ^{31}P NMR spectrum would be $[Me_3Si(PMe_3)][OTf]$, however, Burford *et al.* synthesised $[Me_3Si(PMe_3)][OTf]$ which had showed a singlet at -53.7 ppm in its ^{31}P NMR spectrum, ruling that out.[221]

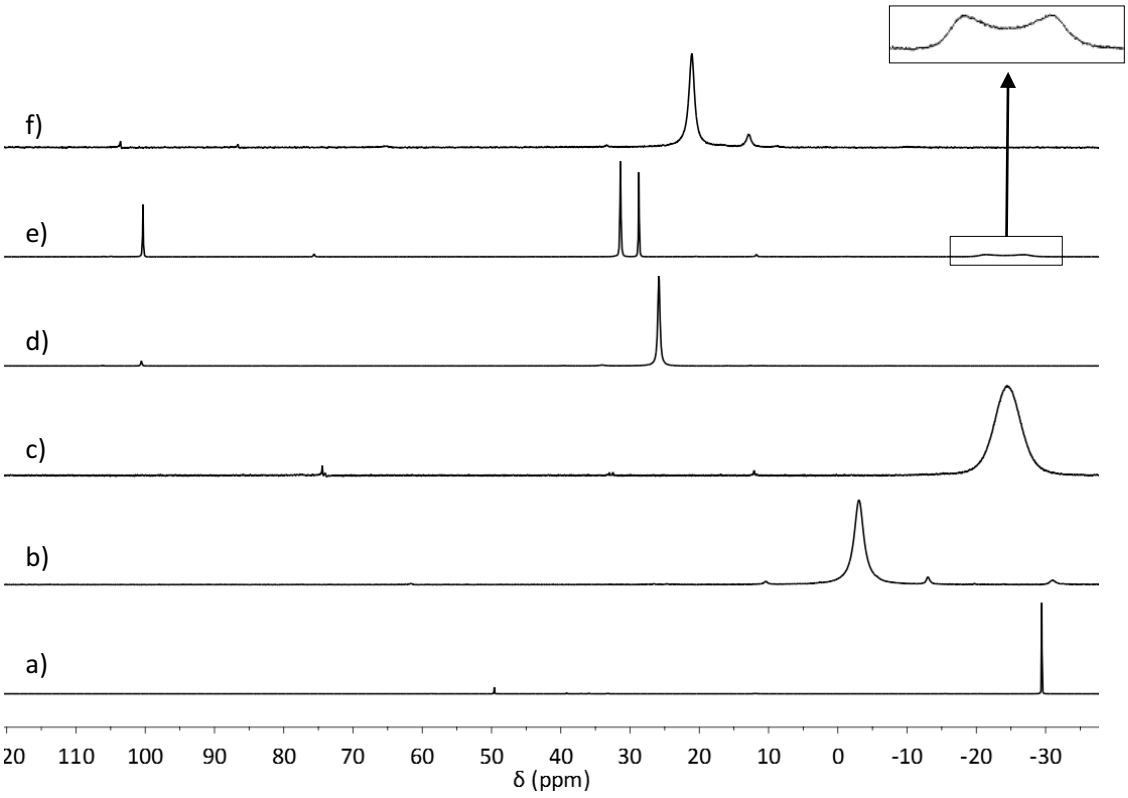

Figure 2.3-4: ^{31}P NMR spectra (neat, DMSO capillary) of a) P_{888}, b) $[SbCl_3(P_{888})_2]$, c) P_{888}-$AlCl_3$ χ_{AlCl3} = 0.50, d) $[SbCl_2(P_{888})_2][AlCl_4]$, e) $[SbCl_3(P_{888})_2]$-2$AlCl_3$ (downfield peak in the insert), and f) $[SbCl_2(P_{888})_2][OTf]$

As with $[SbCl_2(P_{888})_2][AlCl_4]$, when exposed to heat $[SbCl_2(P_{888})_2][OTf]$ darkened noticeably. The ^{31}P NMR spectrum of the heated sample showed formation of the cation $[P_{888}Cl]^+$ at *ca.* 103 ppm, indicating oxidation of the phosphorous, and thus reduction of the antimony (Figure 2.3-11).

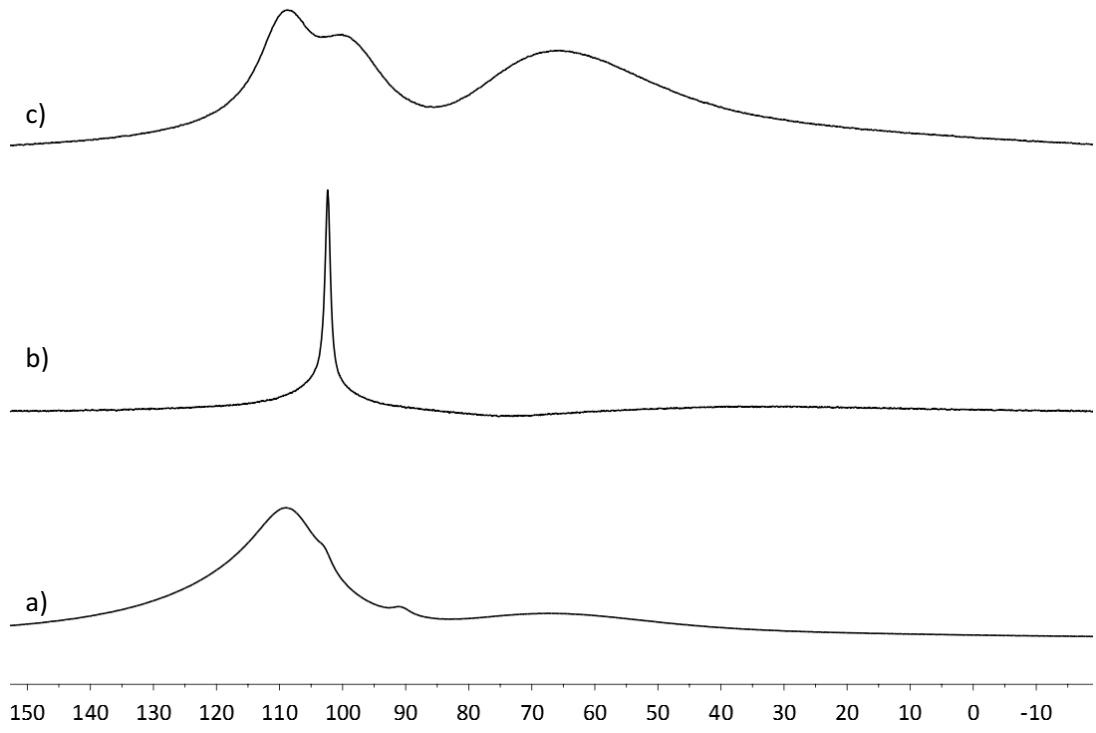

Figure 2.3-5: ^{27}Al NMR spectra (neat, DMSO capillary) of a) P_{888}-$AlCl_3$ χ_{AlCl3} = 0.5, b) $[SbCl_2(P_{888})_2][AlCl_4]$, c) $[SbCl_3(P_{888})_2]$-2$AlCl_3$

The mixture of $[SbCl_3(P_{888}O)_2]$ and $AlCl_3$ has the characteristic peak distribution of the LCC $P_{888}O$-$AlCl_3$ χ_{AlCL3} = 0.50, in both the ^{31}P NMR (Figure 2.3-6-c and Figure 2.3-6-d) and ^{27}Al NMR (Figure 2.3-7-a and Figure 2.3-7-b) spectra, indicating complete transfer of the ligand from $SbCl_3$ to the $AlCl_3$. This is unsurprising, considering high affinity of oxygen to aluminium. Interestingly, for $[SbCl_3(P_{888}O)_2]$-$AlCl_3$, the peak at 103 ppm in the ^{27}Al NMR spectrum, associated with the chloroaluminate anion, is slightly broader than in the benchmark LCC, possibly indicating the dimeric anion $[Al_2Cl_7]^-$ and therefore, to balance charge, the presence of $[SbCl_4]^-$.

The ^{31}P NMR spectrum of $[SbCl_2(P_{888}O)_2][OTf]$ (Figure 2.3-6-e) showed a singlet at 73.99 ppm. The corresponding ^{19}F NMR spectrum also featured a singlet at *ca*. -79 ppm. Again, no signal for Me_3SiCl was seen in the ^{13}C NMR spectrum, only a quartet corresponding to $[OTf]^-$.

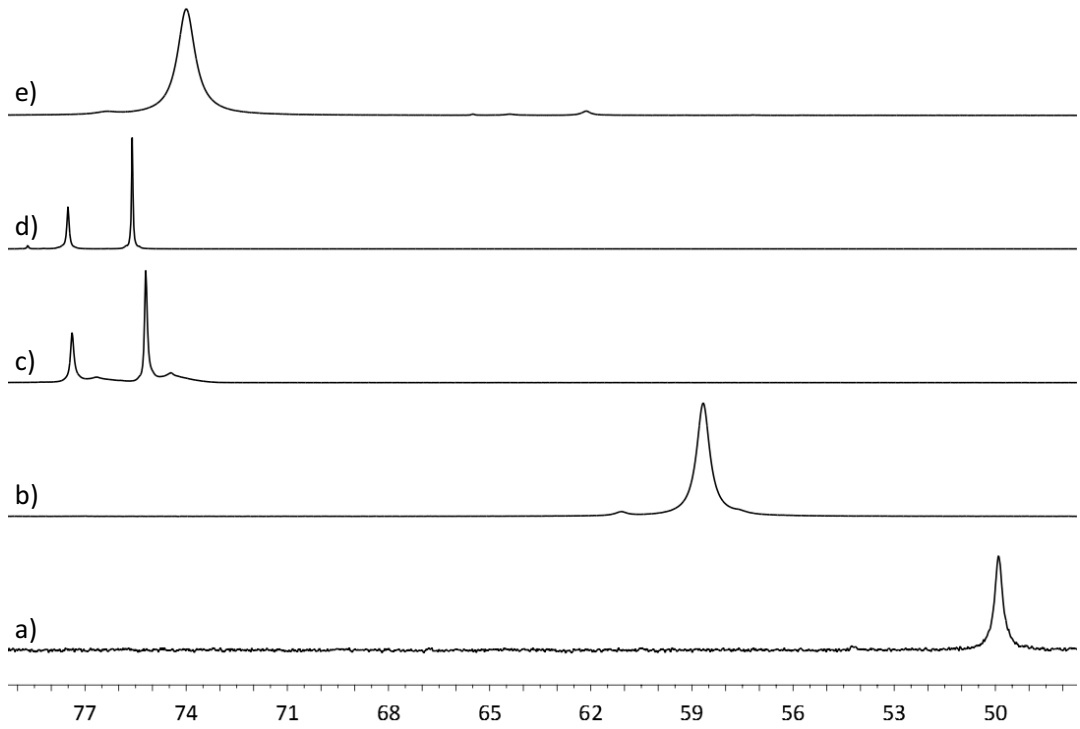

Figure 2.3-6: ^{31}P NMR spectra (neat, DMSO capillary) of a) $P_{888}O$, b) $[SbCl_3(P_{888}O)_2]$, c) $P_{888}O$-$AlCl_3$ χ_{AlCl3} = 0.5, d) $[SbCl_3(P_{888}O)_2]$-$AlCl_3$, and e) $[SbCl_2(P_{888}O)][OTf]$

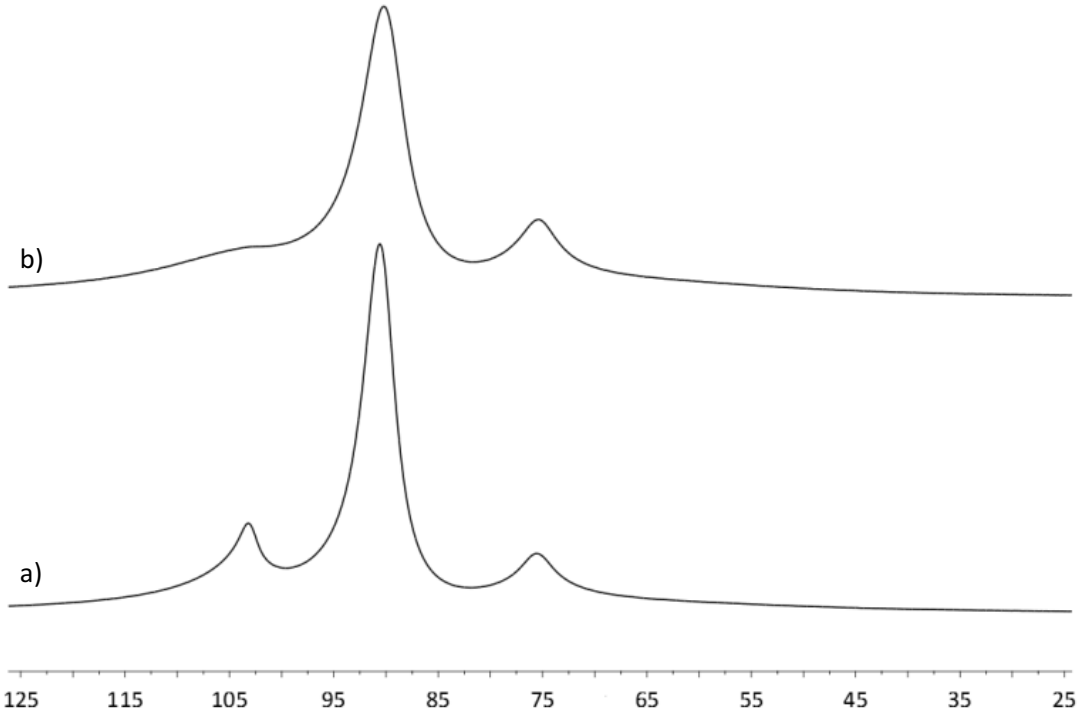

Figure 2.3-7: ^{27}Al NMR spectra (neat, DMSO capillary) of a) $P_{888}O$-$AlCl_3$ χ_{AlCl3} = 0.5, and b) $[SbCl_3(P_{888}O)_2]$-$AlCl_3$

The ^{31}P NMR spectrum of $[SbCl_3(P_{888}S)_2]$-$AlCl_3$ shows a broad singlet at 56.29 ppm, which is more deshielded than the starting complex (Figure 2.3-8-d). $P_{888}S$-$AlCl_3$ χ_{AlCl3} = 0.50 had a signal

at 56.31 ppm in its ^{31}P NMR spectra (Figure 2.3-8-c), as such it could indicate phosphine sulphide coordinating either to Sb or to Al; however. The ^{27}Al NMR spectrum shows a sharp signal at *ca.* 103 ppm associated with the $[AlCl_4]^-$ anion (Figure 2.3-9-b). This suggests that $P_{888}S$ is coordinating to Sb, but not to Al, and the desired ionic liquid was synthesised. Furthermore the stretching frequency of the P=S bond decreased by $\Delta\nu_{P=S}$ = 52 cm^{-1} compared to the free ligand (Table 2.3-3), indicating a change in the coordination environment.

In contrast, in the ^{31}P NMR spectrum of $[SbCl_3(P_{888})_2]$-2$AlCl_3$, there were additional signals present at *ca.* 63 and 64 ppm (Figure 2.3-8-e), integrating to 0.7 and 0.4, next to the main peak (56.67 ppm, integrating to 1.0). The main peak in the spectrum is of a similar chemical shift to both the signal of $[SbCl_2(P_{888}S)_2][AlCl_4]$ (Figure 2.3-8-c) and the signal of $P_{888}S$-$AlCl_3$ χ_{AlCl3} = 0.50, but its peak width is much narrower than the former, and very similar to the later. Moreover, in the corresponding ^{27}Al NMR spectrum there is a significant broadening similar to that in the ^{27}Al NMR spectrum of $P_{888}S$-$AlCl_3$ χ_{AlCl3} = 0.50 (Figure 2.3-9-a and c). This suggests partial migration of $P_{888}S$ to $AlCl_3$.

^{31}P NMR spectrum of $[SbCl_3(P_{888}S)_2][OTf]$ (Figure 2.3-8-f) showed a broad singlet in the at 55.04 ppm (Figure 2.3-8-f), which is more deshielded than $[SbCl_3(P_{888}S)_2]$, and close in both chemical shift and peak width to that of $[SbCl_2(P_{888}S)_2][AlCl_4]$ (Figure 2.3-8-c). In ^{13}C NMR spectrum, the quartet associated with the $[OTf]^-$ anion was seen at *ca.* 119 ppm, but no peaks associated with Me_3SiCl were seen around 3 ppm. Again, the stretching frequency of the P=S bond decreased by $\Delta\nu_{P=S}$ = 52 cm^{-1} compared to the free ligand (Table 2.3-3) indicating a change in the coordination environment. This suggests the desired ionic liquid, $[SbCl_3(P_{888}S)_2][OTf]$, was formed.

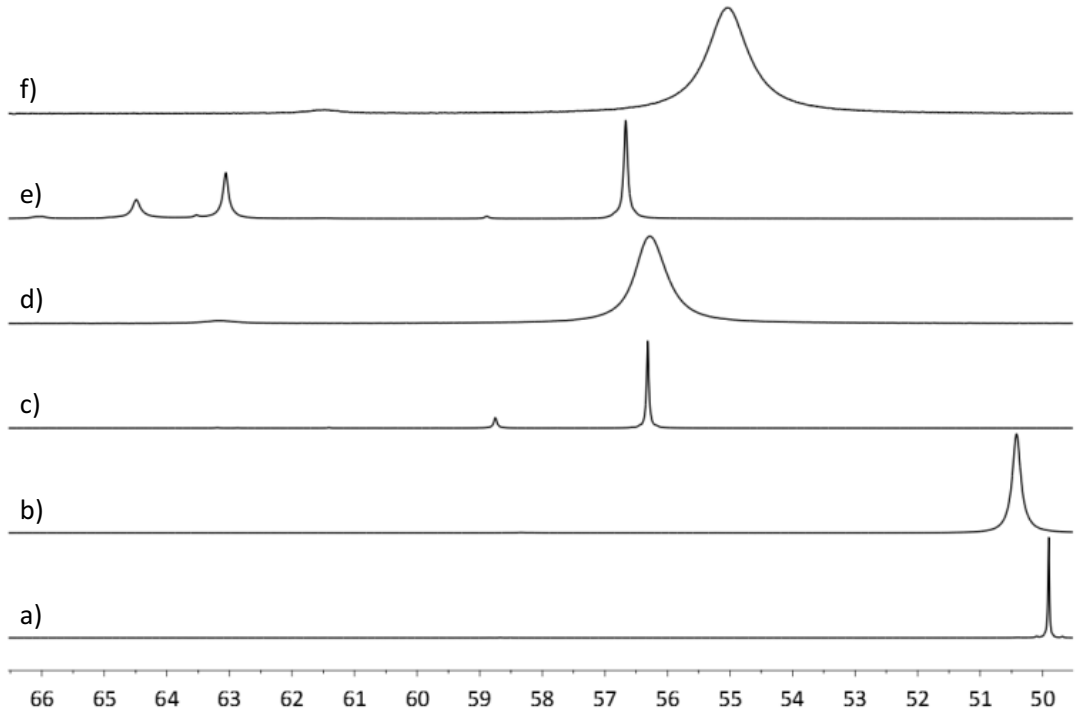

Figure 2.3-8: ^{31}P NMR spectra of a) $P_{888}S$, b) $[SbCl_3(P_{888}S)_2]$, c) $P_{888}S$-$AlCl_3$ χ_{AlCl3} = 0.5, d) $[SbCl_2(P_{888}S)_2][AlCl_4]$, e) $[SbCl_3(P_{888}S)_2]$-$2AlCl_3$ and f) $[SbCl_2(P_{888}S)_2][OTf]$

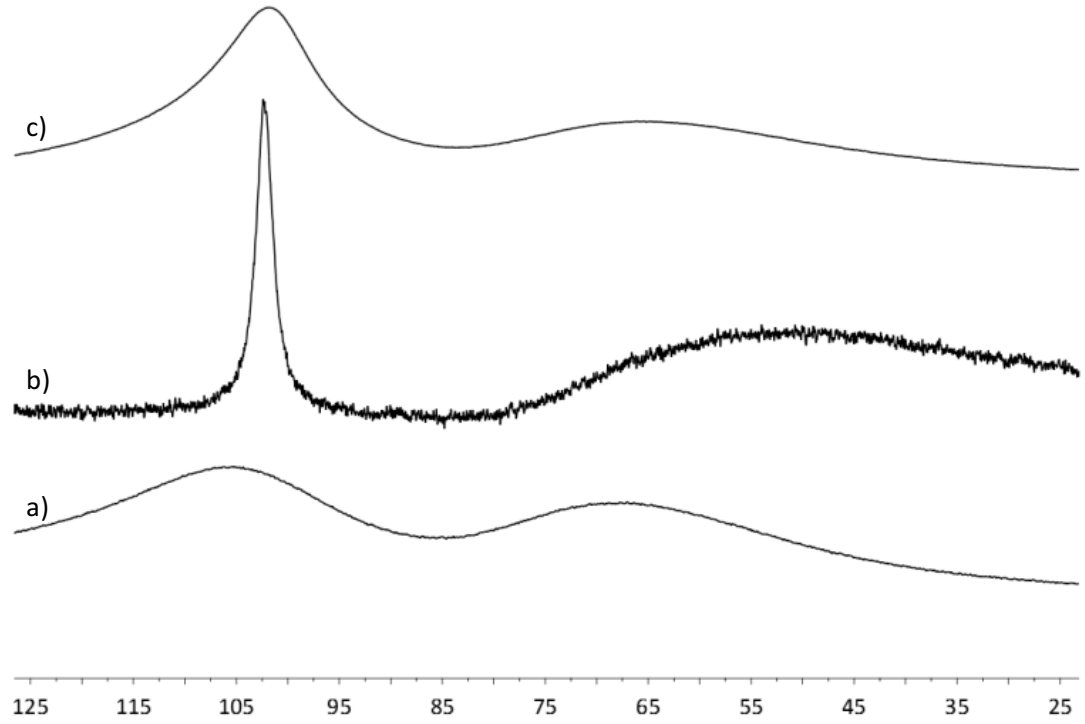

Figure 2.3-9: ^{27}Al NMR spectra (neat, DMSO capillary) of a) $AlCl_3$-$P_{888}S$ x = 0.5, b) $[SbCl_2(P_{888}S)_2][AlCl_4]$ and c) $[SbCl_3(P_{888}S)_2]$-$2AlCl_3$

2.3.3.2.3 Physical property measurements

Densities and viscosities of the five successfully synthesised ionic liquids: $[SbCl_2(P_{888})_2][AlCl_4]$, $[SbCl_2(P_{888})_2][OTf]$, $[SbCl_2(P_{888}O)_2][OTf]$, $[SbCl_2(P_{888}S)_2][AlCl_4]$ and $[SbCl_2(P_{888}S)_2][OTf]$, were measured as described in Chapter 2.1.1.5. No correction factor (Equation 2.1-7) was applied, as the liquids were above the viscosity threshold. As shown in Table 2.3-4 and Figure 2.3-10, density of the ionic liquids varies in a linear fashion with respect to temperature. When fitted by a linear regression, the R^2 values were closely approaching unity. Similarly to the LCCs measured before, the introduction of heavier elements in the ligand resulted in denser liquids.

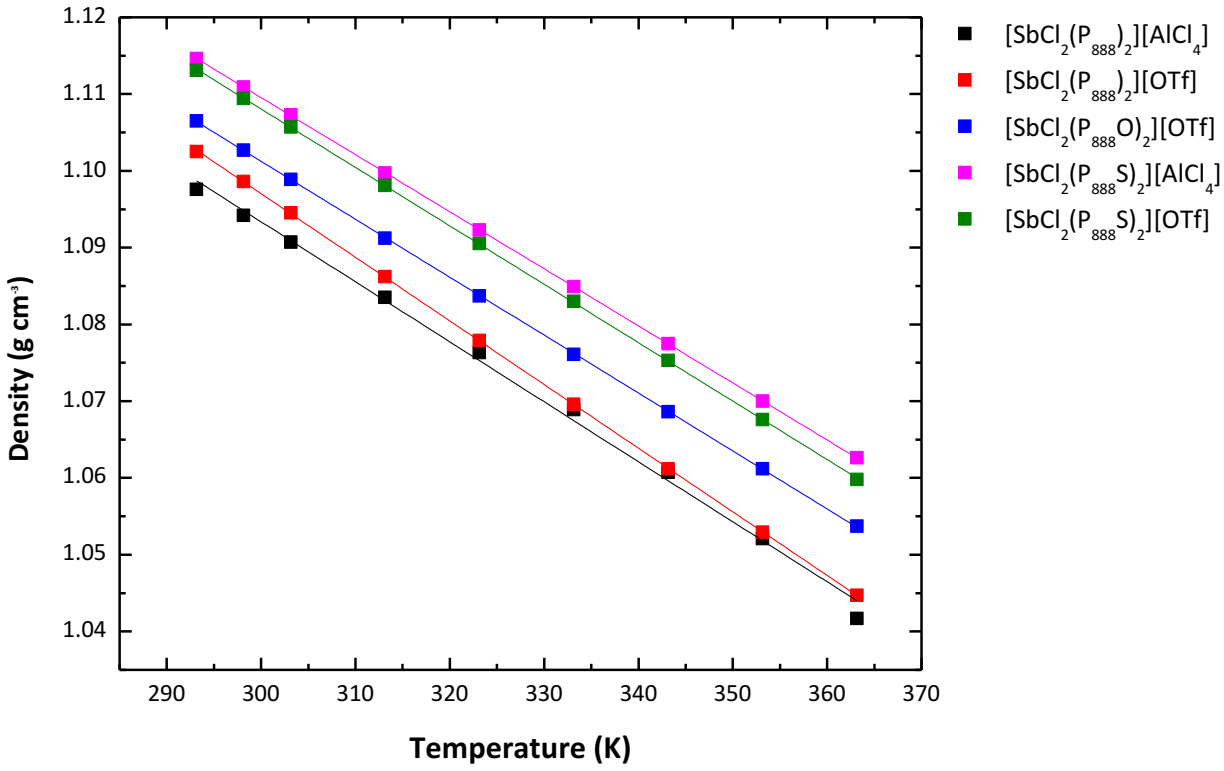

Figure 2.3-10: Densities of antimony(III) chloride ionic liquids *vs.* temperature

Despite high R^2 values, there was a notable discolouration of the ionic liquids with trioctylphosphine ligand, which were studied by ^{31}P NMR spectroscopy post-measurement, to check for possible decomposition. In both $[SbCl_2(P_{888})_2][AlCl_4]$ and $[SbCl_2(P_{888})_2][OTf]$, redox chemistry has been seen to occur. A sharp peak at *ca*. 103 ppm, attributable to the $[P_{888}Cl]^+$ cation, dominates both ^{31}P NMR spectra (see example in Figure 2.3-10). Clearly, at elevated temperature the redox reaction has been accelerated.

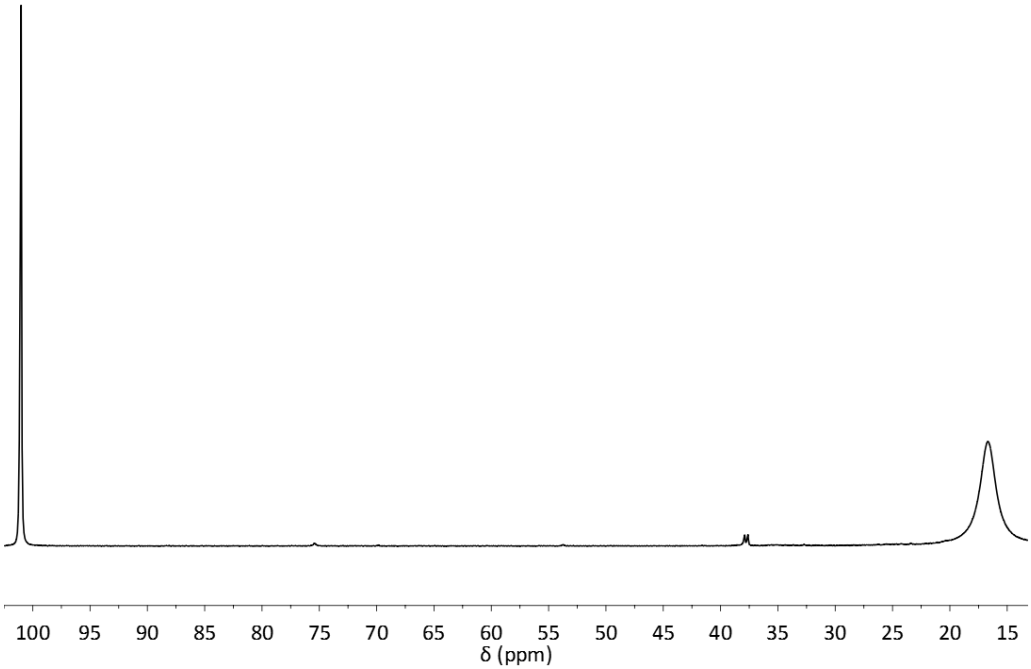

Figure 2.3-11: ^{31}P NMR spectrum (neat, DMSO capillary) of $[SbCl_2(P_{888})_2][OTf]$, recorded after density measurement

Viscosities of the antimony(III) chloride ionic liquids were measured over the temperature range 25 to 70 °C and fitted using the VFT equation (see Chapter 2.1.1.6, Equation 2.1-8 for more details). Results are plotted as a function of temperature in Figure 2.3-12, and additionally tabulated in Table 2.3-4. Viscosities measured vary within a wide range of values, from 589 cP for $[SbCl_2(P_{888}O)_2][OTf]$, to 4199 cP for $[SbCl_2(P_{888}S)_2][OTf]$ at 303 K. Comparing ionic liquids with $[OTf]^-$ anions, viscosities increase for different ligands in the following order: $P_{888}O < P_{888} < P_{888}S$, which is similar to viscosity order noted for LCCs based on these ligands (Chapter 2.1.2.7). Interestingly, whereas $[SbCl_2(P_{888}S)_2][OTf]$ was more viscous than its $[AlCl_4]^-$ analogue, $[SbCl_2(P_{888})_2][OTf]$ was less viscous than the corresponding $[AlCl_4]^-$ ionic liquid. Whilst these ionic liquids contain stibenium cations, they have exceedingly high viscosities, especially compared to LCCs (Table 2.1-13), chloroaluminate ionic liquids[82] and borenium ionic liquids which limits their use as catalysts due to mass transport effects.[223]

Again, after measuring the viscosity at elevated temperature, ionic liquids with the cation $[SbCl_2(P_{888})_2]^+$ were observed to darken. And again, ^{31}P NMR spectra recorded post-measurement featured the peak for $[P_{888}Cl]^+$ at *ca.* 103 ppm, suggesting thermal decomposition of the original ionic liquid to a redox product.

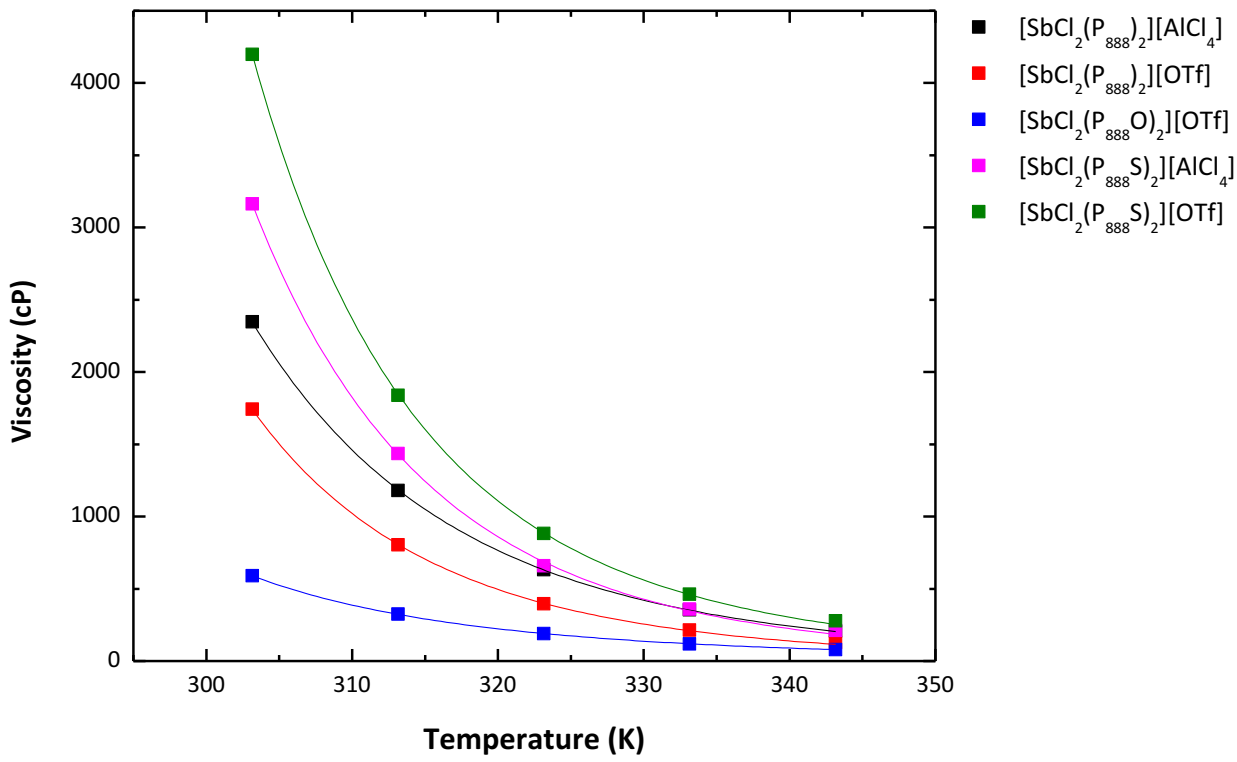

Figure 2.3-12: Viscosities of antimony(III) chloride ionic liquids *vs.* temperature

Table 2.3-4: Density and viscosities of antimony cation ionic liquids

Density / g cm^{-3}					
Temp / K	**$[SbCl_2(P_{888})_2][AlCl_4]$**	**$[SbCl_2(P_{888})_2][OTf]$**	**$[SbCl_2(P_{888}O)_2][OTf]$**	**$[SbCl_2(P_{888}S)_2][AlCl_4]$**	**$[SbCl_2(P_{888}S)_2][OTf]$**
293.15	1.0976	1.1025	1.1065	1.1146	1.1131
298.15	1.0942	1.0986	1.1027	1.1109	1.1094
303.15	1.0907	1.0945	1.0989	1.1073	1.1057
313.15	1.0835	1.0862	1.0912	1.0997	1.0981
323.15	1.0763	1.0779	1.0837	1.0923	1.0905
333.15	1.0689	1.0696	1.0761	1.0849	1.0830
343.15	1.0607	1.0612	1.0686	1.0775	1.0753
353.15	1.0521	1.0529	1.0612	1.0700	1.0676
363.15	1.0417	1.0447	1.0537	1.0626	1.0598
Y	-0.0008	-0.0008	-0.0008	-0.0007	-0.0008
C	1.3278	1.3457	1.3276	1.3325	1.3363
R^2	1.00	1.00	1.00	1.00	1.00
Viscosity / cP					
Temp / K	**$[SbCl_2(P_{888})_2][AlCl_4]$**	**$[SbCl_2(P_{888})_2][OTf]$**	**$[SbCl_2(P_{888}O)_2][OTf]$**	**$[SbCl_2(P_{888}S)_2][AlCl_4]$**	**$[SbCl_2(P_{888}S)_2][OTf]$**
303.15	2346.69	1741.7495	589.2677	3163.23	4198.87
313.15	1179.94	802.6989	323.8303	1436.15	1837.36
323.15	630.86	395.6365	189.1457	659.17	881.56
333.15	354.56	213.5287	119.1208	357.71	461.39
343.15	207.18	126.6203	79.8622	210.70	278.24
A	-11.68	-13.75	-11.89	-12.57	-13.28
B	2098	2499	2097	2174	2499
T_0	136.1	128.44	118.2	144.7	133.3

2.3.4 Conclusions

The strategy used to synthesise borenium ionic liquids was not always directly translatable to antimony systems, nevertheless, some successful synthesis were reported. Attempts to prepare cationic chloroantimonate(V) species failed, which is in agreement with the literature, lacking descriptions of such compounds. In contrast, the synthetic approach was successfully expanded to $SbCl_3$ adducts.

As such, five ionic liquids containing stibenium(III) cations, $[SbCl_2(P_{888})_2][AlCl_4]$, $[SbCl_2(P_{888})_2][OTf]$, $[SbCl_2(P_{888}O)_2][AlCl_4]$, $[SbCl_2(P_{888}S)_2][AlCl_4]$ and $[SbCl_2(P_{888}S)_2][OTf]$, were synthesised, studied spectroscopically, and characterised in terms of viscosities and densities. However, systems which contained the trioctylphosphine ligand were found to be susceptible to redox chemistry, particularly when heated, in agreement with the literature.[217] In conclusion, the three systems: $[SbCl_2(P_{888}O)_2][OTf]$, $[SbCl_2(P_{888}S)_2][AlCl_4]$ and $[SbCl_2(P_{888}S)_2][OTf]$, would be of practical interest for further study.

The nature of the halide extracting agent was crucial for the stability of the antimony cation. Addition of either one or two mol equivalents of $AlCl_3$ to the adduct $[SbCl_3(P_{888}O)_2]$ saw virtually complete transfer of the ligand from the antimony(III) chloride to the aluminium(III) chloride, forming an LCC with dissolved $SbCl_3$, whereas using Me_3SiOTf successfully led to the formation of $[SbCl_3(P_{888}O)_2][OTf]$. At the same time, the reaction with Me_3SiOTf had to be performed slowly to prevent the formation of $[Me_3SiP_{888}O][OTf]$. For the adducts $[SbCl_3(P_{888})_2]$ and $[SbCl_3(P_{888}S)_2]$, significant ligand transfer was only observed if they were reacted with two equivalents of aluminium(III) chloride; *i.e.*, the Lewis acidic $[Al_2Cl_7]^-$ anion was competing for the ligand, whereas the neutral $[AlCl_4]^-$ anion was not.

This methodology potentially represents a suitable method for the synthesis of a soft liquid Lewis acid, of catalytic applications complimentary to those of borenium ionic liquids. Measurements of acidity would be of use to determine the applicability of these acids to catalytic applications. Unfortunately, ionic liquids synthesised in this preliminary study tend to have very high viscosities (> 500 cP), and as such other ligands may be of interest.

2.4 Tin(IV)chloride ionic liquids

2.4.1 Literature review

As discussed in Chapter 1.2.2, chlorostannate(II) ionic liquids have been studied, characterised and utilised in catalytic applications.[65] In contrast, tin(IV) chloride-containing ionic liquids appear to be rarer, and are a noticeable omission from the speciation table produced by Holbrey and co-workers (Figure 1.2-3).[63] Obviously, both hydrolytic and redox instability of tin(IV) makes the handling of chlorostannate(IV) systems more of a challenge.

When performing the Prins condensation of isobutene and formaldehyde, Landau and co-workers reported 1:1 mixtures of organic chloride salts and $SnCl_4$.[115] They describe the anion as being $[SnCl_5]^-$ without spectroscopic or crystallographic evidence, although this does appear to be a reasonable assumption, based on the known behaviour of halometallates across the periodic table (Figure 1.2-3) and observed crystal structure of organotin(IV) chlorides.[224]

Burford and co-workers utilised techniques similar to those seen in Chapter 2.3 for the synthesis of cationic tin(IV) chloride complexes, with some of the crystal structures of $[Sn^{IV}Cl_x(PMe_3)_y]^{z+}$ complexes shown in Figure 2.4-1. The two PMe_3 ligands were shown to prefer *trans* position to each other in the $SnCl_4$ complexes.[225] The complexes were characterised by X-ray diffraction, as well as ^{1}H, ^{31}P and ^{119}Sn NMR spectroscopy, but not ^{27}Al NMR spectroscopy. This is unfortunate, as the X-ray structure revealed a distinctly ionic complex $[SnCl_2(PMe_3)_2][AlCl_4]_2$, but also showed "*interion contacts between tin and chlorine atoms of two anions*", and it would be of interest to see what, if any, effect this has for the ^{27}Al NMR spectrum.

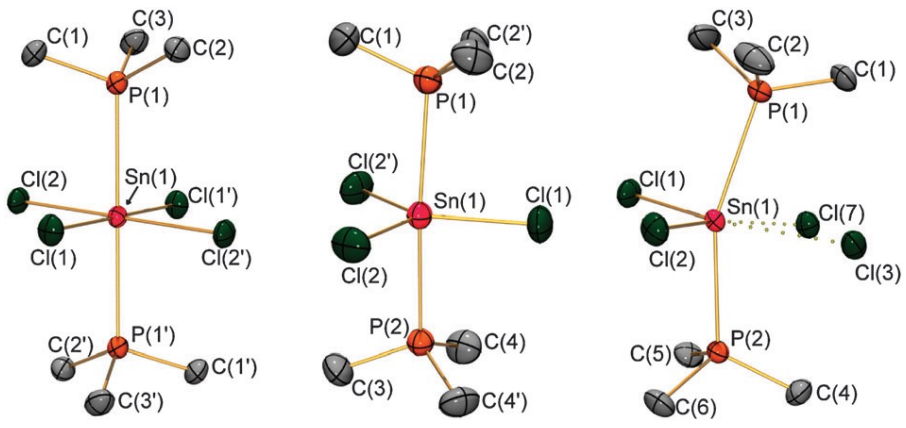

Figure 2.4-1: Crystal structures of $(PMe_3)_2SnCl_4$ (left), $[(PMe_3)_2SnCl_3][AlCl_4]$ (middle) and $[(PMe_3)_2SnCl_2][(AlCl_4)_2]$ (right)[225]

2.4.2 Experimental

2.4.2.1 Materials and methods

All operations were performed in a glovebox (MBraun labmaster dp, <0.3 ppm of H_2O and O_2) or using standard Schlenk techniques with a vacuum and an argon line. All glassware was dried overnight (*ca.* 100 °C) before use.

Tin(IV) chloride (99.99%) was purchased from Sigma Aldrich and used as received.

2.4.2.2 Synthesis of ionic liquids with tin(IV) cation

In the glovebox, $SnCl_4$ (1 g, 3.84 mmol, 1 mol eq.) was added in small portions (0.1 g) to a phosphine or phosphine chalcogenide donor (7.68 mmol, 2 mol eq.). Sufficient time was left between additions to allow for the heat evolved during the reaction to dissipate. Upon complete addition the reaction was stirred overnight to yield clear viscous liquids. Subsequently, 1 or 2 mol equivalents of $AlCl_3$ (0.51 or 1.02 g, 3.84 or 7.68 mmol) were added, and the mixture was stirred overnight. The resulting liquid was filtered (if required) and stored in the glovebox.

2.4.3 Results and discussion

2.4.3.1 Synthesis and analysis of $P_{888}E$-$SnCl_4$ adducts

The synthetic strategy was adopted from the synthesis of LCCs: in a glovebox, neat $SnCl_4$ was added slowly to neat ligands. Tin(IV) chloride reacted rapidly with two mols of each ligand to produce viscous liquids. The equimolar adduct $SnCl_4$-$P_{888}O$ was also prepared. The products were studied by ^{1}H, ^{13}C, ^{31}P (Table 2.4-1) and ^{119}Sn (Table 2.4-3) NMR spectroscopy. In addition, adducts of $SnCl_4$ with $P_{888}E$ (E = O, S) were analysed by FT-IR spectroscopy (Table 2.4-2).

Table 2.4-1: ^{31}P NMR chemical shifts for phosphine/phosphine chalcogenide ligands, their adducts with $SnCl_4$ and ionic liquids

Compound	δ ^{31}P / ppm	$\Delta\delta$ ^{31}P / ppm[(a)]	^{1}J (^{31}P – ^{117}Sn) / Hz	^{1}J (^{31}P – ^{119}Sn) / Hz
P_{888}	-29.44			
$[SnCl_4(P_{888})_2]$	10.91	40.35	2148	2248
$[SnCl_4(P_{888})_2]$-$AlCl_3$	13.80	43.24	2252	2357
$[SnCl_4(P_{888})_2]$-$2AlCl_3$	30.98	60.42	2087	2184
$P_{888}O$	49.91	-	-	-
$[SnCl_4(P_{888}O)_2]$	66.17	16.26	-	-
$P_{888}S$	49.91	-	-	-
$[SnCl_4(P_{888}S)_2]$	53.67	3.76	-	-
$[SnCl_4(P_{888}S)_2]$-$AlCl_3$	57.77	7.86	-	-
$[SnCl_4(P_{888}S)_2]$-$2AlCl_3$	56.35	6.44	-	-

(a) $\Delta\delta$ ^{31}P = δ ^{31}P (complex) - δ ^{31}P (ligand)

Table 2.4-2: IR frequency data for P=E vibrations for phosphine/phosphine chalcogenide ligands, their adducts with $SnCl_4$ and ionic liquids

Compound	ν / cm^{-1}	$\Delta\nu$ / cm^{-1}[(a)]
$P_{888}O$	1144.95	-
$[SnCl_4(P_{888}O)_2]$	1067.38	-77.57
$[SnCl_4(P_{888}O)_2]$-$AlCl_3$	1091.82	-53.13
$[SnCl_4(P_{888}O)_2]$-$2AlCl_3$	1102.47	-42.48
$P_{888}S$	599.36	-
$[SnCl_4(P_{888}S)_2]$	540.92	-58.44
$[SnCl_4(P_{888}S)_2]$-$AlCl_3$	543.67	-55.69
$[SnCl_4(P_{888}S)_2]$-$2AlCl_3$	520.13	-79.23

(a) $\Delta\nu = \nu$ (complex) – ν (ligand)

The ^{119}Sn NMR spectrum of $[SnCl_4(P_{888})_2]$ (Table 2.4-2-b) showed the expected triplet at, at -582 ppm, a similar chemical shift as reported trialkylphosphine adducts of $SnCl_4$.[225–227] The corresponding ^{31}P NMR spectrum (Figure 2.4-3-b) revealed a significantly deshielded peak compared to the free ligand (10.91 *vs*. -29.44 ppm), with coupling constant similar to literature examples (Table 2.4-1).[225–227] Coupling constants measured from the ^{119}Sn NMR spectrum (Table 2.4-3) were in good agreement with those measured from the ^{31}P NMR spectrum (Table 2.4-1).

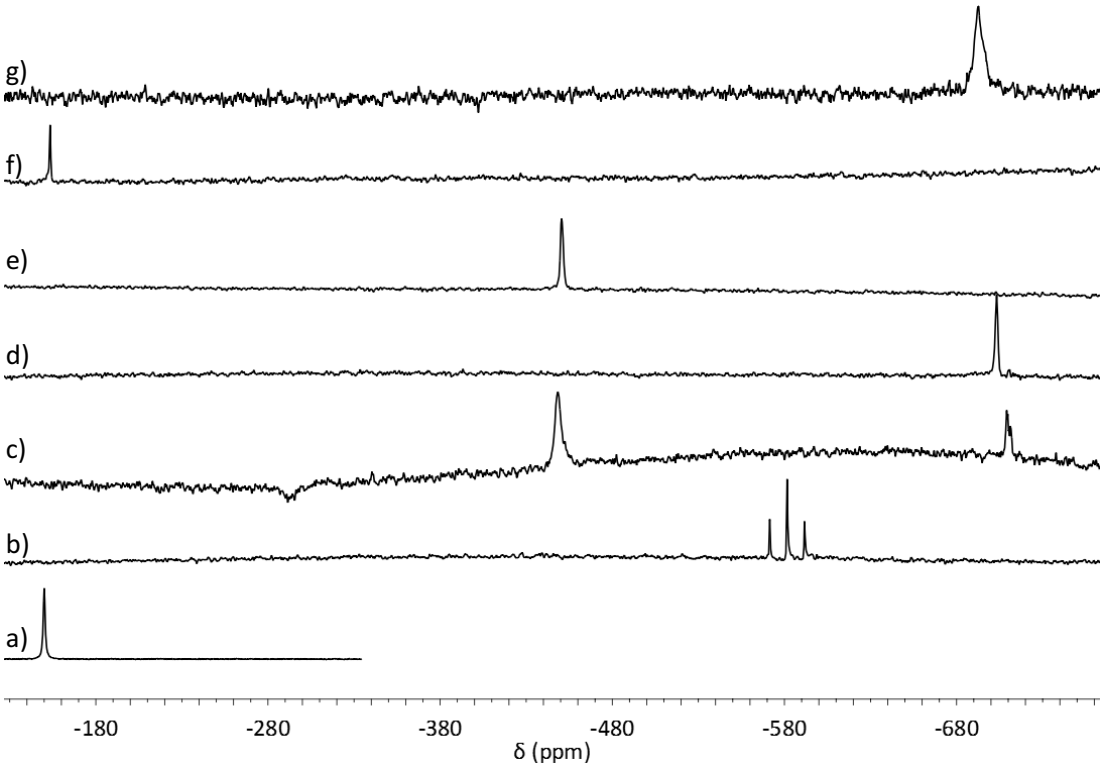

Figure 2.4-2: ^{119}Sn NMR spectra for a) $SnCl_4$, b) $[SnCl_4(P_{888})_2]$, c) $[SnCl_4(P_{888}O)$, d) $[SnCl_4(P_{888}O)_2]$, e) $[SnCl_4(P_{888}O)_2]$-$AlCl_3$, f) $[SnCl_4(P_{888}O)_2$-$2AlCl_3$ g) $[SnCl_4(P_{888}S)_2]$

Table 2.4-3: ^{119}Sn NMR chemical shifts and coupling data

Complex / IL	δ ^{119}Sn (complex)	Δ δ ^{119}Sn [(a)]	^{1}J (^{31}P – ^{119}*Sn*) (Hz)
$SnCl_4(P_{888})_2$	-581.57	-431.57	2256
$SnCl_4(P_{888}O)$	-448.36	-298.36	-
$SnCl_4(P_{888}O)_2$	-703.32	-553.32	-
$SnCl_4(P_{888}O)_2AlCl_3$	-450.54	-300.54	-
$SnCl_4(P_{888}O)_2(AlCl_3)_2$	-153.47	-3.47	-
$SnCl_4(P_{888}S)_2$	-692.83	-542.83	-

(a) Δ δ ^{119}Sn = ^{119}Sn (complex) - δ ^{31}P (ligand) referenced to the appropriate solvent

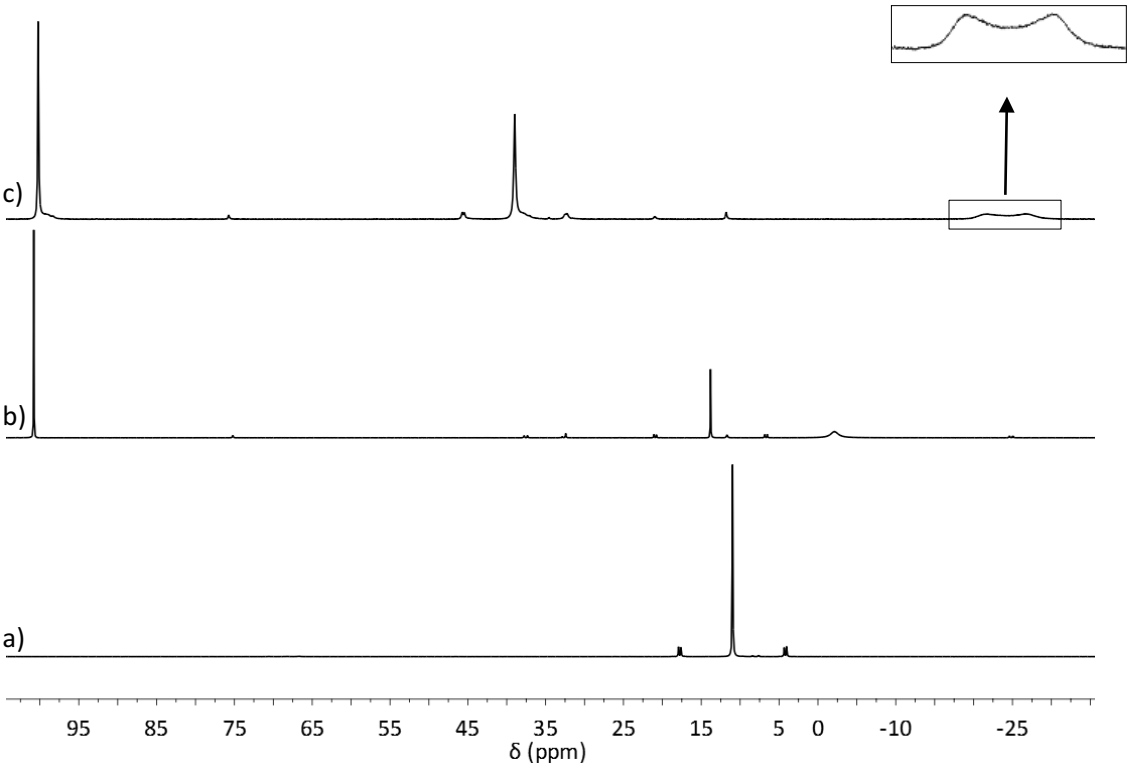

Figure 2.4-3: ^{31}P NMR spectra (neat, DMSO capillary) for a) $[SnCl_4(P_{888})_2]$, b) $[SnCl_4(P_{888})_2]$-$AlCl_3$ and $[SnCl_4(P_{888})_2]AlCl_3)_2$

The ^{31}P NMR spectrum of the $[SnCl_4(P_{888}O)_2]$ adduct (Figure 2.4-3-a) revealed abroad peak, deshielded with respect to $P_{888}O$, at 66.17 ppm. The corresponding ^{119}Sn NMR spectrum (Figure 2.4-5-d) features a singlet at -703 ppm, shifted upfield with respect to $SnCl_4$ by $\Delta\delta$ = 553 ppm (Table 2.4-3) This is supported by a red-shift in the vibrational frequency of the P=O bond, from 1144.9 cm^{-1} in neat $P_{888}O$ to 1067.38 in $SnCl_4$-$P_{888}O$ (Table 2.4-2). The magnitude of the red-shift, $\Delta\nu_{P=O}$ = 77.57 cm^{-1}, confirms complexation to a metal centre.

The ^{31}P NMR spectrum of the $[SnCl_4(P_{888}S)_2]$ adduct (Figure 2.4-5-a) featured a single broad peak at 53.67 ppm (Figure 2.4-5-a), likely due to the viscosity of the medium. As with the complex $[SbCl_3(P_{888}S)_2]$ the ^{31}P NMR peak shift was similar to the free ligand, $\Delta\delta$ ^{31}P = 3.76 for $[SnCl_4(P_{888}S)_2]$, so other spectroscopic techniques were used to confirm coordination of the ligand to the metal halide. The corresponding ^{119}Sn NMR (Figure 2.4-2-g) shows a singlet at -693 ppm, significantly upfield from $SnCl_4$ ($\Delta\delta$ = 543 ppm, see Table 2.4-3). The vibrational data (Table 2.4-2) shows that the P=S vibration has red shifted significantly from free $P_{888}S$, $\Delta\nu_{P=S}$ = 58.44, both of which are indicative of adduct formation.

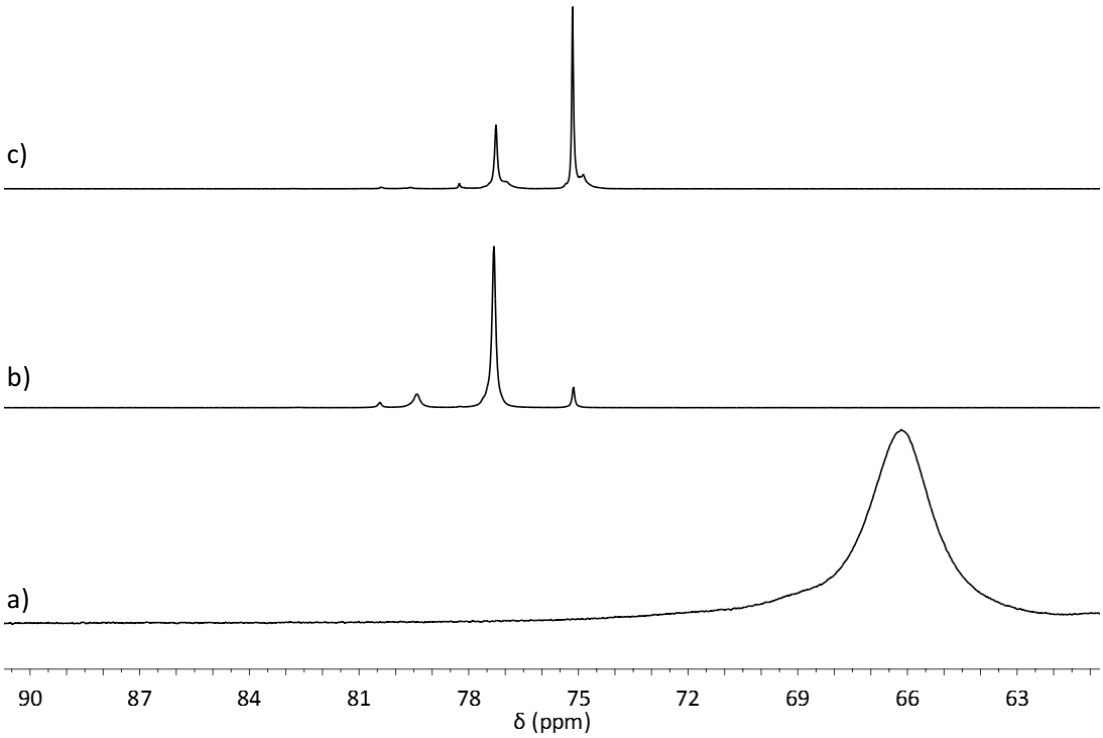

Figure 2.4-4: ^{31}P NMR spectra (neat, DMSO capillary) of a) $[SnCl_4(P_{888}O)_2]$, b) $[SnCl_4(P_{888}O)_2]$-$AlCl_3$ and $SnCl_4(P_{888}O)_2]$-$2AlCl_3$

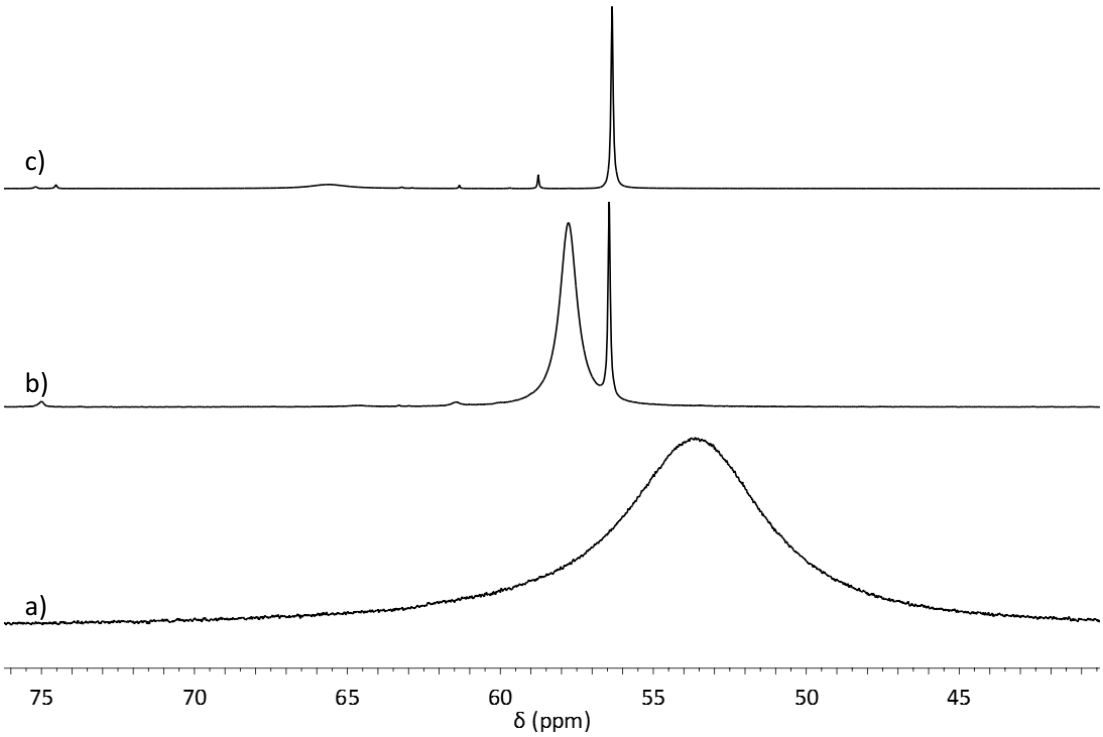

Figure 2.4-5: ^{31}P NMR spectra (neat, DMSO capillary) of a) $[SnCl_4(P_{888}S)_2]$, b) $[SnCl_4(P_{888}S)_2]$-$AlCl_3$ and $[SnCl_4(P_{888}S)_2]$-$2AlCl_3$

2.4.3.1.1 Synthesis and analysis of $P_{888}E$-$SnCl_4$-n$AlCl_3$ ionic liquids

Upon the reaction of $[SnCl_4(P_{888})_2]$ with either one or two equivalents of $AlCl_3$, a white precipitate was observed, which was filtered off before spectroscopic analysis of the liquid. In the ^{31}P NMR spectrum of $[SnCl_4(P_{888})_2]$-$AlCl_3$ (Figure 2.4-3-b), there were two signals, at 13.80 and 103 ppm, integrating to 1 and 2.6, respectively. The peak shifted slightly downfield with respect to the complex (13.80 ppm) displayed satellites (^1J ^{31}P-$^{117/119}Sn$ = 2252 / 2357) associated with P-Sn coupling with good agreement with Burford *et al.,*[225] and was thus assigned to the cationic tin species $[SnCl_3(P_{888})_2]^+$. However, the stronger signal at 103 ppm did not show tin satellites. Again, it is necessary to consider that some authors have reported that synthesis of $SnCl_4$ phosphine complexes have resulted in reduction of the tin centre and the formation of a complex $[SnX_3][XPR_3]$.[219] This redox process appears to occur here only upon the addition of $AlCl_3$. As such, the peak at 103 ppm in the ^{31}P NMR spectrum is attributed to $[P_{888}Cl]^+$, as already discussed *e.g.* for P_{888}-$SbCl_3$ mixtures in Chapter 2.3. The relevant ^{27}Al NMR spectrum (Figure 2.4-6-a) features a very sharp signal at 102 ppm, assigned to $[AlCl_4]^-$. Unfortunately, the ^{119}Sn spectrum did not have any peaks distinguishable from the baseline. It appears that the post-reaction mixture contained mainly the redox product, $[P_{888}Cl][AlCl_4]$, possibly some target $[SnCl_3(P_{888})_2]^+$ complex, exchanging with other Sn species and thus causing the ^{119}Sn NMR signal to disappear in the baseline, possibly due to dynamic exchange between $[SnCl_3(P_{888})_2]^+$ and $[SnCl_2(P_{888})_2]^{2+}$, and/or precipitation of $SnCl_2$ as a white powder.

In the ^{31}P NMR spectrum of $[SnCl_4(P_{888})_2]$-2$AlCl_3$, there are three major peaks observed at -*ca*. -24, 31 and 103 ppm, integrating as 1:1.6:1.3 (Figure 2.4-3-c). The upfield doublet at *ca.* = -24 ppm suggests P_{888} migration from tin to $AlCl_3$. This peak corresponds to the phosphorus-aluminium chloride complexes as reported by Reid and co-workers.[222] The peak at 30.98 ppm with tin satellites, with coupling constants in reasonable agreement with Burford *et al.*[225] (^1J ^{31}P-$^{117/119}Sn$ = 2087 / 2184), was assigned to the dicationic complex $[SnCl_2(P_{888})_2]^{2+}$. Finally, a highly deshielded signal at *ca.* 103 ppm was attributed to $[P_{888}Cl]^+$. In the corresponding ^{27}Al NMR spectrum (Figure 2.4-6-b), was reminiscent of the spectrum observed by Coleman *et al.*[135] for P_{888}-$AlCl_3$ x_{AlCl3} = 0.50, with the major peak at 109 ppm and a slight shoulder at 103 ppm. This suggests partial transfer of the ligand from the Sn to the Al. Again, the ^{119}Sn NMR spectrum did not have any peaks distinguishable from the baseline.

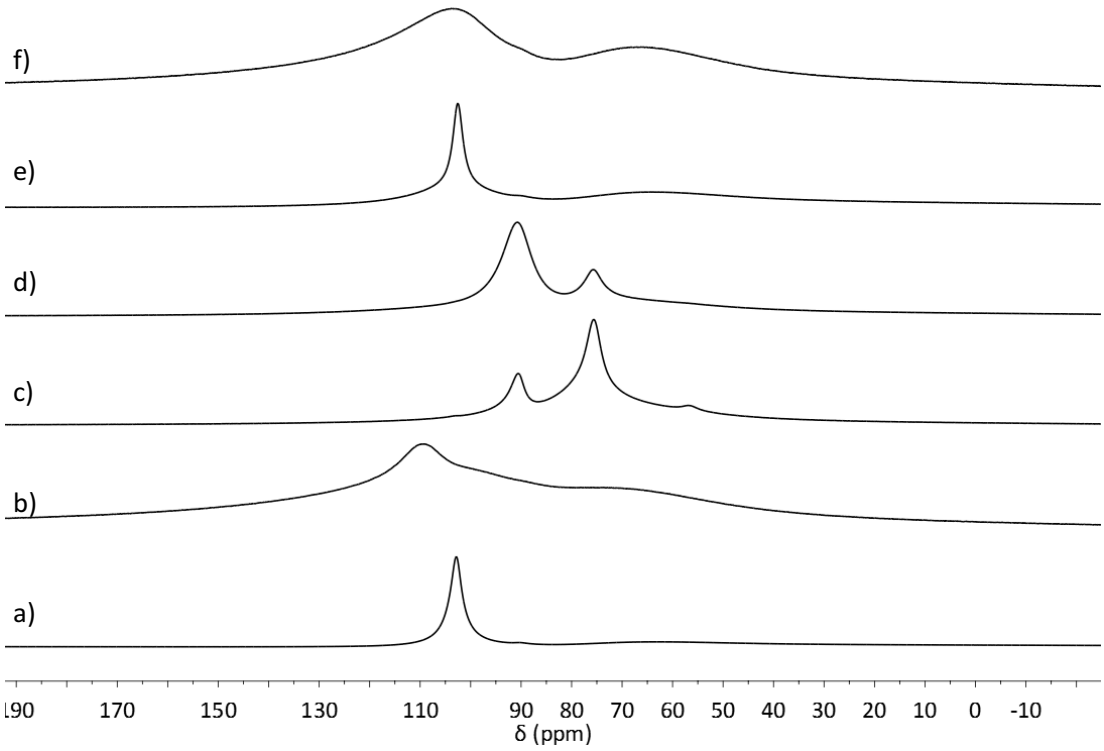

Figure 2.4-6: ^{27}Al NMR spectra for a) $[SnCl_4(P_{888})_2]$-$AlCl_3$, b) $[SnCl_4(P_{888})_2]$-$2AlCl_3$ c) $[SnCl_4(P_{888}O)_2]$-$AlCl_3$, d) $[SnCl_4(P_{888}O)_2]$-$2AlCl_3$ e) $SnCl_4(P_{888}S)_2AlCl_3$, f) $SnCl_4(P_{888}S)_2(AlCl_3)_2$

The ^{31}P NMR spectra of $[SnCl_4(P_{888}O)]$, $[SnCl_4(P_{888}O)_2]$, $[SnCl_4(P_{888}O)_2]$-$AlCl_3$ and $[SnCl_4(P_{888}O)_2]$-$2AlCl_3$ are compared in Figure 2.4-4. There is a stark similarity between the ^{31}P NMR spectra of $[SnCl_4(P_{888}O)_2]$-$2AlCl_3$ (Figure 2.4-4-c) and the LCC $P_{888}O$-$AlCl_3$ χ_{AlCl3} = 0.50 (Figure 2.1-7-a). Also the ^{31}P NMR spectrum of $[SnCl_4(P_{888}O)_2]$-$AlCl_3$ has signals with similar chemical shifts, but at differing ratios (Figure 2.4-4-b). The ^{27}Al NMR spectrum of $[SnCl_4(P_{888}O)_2]$-$AlCl_3$ and $[SnCl_4(P_{888}O)_2]$-$2AlCl_3$ (Figure 2.4-6-c and Figure 2.4-6-d) revealed peak distribution similar to that of $P_{888}O$-$AlCl_3$ χ_{AlCl3} = 0.50 LCC (Figure 2.1-5-a). However, no peaks associated with the chloroaluminate anions (at *ca.* 103 ppm) are visible. The corresponding ^{119}Sn NMR show progressive deshielding of ^{119}Sn as more $AlCl_3$ is added: from -703 ppm for the $[SnCl_4(P_{888}O)_2]$ adduct, through -451 ppm for $[SnCl_4(P_{888}O)_2]$-$AlCl_3$, to -153 ppm for $[SnCl_4(P_{888}O)_2]$-$2AlCl_3$ (Figure 2.4-5, Table 2.4-3). The intermediate chemical shift of -451 ppm, recorded for of $[SnCl_4(P_{888}O)_2]$-$AlCl_3$, corresponds to signal from the adduct $[SnCl_4(P_{888}O)]$, recorded at -448 ppm, indicating that one mole of ligand was abstracted by one mole of $AlCl_3$. The chemical shift at -153 ppm corresponds to that of $SnCl_4$, with two moles of $P_{888}O$ abstracted quantitatively by two moles of $AlCl_3$.

Apparently, the oxophilicity of $AlCl_3$ makes it an effective competitor for the ligand, as shown in Equation 2.4-1 and Equation 2.4-2.

$$[SnCl_4(P_{888}O)_2] + AlCl_3 \rightarrow [SnCl_4(P_{888}O)] + [AlCl_3(P_{888}O)]$$ Equation 2.4-1

$$[SnCl_4(P_{888}O)_2] + 2AlCl_3 \rightarrow SnCl_4 + 2[AlCl_3(P_{888}O)]$$ Equation 2.4-2

The frequency of the P=O stretching frequency It is noteworthy that all compounds in Equation 2.4-1 and Equation 2.4-2 are charge-neutral adducts. Indeed, neither $[AlCl_4]^-$, $[SnCl_5]^-$ or $[SnCl_6]^{2-}$ anions are visible in their respective NMR spectra. This despite the clear visibility of the cationic peak in the $AlCl_4$ spectrum (Figure 2.4-6-c and d). As such there could rapid exchange of chloride anions between the metal centres.

In the ^{31}P NMR spectrum of $[SnCl_4(P_{888}S)_2]$-$AlCl_3$ (Figure 2.4-5-b) there are two main peaks at 56.31 and 57.77 ppm (ratio 1:6). The sharper of the two peaks (56.41 ppm) was of a very similar chemical shift to that observed for $P_{888}S$-$AlCl_3$ χ_{AlCl3} = 0.50 LCC at 56.31 ppm (Figure 2.1-7-b), thus indication ligand transfer to aluminium; the dominant signal at 57.77 ppm is assigned to $[SnCl_3(P_{888}S)_2]^+$. The corresponding ^{27}Al NMR spectrum (Figure 2.4-6-e) showed a sharp peak at 103 ppm associated with the presence of the tetrahedral $[AlCl_4]^-$ anion. The main product appears to be the target ionic liquid, $[SnCl_3(P_{888}S)_2][AlCl_4]$, although some ligand transfer took place. Again, the ^{119}Sn NMR did not yield any observable signals.

The ^{31}P NMR spectrum of $[SnCl_4(P_{888}S)_2]$-$2AlCl_3$ (Figure 2.4-5-c) features the main signal at 56.35, and several trace downfield signals. The main signal corresponds to $P_{888}S$ complexed to $AlCl_3$, rather than to $SnCl_4$. The corresponding ^{27}Al NMR spectrum (Figure 2.4-6-f) shows a broad peak at 103 ppm indicative of the chloroaluminate anion, but is virtually identical to that of $P_{888}S$-$AlCl_3$ χ_{AlCl3} = 0.50 (Figure 2.1-5-b). No signals were observed from the ^{119}Sn NMR spectrum. The observable evidence suggests almost complete ligand transfer from $SnCl_4$ to $AlCl_3$.

2.4.4 Conclusions

The synthesis of ionic liquids with tin(IV) cations was hampered by competitive ligand redistribution upon the addition of aluminium chloride, as well as redox chemistry. Though the desired cations $[SnCl_4(P_{888})_2]$ do appear to have been formed to a certain extent when 1 or 2 eq. of $AlCl_3$ were added to $[SnCl_4(P_{888})_2]$, a significantly deshielded signal (*ca.* 103 ppm) was also observed in the ^{31}P NMR. This signal was attributed to $[P_{888}Cl]^+$ which suggests reduction of the tin(IV) to tin(II). This was accompanied by precipitation of white solid, possibly $SnCl_2$.

As discussed already in Chapter 2.3, $AlCl_3$ successfully extracted $P_{888}O$ from the $[SnCl_4(P_{888}O)_2]$ adduct. This was shown by the similarities of the ^{31}P and ^{27}Al NMR spectra measured here to

those measured in Chapter 2.1 and those published in the literarture.[135] Furthermore the ^{119}Sn spectra showed sequential ligand transfer upon addition of 1 and 2 mol equivalents of $AlCl_3$. (Equation 2.4-1 and Equation 2.4-2).

Upon addition of a single equivalent of $AlCl_3$ to $[SnCl_4(P_{888}S)_2]$, the ^{31}P NMR spectrum showed a signal corresponding to the cationic $[SnCl_3(P_{888}S)_2]^+$ complex, as well as evidence of some ligand transfer to the aluminium, forming $[AlCl_3(P_{888}S)]$. When two mol equivalent of $AlCl_3$ were added, the ligand transfer was nearly quantitative, leading to the formation of a mixture of charge-neutral adducts: $[AlCl_3(P_{888}S)]$ and $[Al_2Cl_6(P_{888}S)]$, and $SnCl_4$.

As the main conclusion from this project, there was a large discrepancy between what was observed by Burford's group in the solid state,[225] and between equilibria found in the ionic liquid environment. It has been explicitly shown, that the existence of a crystal structure of a certain speciation (Figure 2.4-1) does not guarantee analogous speciation being thermodynamically preferable and stable in the liquid phase.

2.5 Summary

The aim of this thesis was to synthesis a range of liquid Lewis acids with main group elements. To that end acids based on aluminium(III), gallium(III), boron(III) and antimony(III) were successfully produced.

LCCs have been studied in the literature (Chapter 1.2.3.2), though the most in-depth speciation studies have been performed on oxygen containing ligands.[135,154] Here the speciation of heavier phosphine chalcogenide donors (sulphur and selenium) were studied. The heavier donor atoms shifted the equilibria present in LCCs (Figure 1.2-8)[135] to prefer neutral species over ionic as evidenced by multinuclear NMR spectroscopy. The physical properties of LCCs were measured. Unexpectedly the neutral LCCs were found to have higher viscosities than the corresponding ionic LCCs. A wide range of $AlCl_3$ and $GaCl_3$ based LCCs were found to be potent Lewis acids, with many being Lewis superacid as measured by the Gutmann acceptor method ($94 \leq AN \leq 109$).

C_7CN-$AlCl_3$ mixtures were shown to exist as ionic liquids rather than LCCs. However as the cation of this ionic liquid was triply charged, $[Al(C_7CN)_6]^{3+}$ it presented a case where Lewis acidic anions could be formed at lower metal chloride loadings (Equation 2.1-4 – Equation 2.1-6) than typical chlorometallate ionic liquids which use organic chloride salts.[83]

Borenium ionic liquids with pyridine ligands were synthesised and characterised by multinuclear NMR. Addition of MCl_3 (M = Al, Ga) to BCl_3-pyridine adducts resulted in ionic liquids with borenium cations. These cations were found to have exceptionally high AN values, up to 180, when measured as a neat ionic liquid. In solution they were found to have lower, but still Lewis superacid, AN values (120). Fluorinated pyridines proved to be unsuitable for ionic liquid synthesis as they showed significant ligand redistribution and or isomerisation, only limited borenium cation formation and typically had a large amounts of precipitate in them.

By applying the technique used to synthesis borenium ionic liquids, five stibenium ionic liquids were successfully synthesised and characterised by multinuclear NMR. Those with phosphorous antimony linkage were found to be susceptible to redox behaviour at elevated temperature. The densities and viscosities of the liquids were measured and though $[SbCl_2L]^+$ cation containing ionic liquids could be synthesised, these liquids were extremely viscous (> 500 cP at 303 K).

Stibonium ionic liquids were not successfully produced due to the highly oxidising nature of Sb(V). Trioctylphosphine and trioctylphosphine sulphide were both rapidly converted to $[P_{888}Cl]^+$ in the presence of $SbCl_5$. Whilst the adduct $[SbCl_5(P_{888}O)]$ was stable, attempts at halide extraction resulted in decomposition of the sample.

The synthetic procedure used for borenium ionic liquids was not successfully applied to tin(IV) chloride. When tin(IV)-phosphine complexes underwent redox chemistry, likely forming the complex $[P_{888}Cl][Sn^{II}Cl_3]$ which itself may be an ionic liquid of interest to study. Tin(IV)-phosphine chalcogenide complexes formed readily, but underwent ligand scrambling upon the addition of the halide abstracting agent $AlCl_3$

However the oxidising potential of Sn(IV) and Sb(V) could be utilised as a legitimate synthetic pathway to make halometallate ionic liquids of the cation $[P_{888}Cl]^+$. Cations of this nature have found application in the conversion of alcohols to chloride functionality.[220]

3 Synthesis of polyalphaolefins

In this chapter, the core application of the developed liquid Lewis acids will be discussed: the synthesis of polyalphaolefins (PAOs), for the use as Group 4 base oils in synthetic automotive lubricants. Two separate projects were carried out, sponsored by two different industrial partners (Petronas and Evonik), exploring two groups of liquid catalysts: LCCs and borenium ionic liquids. The experimental part of this chapter is preceded by introduction to polyalphaolefins.

3.1 Introduction to polyalphaolefins

3.1.1 Lubricants and their properties

Lubricants are substances used to reduce friction between two surfaces. They prevent damage to moving parts of machinery and increase the efficiency of systems by preventing loss of energy to friction. Automotive lubricants are made by the combination of a base oil and additives, which make up to 10% of the lubricant. Base oils are divided into 5 groups with differing physical and chemical properties (Table 3.1-1). Of the base oil groups, groups I-III are derived from mineral oils, group IV is synthetic polyalphaolefins (PAOs) and group V base oils are all other base oils not included in groups I-IV (*e.g.* polyesters, polyethers, long chain fatty acids).[228] Additive packages are used to alter the properties of a base oil, tailoring the finished lubricant to its application.[229] For example, a pour point depression additive may be added to a lubricant intended for use at low temperatures.

Table 3.1-1 Typical properties of base oils[228]

Category	Saturates (%)	Sulphur (%)	Viscosity Index
Group I	< 90	≥ 0.03	80 ≤ VI ≤ 120
Group II	≥ 90	0.03	80 ≤ VI ≤ 120
Group III	≥ 90	0.03	≥ 120
Group IV (PAOs)	100	0	≥ 120

The physical properties of the lubricants are affected by the composition of the base oil. Mineral oil base oils (Groups I-III) contain a broad distribution of hydrocarbons of differing structures. Produced from oil refining processes, the impurities present are heavily dependent upon the quality of the crude oil. These base oils can contain paraffinic, naphthenic and aromatic compounds.[230] In contrast, PAOs are made by the Lewis acid-catalysed oligomerisation of 1-decene, or other alphaolefins, followed by catalytic hydrogenation.[231,232,233] The base oil product contains a distribution of dimers, trimers, tetramers, pentamers and heavier oligomers. The physical properties of the PAO base oil are

dependent upon the oligomers ratio and the branching of the oligomers. Because 1-decene itself is produced through ethylene oligomerisation, which is a very clean feedstock, PAOs tend to have fewer impurities compared to mineral base oils (Table 3.1-1).

There are a host of physical and chemical properties that should be considered when discussing lubricants, of which kinematic viscosity (K_v), viscosity index (VI), pour point (PP), volatility and oxidative stability are most relevant to this work.

Pour point (PP) is the temperature at which the base oil no longer flows, and as such must be low for low temperature applications. High content of aromatic or linear alkyl chains result in an increased pour point. Branched chains and substituted aromatics with longer side chains result in lower pour points.[230]

Viscosity is a measure of the resistance to flow of a liquid and determines the temperature range or application in which a given lubricant may be used. Kinematic viscosities at 40 and 100 °C are routinely measured for lubricant base oils.

Viscosity index (VI) is a measure of the rate of change of viscosity with respect to temperature, with a higher value indicating a lower rate of change of viscosity with changing temperature. Linear and lightly branched alkyl chains tend to have high VIs, whereas short chain substituted rings or highly branched paraffins tend to have lower VIs.[230,234] A high VI is required for applications with variable temperatures, *e.g.* automotive applications. Viscosity number (VN) has been used in place of the viscosity index for low viscosity samples, as the later is not defined for samples with a kinematic viscosity at 100 °C (Kv_{100}) less then 2 cSt.[234,235] Similarly to VI, a high VN indicates a smaller change in viscosity with temperature changes.

Volatility is the tendency of a substance to evaporate. This is measured by the Noack Volatility test, which records the percentage mass lost from a sample held at elevated temperature. Volatility increases with decreasing size of molecules. As such, base oils containing lighter molecules will have higher Noack values than those comprised of heavier molecules. A lower Noack volatility means lubricants used at elevated temperatures are more resistant to compositional change, and therefore will have a longer lifetime.

Oxidative stability is a measure of the chemical inertness of the base oil. In the Hot Oil Oxidation test, air is passed through the base oil at elevated temperatures, with iron used to catalyse oxidation. A number of parameters can be employed to assess the relative oxidative stability of different lubricants, such as: oxygen consumption, increase in the total acid

number, change in viscosity or consumption of antioxidant additives.[236,237] Saturated alkyl chains have high oxidative stability, comparatively unsaturated compounds have lower oxidative stability, thus in PAO production the hydrogenation step is crucial. Impurities can contribute to an accelerated rate of oxidation. A small change in the assessment parameters before and after oxidation indicates a lubricant with a high oxidative stability.

3.1.2 Structure and properties of polyalphaolefins

PAOs used as synthetic lubricant base oils are classed by their kinematic viscosity at 100 °C (Table 3.1-2), with popular classes having Kv_{100} of 2, 4, 6, 8, 10, 40 and 100 cSt. The relative proportion of the oligomers molecular weight determines the viscosity of the base oil, and therefore of the finished lubricant. 1-Decene dimers (C_{20}) are used to make very low viscosity PAO 2. PAO 4 and higher viscosity lubricants exclude the dimer, as this significantly increases the Noack volatility, making the lubricant unsuitable for higher temperature applications. Table 3.1-2 lists typical compositions of various PAO classes produced by Chevron Phillips.

Table 3.1-2: Composition of Synfluid branded PAOs (produced by Chevron Phillips)[238]

Synfluid	Composition
Synfluid PAO 2 cSt	98% decene dimer 1% monomer 1% trimer
Synfluid PAO 2.5 cSt	98% dodecene dimer and impurity: 2% decene/dodecene dimer
Synfluid PAO 4 cSt	85% decene trimer 13% decene tetramer 2% pentamer and higher
Synfluid PAO 5 cSt	87% dodecene, trimer 11% tetramer 2% pentamer and higher
Synfluid PAO 6 cSt	30% decene trimer, 47% decene tetramer, 23% decene pentamer and higher
Synfluid PAO 7 cSt	49% dodecene trimer 39% dodecene tetramer 12% dodecene pentamer and higher
Synfluid PAO 8 cSt	5% decene trimer 48% decene tetramer 47% decene pentamer and higher
Synfluid PAO 9 cSt	16% dodecene trimer 57% dodecene tetramer 27% dodecene pentamer and higher

The skeletal isomerisation of the hydrocarbons is also well known to affect the physical properties of the lubricant. Kioupis and Maginn performed molecular simulations to measure the physical properties of three differing molecular architectures of hydrogenated 1-hexene trimers (C_{18}), namely a "*star*" shaped (7-butyltetradecane), a highly branched (4,5,6,7-tetraethyldecane) and a linear octadecane. The authors showed that a high degree of

branching significantly lowered the pour point of the octadecane. The authors also showed a significant decrease in the viscosity number with an increasing degree of branching.[234] In a corroborating work, Scheuermann *et al*. isolated C_{20} fractions from commercial base oils and measured the viscosity number for C_{20} samples containing varying degrees of branching. Those which were highly branched were found to have significantly lower VN than those which were lightly branched.[235]

For lubricants with the same kinematic viscosity at 100 °C (Kv_{100}), PAOs have a higher VI, lower pour point (PP), and lower Noack volatility than group I-III base oils (Table 3.1-3). PAOs are suitable for use over a wide range of temperatures and are not readily susceptible to changes to their properties due to evaporation of the lubricant. When tested for oxidative stability by the Hot Oil Oxidation test and Panel Cooker test, PAOs show less change in viscosity and less mass gain when compared to mineral oils.[237] Finally, LD_{50} of PAOs was measured to be above 50 g kg^{-1}, as measured in rats, which renders them nontoxic.[237] Considering these advantages, synthetic automotive oils based on group IV base oils are now recommended by virtually all car manufacturers.

Table 3.1-3 Comparison of the physical properties of 4 cSt lubricants[237]

Base Oil (Group)	PAO (IV)	100N (II)	100N (II)	100NLP (II)	VHVI (III)
Kv_{100} (cSt)	3.90	3.81	4.06	4.02	3.75
Kv_{40} (cSt)	16.8	18.6	20.2	20.1	16.2
VI	137	89	98	94	121
PP (°C)	-70	-15	-12	-15	-27
Flash (°C)	215	200	212	197	206
Noack (%)	12.0	37.2	30.0	29.5	22.2

3.1.3 Synthesis of polyalphaolefins

3.1.3.1 Catalysis

It is relatively easy to induce carbocationic oligomerisation of higher olefins using a Lewis or a Brønsted acid, or their combination. However, different catalysts yield different products, with differing molecular weights[54] and branching,[239] which in turn has crucial impact on the base oil properties. Thus, the choice of catalyst is based upon the desired product distribution. As shown in Table 3.1-2, low viscosity PAOs are composed primarily of dimers, trimers, tetramers and pentamers of 1-decene, or sometimes 1-dodecene.

The first patented process for the oligomerisation of 1-decene using BF_3, promoted with *n*-butanol, was released by Brennan of Mobile Oil.[240] Since then, numerous patents have been

released; their key claims are compared in Table 3.1-4. BF_3-promoted oligomerisation is the current industrial standard. It typically gives high conversions with good selectivity to trimers and tetramers of 1-decene. The reaction temperature is quite low, which curtails excessive energy usage due to heating large volumes of reactants. Furthermore, BF_3 is a relatively cheap commodity chemical. On the negative side, BF_3 is a highly toxic and corrosive gas, which requires corrosion-resistant pressurisable equipment, leading to an increase in the cost of plant construction as well as maintenance. This is not considered a problem in established facilities with experienced staff and good safety precautions. However, CAPEX of constructing new oligomerisation facilities is quite high, and operational risks increase in the absence of appropriately trained and experienced workforce.

In more recent patents, the focus has been on diversification of the oligomerisation process, using new co-catalyst mixtures and, in particular, utilising alternative feedstocks, which is driven by the high global demand for 1-decene. Mixtures of olefins also make for interesting alternative feedstocks due to the reduction in processing costs of the feedstock (*e.g.* not having to separate C14, b.p. 251 °C, from C16, b.p. 274 °C).

Aluminium(III) chloride with protic additives has also been reported as a suitable catalyst for the oligomerisation of olefins, however it tends to yield much higher viscosity products (targeting polyalphaolefins classes PAO 40 and PAO 100).[239,241,242]

Table 3.1-4: Summary of selected oligomerisation data from patents utilising BF_3 as a catalyst.

Patent Number (Year)	Olefin	BF_3 Loading (wt%)	BF_3 Pressure (Bar)	Co-catalyst	Co-catalyst Loading (wt%)	Temp (°C)	Time (Hours)	Conversion (%)	Dimer (%)	Trimer (%)	Tetramer (%)	Pentamer + (%)
USP 3382291 (1968)[240]	C_{10}	0.54	-	nBuOH	-	30 - 50	1	> 80	< 15	37 - 55	-	-
USP 3763244 (1973)[243]	C_{10}	-	-	H_2O	-	25 - 27	2	96.4	18.5	77.9	Trace	-
USP 3780128 (1973)[244]	C_{10}	-	Continuous bubbling	nDecOH	-	25 - 32	2.5	100	30	70	-	-
	C_{10}	-	Continuous bubbling	nPrOH	1	25-35	2	100	1.7	54	43.2	-
USP 3997621 (1976)[245]	C_{10}	0.54	-	H_2O or Alcohol + Ester	-	15 - 50	1.5 - 4	-	-	35 -60	-	-
USP 4032591 (1977)[246]	C_{10}	-	3.44	nBuOH	-	40	-	79.8	9.4	44.7	19.2	6.5
USP 4045507 (1977)[247]	C_{10}	-	3.44	nBuOH	0.6	43.3	-	52.7	24.1	58.8	14.4	2.7
	C_{10}	-	3.44	nBuOH	0.6	43.3	-	90.5	3.8	35.1	48	13.1
	C_{10}	-	3.44	nBuOH	0.6	43.3	-	57.6	28.5	55.6	14.2	1.7
	C_{10}	-	3.44	nBuOH	0.6	43.3	-	98.7	3.6	31.6	51.3	13.5

USP 4376222 (1983)[248]	C_6	-	Continuous bubbling	$BF_3{\cdot}2H_2O$	0.075 ml	20 - 50	1.33 - 3.75	>99	0-14	62-76	19-31	-
USP 4409415 (1983)[249]	C_{10}	0.63	1.37	nBuOH	0.56	49 - 52	-	90	7.8	50.1	25.2	6.9
	C_{10}	0.53	1.37	nBuOH + Ethylene Glycol	0.4	48 - 50	-	91.8	9.4	52.8	23.7	5.9
USP 4587368 (1986)[250]	C_{10}	1.36	-	nHexOH + nPrOH	-	25	1.5 + 2	97.12	1.64	26.93	28.84	24.31
USP 6646174 (2003)[251]	$C_{10} + C_{12}$	-	2.5	nBuOH + EtOH	< 0.6	35	1 + 1	99.1	13.7	56.8	22.1	6.5
USP 7562497 (2009)[252]	$C_8 + C_{10} + C_{12}$	-	0.137-3.44	nBuOH		15 - 70	0.75 - 5	-	-	-	-	-
USP 8455416 (2013)[253]	$C_{14} + C_{16}$	-	3.5	nBuOH + Butyl Acetate	0.2	30	-	> 80	95	3	-	-

Whilst BF_3 is the catalyst of choice for industry, academic research has focused on alternative catalysts. Supported metal chlorides ($AlCl_3$, $FeCl_3$, $ZnCl_2$) and zeolites were used by Yadav and Doshi for the oligomerisation of 1-decene, as greener alternatives to BF_3. The catalysts required high temperatures (≥ 190 °C) and had a very high selectivity to the dimer.[254] The products properties were close to those of commercial PAO 2, however, this grade is of much lower commercial value than other PAO grades. Huang *et al.* utilised $AlCl_3$, $TiCl_4$ and $EtAlCl_2$ supported on $MgCl_2$[255] and SiO_2[256] to oligomerise 1-decene. Analysing the products by GC-MS and ^{13}C NMR, they authors showed that the products consisted of a mix of desired lightly branch PAOs and of highly branched oligomers.

Wassercheid and co-workers reported the use of chromium complexes, widely used in the selective trimerisation of ethene, for the selective trimerisation of 1-decene in a homogenous process.[257] The exceptionally high selectivity to the trimer product was due mechanistic difference between traditional carbocationic process and Cr-promoted synthesis. The products were lightly branched and had excellent VI upon hydrogenation (VI ≥ 125), though the Kv_{100} was typically around 3.2 cSt for the decene feedstock. Dodecene had a slightly higher Kv100 (4.3) and a high VI (150).

There was a number of attempts to use chloroaluminate(III) ionic liquids as catalysts For example, Ibragimova and colleagues oligomerised C_8 and C_{10} olefins using pyridinium and imidazolium chloroaluminate(III) ionic liquids. After removing all hydrocarbons with boiling points below 330 °C, they found the average carbon chain length to be greater for oligomerised 1-octene than 1-decene. Crucially, the oligomers had high viscosity (Kv_{100} > 8 cSt), whilst still containing low boiling point fraction. Should this be completely removed, further increase in the Kv_{100} would be expected. In general, the issue observed for catalysis with chloroaluminate(III) ionic liquids and no modifiers is similar to that with $AlCl_3$ used as catalysts - they are very active, but yield heavy oligomers with Kv_{100} values making them unsuitable for low viscosity lubricant production.

Stenzel *et al.* used $[C_4C_1im]Cl$-$[AlCl_4]$ χ_{AlCl3} = 0.52 with added $EtAlCl_2$ for the oligomerisation of C_2 - C_8 olefins.[127] The addition of $EtAlCl_2$, minimised cationic side reactions, resulting in low conversions and high selectivity to dimeric products. When $TiCl_4$ was added as a catalyst, narrow polydispersity atactic polymers were obtained, with average MW = 650 to 1620 g mol^{-1}, depending on the feedstock.

In search for alternatives to chloroaluminate(III) ionic liquids, Ding *et al.* compared chloroaluminate(III) and chloroferrate(III) systems as catalysts for oligomerisation of 1-decene at elevated temperature (160 °C). $[C_4C_1im][Al_2Cl_7]$ yielded twice the conversion and a much higher selectivity to trimers and tetramers compared to $[C_4C_1im][Fe_2Cl_7]$, likely due to the higher acidity of the former.[258] However, the quality of this publication is rather dubious. The authors report low conversions when using $[C_4C_1im][Al_2Cl_7]$ at 3 wt % when others have reported chloroaluminate ionic liquids to be very active.

Swadźba-Kwaśny, *et al.* oligomerised 1-pentene using chlorogallate(III) ionic liquids at ambient and lower temperatures. The design of experiment approach was used to establish the relationships between reaction conditions and products.[259] Catalyst concentration, temperature and reaction time were found - expectedly - to have a large effect on the product distribution, and by altering these reaction conditions the yield of unwanted heavy oligomers could be minimised. Unfortunately, chlorogallate(III) ionic liquids are prohibitively expensive, thus the study was only of academic interest. In addition, physical properties of 1-pentene oligomers, such as viscosity and pour point, were not reported.

In summary to this section, despite the plethora of studied catalytic systems (only representative selection of which were discussed above), it has proven challenging to find catalysts that would be economically viable, environmentally benign, and would deliver product distribution on par with that produced using the BF_3 catalyst family.

3.1.4 Carbocationic oligomerisation

As noted in the preceding chapter, different Lewis acid catalysts can have drastically differing product distributions. In order to understand why the oligomerisation process is so sensitive to the catalyst type and reaction conditions, mechanistic insight into carbocationic polymerisation (or oligomerisation) is needed. Carbocation polymerisation chemistry has been widely studied due to its commercial importance, in particular in the production of polyisobutene, which is used to make butyl rubber.

Carbocationic polymerisation is defined by three key steps: initiation, propagation and termination. The initiation step is the generation of the carbocation itself. Propagation is the addition of a nucleophilic monomer to the electrophilic carbocation, and termination is the neutralisation of the cation. In addition, the propagating cation may also transfer the charge from itself to another chain, terminating itself but without loss of the propagating species. This phenomenon is known as a chain transfer.

3.1.4.1 Initiation

3.1.4.1.1 Types of initiators

Kennedy described the numerous ways in which initiation process can occur[54] Chemical methods can be divided into two-electron (heterolytic) and one-electron (homolytic) transpositions. Heterolytic transpositions require a Brønsted acid, a Lewis (Friedel Crafts) acid, or a carbenium ion salt. Homolytic transpositions occur in direct radical oxidations and charge-transfer polymerisations. Finally, there are physical initiation methods which involve ionising radiation, UV radiation, field emission and field ionisation in an electric field, and electroinitiation. Lewis acids are of the greatest interest here and are discussed subsequently.

3.1.4.1.2 Initiating species in Lewis acid catalysis

As already discussed, of key industrial interest in the production of PAOs are Lewis acids, which incur chemical, two-electron initiation. Irrespective of the initiator, the two-electron systems generate a positively charged species which is capable of interacting with an electron rich centre, typically a C=C bond,[54,260] yielding a carbocation capable of propagation. In Brønsted acids, the initiating species is obviously a proton. In carbenium salts, it is the carbenium cation, produced by dissociation of this salt. In the case of Lewis acids, the question of the actual initiating species is slightly more problematic.

It has been shown that Friedel Crafts acids often require co-initiators to catalyse polymerisation. Whilst Friedel and Crafts had shown the catalytic ability of $AlCl_3$ and other metal halides in their early pioneering work, it is dubious that their work was carried out under strictly anhydrous conditions.[194] Evans and Polanyi showed that the polymerisation of isobutene using BF_3 was stalled under ultra-dry conditions.[261] Conversely, when the reactants weren't dried thoroughly, the addition of BF_3 to isobutene resulted in near-instantaneous polymerisation to very high molecular weight products. Isobutene with tertiary butanol impurities also polymerised rapidly in the presence of BF_3. Evans and Polanyi put forth the mechanism described in Equation 3.1-1 and Equation 3.1-2 to explain the initiation of the reaction.[261]

$$BF_3 + HA \longrightarrow F_3BHA \qquad \text{Equation 3.1-1}$$

$F_3BHA + CH_2=C(CH_3)_2 \rightarrow F_3BA^- + CH_3\text{-}C^+(CH_3)_2$ Equation 3.1-2

Where: A = conjugate base (*e.g.* OH^-, BuO^-)

Studies using deuterated water show exchange of the deuterium between the initiator and the product, reinforcing the view that in many Lewis acid catalysed carbocationic processes, proton exchange is necessary for the formations of the carbocation.[262] This is why Lewis acids reported to catalyse PAOs synthesis typically require protic co-catalysts. These protic initiating systems do not impart any functionality on the polymer, as only a proton is added to the terminal carbon.

In contrast, some initiating systems do not require protic activators. For example, Friedel Crafts acids combined with organohalides can be used to give functionalised head groups to polymers. The initiating species here is the carbocation generated when the metal halide extracts a halide ion from the organic molecule (Equation 3.1-3), generating a carbocation. The carbocation then acts as a Lewis acid and accept electrons from the monomer, forming the propagating chain (Equation 3.1-4). This method allows functionality to be bestowed upon the polymer.

$RX + MX_n \rightarrow R^+ + MX^-_{n+1}$ Equation 3.1-3

$R^+ + C=C \rightarrow R\text{–}C\text{–}C^+$ Equation 3.1-4

Polymerisation in some other systems was also found to proceed with rigorous drying and without the use of co-initiators, although Kennedy does point out the "*futility of chasing the last trace of water*", as the concentration of water required for polymerisation can be significantly below the detection limit of water.[54] For example, experiments carried out using 2,6-di-tert-butylpyridiene as a proton scavenger, showed that BCl_3 was capable of polymerising isobutene in absence of other initiators. This was shown to give lower weight polymers and slower reactions rates.[263,264]

There have been three routes of proton-free initiation proposed for Lewis acidic metal halides. The Sigwalt-Olah theory suggests direct halometallation of the double bond (Equation 3.1-5), which can be then ionised by a second Friedel Craft acid molecule (Equation 3.1-6).[54, 263, 264]

$MX_n + CH_2=CHR \rightarrow X_{n-1}M\text{–}CH_2\text{–}CRHX$ Equation 3.1-5

$$X_{n-1}M–CH_2–CHRX + MX_n \rightleftharpoons [X_{n-1}M–CH_2–C^+RH] + [MX_{n+1}]^-$$ Equation 3.1-6

The theory of autoionisation assumes, as the name suggests, autoionisation reaction of the Friedel Craft acid (Equation 3.1-7). These then react with the monomer (Equation 3.1-8), to give the same carbocation and counterion pair as in Equation 3.1-6.

$$2MX_n \rightleftharpoons [MX_{n-1}][MX_{n+1}]$$ Equation 3.1-7

$$[MX_{n-1}][MX_{n+1}] + CH_2=CRH \rightarrow [X_{n-1}M–CH_2–C^+RH] + [MX_{n+1}]^-$$ Equation 3.1-8

Finally, the Kennedy theory arises from the observation that carbocationic polymerisation can be halted in extremely dry styrene and butadiene, but not in isobutylene, isoprene and other systems with an allylic hydrogen. It suggests the metal halide is capable of hydride extraction from allyl (Equation 3.1-9).

$$CH_2=CR-CR_2H + MX_n \rightarrow CH_2=CR-C^+R_2 + [MX_nH]^-$$ Equation 3.1-9

Faust *et al.*[263] studied BCl_3-catalysed polymerisation of isobutene using ^1H and ^{11}B NMR spectroscopy, and reported that a boron head group existed in their quenched polymer. The reaction product, quenched with methanol, featured a peak at 32 ppm in their ^{11}B NMR spectrum. Subsequent addition of trimethoxyboron resulted in an additional peak appearing at 18 ppm, whereas the addition of isobutyldimethoxyboron resulted in the sharpening of the peak at 32 ppm. In addition, the ^1H NMR spectra of the system quenched with methanol gave a peak at 3.5 ppm, which was not present when quenched with CD_3OD. This suggests that a dimethoxyboron head group has been incorporated into the polymer. Finally Faust *et al.* used elemental analysis to see the difference in boron content of the polymer produced by BCl_3 alone, and BCl_3 with an alkyl halide co-initiator, 2,4,4-trimethylpentyl chloride. Both reactions were carried out in the presence of proton scavengers. They found significantly reduced boron content in the second system, with the small boron content being attributed to impurities or due to competition between the two initiation processes.

The above analysis highlights the fact that alterations in the catalytic system can result in significant mechanistic changes, thus leading to dramatically different reaction products.

3.1.4.2 Propagation

Propagation and termination in carbocationic processes are not firmly understood due to their complexity, difficulty in the elucidation of propagating structures and identifying termination points. The rapidity of carbocationic polymerisation, as well as sensitivity to

impurities, causes difficulty in measuring reaction rates and isolating or observing active species.

A key mechanistic point that is immediately obvious is that carbocationic polymerisation often takes places in organic solvents with a low dielectric constant. This would suggest that the cation and counter anion would be associated, and as such the initiating species that lead to generation of the carbocation-counterion pair have an important influence on the propagation and termination rates.[265, 266]

Styrene polymerisation, catalysed with acetyl perchlorate, resulted in a bimodal molecular weight distribution, with average MW values of 2,000 and 20,000 g mol^{-1}.[54, 267] The ratio of the two polymeric products was heavily affected by the polarity of the solvent. Reactions in solvents ranging from a mixture of nitrobenzene and dichloromethane (1:7), to a mixture of dichloromethane and benzene (2:1), saw a drop in the high molecular weight product and a rise in the low molecular weight product. Moreover, addition of *n*-Bu_4NClO_4 salt to the reaction supressed the formation of the high weight polymer, but not the low weight polymer. It has been suggested that this is due to two separate propagation mechanisms, with the high molecular weight polymer being produced *via* dissociated ions (favoured in more polar solvent), and the low by associated ions (favoured in low polarity solvent).

Sawamoto and Higashimura measured the polymerisation of *p*-methoxystyrene in 1,2-dichloroethane using four different initiating systems: I_2, CH_3SO_3H , $BF_3{\cdot}O(C_2H_5)_2$ and $SnCl_4$.[268] Addition of each initiator to the monomer resulted in a peak at 380 nm in a UV-Vis spectrum, which increased with time before reaching a maximum absorbance, and then decreased slowly. Monomer consumption, monitored at 295 nm, was largest when the absorbance at 380 nm was greatest, which suggests that the signal originates from a reactive intermediate (carbocation). The peak appeared at different rates for the different initiators, but with consistent maximum at 380 nm. Furthermore, propagation rate constants and molecular weights of the products were broadly similar for all four initiators. It was also observed that addition of *n*-Bu_4NI to all reactions suppressed the peak at 380 nm and monomer consumption rate. This led to conclusion that propagation in this case was taking place by a dissociated mechanism.

In the follow-up work,[269] Sawmoto and Higashimura discussed the effect of solvent polarity on the same polymerisation with the same initiators, using dichloromethane and dichloromethane/carbon tetrachloride mixtures as solvents. With increasing CCl_4 concentrations, the absorption peak at 380 nm was reduced, and was not replaced by other

peaks in the measured range, indicating significant decrease in the concentration of the propagating species with increasing volume of CCl_4. In contrast to what could be expected, however, the propagation rate constant was largely unaffected for the metal halide initiators, and was found to increase for iodine and CH_3SO_3H initiators, as polarity of the solvent decreased. It appeared that a second propagating species was present, undetectable by UV-Vis spectrometry, arguably related to an associated carbocation-counterion pair. When molecular weights of the products were compared, decreasing solvent polarity had little effect on the product of the $BF_3{\cdot}O(C_2H_5)_2$ system, but the product weight decreased significantly for CH_3SO_3H,. This could be interpreted as the $[CH_3SO_3]^-$ counteranion having a greater interaction with the carbocation than the fluoroborate anion, which is indeed consistent with their donor abilities.

Following on from these examples, as a general rule it must be noted that, although proton is often the key to the initiation step, mineral acids are poor catalysts for oligomerisation or polymerisation, often requiring extreme conditions, typically yielding only very low molecular weight oliogmers.[270,271] This can be associated with relatively strong interactions of conjugate bases of these acids with propagating carbocations. In contrast, Brønsted superacids, generated from the combination of Lewis and Brønsted acids, were found to induce a very rapid polymerisation of olefins to a high molecular weight products.[54,194] This is because conjugated bases of Brønsted superacids, generated by the reaction of a Lewis acid with a conjugate base of a Brønsted acid, are in general extremely non-coordinaing (*viz*. Chapter 1.1.5.1).

Propagation is further complicated by the fact that a carbocation can isomerise (Figure 3.3-1), with each carbocation having a differing stability and reactivity. Scheuermann *et al.* showed that the isomers formed as products of Lewis acid catalysed 1-decene oligomerisation could not all be accounted for by simple acid catalysed isomerisation of the 1-decene.[235] Cupples *et al.* measured ^{1}H NMR spectrum of oligomer products and found that the number of methyl branches was higher than that theoretically predicted by the accepted mechanism.[272] Shubkin and co-workers found that BF_3 catalysed oligomerisation of 1-decene resulted in products with differing physical properties than was expected by the conventional acid catalysed isomerisation of the olefin, due to the product having a higher than expected amount of methyl branching.[233]

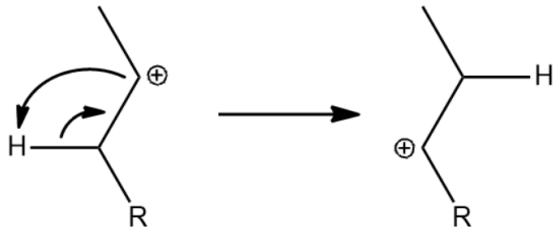

Figure 3.1-1: Simplified carbocation isomerisation

Shubkin and co-workers proposed isomerisation of cyclopropyl intermediates of the cationic dimer, driven by the formation of a tertiary carbocation, at the expense of a less thermodynamically stable secondary carbocation.

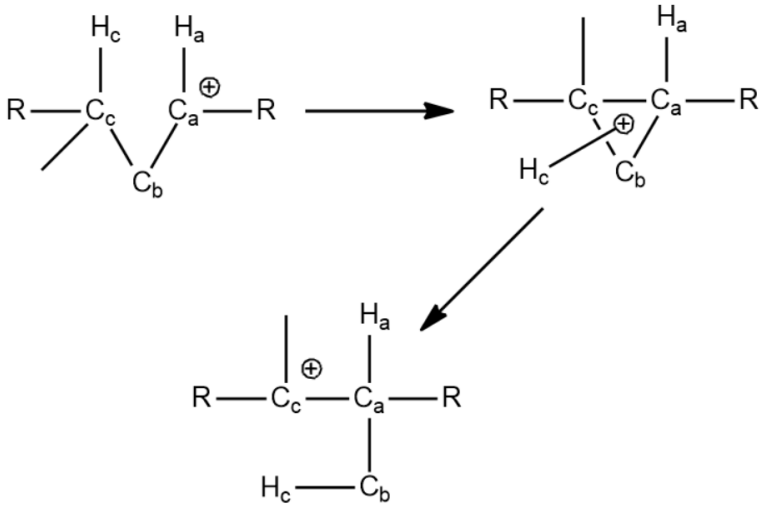

Figure 3.1-2: Shubkin's proposed mechanism for cyclopropyl rearrangement resulting in methyl branching (atoms labled for clarity)[233]

Cupples *et al.* also suggested that methyl migration must be possible for the monomer also.[272] They reported that with high 1-decene conversion (90%) the unreacted monomer contain a significant proportion of methylnonenes (1.5%), whereas at low conversions (30%), the unreacted decene contained a lower proportion of methylnonenes.

Ghosh *et al.* measured the kinetics of $[C_1C_1C_1NH][Al_2Cl_7]/H_2O$ catalysed oligomerisation of various octenes.[273] 1-octene was found to oligomerisise rapidly reaching near 91% conversion within 15 mins. Within the same time, a mix of *trans*- and *cis*-2-octene reached only 15% conversion, with significant preference for *cis*-2-octene conversion, and the mixture of *trans*-3-octene and *trans*-4-octene only reached 5.8% and 6.2% conversion respectively. The analysis of the polyoctenes showed decreasing oligomer chain lengths when internal olefins were used (Table 3.1-5).

Table 3.1-5: Relative oligomer chain lengths of $[C_1C_1C_1NH][Al_2Cl_7]$-catalysed octane oligomerisation

Octene	Trimer	Tetramer	Pentamer	Hexamer
1-octene	30.4	30.3	29.0	29.0
***Cis*- and *trans*-2-octene**	37.3	39.9	18.2	18.2
***Trans*-3-octene**	87.0	12.5	12.5	0.4
***Trans*-4-octene**	83.3	17.0	17.0	0.0

3.1.4.3 Termination and chain transfer

Termination of the propagating carbocationic chain can occur in a number of ways. Nucleophilic addition to the carbocation results in termination of the propagating chain. The counter anion can attack the carbocation forming a neutral species. Depending on the nucleophilicity of the counter anion this reaction can be rapid, and result in early chain termination, *i.e.* an addition reaction rather polymerisation. With decreasing nucleophilicity, the chain propagation can continue to greater lengths.[54] Chain transfer terminates the propagation of a chain and curtails the length of a polymer chain, but crucially does not result in the loss of the propagating species. *Quasi*-living polymers have a rapid equilibrium between a stable intermediate and the reactive carbocation. If the equilibrium can be shifted to the stable intermediate under certain conditions, polymerisation can be temporarily terminated in a controlled manner.[274]

The relative rates of propagation, chain transfer and termination are the deciding factors in whether polymerisation or oligomerisation takes place. Again, this illustrates the difficulty in adjusting the catalyst and reaction parameters in such manner, that the resulting product will have the desired molecular weight distribution.

3.2 LCCs catalysed oligomerisation of 1-decene

This project was sponsored by Petronas, the Malaysian national oil company, who were looking for new IP to edge into the synthetic lubricant market, currently dominated by three large companies: Chevron Phillips, INEOS and Exxon Mobile. Their strategy was to seek innovation in two areas: developing a new catalyst for a proprietary process, and developing a process that uses bio-sourced 1-decene. This feedstock had two advantages: its supply could be secured despite high demand of conventional petrochemical 1-decene in the market, and it gave a competitive edge in lubricant marketing.

The author has joined the project at stage 2, one year into the duration of the project. In the first stage, chlorometallate ionic liquids had been tried as catalyst with little success, and subsequently LCCs had been demonstrated to be viable candidates for further investigation. The body of work regarding this project was concerned with the synthesis of a wide range of LCCs (Chapter 2.1), and assessing their performance as catalysts on the small scale (40 ml feedstock). Reaction parameters were altered to assess their effect on the product distribution. Selection of the catalyst was based upon both catalyst performance and economics. Working with a PDRA employed for the scale-up phase of the project, the selected catalyst was tested on the large scale (3-5 L feedstock), with the ultimate aim of producing two lubricant samples, 3 L of PAO 4 and PAO 6 each. Overall duration of the stage 2 of the project was 12 months.

3.2.1 Experimental

3.2.1.1 Materials and methods

1-decene was obtained from Alfa Aesar and Sigma Aldrich and was used as received unless otherwise stated. Samples of $[C_2C_1im][Al_2Cl_7]$, $[C_8C_1im][Al_2Cl_7]$, $[C_2C_1im][Ga_2Cl_7]$ and $[C_8C_1im][Ga_2Cl_7]$ were synthesised following literature methods[25] and stored in the glovebox. Tetrabutylphosphonium chloride and trihexyl(tetradecyl)phosphonium chloride were provided by Cytec and dried at reduced pressure (80 °C, 24 h, ≤ 1 mbar) before use. The phosphonium chloroaluminate(III) ionic liquids were synthesised in the same manner as the 1,3-dialkylimidazolium analogues.

Synthesis of LCCs at small scale was described in Chapter 2.1.1. For the scale up reactions (Chapter 3.2.3.4), aluminium(III) chloride was purchased at lower purity grade (98 %) and was doubly sublimed[275] before use.

3.2.1.2 Small-scale oligomerisation

A battery of 8 computer controlled H.E.L. reactors (Figure 3.2-1) were used for small-scale oligomerisation. Prior to use, the reaction vessel and stirrer blades were dried in the oven overnight. The rest of the assembly could not be easily dismantled, and so was dried immediately prior to use with a heat gun. Olefin (1-decene, recycled decene and/or dimer, 40 ml) was added to the reaction vessel, which was then purged of air by positive argon pressure. The reaction vessel was set to desired reaction temperature (40 - 160 °C) and allowed to equilibrate whilst stirred at 600 rpm. The Lewis acidic catalyst (1.707 mmol – 5.121 mmol MCl_3 eq.) was loaded into a pre-dried gas-tight Hamilton syringe. The Lewis acid was added to the olefin and the reaction was allowed proceed for the allotted time (30 min - 2 h). Subsequently, the reaction was quenched with water, the organic phase dried and analysed by simulated distillation gas chromatography (SimDist GC).

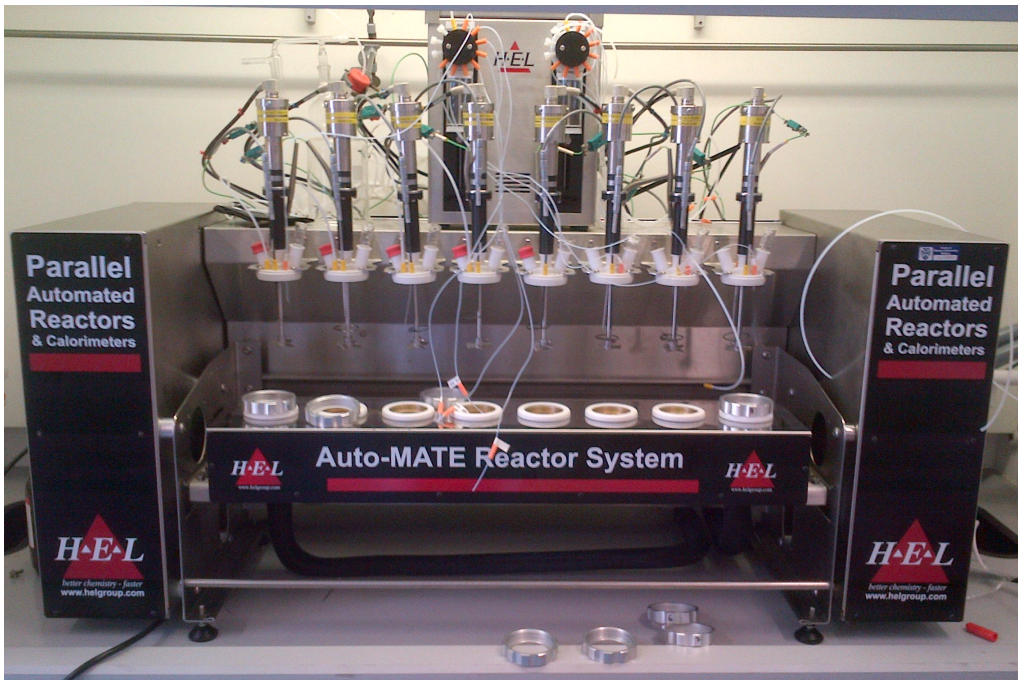

Figure 3.2-1: H.E.L. automated reactors used for small-scale oligomerisation experiments

3.2.1.3 Large-scale oligomerisation

The H.E.L. automated reactor with a 5 L vessel (Figure 3.2-2) was dried prior to use under vacuum (60 °C, 30 min) to remove residual cleaning solvents. It was then filled with decene

(2 kg, 2.7 L) and purged of air by positive pressure of argon. The decene was equilibrated at the required temperature (60 - 160 °C). The catalyst, Ur-$AlCl_3$ χ_{AlCl3} = 0.60, (0.25 - 3 wt%) was loaded into a pre-dried gas-tight Hamilton syringe, and added drop-wise to the decene. The reaction was left for the allotted time (1 - 2 h) and subsequently quenched with deionised water (3 x 1 L). The organic phase was retained, dried over $MgSO_4$ and analysed with SimDist GC.

Figure 3.2-2: H.E.L. automated reactor used for large-scale oligomerisations

3.2.1.4 Distillation

Prior to distillation, the crude oligomerised product was dried over $MgSO_4$ and filtered, to prevent bumping. Any residual solvents from cleaning the distillation rig were removed under reduced pressure (0.10 mmHg, 30 min). SimDist GC was used to predict expected volumes of different oligomers. Fractionated distillation of crude product was carried out using protocols set in ASTM D5236,[276] using a Distrilab D5236 Crude Oil Distillation System.

Figure 3.2-3: Distrilab D5236 Crude Oil Distillation System used to fractionate samples

The conditions and fractionation pattern of a typical distillation procedure are summarised in Table 3.2-1.

Table 3.2-1: Typical parameters for the distillation process

Fraction	Pressure (mm Hg)	Pot Temp (°C)	Vapour Temp (°C)	Vapour AET (°C)	Weight (g)
C_{10}	10	70-140	53-56	170-180	850
C_{20}	0.15	116	57	365	426.32
Cold Trap	-	-	-	-	108.28
C_{30} F1	0.15	180-198	107-150	330-386	38.20
C_{30} F2	0.15	198-201	150-173	386-414	45.76
C_{30} F3	0.15	201-204	173-177	414-421	42.07
C_{30} F4	0.15	204-206	177-182	421-426	44.53
C_{30} F5	0.15	206-208	182-185	426-430	40.69
C_{30} F6	0.15	208-209	185-187	430-432	38.74
C_{30} F7	0.15	209-211	187-189	432-434	42.41
Pot	-	-	-	-	216.79

3.2.1.5 Physical properties measurements

3.2.1.5.1 Kinematic viscosity and viscosity index

Kinematic viscosities measured according to ASTM D445-15a.[277] Kinematic viscosity was calculated by measuring flow of the PAO through calibrated Canon-Fenske routine

viscometers. The measurements were taken at 40 and 100 °C, which were used to calculate the viscosity index using ASTM D2270 – 10 (2016).[278]

3.2.1.5.2 Pour point

The pour point was measured according to ASTM D97-16,[279] using a Stanhope-Seta pour point cryostat, Model 93531-7, which was validated against a standard gas oil sample (99851-0, pour point -15 °C, cloud point -4 °C).

3.2.1.6 Simulated distillation gas chromatography (SimDist GC)

Samples for SimDist GC analysis were dissolved in toluene (100 mg cm^{-3}), dried over magnesium sulphate, filtered and analysed according to ASTM D6352.[280] The analysis were carried out using Agilent 6890N GC, fitted with an Agilent J&W DB-HT SimDist column, equipped with an FID detector and a high-performance HT PTV (high-temperature program - mable temperature vaporising) inlet with optimised design for SimDist applications.

3.2.2 Analysis of benchmark commercial samples

3.2.2.1 Physical properties

A number of commercial samples were analysed to validate in-house analytical procedures, and serve as benchmarks. Tested samples ranged from PAO 2 to PAO 100, and included several brands: Durasyn by Ineos, SpectraSyn by Exxon Mobil, Synfluid by Chevron Phillips and NEXBASE by Neste Oil.

Analysis of the physical properties, following ASTM methods, included measuring pour point[279] and kinematic viscosities at 40 and 100 °C,[277] and subsequently calculating the viscosity index (Table 3.2-2).[278]

Table 3.2-2: Measured and reported by the manufacturer physical properties of commercial samples of PAO

PAO	Kv 40 (cSt) Reported	Kv 40 (cSt) Measured	Kv 100 (cSt) Reported	Kv 100 (cSt) Measured	VI Measured	Pour Point (°C)
PAO 2 SpectraSyn	5.00	6.36	1.70	2.2	177	-51
PAO 4 Synfluid	16.80	16.6	3.90	4.02	146	<-63
PAO 4 Durasyn	17.25	16.02	3.92	3.85	137	<-63
PAO 4 SpectraSyn	18.14	17.17	4.03	4.12	147	<-63
PAO 6 Synfluid	30.50	27.94	5.80	5.43	133	-60
PAO6 Durasyn	30.22	27.62	5.76	5.23	123	-57
PAO 8 NEXBASE	48.50	43.28	7.90	7.46	138	-51
PAO 8 Durasyn	47.00	42.85	7.77	7.2	130.41	-57
PAO 40 Durasyn	396.00	371.51	39.00	41.13	163.51	-36
PAO 100 Durasyn	927.50	1,075.24	98.00	93.68	174.30	-27

3.2.2.2 Composition - distribution of oligomers by SimDist GC

The composition of commercial base oils was elucidated using simulated distillation gas chromatography (SimDist GC). Discussion of the results obtained for commercial base oils will be simultaneously used to discuss underlying principles of the technique.

SimDist GC is an ASTM[280] method of accurately determining the product distribution of a sample by the boiling point of the samples' components, much like True Boiling Point Distillation (TBP),[281] but using a much smaller sample, within shorter timeframe.[282] A sample is passed through a GC column with a non-polar stationary phase, which, in contrast to typical GC analysis, is not designed to preferentially retain samples based on polarity. Instead, samples elute directly in order of their boiling points. The temperature of the column is raised slowly in a linear fashion. The components of the sample are detected by a FID detector, which gives a chromatogram of signal intensity *vs.* retention time.

The SimDist GC is calibrated using a mix of paraffins of known boiling point (Figure 3.2-4). This allows retention time to be correlated to boiling point directly. Each peak of the calibration is also correlated with a response factor, which allows for relative peak size to be correlated with percentage mass eluted, making the analysis fully quantitative. This allows constructing boiling point curves from a GC experiment, rather than from an actual distillation and gives a complete percentage yield, which shows the atmospheric eqviulent boiling temperature at each 1% of mass eluted. The first and last 0.5% of mass eluted is disregarded to avoid giving inacurate Initial and Final Boiling Points (IBP and FBP).

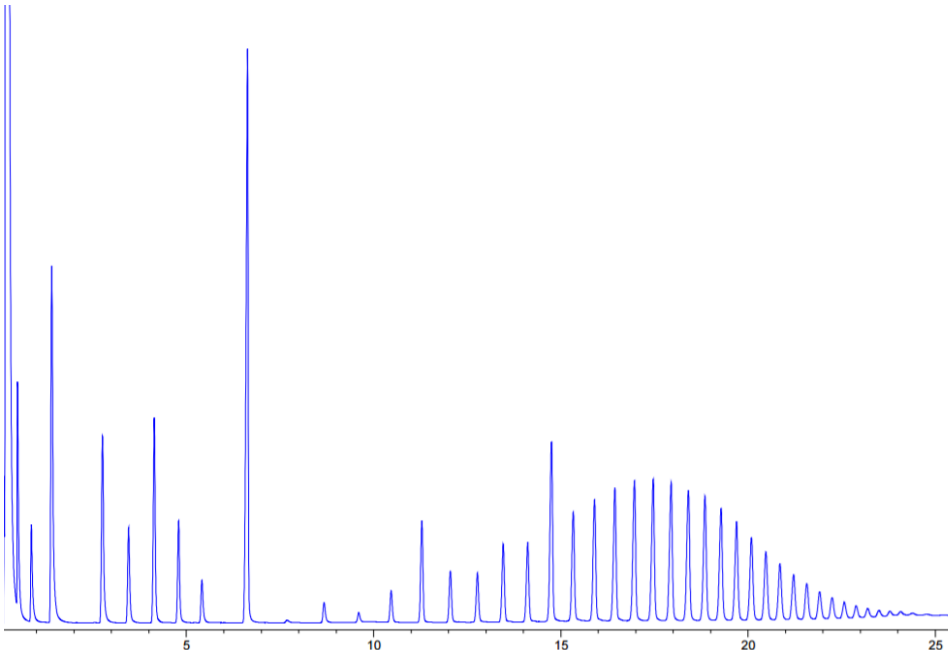

Figure 3.2-4: Chromatogram of boiling point calibration kit #1 and polywax 655 spiked with C_{20}, C_{30} and C_{40} for peak identification

Selected chromatograms of commercial base oils are shown in Figure 3.2-5. Discrete retention time ranges for all fractions of C_{10} oligomers could be assigned. Since retention times are correlated with temperatures, boiling points of each fraction could easily be determined. The temperature at troughs between each peak was taken as the boundaries for each oligomeric fraction. For example, the troughs either side of the C_{30} peak corresponded to boiling points of 370 and 450 °C, which were taken as boundaries for distillation of this fraction. Oligomers of C_{70+} are heavy (undesired) waste, and as such no distinction was made between C_{70}+ oligomers.

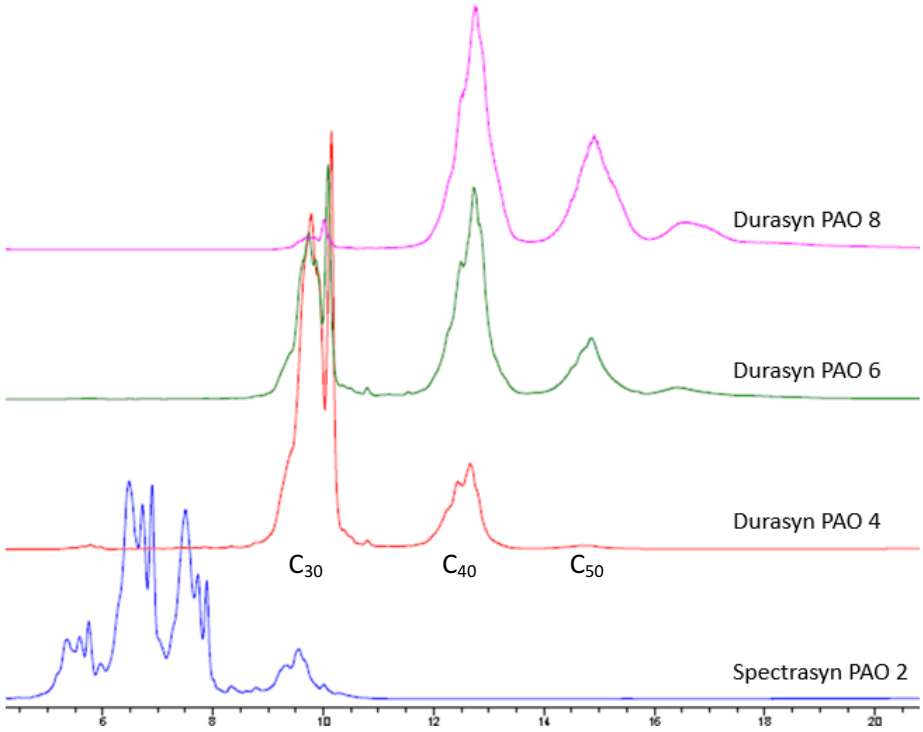

Figure 3.2-5: SimDist GC chromatogram of commercial samples of lubricant of varying Kv100

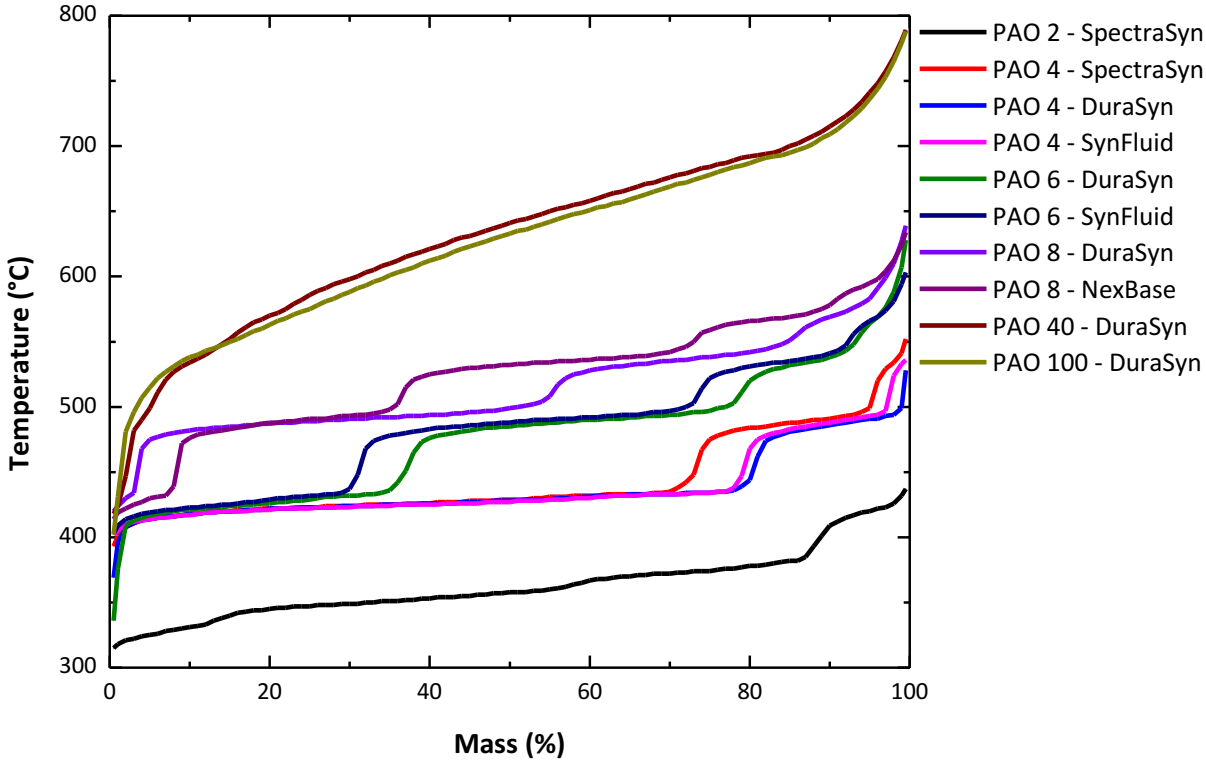

Figure 3.2-6: Boiling point curves of different commercial lubricants

Using the retention time and response factors the above chromatograms were converted to boiling point curves, which show cumulative mass % of a sample boiling at a given temperature (Figure 3.2-6). The 'steps' in PAO 4, PAO 6 and PAO 8 distillation curves correspond to distinct oligomeric fractions (C_{30}, C_{40} *etc*.)

Using boiling point thresholds established based on chromatograms (Figure 3.2-5), and quantitative data from distillation curves (Figure 3.2-6), composition of each base oil was calculated (Table 3.2-3). All oligomeric distributions are reported by mass %.

Table 3.2-3: Oligomer distribution of commercial lubricants

Brand	PAO	C_{30} (%)	C_{40} (%)	C_{50} (%)	C_{60} (%)	C_{70+} (%)
SpectraSyn	**PAO 4**	73.23	22.22	4.55	0.00	0.00
DuraSyn	**PAO 4**	80.30	19.19	0.51	0.00	0.00
SynFluid	**PAO 4**	79.29	18.18	2.53	0.00	0.00
DuraSyn	**PAO 6**	36.87	42.42	14.14	4.04	2.53
SynFluid	**PAO 6**	30.81	42.42	19.19	6.06	1.52
DuraSyn	**PAO 8**	2.53	52.53	30.30	9.09	5.56
NexBase	**PAO 8**	7.85	28.28	37.37	17.17	9.60
DuraSyn	**PAO 40**	1.52	4.04	9.09	9.09	76.26
DuraSyn	**PAO 100**	0.51	3.03	13.13	10.10	73.23

From Table 3.2-3 it is clear the key oligomers for the target PAOs (PAO 4 and PAO 6) are the trimer, tetramer and pentamer, with small amounts of higher oligomers in the PAO 6 samples. Therefore, reduction of waste C_{70}+ oligomers is of critical importance. Unreacted decene can potentially be recycled and the dimer can be either sold at a lower price as PAO 2, or potentially recycled back into the reaction. However, ideally, the percentage of C_{10} and C_{20} fractions in the post-reaction mixture should also be minimised.

3.2.3 Oligomerisation of petrochemical 1-decene using LCCs

3.2.3.1 General observations

The addition of the Lewis acidic catalysts to 1-decene typically resulted in a rapid increase in the temperature, due to the exothermic formation of the carbocation and rapid oligomerisation. The temperature would then drop to the baseline reaction temperature over the next 5-10 min as the rate of reaction decreased as monomer concentration dropped. The colour of the reaction took on a golden hue which was lost upon quenching the reaction with water. Though the oligomers of 1-decene have a higher viscosity that 1-decene, increasing viscosity was not an issue during the reaction due to the high temperatures used,

which kept viscosities relatively low. Upon cooling the product was noticeable more viscous than the starting material and had a slight yellow tinge, likely caused by unsaturated compounds in the product.

3.2.3.2 Reproducibility studies

As discussed in Chapter 3.1.4 carbocationic oligomerisation is extremely sensitive not only to the catalyst used and reaction conditions, but also to trace impurities, such as moisture. This required developing and maintaining very consistent procedures, in order to ensure reproducibility of the results.

To establish the reproducibility of the oligomerisation reaction, a number of repeated experiments were performed, using three catalyst systems: Ur-$AlCl_3$ χ_{AlCl3} = 0.60, DMA-$GaCl_3$ χ_{GaCl3} = 0.67, and Ur-$GaCl_3$ χ_{GaCl3} = 0.67. The distribution of oligomeric products is reported by mass % of the converted of 1-decene (see Table 3.2-4, Table 3.2-5, Table 3.2-6). For example, the first entry of Table 3.2-4 shows a total 1-decene conversion of 78.50%, of which 34.84 % is C_{20}. The average (*i.e.* arithmetic mean) and the standard deviation (StDev) was calculated for each oligomeric fraction. All reactions in the screening were performed for 1 hour at 120 °C.

Table 3.2-4: Product distribution for $AlCl_3$-Ur χ_{AlCl3} = 0.60, 1.707 mmol of MCl_3, 120 °C, 1 h

Entry	Conversion (%)	C_{20} (%)	C_{30} (%)	C_{40} (%)	C_{50} (%)	C_{60} (%)	C_{70+} (%)
1	78.50	34.84	37.42	15.48	5.16	5.16	1.94
2	80.50	30.19	36.48	17.61	8.81	3.77	3.14
3	77.50	37.91	33.99	15.69	7.84	2.61	1.96
4	78.50	37.42	29.68	14.19	9.03	5.16	4.52
5	78.50	36.13	30.97	16.77	9.03	3.87	3.23
Average	78.70	35.30	33.71	15.95	7.97	4.12	2.96
StDev	1.10	3.10	3.36	1.30	1.65	1.07	1.07

Table 3.2-5: Product distribution for DMA-$GaCl_3$ χ_{GaCl3} = 0.67, 1.707 mmol of MCl_3, 120 °C, 1 h

Entry	Conversion (%)	C_{20} (%)	C_{30} (%)	C_{40} (%)	C_{50} (%)	C_{60} (%)	C_{70+} (%)
1	79.50	33.12	28.03	16.56	11.46	6.37	4.46
2	85.50	33.14	26.04	16.57	10.65	7.10	6.51
3	84.50	32.34	26.35	15.57	11.98	8.38	5.39
4	83.50	31.52	27.88	15.76	10.91	7.27	6.67
Average	83.25	32.53	27.07	16.11	11.25	7.28	5.76
StDev	2.63	0.77	1.03	0.53	0.59	0.83	1.04

Table 3.2-6: Product distribution for Ur-$GaCl_3$ χ_{GaCl3} = 0.67, 1.707 mmol of MCl_3, 120 °C, 1 h

Entry	Conversion (%)	C_{20} (%)	C_{30} (%)	C_{40} (%)	C_{50} (%)	C_{60} (%)	C_{70+} (%)
1	73.50	40.00	35.86	13.79	6.90	2.76	0.69
2	71.50	32.62	35.46	17.02	8.51	4.26	2.13
3	76.50	31.79	34.44	17.22	10.60	3.97	1.99
4	72.50	32.17	34.97	16.78	9.79	4.20	2.10
Average	73.50	34.15	35.18	16.20	8.95	3.80	1.73
StDev	2.16	3.92	0.62	1.62	1.62	0.70	0.69

From these three sets of experiments, experimental error for conversions and yields in all fractions was set. The largest standard deviation for each parameters was taken and rounded to one significant number, given in mass %, as listed in Table 3.2-7.

Table 3.2-7: Experimentally established error of quantifying yield and content of each oligomer fraction in small-scale oligomerisation reactions, analysed by SimDist GC

	Conversion (%)	C_{20} (%)	C_{30} (%)	C_{40} (%)	C_{50} (%)	C_{60} (%)	C_{70+} (%)
Error	± 3	± 4	± 3	± 2	± 2	± 1	± 1

The most likely cause of error in the results is due to the varying quantity of residual moisture present. As pointed out by Kennedy (Chapter 3.1.4.1),[54] a quantity of water below detection limits can be sufficient to enable polymerisation to occur. It is bordering on impossible to remove virtually all water from the equipment used, which would as a matter of fact be disadvantageous, as adventitious water acts as co-catalysts. As has been shown in various patents (Table 3.1-4), variation in co-catalyst concentration can significantly alter the results of the oligomerisation. In order to maintain similar water contents between experiments, a great care was taken to maintain constant procedures of drying the equipment and setting up the reactions.

3.2.3.3 Influence of LCC ligand

3.2.3.3.1 Ligand screening

The ligands used in this study can be divided into two categories, those featuring at least one long alkyl chain ($P_{222}O$, $P_{888}O$, P_{888}, C_7CN) and the very polar ones, with urea-like structures (Ur, SUr, DMA, AcA). The LCCs made using these ligands, with both $AlCl_3$ and $GaCl_3$, were screened as catalysts for the oligomerisation of 1-decene. The C_7CN-$AlCl_3$ χ_{AlCl3} = 0.60 system was excluded from the study, since this composition contained significant amount of

precipitation (Chapter 2.1.2.5). For meaningful comparison, all reactions in the screening were carried out for 1 h, at 120 °C. LCCs were used at constant composition, fixed for each metal chloride: χ_{AlCl3} = 0.60 and χ_{GaCl3} = 0.67. LCC catalysts were used at quantities normalised to contain 1.707 mmol of metal chloride equivalent per 40 ml of 1-decene feedstock.

Conversions and product distributions are listed in Table 3.2-8 for L-$GaCl_3$ χ_{GaCl3} = 0.67, and in Table 3.2-9 for L-$AlCl_3$ χ_{AlCl3} = 0.60. The conversion of 1-decene was typically 75 – 85% for all the LCCs used (Table 3.2-8 and Table 3.2-9), irrespective of metal or ligand, with the noticeable exception of $P_{888}O$-$AlCl_3$ χ_{AlCl3} = 0.60, which only gave 61.5% conversion. Distribution of products is a more complex matter, as discussed below the two tables.

Table 3.2-8: 1-Decene conversions and product distributions achieved with L-$GaCl_3$ χ_{GaCl3} = 0.67 LCCs as catalysts (1.707 mmol of MCl_3 per 40 ml of 1-decene, 120 °C, 1 h). Results are listed in order of highest to lowest proportion of C20 in the product

Ligand (χ_{GaCl3} = 0.67)	Conversion (± 3 %)	C_{20} (± 4 %)	C_{30} (± 3 %)	C_{40} (± 2 %)	C_{50} (± 2 %)	C_{60} (± 1 %)	C_{70+} (± 1 %)
$P_{888}O$	81.50	45.96	33.54	14.91	4.97	0.62	0.00
P_{888}	76.50	43.71	35.76	14.57	5.30	0.66	0.00
C_7CN	86.50	42.11	33.92	15.20	5.85	2.34	0.58
$P_{222}O$	85.50	27.22	27.22	17.75	11.83	8.28	7.69
SUr	80.50	38.99	40.25	15.09	5.03	0.63	0.00
DMA	84.50	32.34	26.35	15.57	11.98	7.19	6.59
Ur	75.50	32.21	33.56	17.45	9.40	5.37	2.01
AcA	82.50	31.90	34.36	17.18	9.82	4.91	1.84

Table 3.2-9: 1-Decene conversions and product distributions achieved with L-$AlCl_3$ χ_{AlCl3} = 0.60 LCCs as catalysts (1.707 mmol of MCl_3 per 40 ml of 1-decene, 120 °C, 1 h). Results are listed in highest to lowest proportion of C20 in the product

Ligand (χ_{AlCl3} = 0.60)	Conversion (± 3 %)	C_{20} (± 4 %)	C_{30} (± 3 %)	C_{40} (± 2 %)	C_{50} (± 2 %)	C_{60} (± 1 %)	C_{70+} (± 1 %)
Ur	78.50	37.42	29.68	14.19	9.03	5.16	4.52
P_{888}	81.50	33.54	37.27	18.63	7.45	2.48	0.62
SUr	87.50	30.06	35.84	19.65	9.25	3.47	1.73
DMA	81.50	29.81	23.60	14.91	12.42	8.70	10.56
AcA	79.50	28.03	33.12	17.83	11.46	5.10	4.46
$P_{888}O$	61.50	19.83	36.36	19.83	13.22	6.61	4.13
$P_{222}O$	87.50	16.18	17.34	17.34	16.18	13.87	19.08

Of the four LCCs based on urea-like ligands, Ur-MCl_3 $\chi_{MCl3} \geq 0.60$ and AcA-MCl_3 $\chi_{MCl3} \geq 0.60$ behaved in a similar fashion. The use of Ur-$GaCl_3$ and AcA-$GaCl_3$ χ_{GaCl3} = 0.67 resulted in near identical product distributions (Figure 3.2-7), though the former converted 7% less decene (Table 3.2-8). Only small discrepancies were noted between oligomers produced using Ur-$AlCl_3$ and AcA-$AlCl_3$ χ_{AlCl3} = 0.60 (Figure 3.2-8): the former gave 9% more dimer than the later, but *ca*.

3.5% less trimer and tetramer, and there was no significant difference in the proportion of C_{60} and C_{70+} produced, nor in the conversion of 1-decene (Table 3.2-9).

Like Ur and AcA, DMA is an *O*-donor, structurally very similar to the two others. Surprisingly, catalysis with DMA-MCl_3 LCCs, irrespective of metal, resulted in a significantly different product distribution compared to the AcA-MCl_3 and Ur-MCl_3 analogues. Firstly, an experimental error was considered as the potential explanation. DMA is a liquid at room temperature, hence it was dried over molecular sieves, as opposed to being dried by heating under vacuum, like AcA and Ur. Potentially, differences in treatment could lead to varying moisture contents, with DMA-LCCs containing greater concentration of superacidic protons, which in turn has been shown shift the distribution to heavier oligomers.[239] However, molecular sieves have been shown to be effective at removing water from hydroscopic polar solvents,[283] and using freshly distilled DMA made no difference in the reaction outcome. An alternative explanation, which appears to be an overarching theme of this thesis, lies in speciation. Liu *et al*. report significant differences in coordination of DMA and AcA to $AlCl_3$ (Chapter 1.2.3.2).[154] This results in differences in the speciation of the catalyst. The sum of the cation and anion integral area increased in the order AcA<DMA<NMA for L-$AlCl_3$ $0.50 \leq \chi_{MCl3} \leq 0.60$ ergo, DMA LCCs have a higher concentration of Lewis acidic anions than AcA LCCs which will alter initiation propagation and termination rates, as discussed in Chapter 3.1.4.

For SUr-$AlCl_3$ χ_{AlCl3} = 0.60 and SUr-$GaCl_3$ χ_{GaCl3} = 0.60 LCCs the products of oligomerisation were typically enriched in C_{20} and C_{30} and had little C_{60} and C_{70} (Table 3.2-8 and Table 3.2-9). SUr-$AlCl_3$ χ_{AlCl3} = 0.60 had the 2nd highest and highest proportions of C_{20} and C_{30} (30.06% and 35.84%) and the least C_{60} and C_{70}+ (3.47% and 1.73%) of the urea like family of catalysts with $AlCl_3$. Similarly SUr-$GaCl_3$ χ_{GaCl3} = 0.60 had the highest C_{20} and C_{30} (38.99% and 40.25%) and least C_{60} and C_{70+} (0.63% and 0%) of the urea like family of catalysts with $GaCl_3$. This would appear to follow the iconicity trend of the oxygen donors, as sulphur donors were shown to more likely to form neutral complexes than oxygen donors (Chapter 2.2). A less ionic catalyst would likely push the carbocation to a more associated pair with its counteranion, increasing the energy demand to separate them and thus slowing propagation.

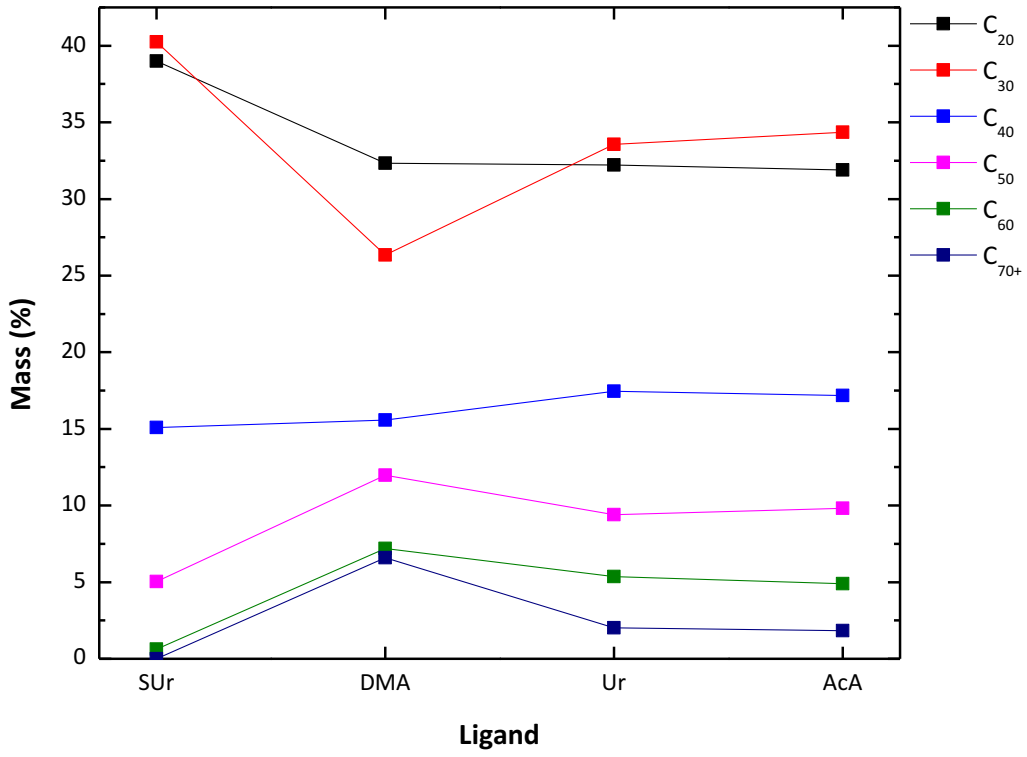

Figure 3.2-7: Products distribution achieved using L-$GaCl_3$ χ_{GaCl3} = 0.67 LCCs as catalysts (1.707 mmol of MCl_3, 120 °C, 1 h)

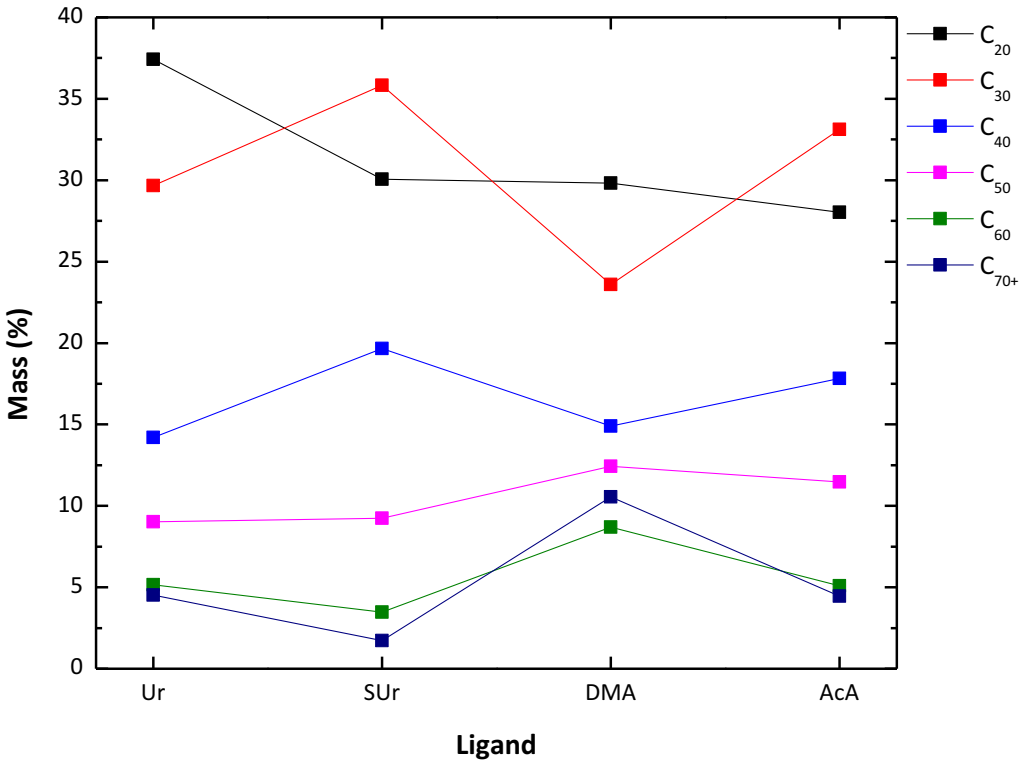

Figure 3.2-8: Products distribution achieved using L-$AlCl_3$ χ_{AlCl3} = 0.60 LCCs as catalysts (1.707 mmol of MCl_3, 120 °C, 1 h)

L-$GaCl_3$ χ_{GaCl3} = 0.67 catalysts based on ligands with octyl alkyl chains gave, in general, similar products distribution (Figure 3.2-9, Table 3.2-8), irrespective of the donor atom. The products were on average lighter compared to the corresponding LCCs with urea-like ligands (Figure 3.2-7). Interestingly, the product distribution obtained with C_7CN-$GaCl_3$ χ_{GaCl3} = 0.67 is not significantly different to those obtained with P_{888}-$GaCl_3$ χ_{GaCl3} = 0.67 and $P_{888}O$-$GaCl_3$ χ_{GaCl3} = 0.67. In Chapter 2.1.2.5 it was seen that C_7CN-$AlCl_3$ mixtures were ionic liquids rather than LCCs. Assuming a similar speciation for C_7CN-$GaCl_3$ mixtures and extrapolating from Equation 2.1-6, it would appear that the main chlorometallate anion in this composition is $[Ga_4Cl_{10}]^-$, with some $[Ga_3Cl_7]^-$ (Equation 3.1-2, see also Chapter 2.1.2.5), as opposed to $[Ga_3Cl_7]^-$ only for LCCs (Figure 1.2-8).[135]

$$12GaCl_3 + 6C_7CN \rightarrow [Ga(C_7CN)_6]^{3+} + 2[Ga_4Cl_{10}]^- + [Ga_3Cl_7]^- \quad (\chi_{GaCl3} = 0.67) \qquad \text{Equation 3.2-1}$$

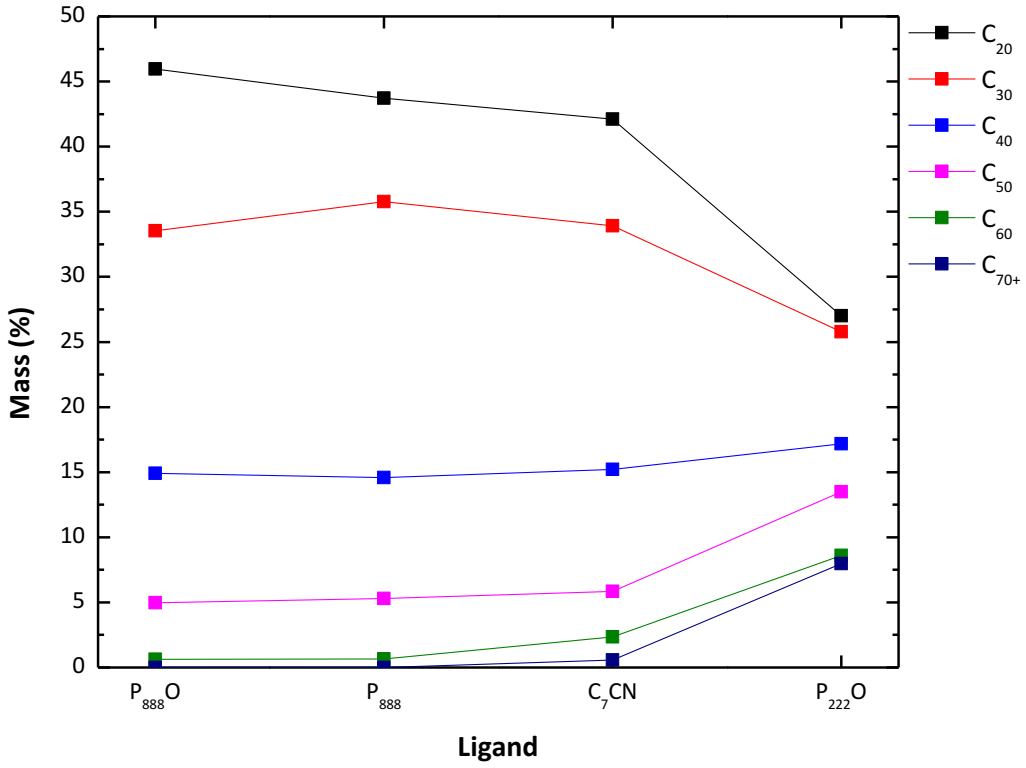

Figure 3.2-9: Products distribution achieved using L-$GaCl_3$ χ_{GaCl3} = 0.67 LCCs as catalysts (1.707 mmol of MCl_3, 120 °C, 1 h)

P_{888}-$AlCl_3$ χ_{AlCl3} = 0.60 gave product distribution similar to that obtained with corresponding LCCs with urea-like ligands (Figure 3.2-10, Table 3.2-9) though typically with led C_{50+} content in the product. In contrast, reaction catalysed with $P_{888}O$-$AlCl_3$ χ_{AlCl3} = 0.60 (Figure 3.2-10, Table

3.2-9) yielded relatively little dimer and a lot of trimer. Coupling it with lower conversion, it appears that the rate of termination, compared to chain transfer, is higher in $P_{888}O$-$AlCl_3$ χ_{AlCl3} = 0.60 than in any other LCC.

It is interesting to compare products synthesised with $P_{222}O$-MCl_3 *vs*. those synthesised with corresponding $P_{888}O$-MCl_3. In both cases, the short-chain ligand in LCC induces the synthesis of much heavier products. Considering chemical similarities, this may arise from phase behaviour rather than speciation; *i.e.*, complexes containing $P_{888}O$ are expected to be much more lipophilic than those based on $P_{222}O$. This is somewhat surprising, because more lipophilic ligands would be expected to remain dissolved in the oligomerising mixture for longer, therefore allowing for longer oligomers. More polar ligands should induce fast phase-separation of the catalyst. Here, the results show exactly the opposite outcome.

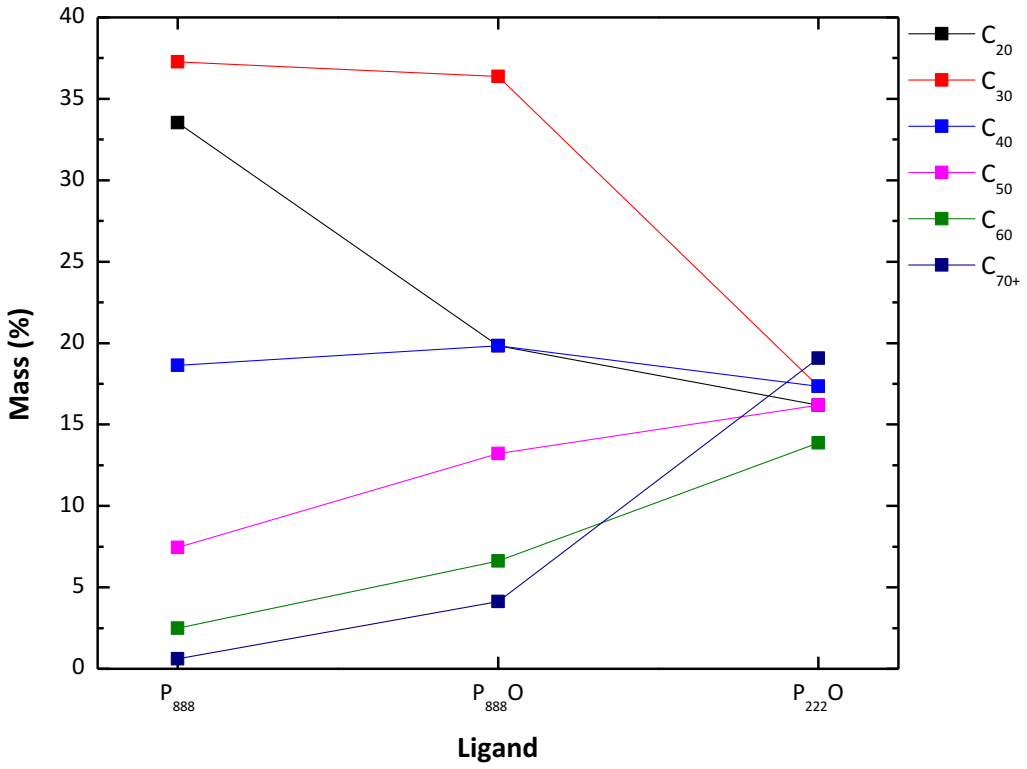

Figure 3.2-10 Products distribution achieved using L-$AlCl_3$ χ_{AlCl3} = 0.60 LCCs as catalysts (1.707 mmol of MCl_3, 120 °C, 1 h)

3.2.3.3.2 Comparison with ionic liquid catalysts

To further the understanding as to why different ligands should cause different distributions, comparative reactions catalysed with solid aluminium(III) chloride, and several chlorometallate(III) ionic liquids, were studied (

Table 3.2-10, Figure 3.2-11). The ionic liquids chosen used the commonly used imidazolium and phosphonium cations. As miscibility of the catalysts and 1-decene was suspected to play a role what oligomer distribution was obtained, both short chain, $[C_2C_1im]^+$ and $[P_{4444}]^+$, and long chain, $[C_8C_1im]^+$ and $[P_{66614}]^+$, examples of the each cation were used. Furthermore $GaCl_3$-imidazolium ionic liquids were used to check parity of behaviour between $AlCl_3$ and $GaCl_3$ based catalysts.

Table 3.2-10: Decene conversions and product distributions achieved with L-$AlCl_3$ χ_{AlCl3} = 0.60 LCCs as catalysts (1.707 mmol of MCl_3 per 40 ml of 1-decene, 120 °C, 1 h).

Catalyst	Conversion (± 3 %)	C_{20} (± 4 %)	C_{30} (± 3 %)	C_{40} (± 2 %)	C_{50} (± 2 %)	C_{60} (± 1 %)	C_{70+} (± 1 %)
$AlCl_3$	55.50	18.35	29.36	23.85	20.18	8.26	0.00
$[C_2C_1im][Al_2Cl_7]$	79.50	31.85	24.20	15.29	14.01	8.92	5.73
$[C_8C_1im][Al_2Cl_7]$	86.50	17.54	19.88	16.37	15.20	11.70	19.30
$[C_2C_1im][Ga_2Cl_7]$	89.50	20.34	25.99	20.34	15.82	9.04	8.47
$[C_8C_1im][Ga_2Cl_7]$	90.50	15.64	24.58	20.11	17.88	11.17	10.61
$[P_{4444}][Al_2Cl_7]$	85.50	20.12	27.22	20.12	16.57	9.47	6.51
$[P_{66614}][Al_2Cl_7]$	95.50	5.29	12.70	14.81	19.05	19.05	29.10

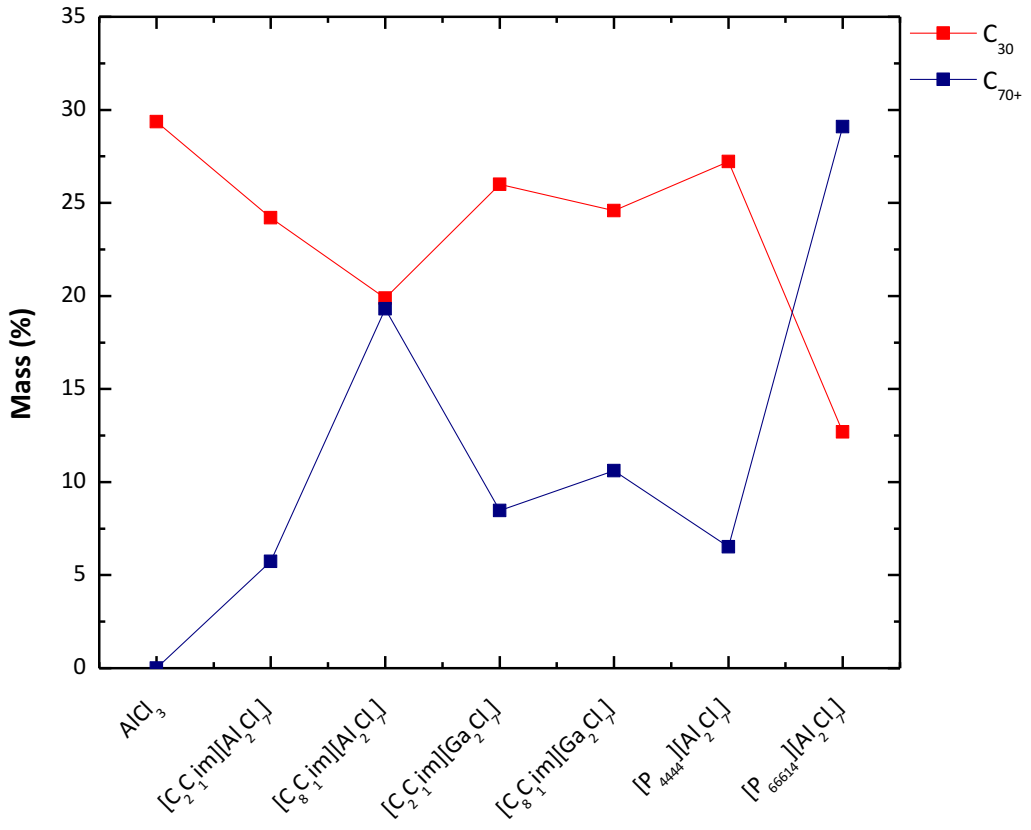

Figure 3.2-11: Distribution of two product fractions for $AlCl_3$ and ionic liquid-catalysed oligomerisation of 1-decene, χ_{AlCl3} = 0.60, 1.707 mmol MCl_3. Other fractions omitted for clarity.

Within each group of ionic liquids used here, there is a clear trend of increasing heavy oligomer production with increasing alkyl chain length, *i.e.* increasing lipophilicity (

Table 3.2-10). This trend is strongest in phosphonium cation group, *i.e.* changing $[P_{4444}][Al_2Cl_7]$ to $[P_{66614}][Al_2Cl_7]$ resulted in *ca.* 15% decrease in dimer content, and increase of *ca.* 23% in C_{70+} content, with 10% increase in conversion. The high conversion and selectivity to heavier oligomers seen with $[P_{66614}][Al_2Cl_7]$ is contrasted by the low conversion (55.50%) and higher trimer selectivity achieved with powdered $AlCl_3$. The influence of cation lipophilicity on both conversion and product distribution is much smaller in chlorogallate(III) ionic liquids, compared to chloroaluminate(III) systems. When changing the cation from polar $[C_2C_1im]^+$ to more lipophilic $[C_8C_1im]^+$, there was a 14.31% decrease in dimer for chloroaluminates(III), but only 4.70% decrease for chlorogallates(III). At the same time, the C_{70+} fraction increased by 13.57% for chloroaluminates(III), and by 2.41% for chlorogallates(III).

Olivier-Bourbigou *et al.* found 1-hexene hydroformylation was accelerated in alkylmethylimidizolium ionic liquids for a given anion by increasing the length of the alkylchain on the imidazolium ring.[284] This in turn was correlated with an increased miscibility between the ionic liquid and the alkene, which was related to a decrease in columbic interactions between anion and cation with increasing chain length.[134]. Both chloroaluminate(III) and chlorogallate(III) ionic liquids see a significant shift in the product distribution towards heavier oligomer with increasing chain length. Combined with the low conversion of aluminium chloride, which is not readably soluble in hydrocarbons, it would suggest that miscibility of the catalyst and feedstock is a factor in determining the product distribution, with high miscibility increasing the relative rate of propagation *vs.* termination of the carbocation. Very surprisingly, in the LCCs with long alkyl chains (P_{888}, $P_{888}O$ and C_7CN) do not enhance the production of heavy oligomers. In fact, the opposite trend is observed: the comparison of $P_{888}O$-MCl_3 $\chi_{MCl3} \geq 0.6$ and $P_{222}O$-MCl_3 $\chi_{MCl3} \geq 0.6$ shows the product distribution to be shifted to the heavier oligomers with a decreased chain length.

3.2.3.3.3 Conclusions from ligand screening

There are two clear criteria that have been shown to significantly affect how the carbocationic oligomerisation of 1-decene proceeds. From the LCC study, the comparison of the urea-like ligand containing catalysts show that ionicity/polarity is a significant factor. By comparing the product distribution achieved using AcA-MCl_3 $\chi_{MCl3} \geq 0.6$ and DMA-MCl $\chi_{MCl3} \geq 0.6$ with the sum of the anion and cation peaks in the ^{27}Al NMR spectra measured by Liu *et al.* it appears that a higher ionicity results in a shift to heavier oligomers. Conversely sulphur was shown in Chapter 2.1.2.4 to promote the formation of molecular adducts of the ionic LCCs,

and as such SUr-MCl_3 χ_{MCl3} ≥ 0.6 gave product distributions more focused on the light oligomers.

The ionic liquid study also showed that lipophilicity was a key factor. Ionic liquids with the same anion showed a marked increase in the conversion of 1-decene and of heavier oligomers in the product. This is best exemplified by the difference in the product distributions of $[P_{4444}][Al_2Cl_7]$ and $[P_{66614}][Al_2Cl_7]$ (Figure 3.2-11).

As there are a wide range of ligand available to choose from to make LCCs, there is a degree of tunability which would make LCCs interesting to study in a range of carbocationic processes.

3.2.3.3.4 Influence of catalyst loading

The distribution of oligomers were studied as a function of catalyst loading, using the catalytic system Ur-$AlCl_3$ χ_{AlCl3} = 0.60 (Figure 3.2-12, Table 3.2-11). Catalyst loading can be seen to have two important effects upon the reaction. Firstly, conversion is increased by 12% upon tripling the catalyst loading. Secondly, there was a shift towards the heavier oligomers. The C_{20} fraction was seen to drop by 4% upon tripling the catalyst loading. Simultaneously, heavier C_{60} and C_{70+} fractions amount decrease by 1.72% and 1.63%. This could be down to greater number of initiating protons, resulting in more propagating chains reacting with the 1-decene.

Increased yield of desired C_{30} and C_{40} fractions and increased conversion are both an advantage; as a higher value product is obtained, with less starting material to be recycled, leading to a decrease in OPEX. At the same time, although the Ur-$AlCl_3$ χ_{AlCl3} = 0.60 is a very cheap system, tripling its loading is bound to increase OPEX of the process. To find optimum catalyst loading in such case is not a trivial task, and techno-economical evaluation of the entire process is necessary.

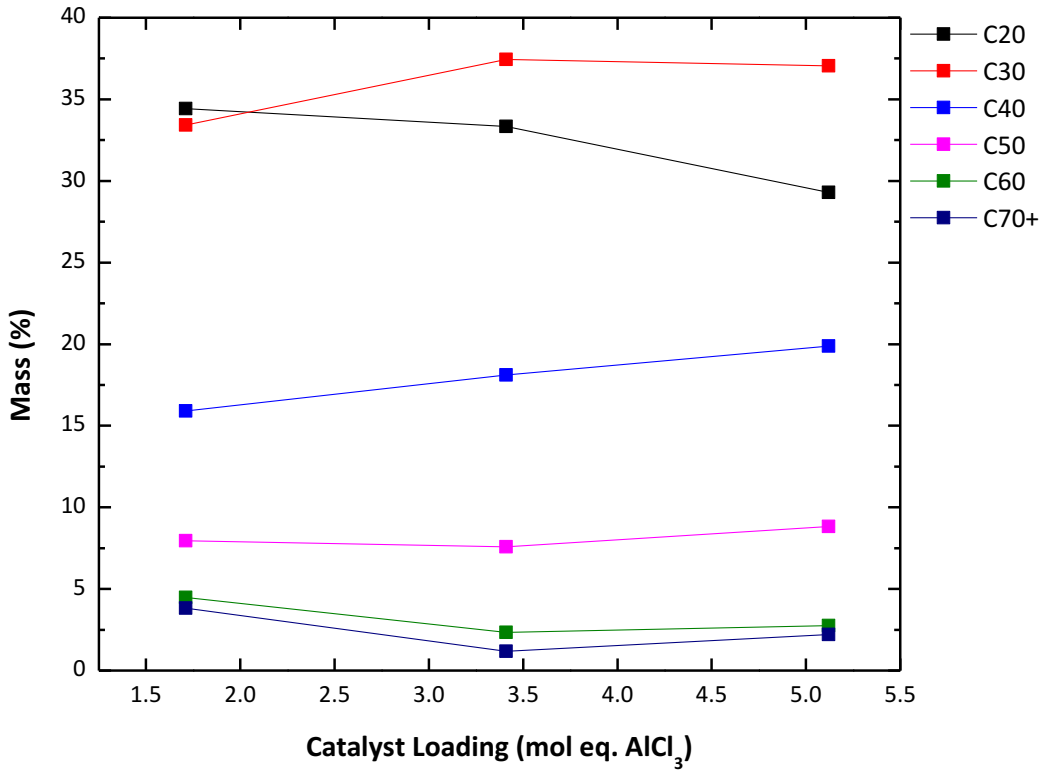

Figure 3.2-12: Product distribution achieved using Ur-$AlCl_3$ χ_{AlCl3} = 0.60 as the catalyst, with variable loadings (120 °C, 1 h)

Table 3.2-11: Product distribution achieved using Ur-$AlCl_3$ χ_{AlCl3} = 0.60 as the catalyst, with variable loadings (120 °C, 1 h)

Catalyst	Conversion (± 3 %)	C_{20} (± 4 %)	C_{30} (± 3 %)	C_{40} (± 2 %)	C_{50} (± 2 %)	C_{60} (± 1 %)	C_{70+} (± 1 %)
5.12	91.50	29.30	37.04	19.88	8.82	2.75	2.21
3.41	86.50	33.33	37.44	18.12	7.59	2.34	1.17
1.71	79.50	34.43	33.42	15.91	7.96	4.47	3.82

3.2.3.3.5 Influence of catalyst composition

As noted in Chapter 2.1.2.1, gallium(III) chloride LCCs can form higher anionic oligomers than aluminium(III) chloride analogues, and as such they are liquid over a larger range of χ_{GaCl3} values.[143] To study the influence of metal to ligand ration in an LCC catalyst, DMA-$GaCl_3$ was used, with χ_{GaCl3} = 0.50, 0.60, 0.67 and 0.75. For each oligomerisation experiment, the catalyst amount used was normalised to contain mole equivalent of 1.707 mmol of $GaCl_3$. With this approach, the investigated parameter was the speciation of chlorogallate(III) complexes in the LCC, not the concentration of LCC. Conversions and product distributions obtained as a function of χ_{GaCl3} value of the catalyst are compared in Figure 3.2-13 and Table 3.2-12.

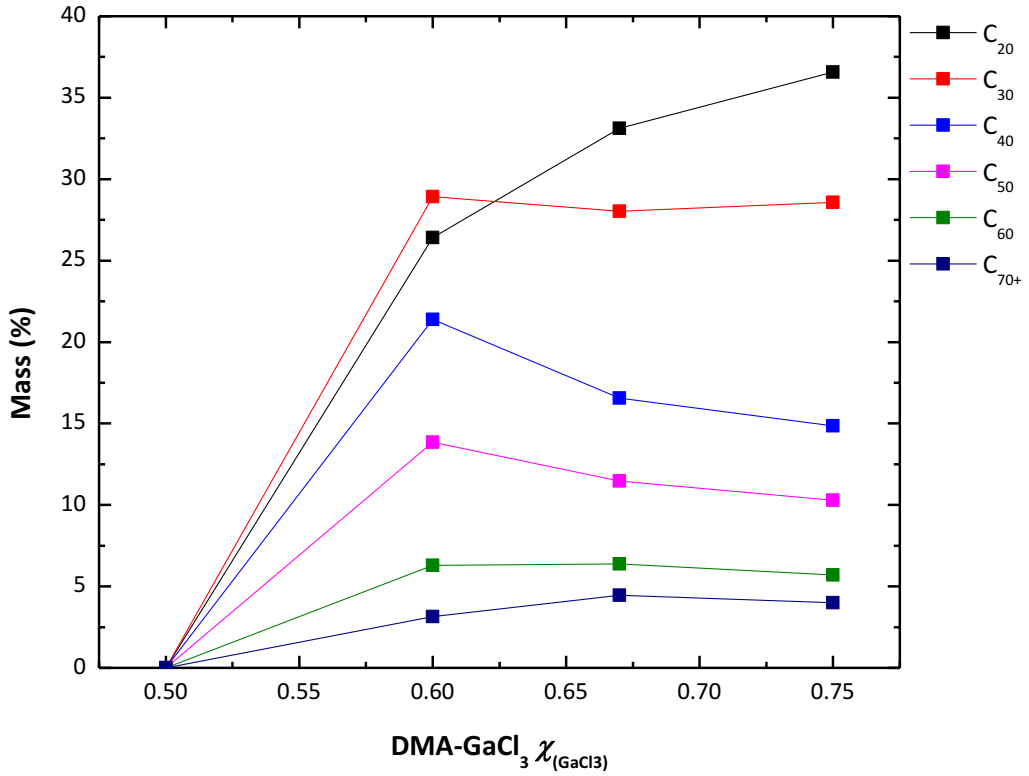

Figure 3.2-13: Product distribution achieved using DMA-$GaCl_3$ as the catalyst, with variable χ_{GaCl3} values (1.707 mmol of MCl_3, 120 °C, 1 h)

Table 3.2-12: Product distribution achieved using DMA-$GaCl_3$ as the catalyst, with variable χ_{GaCl3} values (1.707 mmol of MCl_3, 120 °C, 1 h)

Catalyst	χ_{GaCl3}	Conversion (± 3 %)	C_{20} (± 4 %)	C_{30} (± 3 %)	C_{40} (± 2 %)	C_{50} (± 2 %)	C_{60} (± 1 %)	C_{70+} (± 1 %)
DMA-$GaCl_3$	0.50	0.00	0.00	0.00	0.00	0.00	0.00	0.00
	0.60	80.50	26.42	28.93	21.38	13.84	6.29	3.14
	0.67	79.50	33.12	28.03	16.56	11.46	6.37	4.46
	0.75	88.50	36.57	28.57	14.86	10.29	5.71	4.00

The first and foremost observation is, that for χ_{GaCl3} = 0.50 there was no conversion (Table 3.2 12). At this composition the main anion is $[GaCl_4]^-$, which is not Lewis acidic, and was not expected to catalyse the reaction. At high χ_{GaCl3} values there is a gradual shift towards larger oligomeric species, such as $[Ga_2Cl_7]$-, and then $[Ga_3Cl_{10}]^-$ [135]. The C_{20} content of the product is decreased by 10.15% when the chi value is raised from χ_{GaCl3} = 0.60 to χ_{GaCl3} = 0.75. Over the same range C_{40} and C_{50} content is decreased by 6.52% and 3.55% respectively. The content of C_{30}, C_{60}, and C_{70+} all remain within error bars. Whether higher or lower metal loading is presents the best case for an industrial process is dependent upon the process costs. The highest C_{30} and C_{40} content of the product is realised when χ_{GaCl3} = 0.60. This would reduce catalyst cost by decreasing the metal chloride content, but this will in turn will invoke higher energy costs to remove unreacted decene and dimer.

3.2.3.3.6 Influence of temperature

Based on the preliminary studies, Ur-$AlCl_3$ χ_{AlCl3} = 0.60 was selected as the catalyst of choice for the optimisation stage. Though $GaCl_3$-LCCs gave lighter oligomers and less heavy waste, the relative cost of $GaCl_3$ *vs*. $AlCl_3$ was too great to base an industrial process upon. Whilst thiourea as a ligand also gave good results, urea was chosen due to its relatively low toxicity, high biodegradability and its availability as the industrial partners are producer of urea.

The first step in optimisation of the small scale process was testing the catalyst at a wide range of temperatures and comparing the distribution of products to the desired outcome, aiming to get the correct distribution of C_{30+} fractions (Table 3.2-13, Figure 3.2-14).

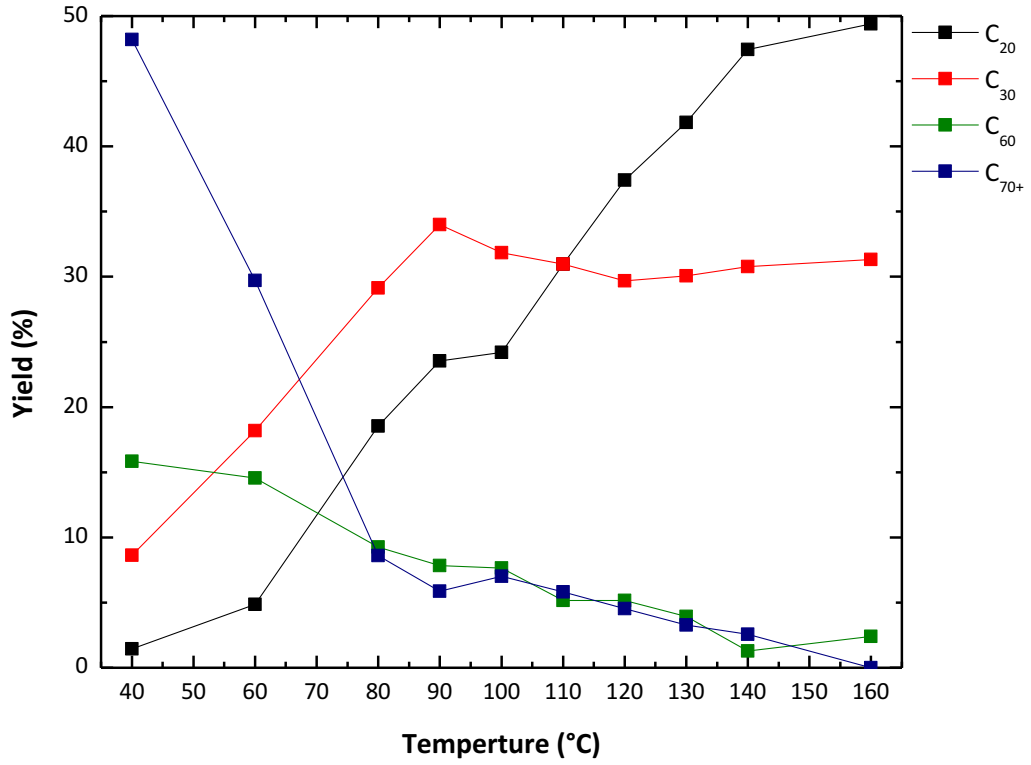

Figure 3.2-14: Distribution of selected 1-decene oligomers in Ur-$AlCl_3$ χ_{AlCl3} = 0.60 catalysed oligomerisation (1 wt% of catalyst, 1 h), as a function of reaction temperature. C_{40} and C_{50} fractions removed for clarity

Table 3.2-13: Conversion of 1-decene and distribution of 1-decene oligomers in Ur-$AlCl_3$ χ_{AlCl3} = 0.60 catalysed oligomerisation (1 wt% of catalyst, 1 h), as a function of reaction temperature.

Temp °C	Conversion (± 3 %)	C_{20} (± 4 %)	C_{30} (± 3 %)	C_{40} (± 2 %)	C_{50} (± 2 %)	C_{60} (± 1 %)	C_{70+} (± 1 %)
160	83.50	49.40	31.33	13.25	3.61	2.41	0.00
140	78.50	47.44	30.77	11.54	6.41	1.28	2.56
130	77.50	41.83	30.07	13.07	7.84	3.92	3.27
120	78.50	37.42	29.68	14.19	9.03	5.16	4.52
110	78.50	30.97	30.97	16.77	10.32	5.16	5.81
100	79.50	24.20	31.85	17.83	11.46	7.64	7.01
90	77.50	23.53	33.99	18.30	10.46	7.84	5.88
80	76.50	18.54	29.14	18.54	15.89	9.27	8.61
60	83.50	4.85	18.18	13.33	19.39	14.55	29.70
40	70.50	1.44	8.63	8.63	17.27	15.83	48.20

As expected with carbocationic processes, the average chain length of the oligomeric product is inversely proportional to the reaction temperature.[54] Therefore, the easiest way to cut down on unwanted heavy waste is to increase the temperature. This does however significantly increase the dimer by-product, which is also undesired in large quantities, due to its low economic value. Increased temperature also increases the operational cost, although this relationship is not linear, and site-dependent.

Reaction temperature affects also distribution of isomers in each fraction, *i.e*. degree of branching. The chromatograms of oligomers synthesised at different temperatures are compared in Figure 3.2-15. One can see peaks shifting towards shorter retention times for lubricants produced at higher temperatures. The shape of the C_{20} peak clearly shows that a lower boiling point, more branched isomer,[235] is the preferred product at higher temperature. The maximum in the C_{40} peaks decreases from 12.26 min at 60 °C to 11.89 min at 160 °C, which indicates significant increase in branching of this fraction.

It is known that pour point is lower for more branched oligomers, which is a desired property (Chapter 3.1).[229] At the same time, VI decreases with increased branching, which is a negative outcome (Chapter 3.1).[234,235] An optimum must be found, where both these properties are within commercial specifications. However, these parameters will only be known upon scale-up, fractionation and tests of appropriate blended fractions.

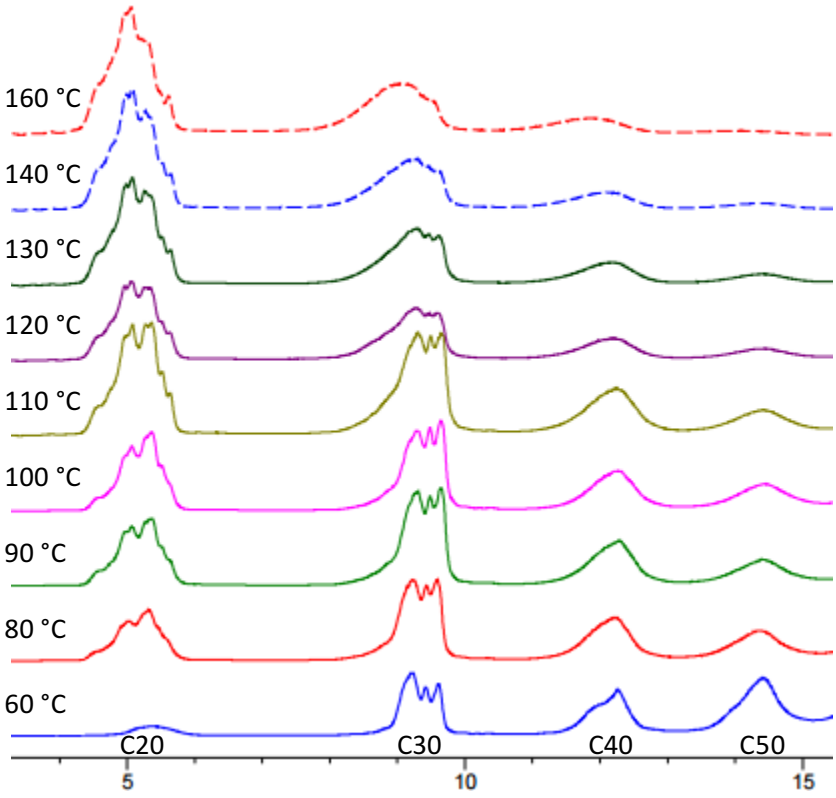

Figure 3.2-15: SimDist chromatogram for lubricants produced with 1wt % Ur-$AlCl_3$ χ_{AlCl3} = 0.60 at various temperatures

3.2.3.4 Scale up

3.2.3.4.1 Exotherm considerations

One of the first major concerns with scaling up the reaction is the exothermic nature of the reaction. With the reaction performed at high temperatures, it is not inconceivable that the boiling point of decene (*ca.* 171 °C) could easily be reached. In fact, temperature on the small scale often reached 170 °C for a short period of time, despite the efficient temperature control system (Chapter 3.2.1.2). Considering this, 140 °C was chosen as the reaction temperature, giving a balance between lowering the heavy oligomers content in the product and the health and safety issue presented. Furthermore, the catalyst was added at a considerably slower rate to prevent thermal runaway, which resulted in the overall reaction time to be extended to 1.5 h.

In the initial set of trial experiments, for a typical 2.5 L reaction performed at 140 °C, 1 wt% of the Ur-$AlCl_3$ χ_{AlCl3} = 0.60 catalyst (18.5 g, 12 ml) was used. LCC was added to the large reactor at a rate of 0.5 ml min^{-1}. After 6 min, no increase in temperature was seen, but the reaction mixture had begun to develop a light yellow tinge. After about 10 min, the

temperature began to increase rapidly and the colour of the reaction turned a more intense golden colour. Catalyst addition was immediately ceased. The temperature began to rise, peaking 181 °C before cooling back to 140 °C. The addition of the rest of the catalyst did not result in another large exotherm. The experiment was repeated, but this time the 2nd half of the catalyst being rapidly added. Again, no exotherm was seen upon the addition of the 2nd part.

3.2.3.4.2 Adjustment in catalyst loading

Following on from this observation, experiments with a decreased amount of catalyst were carried out, to investigate the effect of catalyst concentration at the large scale. Results for 1.00 to 0.25 wt% loading are shown in Table 3.2-14.

Table 3.2-14: Product distribution achieved with varying loadings of the catalyst, Ur-$AlCl_3$ χ_{AlCl3} = 0.6, (140 °C, 1.5 h)

Catalyst Mass (wt %)	Conversion (± 3 %)	C_{20} (± 4 %)	C_{30} (± 3 %)	C_{40} (± 2 %)	C_{50} (± 2 %)	C_{60} (± 1 %)	C_{70+} (± 1 %)
1.00	77.50	54.64	29.67	10.05	2.61	2.16	0.87
0.50	75.50	60.40	28.19	9.40	2.01	0.00	0.00
0.25	77.50	57.52	28.76	9.15	2.61	1.96	0.00

As shown in Table 3.2-14, for 1.00 to 0.25 wt% loading, conversion was independent from the catalyst amount, within error bars. Furthermore, on the larger scale, there was a significant shift observed towards the light oligomers compared with the same conditions on the small scale. Product distribution with varying catalyst loading was also largely constant within the error bars for each product fraction allowing the catalyst loading to be lowered to 0.25 wt%.

It is known that the relative amount of adventitious water is scale-dependent. For small-scale reactors, the surface area of reactor walls, stirrer etc. was significantly larger with respect to the catalyst amount, than it was in the large scale. Furthermore, the large scale reactor was dried entirely at elevated temperature under vacuum before use (60 °C, 1 h). Therefore, it must be assumed that the degree of hydrolysis of the catalyst was larger at the small scale, thus more catalyst was required. In confirmation of this hypothesis, reactions on the large scale gave far greater reproducibility between the runs, which was attributed to better control over the moisture content, and lower error on measuring out the catalyst amount.

3.2.3.4.3 Reaction kinetics

Attempts to measure reaction kinetics on the small scale resulted in poor quality data, likely due to the introduction of statistically significant traces of water every time a needle was

introduced to the reactor to collect a GC sample. On the large scale, with a larger catalyst amount, it was possible to sample the reaction mixture without compromising data quality. The reaction temperature was dropped to 100 °C for the kinetic measurements, there was a significant shift to dimer production and a decrease in the production of the desired C_{30} and C_{40} fractions. Product distribution and conversion, as a function of reaction time, are shown in Table 3.2-15 and Figure 3.2-16.

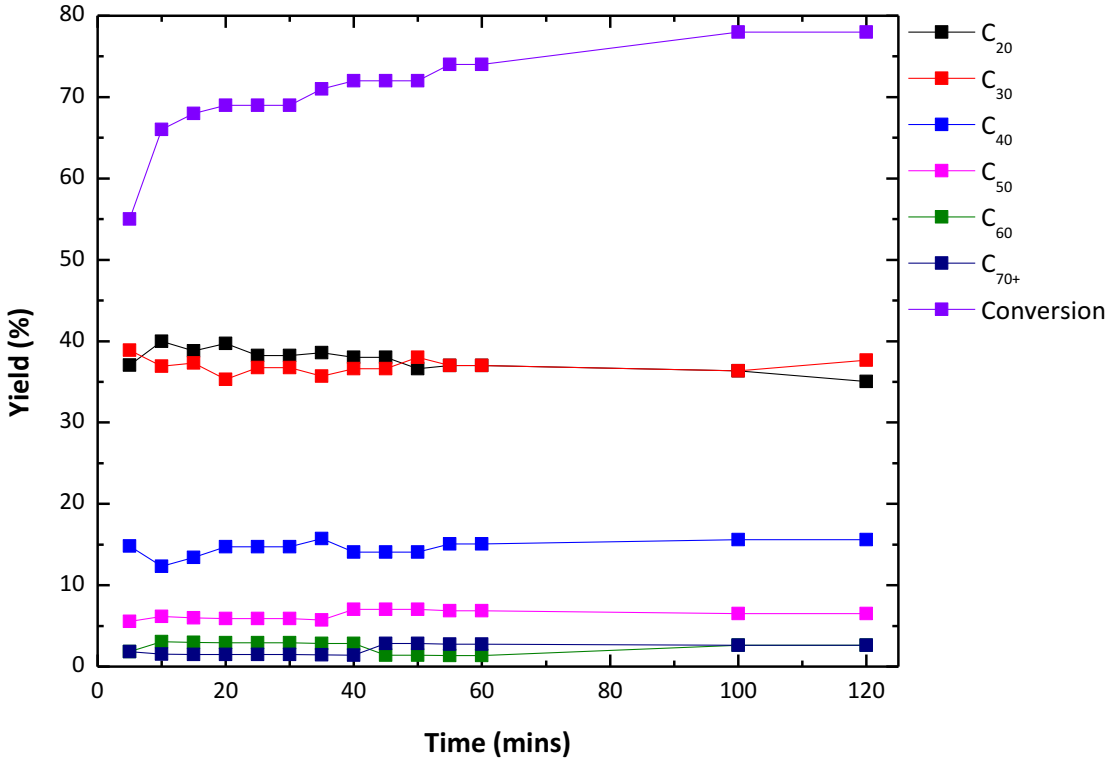

Figure 3.2-16: Kinetic study of large scale oligomerisation, 100 °C, 0.25 wt% of LCC: Ur–$AlCl_3$, χ_{AlCl3} = 0.60

It is of great interest to note that, within the entire duration of the experiment, the product distribution remained constant within the experimental error, with increasing conversion (Figure 3.2 16). Conversion increase was extremely rapid at first 10 min, followed by a period of a steady slow increase above 66%. The rate of reaction is understood to be retarded by both the decreased concentration of 1-decene, due to oligomerisation and isomerisation, and due to competitive chain termination reactions. Reactions were subsequently performed for 1.5 h as the conversion was seen to stall after 100 min.

Table 3.2-15: Kinetic study of large scale oligomerisation, 100 °C, 0.25 wt% of LCC: Ur–$AlCl_3$, χ_{AlCl3} = 0.60

Time	Conversion (± 3 %)	C_{20} (± 4 %)	C_{30} (± 3 %)	C_{40} (± 2 %)	C_{50} (± 2 %)	C_{60} (± 1 %)	C_{70+} (± 1 %)
5	55.00	37.04	38.89	14.81	5.56	1.85	1.85
10	66.00	40.00	36.92	12.31	6.15	3.08	1.54
15	68.00	38.81	37.31	13.43	5.97	2.99	1.49
20	69.00	39.71	35.29	14.71	5.88	2.94	1.47
25	69.00	38.24	36.76	14.71	5.88	2.94	1.47
30	69.00	38.24	36.76	14.71	5.88	2.94	1.47
35	71.00	38.57	35.71	15.71	5.71	2.86	1.43
40	72.00	38.03	36.62	14.08	7.04	2.82	1.41
45	72.00	38.03	36.62	14.08	7.04	1.41	2.82
50	72.00	36.62	38.03	14.08	7.04	1.41	2.82
55	74.00	36.99	36.99	15.07	6.85	1.37	2.74
60	74.00	36.99	36.99	15.07	6.85	1.37	2.74
100	78.00	36.36	36.36	15.58	6.49	2.60	2.60
120	78.00	35.06	37.66	15.58	6.49	2.60	2.60

3.2.3.4.4 Production of commercial samples of PAO 4 and PAO 6

After preliminary experiments at a large scale, reaction under optimised conditions (100 – 160 °C, 1.5 h, 0.25 wt % Ur–$AlCl_3$, χ_{AlCl3} = 0.60) was repeated a number of times, in order to produce 3 L of PAO 4 and 3 L of PAO6. After neutralisation and drying, using the distillation rig (Figure 3.2-3), the lightest fractions (C_{10} and C_{20}) were removed and the trimer was fractionated from the pot to be blended with the heavier oligomers (C_{40+}) as required. Typical distillation conditions are shown in (Table 3.2-1). The first C_{30} fraction typically contained some C_{20} due to imperfect separation during distillation. The later fractions also contained a small proportion of C_{40} due to co-distillation. The first samples of PAO were produced at 140 °C. It was discovered that by matching the commercial blends distribution (Table 3.1-2), the Kv_{100} of produced samples was typically higher than commercial samples, because for each catalyst and reaction conditions, specific degrees of branching are obtained, giving oligomers with different physical properties. Also the heaviest oligomers could not be separated on the distillation column due to their extreme boiling points. It was found that a higher proportion of C_{30} was required to compensate for the excess heavy oligomers.

Having reached the correct Kv_{100}, it was discovered that the blends had higher than anticipated Kv_{40} values, and as a consequence - low VIs (Table 3.2-16). Initially, this was attributed to the higher heavy oligomers content, so reactions were carried out at higher temperatures (with 0.25% catalyst loading, it was feasible to raise the reaction temperature up to 160 °C). However, having achieved reduced heavy oligomer content from products synthesised at 160 °C, the correct VI still could not be achieved. It was postulated in the literature that higher temperatures may be causing excessive branching leading to a decrease

in the VI.[234,235] Thus the reaction temperature was lowered and samples of PAOs were produced from reactions performed at 100 and 120 °C. Samples produced at lower temperatures were shown to give a better VI, despite having a higher C_{50+} content.

Table 3.2-16: Physical properties of the PAO samples produced with respect to temperature

PAO Sample	Reaction Temp	C_{30} (%)	C_{40} (%)	C_{50+} (%)	Kv 100 (cSt)	Kv 40 (cSt)	VI
OL Dist 02.12.13	160 °C	47.00	36.00	17.00	5.84	35.16	108
OL Dist 04.12.13		48.48	35.35	16.16	5.68	32.32	115
OL Dist 13.01.14		29.29	45.45	25.26	6.72	43.87	106
OL Dist 14.01.14		14.14	54.55	31.31	7.79	53.93	109
OL Dist 20.11.13	140 °C	47.00	35.00	18.00	6.39	39.61	111
OL Dist 21.01.14	120 °C	46.46	31.31	22.22	5.22	26.88	127
OL Dist 31.01.14		42.00	36.00	22.00	5.79	31.46	126
OL Dist 21.11.13	100 °C	45.45	32.32	22.23	5.27	26.19	137

Indeed, an overlay of the chromatograms of the commercial sample and the samples produced in this work (Figure 3.2-15) showed that peak retention times were shifted to lower retention times (indicating higher branching) with higher reaction temperatures. The PAO sample produce at 120 °C showed similar retention times to the commercial sample.

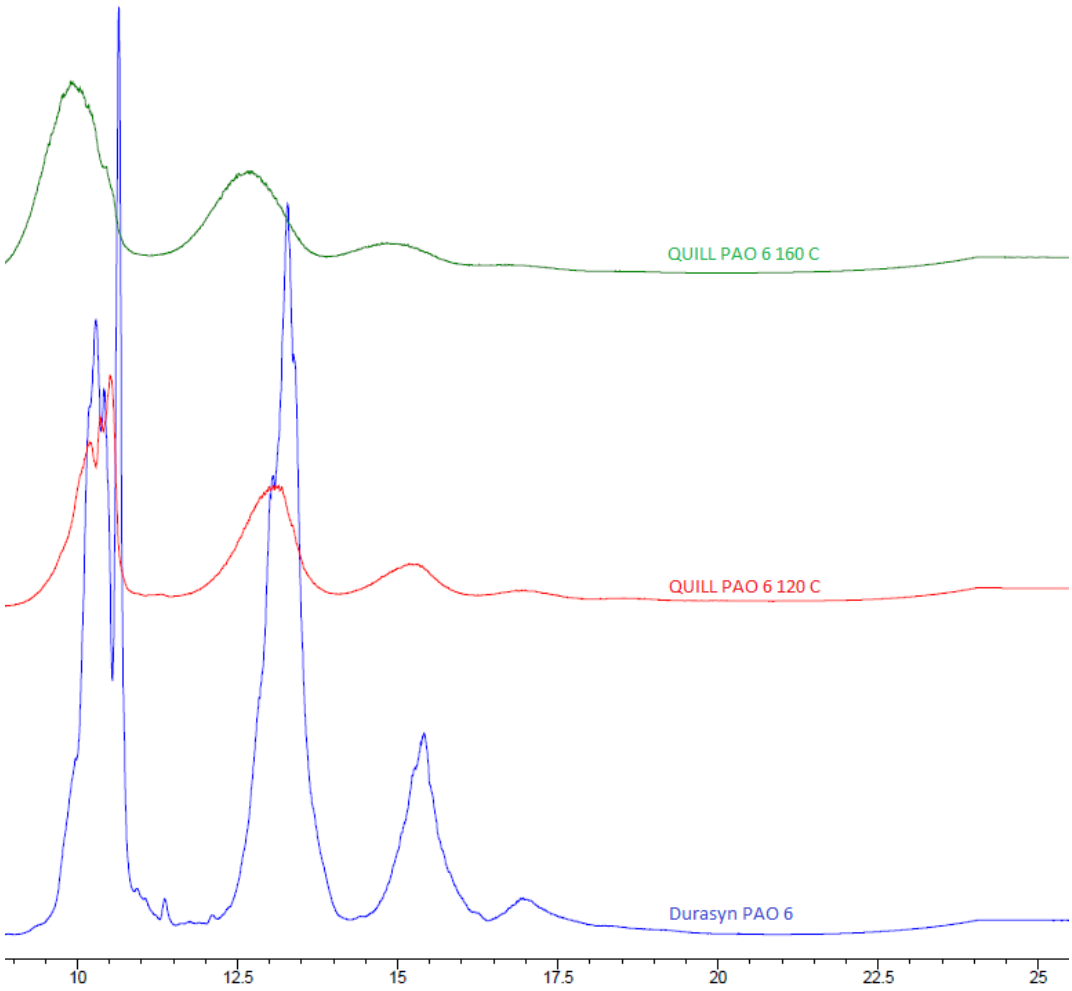

Figure 3.2-17: SimDist GC Chromatogram of PAO 6 produced at 160 °C (green), 120 °C (red) and commercial product (blue)

To gain more insight into branching, ^{1}H NMR spectra of the PAO samples produced were recorded and showed 3 broad peaks which could be assigned to *CH*, CH_2 and CH_3 groups. From these spectra, the ratio of terminal CH_3 groups to CH_2 and *CH* groups was assessed by integration of the peaks. In linear oligomers, the number of *CH* groups would be lower, and CH_2 groups, higher, compared to branched products. The same analysis was carried out on the commercial samples, with results are compared in Table 3.2-17. It is visible, there is a correlation between the reaction temperature and the oligomer branching. With higher reaction temperatures the rate of isomerisation was increased rapidly, as shown by the decrease of CH_2 peaks. At 100 °C the samples produced showed higher branching than commercial samples.

Table 3.2-17: ^{1}H NMR data showing ratio of terminal to chain carbons in different PAO 6 samples

PAO 6	*CH*	*CH_2*	*CH_3*
Synfluid 6	0.06	4.36	1
Durasyn 6	0.03	4.31	1
PAO 6 100 °C	0.24	3.22	1
PAO 6 120 °C	0.26	2.97	1
PAO 6 160 °C	0.23	2.46	1

Based on the above investigation, the required 3 L samples of PAO 4 and PAO 6 were produced, and shipped to Petronas laboratories for further evaluation. PAO 6 was achievable at 120 °C, however PAO 4 was more difficult to blend, and required lower temperatures of 100 °C to ensure a VI over 120. The final specifications of the products, compared to commercial examples, are listed in Table 3.2-18.

Table 3.2-18: Physical properties and oligomer distribution of non-hydrogenated PAO samples produced and shipped to Petronas for further testing

PAO	KV 100 (cSt)	KV40 (cSt)	VI	PP (°C)	C_{30} (%)	C_{40} (%)	C_{50} (%)	C_{60+} (%)
LCC PAO 6	5.74	31.49	126	< -60	42.15	37.46	12.84	7.55
Durasyn PAO 6	5.76	30.22	135	-57	36.87	42.42	14.14	6.57
LCC PAO 4	4.31	20.11	123	< -60	76.94	15.88	4.23	2.94
Durasyn PAO 4	3.92	17.25	137	< -60	80.30	19.19	0.51	0.00

3.2.3.5 Techno-economic evaluation

In parallel to scale-up studies, Process Design Centre (PDC) was invited to assist with a techno-economic evaluation of the process. Experimental data were provided to PDC for comparison with current market technologies, in order to assess the economic viability of the process. Full mass balances for each process (PAO 4 and PAO 6 synthesis) were provided, along with reaction conditions and distillation regimes.

3.2.3.5.1 Conclusions from techno-economical evaluation

PDC provided a number of suggestions to improve the process, summarised in Table 3.2-19.

Comparing the experimental data with the reference data, a number of improvement areas were determined, in order to make the LCCs process a viable alternative to BF_3-based benchmark. The conversion needed to be increased to 90%, and the product distribution needed optimisation towards a higher yield of PAO 4 (that is, with less C_{20} being produced). Though C_{20} could be sold as low viscosity PAO 2 for drilling fluids, the market for this PAO grade was small, and the price markedly lower than other PAO grades.

Table 3.2-19: Techno-economic evaluation summary

Area of improvement	BF_3/*n*BuOH Reference	Ur-$AlCl_3$ χ_{AlCl3} = 0.60	Area to be investigated
Conversion per pass	90-95%	75%	Increase conversion
Recycling of C_{10}	5-10% (Linear Olefins)	25% (Internal Olefins)	***To conduct experiment on the conversion and product distribution using recycle C10 at various ratio***
Reduce C_{20} by recycling	20%	50%	C20 recycling experiments
Increase PAO 4 yield	45%	30-35%	***By varying the C10 addition*** ***By varying the amount of catalyst***
Catalyst cost $/t	53	12-14	New catalyst is currently predicted to be cheaper than the reference case

The strong points of the LCC case were: reduced cost of the catalyst compared to the BF_3 benchmark, and the reduced CAPEX, as BF_3 is a toxic gas which must be handled under higher than atmospheric pressure and in higher grade steel. Furthermore, waste by-products of the LCC catalyst are less dangerous compared to the BF_3 case, and thus less expensive to treat. Finally, in terms of safety, upon release, gaseous BF_3 hydrolyses to release HF, whereas Ur-$AlCl_3$ LCC is a liquid and releases HCl which is significantly less toxic.

3.2.3.5.2 Recycling of C_{10} fraction

Recycling of post-oligomerisation C_{10} was carried out on the small scale (Table 3.2-20). Notably, there was a significantly diminished exotherm when using high proportions of recycled decene. The experiments were repeated with 3 wt% catalyst in order to stimulate the carbocation formation, but with limited success. The reaction could be forced to progress by increasing the amount of catalyst used, allowing for 75% conversion with 50% recycled decene, but such high amounts of catalyst favour heavy oligomer production. The experiments with a lower proportion of recycled decene (up to 25%) were more successful, though not with the same size of exotherm as that seen for fresh feedstock.

Table 3.2-20: Exotherm, conversion and product distribution achieved using recycled-fresh 1-decene mixtures (Ur-$AlCl_3$ χ_{AlCl3} = 0.60, 1.707 mmol of MCl_3 per 40 ml of 1-decene, 120 °C, 1 h)

Recycled C_{10} (%)	Catalyst Mass (wt %)	Exotherm (° C)	Conversion (± 3 %)	C_{20} (± 4 %)	C_{30} (± 3 %)	C_{40} (± 2 %)	C_{50} (± 2 %)	C_{60} (± 1 %)	C_{70+} (± 1 %)
100	1	3.23	5.00	-	-	-	-	-	-
75	1	3.87	6.00	-	-	-	-	-	-
50	1	5.45	10.00	-	-	-	-	-	-
25	1	24.61	81.00	31.25	27.50	17.50	10.00	5.00	8.75
0	1	29.54	79.00	35.90	30.77	16.67	8.97	3.85	3.85
100	3	9.70	53.00	46.15	36.54	11.54	1.92	1.92	1.92
75	3	27.94	76.00	26.67	32.00	20.00	10.67	5.33	5.33
50	3	52.96	88.00	24.14	27.59	19.54	11.49	5.75	11.49
25	3	62.43	88.00	28.74	27.59	17.24	9.20	5.75	11.49

The two plausible reasons for diminished exotherm were: (i) recycled decene had undergone saturation of the double bond, or (ii) the double bond had isomerised to the internal position, rendering it less active. ^{1}H NMR studies were carried out on the recycled sample to determine the answer (Figure 3.2-18). It is clear from Figure 3.2-18 this that decene is isomerised to internal olefin, and further validates the earlier hypotheses (Chapter 3.2.3.4.4) that PAOs synthesised at higher temperature have low VIs at least partially due to excessive isomerisation. Furthermore, it was quantified that isomerisation degree increased with reaction temperature (Table 3.2-21).

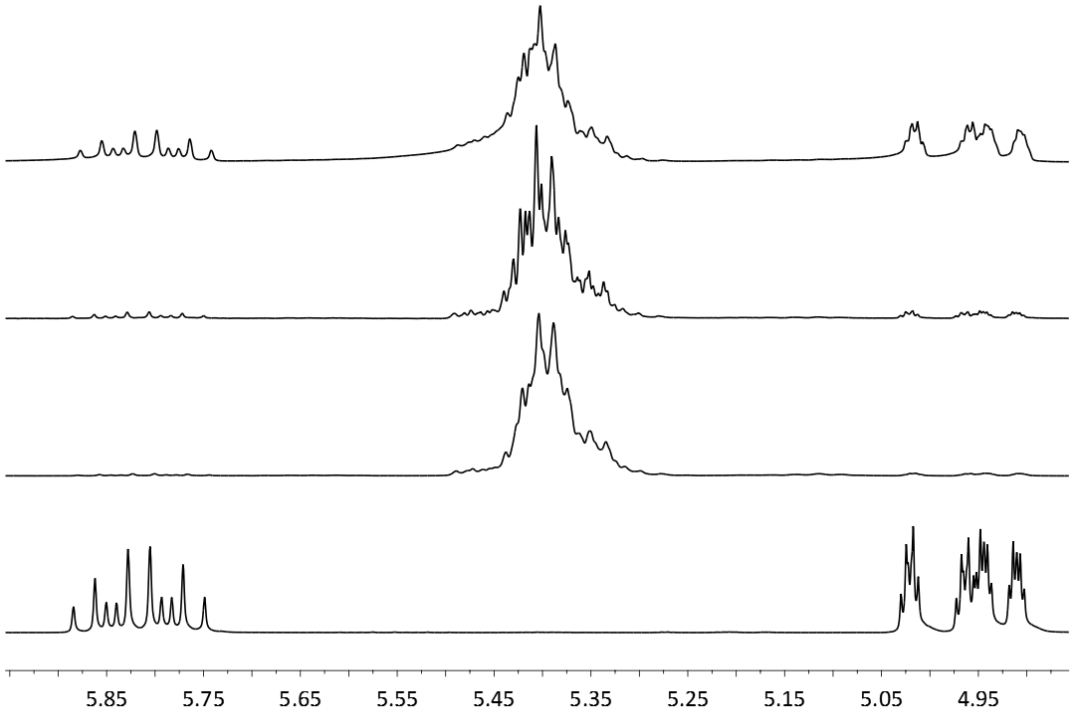

Figure 3.2-18: NMR of double bond region of fresh and recycled 1-decene from reactions at a) fresh 1- decene b) 120 °C, c) 100 °C and d) 80 °C

Table 3.2-21: Ratio of isomerised to linear decene present in recycled C_{10} fraction

Reaction temperature	5.8 ppm : 5.4 ppm Signal ratio
120 °C	1 : 109
100 °C	1 : 29
80 °C	1 : 6
Fresh Decene	33:1

Since branched alkenes are less reactive the oligomerisation does not progress using 50 % or more recycled decene with 1 wt% catalyst (Table 3.2-20). Nevertheless, at 25% loading of recycled decene a good degree of conversion (80%) was seen; following the requirement of achieving 90% conversion in the first place, it was estimated that 10% replacement with recycled decene would be viable. Using recycled decene, increased the proportion of heavy oligomers produced, compared to reactions of fresh 1-decene.

To address recycling of decene, increased catalyst loading was used (2 and 3 wt%), with otherwise unaltered conditions (1 h, 120 °C). On the small scale, higher catalyst loadings did increase conversion of the decene, and shifted the distribution towards a higher proportion of favourable trimers and tetramers (Table 3.2-22).

Table 3.2-22: Product distribution for varying wt%, Ur-$AlCl_3$ χ_{AlCl3} = 0.60, 120 °C, 1.5 h

Cat Mass	Conversion (± 3 %)	C_{20} (± 4 %)	C_{30} (± 3 %)	C_{40} (± 2 %)	C_{50} (± 2 %)	C_{60} (± 1 %)	C_{70+} (± 1 %)
3 wt%	93.00	28.26	35.87	20.65	9.78	3.26	2.17
	90.00	30.34	38.20	19.10	7.87	2.25	2.25
2 wt%	88.00	33.33	36.78	18.39	8.05	2.30	1.15
	85.00	33.33	38.10	17.86	7.14	2.38	1.19
1 wt%	79.00	37.18	29.49	14.10	8.97	5.13	5.13
	79.00	35.90	30.77	16.67	8.97	3.85	3.85

As shown in the scale-up study, this shift may be somewhat counteracted on the large scale, but at the same time - the catalyst demand on the large scale is likely to decrease as well.

3.2.3.5.3 Recycling of C_{20} fraction

Direct oligomerisation of C_{20} by solid-supported organo-aluminium catalysts has been reported.[285] The authors obtained linear C_{20} in good yield and selectivity using a zirconacene-MAO catalyst, and then directly oligomerised C_{20} using $EtAlCl_2/SiO_2$ for 7 h. Taking this publication as the starting point, a screening study was performed using both Ur-$AlCl_3$ χ_{AlCl3} = 0.60 LCC and $AlCl_3$ powder, over long reaction times. Summary of this attempts is show in Table 3.2-23.

Table 3.2-23: Product distribution achieved for oligomerisation of recycled C_{20}, 5.1 mmol $AlCl_3$ eq., at 140 °C

Catalyst (Time)	C_{20} (± 4 %)	C_{30} (± 3 %)	C_{40} (± 2 %)	C_{50} (± 2 %)	C_{60} (± 1 %)	C_{70+} (± 1 %)
feedstock (0 h)	93.75	6.25	-	-	-	-
Ur-$AlCl_3$ (4 h)	73.20	12.37	10.31	2.06	2.06	0.00
$AlCl_3$ (4 h)	61.62	14.14	16.16	5.05	2.02	1.01
Ur-$AlCl_3$ (24 h)	59.60	16.16	17.17	4.04	2.02	1.01
$AlCl_3$ (24 h)	42.42	17.17	25.25	9.09	4.04	2.02

Though oligomerisation of C_{20} is possible, reaction times appear to be prohibitively long, even with large catalyst loadings, either using the LCC system or aluminium(III) chloride powder. In contrast to the literature report,[285] where a metalocene catalyst was used to produce a linear C_{20}, which was then oligomerised in a carbocationic process, here two consecutive carbocationic processes took place. Carbocationic processes result in highly isomerised C_{20}, which had decreased reactivity due to steric hindrance. As such, direct oligomerisation of the dimer by secondary carbocationic oligomerisation was not deemed to be economically feasible.

3.2.3.6 Conclusions

LCCs were shown to be effective 1-decene oligomerisation catalysts. The reaction conditions could be varied to effect the product distribution. Ionicity of the catalyst and miscibility of catalyst and feedstock were shown to be crucial factors in whether lighter or heavier oligomers were favoured, as was temperature, which is to be expected for a carbocationic process.

The catalytic system Ur-$AlCl_3$ χ_{AlCl3} = 0.60 / H_2O was successfully employed on a 3 L scale to produce 1-decene oligomers which were fractionated and blended to give PAO 4 and PAO 6 samples (non-hydrogenated). Temperature of the reaction was found to have a large affect upon the physical properties of the samples produced. Higher temperatures induced excessive branching of the oligomers yielding PAO sample with VI < 120. As such the temperature of the reaction had to be kept at 120 and 100 °C for PAO 6 and PAO 4 respectively to meet the requirements for physical properties.

Distilled decene could be recycled, however it was found that the recycled decene was highly isomerised and less reactive than fresh decene. As such only a blend up to 25% recycled decene to 75% 1-decene could be successfully oligomerised under the same conditions as fresh decene without noticeable loss of conversion. The recycled dimer when oligomerised proved to be unreactive and took prohibitively long reaction times to achieve low conversion.

3.3 Borenium ionic liquid catalysed oligomerisation of 1-decene

This project was sponsored by Evonik, who are a major German chemical company. They were interested in developing and licensing a catalyst for the production of PAOs, but were not interest in undertaking that production themselves. To interest potential partners, they needed a new Lewis acidic catalyst (to generate new IP), and proof of concept data about the catalysts' performance, the quality of the product and the recyclability of materials. Overall duration of the project was 6 months. Work regarding scale-up was carried out together with a PDRA employed on the project.

3.3.1 Experimental

Borenium ionic liquids were synthesised as detailed in Chapter 2.2.2, however, for scale up reactions, aluminium(III) chloride was purchased as lower purity grade (98%) and was doubly sublimed[275] before being used.

All oligomerisation experimental details are as described in Chapter 3.2.1, except borenium ionic liquids were used as catalysts in place of liquid coordination complexes. Moreover, upon quenching large-scale reactions with water, the resulting mixture was stirred at 95 °C to ensure dissolution of boron impurities.

3.3.2 Results and discussion

3.3.2.1 Influence of anion

From the experiments in Chapter 3.2 some general conclusions could be drawn about temperature, reaction time and catalyst loading influence on conversion and selectivity. Upon starting this project, the unknown was associated mainly with the chemistry of the new catalytic system itself. As discussed in Chapter 2.2, borenium ionic liquids can have acidity in both the cation and the anion. To study the influence of the anion, the ionic liquids $[BCl_2(3pic)][MCl_4]$ and $[BCl_2(3Pic)][M_2Cl_7]$ (M = Al, Ga) were synthesised and used as catalysts for the oligomerisation of 1-decene (Table 3.3-1). 3-Picoline was the ligand of choice, as its asymmetry helps to lower the melting point of the ionic liquid (the crystal structures for some borenium cations with symmetrical pyridines used as the ligand have been reported).[204] To ensure comparability of results, each reaction was run with a constant molar equivalent of borenium ionic liquid (0.62 mmol).

There was a noticeable difference in the exotherms which occurred with the $[MCl_4]^-$ counterion compared to those with the $[M_2Cl_7]^-$ counterion (Table 3.3-1). $[BCl_2(3pic)][AlCl_4]$ resulted in an exotherm of 20 °C compared to 80 °C seen when $[BCl_2(3pic)][Al_2Cl_7]$ was used as the catalyst. Similarly, when $[BCl_2(3pic)][GaCl_4]$ was used as the catalyst an exotherm of only 8 °C was recorded, compared to 55 °C seen when $[BCl_2(3pic)][Ga_2Cl_7]$ was used. The monomeric anion is non-Lewis acidic itself, as such when using the dimeric anion the concentration of Lewis acidic species is effectively doubled, no doubt resulting in more rapid formation of the carbocation and therefore increased exotherms. Furthermore, there is stronger interaction of the monomeric anion with the borenium cation (Chapter 2.3), possibly lowering the rate of interaction of borenium cation with adventitious water.

Conversions and product distributions achieved with the four ionic liquids are listed in Table 3.3-1. It can be seen that conversions of 1-decene obtained with $[BCl_2(3pic)][AlCl_4]$ and $[BCl_2(3pic)][Al_2Cl_7]$ were the same (within error bars), but the product distribution displayed a significant shift to heavier oligomers using the former catalyst. For $[BCl_2(3pic)][Al_2Cl_7]$, the amount of C_{20} increased by 4.52 % and both C_{60} and C_{70+} decreased by 1.21 % and 1.81 %

respectively. This is likely due to the differences in exotherm, *i.e.* the later reaction reached a higher temperature, which will curtail oligomer chain length whilst at the elevated temperature so a higher proportion of propagating chains will be terminated at the dimer intermediate.

In contrast to borenium ionic liquids with chloroaluminate(III) anions, using $[BCl_2(3pic)][GaCl_4]$ resulted in a significantly decreased conversion (52.5%), compared to using $[BCl_2(3pic)][Ga_2Cl_7]$ as the catalyst (77.0%) of the 1-decene. This trend does correlate with the acceptor numbers measured for these ionic liquids.[52] It appears that $[GaCl_4]^-$ interacts with the borenium cation much stronger than $[AlCl_4]^-$, making it less available for substrates. Confirming this theory would require computational chemistry studies, and would be very interesting for further design of new generations of borenium ionic liquids.

Table 3.3-1: Conversions, product distribution and exotherms in $[BCl_2(3pic)][M_nCl_{3n+1}]$-catalysed oligomerisation, 0.62 mmol of catalyst, 1 h, 100 °C, M = Al or Ga, *n* = 1 or 2

Anion	Conversion (± 3 %)	C_{20} (± 4 %)	C_{30} (± 3 %)	C_{40} (± 2 %)	C_{50} (± 2 %)	C_{60} (± 1 %)	C_{70+} (± 1 %)	Exotherm (°C)
$[AlCl_4]^-$	82.00	27.78	34.58	16.66	8.64	4.94	7.40	20
$[Al_2Cl_7]^-$	80.50	32.30	32.92	16.77	8.70	3.73	5.59	80
$[GaCl_4]^-$	52.50	48.54	29.13	9.71	4.85	3.88	3.88	8
$[Ga_2Cl_7]^-$	77.00	42.76	34.85	12.50	5.27	1.95	2.67	55

The chromatograms of 1-decene oligomers obtained with $[BCl_2(3pic)][AlCl_4]$ and $[BCl_2(3pic)][Al_2Cl_7]$ were compared (Figure 3.3-1,) showing that the difference in anion has visible effect on the linearity of the oligomers. When the counter ion is $[Al_2Cl_7]^-$, there is a shift to lower boiling, and therefore more branched, oligomers compared to when $[AlCl_4]^-$ was the counter ion present. Comparing oligomers produced with BF_3 and $AlCl_3$ (Figure 3.2-17) one may speculate that Al-centred Lewis acids somehow promote isomerisation more than those based on boron. In addition, it should be noted that $[Al_2Cl_7]^-$ is less coordinating than $[AlCl_4]^-$, thus would leave the generated carbocation more 'free' to isomerise. Isomerised chains would contain more stable carbocations, which in turn would be less active in

propagation - thus shorter oligomers were produced. Again, confirming these hypothesis would require much more in-depth investigation.

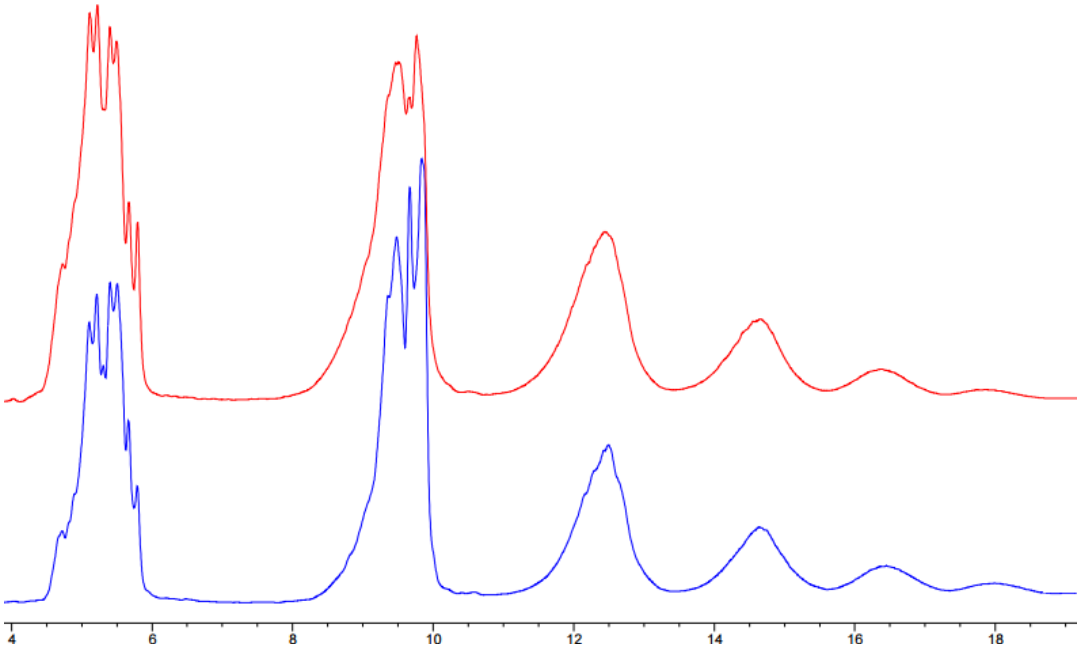

Figure 3.3-1: Chromatogram showing oligomer distributions when using a) $[BCl_2(3pic)][AlCl_4]$ and b) $[BCl_2(3pic)][Al_2Cl_7]$ as catalysts.

3.3.2.2 Influence of ligand

A range of pyridine ligands were chosen to assess the steric and electronic effects upon the oligomerisation of decene. Methyl substituents on the pyridine ring are weakly electron donating, and in the 2-position act to weaken the stability of the $[BCl_3(2pic)]$ complex by steric effects (Chapter 2.2.3.1). Conversely, due to its high electronegativity, fluorine is an electron-withdrawing group. To ensure all adducts were liquid at room temperature, only ionic liquids with dimeric counter anions, *i.e.* $[M_2Cl_7]^-$, were tested. As mentioned in Chapter 2.2, ionic liquids with fluoropyridine-substituted borocations contained a significant amount of precipitate. These liquids were filtered before use.

Results of oligomerisation experiments with a range of ligands on boron are shown in Table 3.3-2 and Figure 3.3-2 for borenium ionic liquids with chloroaluminate(III) anions, and in Table 3.3-3 and Figure 3.3-3 for those with chlorogallate(III) anions. There was a significant difference in product distribution between aluminium(III) chloride and gallium(III) chloride containing borenium ionic liquids. Catalysts with the $[Ga_2Cl_7]^-$ family typically have a higher conversation

and smaller chains, indicating a greater rate of chain transfer with respect to propagation, than catalysis with the $[Al_2Cl_7]^-$ family.

For the non-fluorinated pyridine ligands, the position of the methyl substituent on the pyridine ring affected slightly the proportion of heavy oligomers (C_{70+}) produced: $[BCl_2(4pic)][Al_2Cl_7]$ resulted in 1.19 % more C_{70+} than $[BCl_2(py)][Al_2Cl_7]$ did. However, there was no significant variation in the product distribution, regarding C_{20} – C_{60}, fractions when using the ligands py, 2pic, 3pic and 4pic. The conversion achieved with $[BCl_2(2pic)][Al_2Cl_7]$ was lower than other pyridines, by > 4%. The fact that the 2-picoline boron adduct was shown to be less stable in solution than the other pyridines-boron adducts may indicate the catalyst degrades more quickly.

In contrast, when $[BCl_2(2Fpy)][Al_2Cl_7]$ was used as the catalyst, decreased conversion and a significantly heavier product distribution was noted. This can be explained by speciation, as evidenced by the ^{11}B and ^{27}Al NMR spectra (Figure 2.2-13 and Figure 2.2-17). The ^{11}B NMR spectrum shows only a peak at 6.21 ppm suggesting tetrahedral boron, whilst the ^{27}Al NMR spectrum shows significant broadening, typical of dimeric aluminium species. As such, it is likely the only catalytically active species is an Al-Lewis acid, meaning the product distribution would be different, and that the effective loading of Lewis acidic species in the ionic liquid added was lower. $[BCl_2(3Fpy)][Al_2Cl_7]$ used as a catalyst gave high conversions, though with an increased C_{70+} content with respect to the ionic liquids containing non-fluorinated pyridine ligands. Although NMR spectroscopy of the liquid showed the presence of a borenium cation (Figure 2.2-13-f), there was also significant ligand redistribution and decomposition noted. As carbocationic processes can be sensitive to small impurities, it is not surprising to see such a deviation from the general trend.

Table 3.3-2: Conversion and product distribution achieved in $[BCl_2L][Al_2Cl_7]$ catalysed oligomerisation, 0.62 mmol, 1 h, 100 °C

Ligand	Conversion (± 3 %)	C_{20} (± 4 %)	C_{30} (± 3 %)	C_{40} (± 2 %)	C_{50} (± 2 %)	C_{60} (± 1 %)	C_{70+} (± 1 %)
py	81.50	31.89	33.15	17.18	9.20	3.68	4.90
2pic	76.00	30.91	33.55	17.77	8.56	3.95	5.27
3pic	80.50	32.30	32.92	16.77	8.70	3.73	5.59
4pic	82.00	29.88	32.93	17.07	9.76	4.27	6.09
2Fpy	74.50	20.76	23.45	14.09	12.10	8.07	21.54
3Fpy	84.00	34.53	31.55	14.88	7.74	3.57	7.74

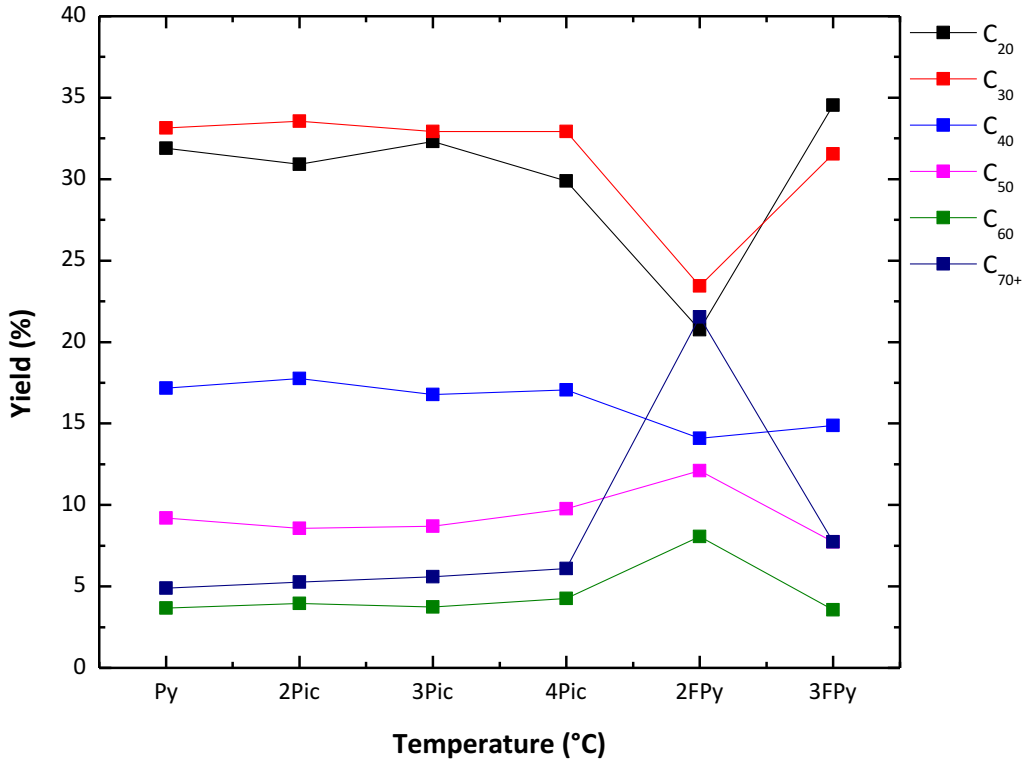

Figure 3.3-2: Product distribution achieved in $[BCl_2L][Al_2Cl_7]$ catalysed oligomerisation, 0.62 mmol, 1 h, 100 °C

Analogous trends were found for catalysis with chlorogallate borenium ionic liquids: $[BCl_2(4pic)][Ga_2Cl_7]$ yielded a significant higher content of C_{70+} than $[BCl_2(py)][Ga_2Cl_7]$, and catalysis with $[BCl_2(4pic)][Ga_2Cl_7]$ also resulted in > 4% less C_{20} in the product distribution, compared to when py, 2pic and 3pic were used as ligands.

The $[BCl_2(2Fpy)][Ga_2Cl_7]$ system showed a downfield shift in its ^{11}B NMR spectrum (Figure 2.2-14), typically associated with tricoordinate boron species, unlike $[BCl_2(2Fpy)][Al_2Cl_7]$, and as such its product distribution remains largely similar to other $[BCl_2(L)][Ga_2Cl_7]$ catalysed oligomerisations. Both $[BCl_2(2Fpy)][Ga_2Cl_7]$ and $[BCl_2(3Fpy)][Ga_2Cl_7]$ as catalytic systems produced significantly more C_{60} and C_{70+} than their non-fluorinated counterparts, no doubt in part due to impurities in the ionic liquid (Chapter 2.2.3.2).

Table 3.3-3: Conversion and product distribution achieved in $[BCl_2L][Ga_2Cl_7]$ catalysed oligomerisation, 0.62 mmol, 1 h, 100 °C

Ligand	Conversion (± 3 %)	C_{20} (± 4 %)	C_{30} (± 3 %)	C_{40} (± 2 %)	C_{50} (± 2 %)	C_{60} (± 1 %)	C_{70+} (± 1 %)
py	84.00	41.08	33.93	13.69	4.76	2.38	4.17
2pic	83.50	40.72	33.53	13.77	5.99	2.40	3.59
3pic	77.00	42.76	34.85	12.50	5.27	1.95	2.67
4pic	84.50	36.09	30.77	13.61	6.51	4.14	8.88
2Fpy	82.00	36.60	30.50	15.24	7.92	4.26	5.49
3Fpy	85.00	38.82	31.17	13.53	5.88	3.53	7.06

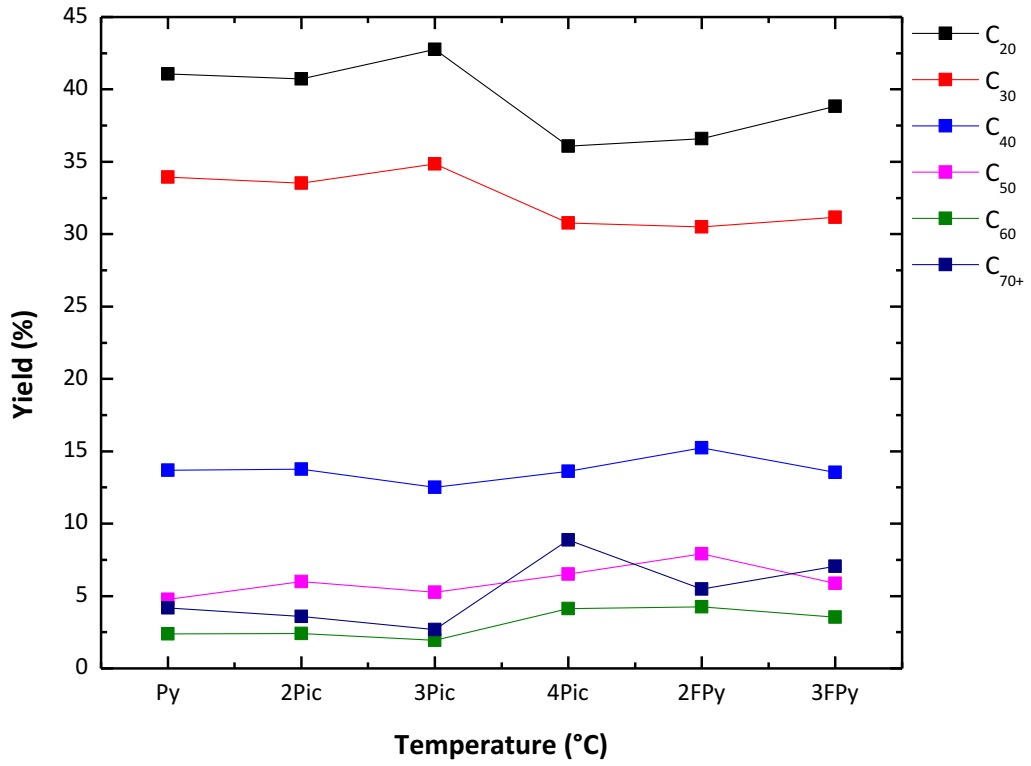

Figure 3.3-3: Product distribution achieved in $[BCl_2L][Ga_2Cl_7]$ catalysed oligomerisation, 0.62 mmol, 1 h, 100 °C

The SimDist chromatograms were compared, in order to contrast the degree of isomerisation. As explained already in Chapter 3.2.6.1, SimDist separates chemical species by their boiling point only, with higher boiling species having longer retention times.[286] As the boiling point each oligomer is highly affected by branching, a decrease in retention time is indicative of the degree of branching present. Peak shape would also be affected by branching, because more different isomers results in broader peak with more 'spikes'. Figure 3.3-4 shows the comparison of oligomerised 1-decene.

Chlorogallate(III) systems with fluorinated ligands appear to yield broader peaks than their non-fluorinated chloroaluminate(III) counterparts, indicating increased isomerisation of the carbocation during the reaction. Unfortunately, the samples produced are too small for effective distillation, blending and comparison of VI and PP - both of which are affected by branching as well.

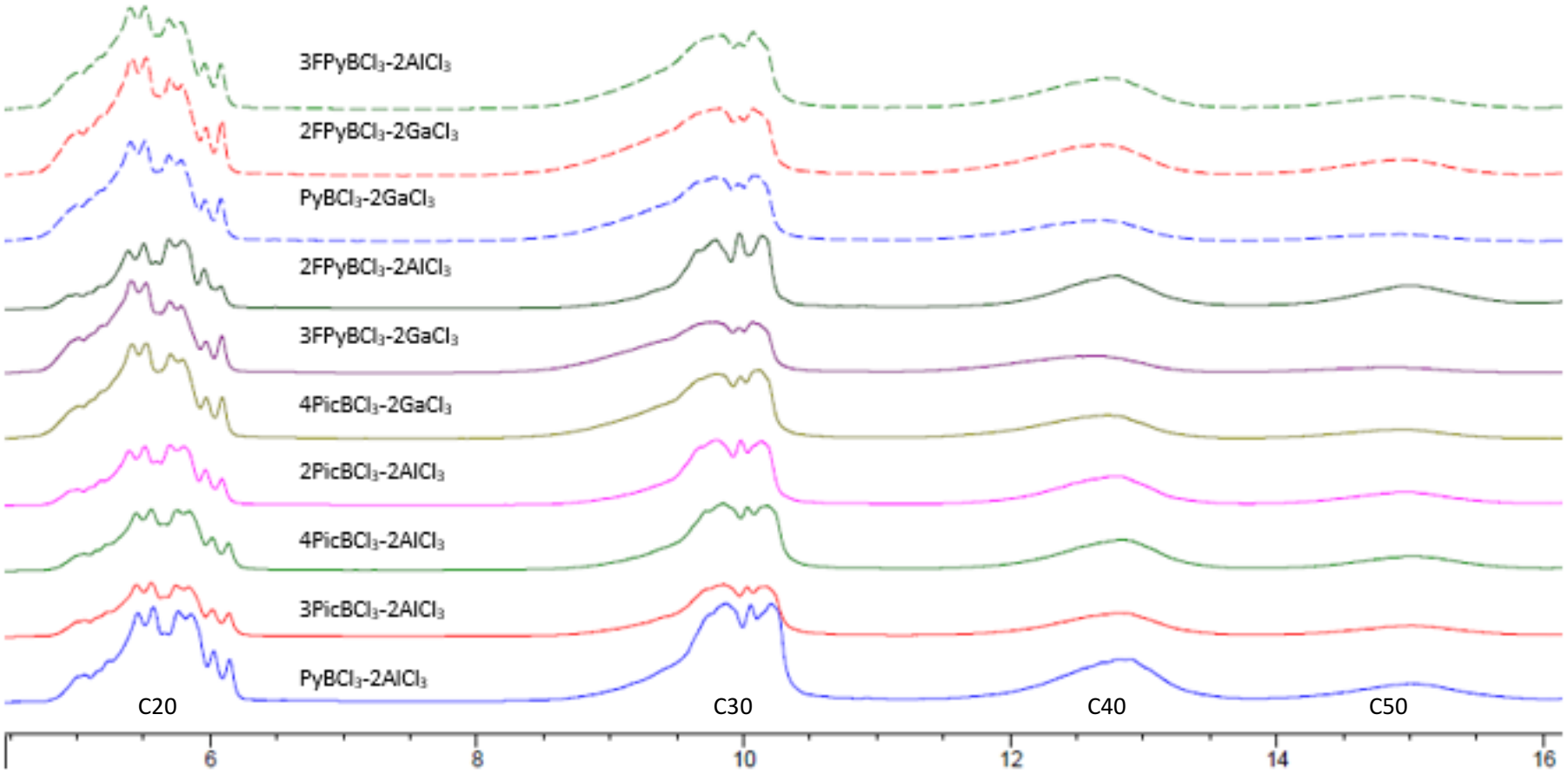

Figure 3.3-4: Chromatograms of oligomeric products obtained using different borenium ionic liquids.

3.3.2.3 Influence of temperature

Oligomerisations were carried out at a range of temperatures, to assess the effect temperature on product distribution. From previous studies it was known that higher temperature leads to shorter oligomers and more branching, thus a decrease in VI (Table 3.2-16). Therefore, lower reaction temperatures are desirable; however this unfortunately leads to an increase in undesired heavy oligomer content (Table 3.2-13) which has a detrimental effect upon the pour point.[229]

The catalyst $[BCl_2(2pic)][Al_2Cl_7]$ was the first to be assessed over a range of temperatures (Figure 3.3-5 and Table 3.3-4). As already shown in Chapter 3.2.1.2, temperature is an important factor shaping product distribution, with the expected preference for shorter oligomer chains noted at higher temperatures. The proportion of C_{20} in the product dropped by 17.05% between reactions performed at 130 and 80 °C. Conversely, the proportion of C_{70+} rose by 3.76% across the same temperature range. For comparison - the LCC catalyst, Ur-$AlCl_3$ χ_{AlCl3} = 0.60, studied across the same temperature range, saw a decrease of 23.29% of C_{20} and an increase of 5.34% of C_{70+}. This suggests that the LCC catalyst product distribution is more sensitive to temperature than the borenium ionic liquid, which may be caused by changes in the LCC catalyst speciation with temperature.[135]

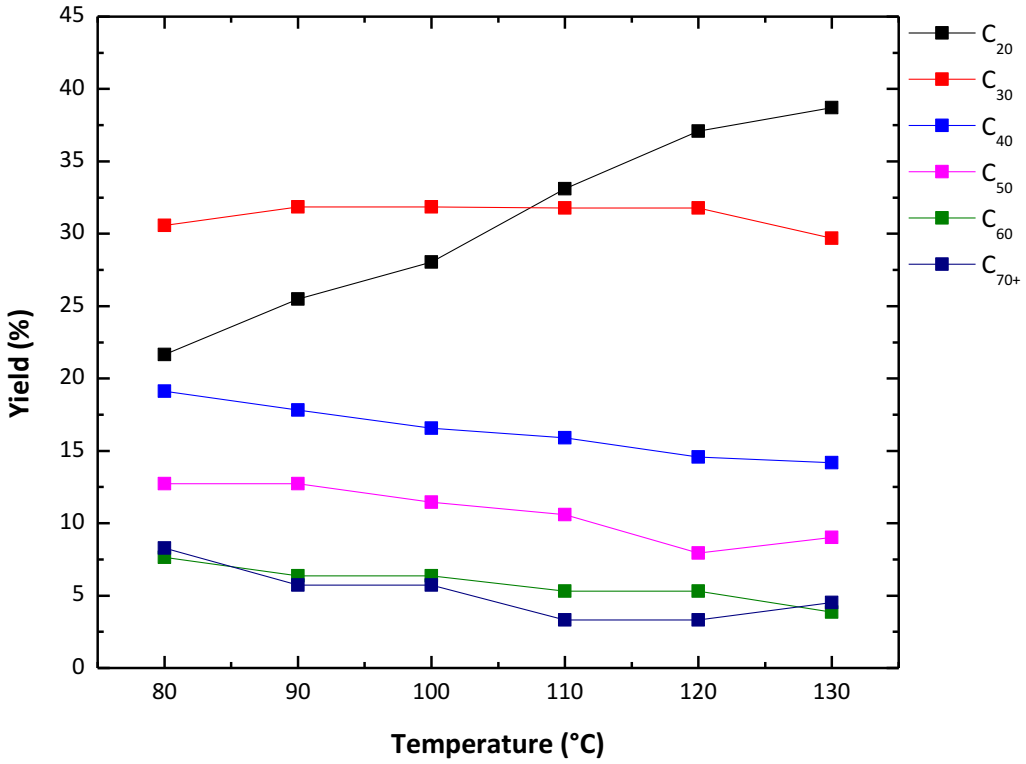

Figure 3.3-5: Product distribution achieved during $[BCl_2Pic][Al_2Cl_7]$ catalysed oligomerisation, 0.62 mmol, 1 hour,

Table 3.3-4: Product distribution achieved during $[BCl_2Pic][Al_2Cl_7]$ catalysed oligomerisation, 0.62 mmol, 1 hour, 100 °C

Temp (°C)	Conversion (± 3 %)	C_{20} (± 4 %)	C_{30} (± 3 %)	C_{40} (± 2 %)	C_{50} (± 2 %)	C_{60} (± 1 %)	C_{70+} (± 1 %)
130	78.50	38.71	29.68	14.19	9.03	3.87	4.52
120	76.50	37.09	31.79	14.57	7.95	5.30	3.31
110	76.50	33.11	31.79	15.89	10.60	5.30	3.31
100	79.50	28.03	31.85	16.56	11.46	6.37	5.73
90	79.50	25.48	31.85	17.83	12.74	6.37	5.73
80	79.50	21.66	30.57	19.11	12.74	7.64	8.28

The SimDist chromatograms of the samples listed in Table 3.3-4 were compared with a previously synthesised PAO 6 (Table 3.2-18), to assess the difference in branching and thus, potentially, difference in physical properties, especially in VI. As the retention time of isomerised paraffins is lower than linear ones[235] the retention time of the maximum height of a peak can be used to estimate the degree of isomerisation. As such, peaks with a similar retention time as the PAO 6 sample should have a similar set of isomers present and therefore similar viscosity properties. From this reasoning, it can be inferred that temperatures below 110 °C would likely give an acceptable VI, seeing as the C_{30} and heavier oligomers have a similar or longer retention times, indicating lower branching. (Figure 3.3-6).

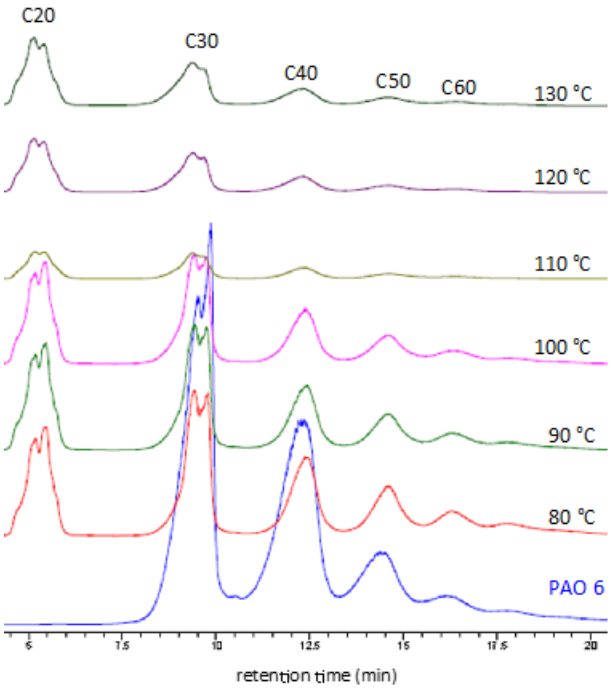

Figure 3.3-6: SimDist chromatogram of unfractionated oligomers obtained with $[BCl_2(2pic)][Al_2Cl_7]$ *vs.* PAO 6 (VI = 132) produced with Ur-$AlCl_3$ χ_{AlCl3} = 0.60

From previous economic evaluation, high conversion (90% minimum) was required (Table 3.2-19), particularly when a high proportion of the product is the undesired C_{20} fraction. As such, the catalyst amount was raised to 1.24 mmol to increase conversion. Furthermore, Table 3.3-2 shows that $[BCl_2(2pic)][Al_2Cl_7]$ gave lower conversions than other catalysts at the equivalent temperature. As such, catalysis with $[BCl_2(4pic)][Al_2Cl_7]$ (Figure 3.3-7) and $[BCl_2(py)][Al_2Cl_7]$ (Figure 3.3-8) was also evaluated as a function of temperature.

Both $[BCl_2(py)][Al_2Cl_7]$ (Table 3.3-5) and $[BCl_2(4pic)][Al_2Cl_7]$ (Table 3.3-6) showed the expected trend, and produced less dimer and more heavy oligomers with decreasing temperature. For $[BCl_2(py)][Al_2Cl_7]$, there was a more significant drop in the dimer content with decreasing temperature. C_{20} went from making up 36.04% of the oligomers at 120 °C to 14.89% at 60 °C. The C_{70+} content rose in tandem by 6.29% over the same range, from 1.16% at 120 °C to 7.45 % at 60 °C.

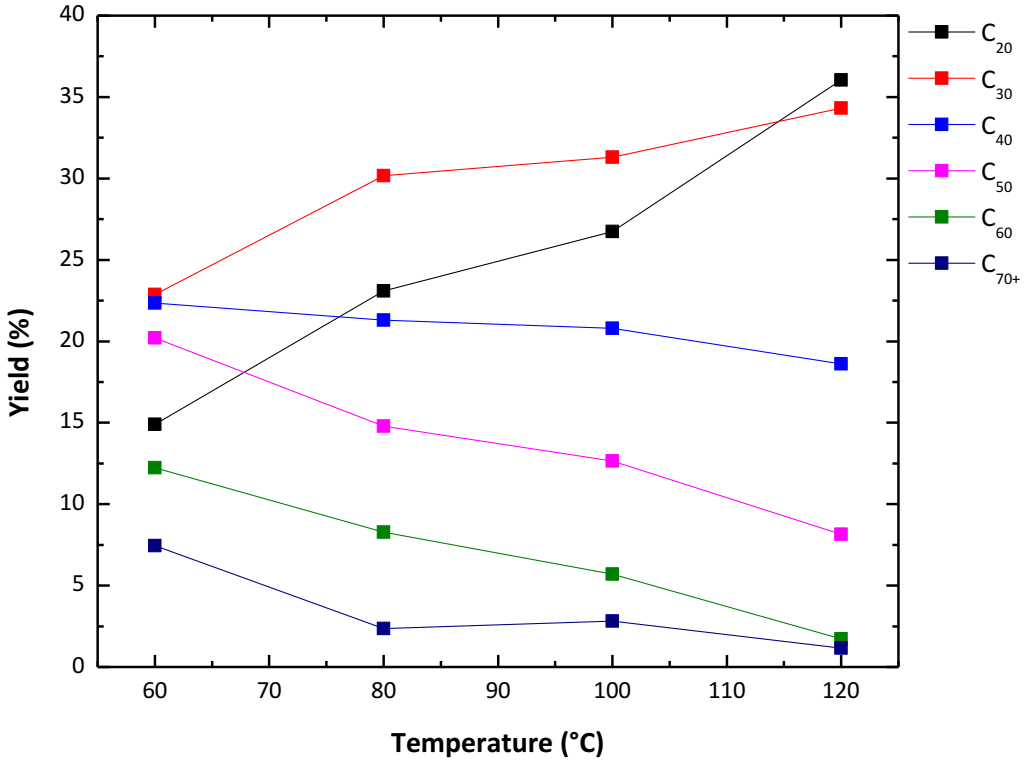

Figure 3.3-7: Product distributions achieved in $[BCl_2(py)][Al_2Cl_7]$ catalysed oligomerisation, 1.24 mmol, 1 h, 100 °C

Table 3.3-5: Conversions and product distributions achieved in $[BCl_2(py])[Al_2Cl_7]$ catalysed oligomerisation, 1.24 mmol, 1 h, 100 °C

Temp (°C)	Conversion (± 3 %)	C_{20} (± 4 %)	C_{30} (± 3 %)	C_{40} (± 2 %)	C_{50} (± 2 %)	C_{60} (± 1 %)	C_{70+} (± 1 %)
120	86.00	36.04	34.31	18.61	8.14	1.73	1.16
100	86.50	26.73	31.31	20.80	12.64	5.70	2.82
80	84.50	23.09	30.18	21.30	14.79	8.28	2.37
60	94.00	14.89	22.87	22.34	20.21	12.23	7.45

Of particular interest was that for $[BCl_2(4pic)][Al_2Cl_7]$ catalysed oligomerisations, the C_{70+} fraction of the product was only increased by 1.47% upon decreasing the temperature from 100 to 60 °C, resulting in C_{70+} only making up 2.60 % of the oligomers at the lower temperature. This suggested that, on the large scale, $[BCl_2(4pic)][Al_2Cl_7]$ may offer a way to further increase the yields of the desired $C_{30} – C_{50}$ fraction (which at the small scale increased from 59.32% to 71.87% upon decreasing the temperature 100 to 60 °C), without compromising the low temperature physical properties, such as pour point.

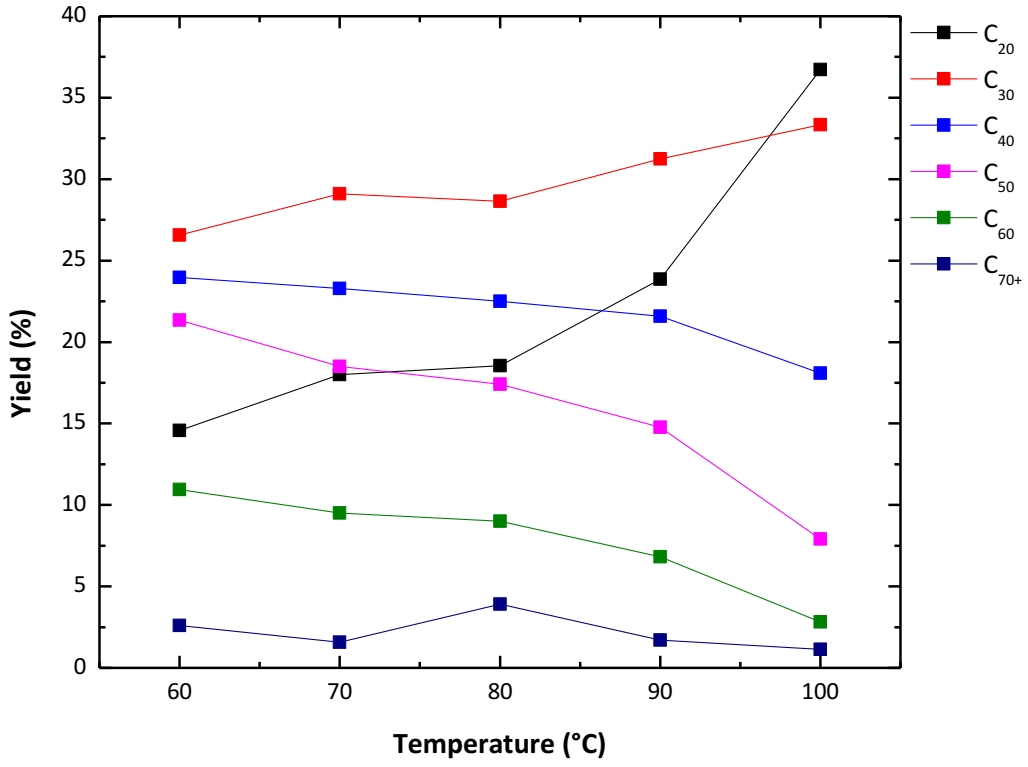

Figure 3.3-8: Product distributions achieved in $[BCl_2(4pic)][Al_2Cl_7]$ catalysed oligomerisation, 1.24 mmol, 1 h, 100 °C

Table 3.3-6: Conversions and product distributions achieved in $[BCl_2(4pic)][Al_2Cl_7]$ catalysed oligomerisation, 1.24 mmol, 1 h, 100 °C

Temp (°C)	Conversion (± 3 %)	C_{20} (± 4 %)	C_{30} (± 3 %)	C_{40} (± 2 %)	C_{50} (± 2 %)	C_{60} (± 1 %)	C_{70+} (± 1 %)
100	88.50	36.73	33.33	18.08	7.91	2.82	1.13
90	88.00	23.85	31.25	21.59	14.77	6.82	1.71
80	89.00	18.54	28.63	22.50	17.42	9.00	3.92
70	94.50	18.01	29.10	23.29	18.51	9.51	1.58
60	96.00	14.58	26.56	23.96	21.35	10.94	2.60

In concluding this chapter, one must note that in all carbocationic oligomerisations and polymerisations, a lower reaction temperature is expected to result in a shift towards heavier products.[54] Interestingly, comparing the reaction temperature profiles using borenium ionic liquids (Table 3.3-4, Table 3.3-5, Table 3.3-6) and liquid coordination complexes (Table 3.2-13) as catalysts, for the former ones the shift to heavy oligomers is less rapid with decreasing temperature. This is a very favourable feature, possibly allowing for lower temperatures to be used, which would have a positive effect on VI without compromising PP. Through increasing the catalyst amount and lowering the reaction temperature, it was possible to push the conversion up towards the desired 90%+ region (Table 3.3-5, Table 3.3-6).

3.3.2.4 Scale up

From previous work using LCCs (Chapter 3.2) it was known that temperature had to be controlled carefully to balance oligomer distribution with the physical properties of the finished lubricant. From the small scale reactions using borenium ionic liquids (Figure 3.3-5: , Figure 3.3-8), it was known that less heavy oligomers were produced at low reaction temperatures than when using LCCs at the same temperatures (Figure 3.2-14). As such, reactions were generally carried out at lower temperatures using borenium ionic. Furthermore, the catalyst loading was decreased due to the exceptionally high exotherms seen on the small scale (Chapter 3.3.2.2).

The preliminary large-scale reactions were performed in triplicate (Table 3.3-7) using 0.25 wt% catalyst (0.16 mmol), and had a significantly decreased conversion compared to the small scale. Comparing the large scale and small scale results for $[BCl_2(2pic)][Al_2Cl_7]$ (Table 3.3-4 and Table 3.3-7), there was a significant shift to the lighter oligomers. For the product synthesised at 100 °C, the C_{20} fraction constituted *ca*. 50% of the product on the large scale, compared to 28% on the small scale. This difference in distribution was seen also for Ur-$AlCl_3$ χ_{AlCl3} = 0.60 (compare Table 3.2-13 and Table 3.3-7).

Table 3.3-7. Conversion and products distribution in scale-up oligomerisation of petrochemical 1-decene, catalysed by borenium IL catalyst (100 °C, 1 h, 0.25 wt%).

Catalyst	Conversion (± 3 %)	C_{20} (± 4 %)	C_{30} (± 3 %)	C_{40} (± 2 %)	C_{50} (± 2 %)	C_{60} (± 1 %)	C_{70+} (± 1 %)
$[BCl_2(4pic)][Al_2Cl_7]$	69.0	50.7	31.9	13.0	2.9	1.5	0.0
$[BCl_2(2pic)][Al_2Cl_7]$	65.5	49.6	31.0	12.4	3.1	1.5	2.3
$[BCl_2(2pic)][Al_2Cl_7]$	62.5	50.4	30.9	11.4	3.2	1.6	2.4

Following these preliminary results it was ensured that reproducibility on the large scale was very good, but modifications were required. Since 90% conversion was required to match the industrial benchmark catalyst, BF_3/nBuOH (Table 3.2-19), the catalyst amount was increased to 1.25 wt% (0.78 mmol) (Table 3.3-8). Since, on the small scale, $[BCl_2(py)][Al_2Cl_7]$ produced less heavy oligomers than systems with other pyridine ligands at the same temperature, it was selected as the catalyst of choice. Using 1.25 wt% of the $[BCl_2(py)][Al_2Cl_7]$ catalyst, large-scale temperature screening was carried out to see how far the reaction temperature could be lowered without drastically increasing the heavy oligomer content (Table 3.3-8, Figure 3.3-9).

Table 3.3-8. Conversion and products distribution achieved in $[BCl_2(py)][Al_2Cl_7]$ catalysed oligomerisations at a range of temperatures (1 h, 1.25 wt% catalyst loading)

Reaction Temperature (°C)	Conversion (± 3 %)	C_{20} (± 4 %)	C_{30} (± 3 %)	C_{40} (± 2 %)	C_{50} (± 2 %)	C_{60} (± 1 %)	C_{70+} (± 1 %)
100	83.00%	39.76%	36.14%	18.07%	6.02%	0.00%	0.00%
80	86.00%	33.72%	32.56%	18.60%	10.47%	3.49%	1.16%
60	86.00%	22.09%	32.56%	22.09%	16.28%	5.81%	1.16%

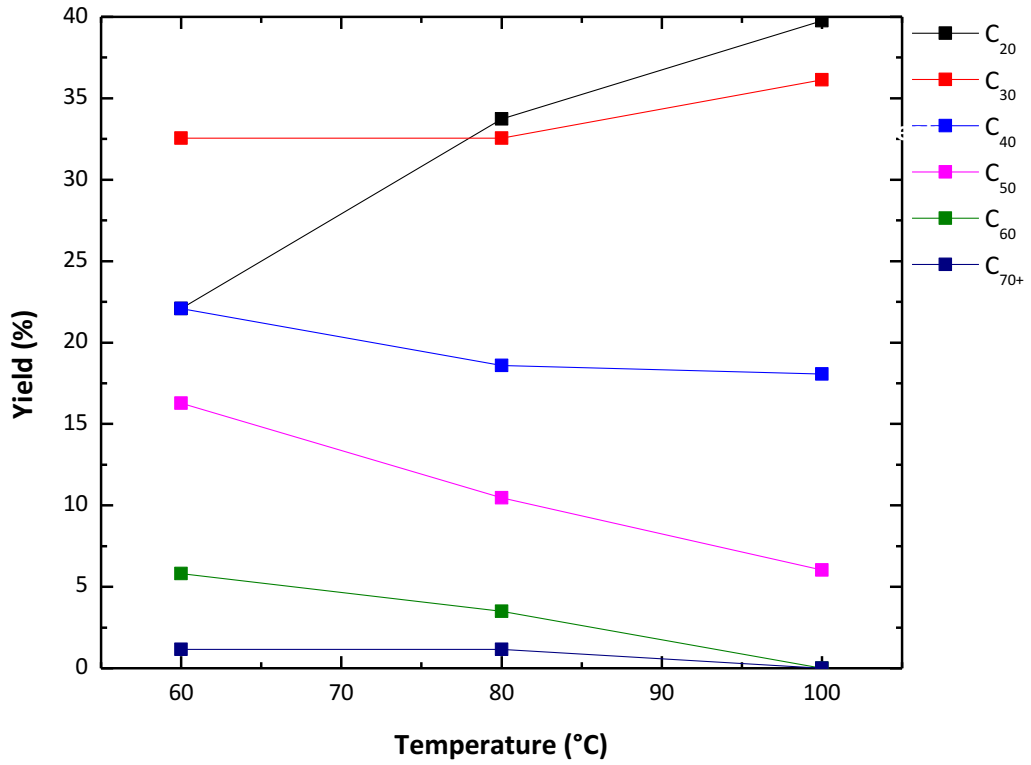

Figure 3.3-9: Products distribution achieved during $[BCl_2(py)][Al_2Cl_7]$ catalysed oligomerisations at different temperatures. (1 hour, 1.25 wt%)

Using $[BCl_2(py)][Al_2Cl_7]$ as the catalyst, the dimer content of the product could be significantly reduced by lowering the temperature to 60 °C, without increasing the heavy content drastically (Figure 3.3-9). However, disappointingly, the produced PAOs were found to have exceptionally low VIs (VI > 100) which originated from the relatively high isomerisation rate promoted by this catalyst. Decene fraction recycled from several reactions using $[BCl_2(py)][Al_2Cl_7]$, at different temperatures, showed much higher rates of isomerisation than other borenium ionic liquid catalysts (Table 3.2-9).

Table 3.3-9: Ratio of isomerised to linear decene present in recycled decene

Temperature of Reaction [Catalyst]	5.8ppm : 5.4ppm Peak Ratio
100 °C $[BCl_2(2pic)][Al_2Cl_7]$	1 : 21
100 °C $[BCl_2(4pic)][Al_2Cl_7]$	1 : 6
100 °C $[BCl_2(py)][Al_2Cl_7]$	1 : 95
80 °C $[BCl_2(py)][Al_2Cl_7]$	1 : 84
60 °C $[BCl_2(py)][Al_2Cl_7]$	1 : 33
Fresh Decene	33:1

The oligomeric product generated using $[BCl_2(py)][Al_2Cl_7]$ also precipitated a fine white powder, which was possible to remove by repeated high temperature water washing, but not by filtration. This powder was found to be extremely fine boric acid powder. The oligomeric product was analysed with ^{11}B NMR spectroscopy immediately post reaction to determine whether boron was dissolved in the product as boric acid, or chemically bound to the oligomers and subsequently hydrolysed - but no ^{11}B peaks were distinguishable from the baseline.

Considering that pyridine-based system was obviously unsuitable, it was decided to use $[BCl_2(2pic)][Al_2Cl_7]$ as the catalyst for 1-decene oligomerisation, with the experiments repeated several times to produce sufficient material for fractionation and blending (Table 3.3-10), yielding yellow, non-hydrogenated samples of PAO4 and PAO 6. The PAO 6 sample produced using $[BCl_2(2pic)][Al_2Cl_7]$ was additionally hydrogenated (Pd/C, 100 °C, 40 bar H_2), giving a clear colourless liquid. The samples produced using borenium ionic liquids and LCCs as catalysts are compared below (Table 3.3-10) along with a commercial sample. The physical properties of the hydrogenated sample showed a slight increase in Kv_{100} compared to the non-hydrogenated sample The PP increased up to -57 °C, as expected when converting unsaturated to saturated oligomers, but all parameters remained within required specifications for base oils.

Table 3.3-10: Composition and physical properties of PAO samples produced using borenium ionic liquids, LCCs and compared to commercial PAO samples

Catalyst (Temperature)	KV 100 (cSt)	KV40 (cSt)	VI	PP (°C)	C_{30} (%)	C_{40} (%)	C_{50+} (%)
$[BCl_2(2pic)][Al_2Cl_7]$ (100 °C)	6.18	33.35	136	< -60	39	36	25
$[BCl_2(2pic)][Al_2Cl_7]$ (100 °C, Hydrogenated)	6.45	35.30	137	-57	39	36	25
LCC PAO 6	5.74	31.49	126	< -60	42.15	37.46	12.84
Durasyn PAO 6	5.76	30.22	135	-57	36.87	42.42	14.14
$[BCl_2(2pic)][Al_2Cl_7]$ (100 °C)	4.23	18.87	132	< -60	80	14	6
LCC PAO 4	4.31	20.11	123	< -60	76.94	15.88	4.23
Durasyn PAO 4	3.92	17.25	137	< -60	80.30	19.19	0.51

3.3.2.5 Recycling of C10 + C20

It was demonstrated that synthesis of high quality PAOs was possible using borenium catalysts. However, in order to ensure economic appeal of the process, either a high conversion per reaction, or recyclability of the unreacted C_{10} and C_{20} fraction would be needed to increase the selectivity to the desired C_{30}-C_{50} oligomers as stated in the techno-economical evaluation provided by PDC (Table 3.2-19).

As already mentioned, the ^{1}H NMR spectra of recycled decene fractions from several reactions were compared, with the purpose of assessing the isomerisation of the decene (Table 3.3-9). For the linear 1-decene, the hydrogen atoms on the double bonds have peaks at *ca.* 5.8 and 4.95 ppm. The recycled decene showed the original peaks with the same splitting pattern, and a new signal at *ca.* 5.4 ppm, assigned to the isomerised decene (internal olefin). From this signal ratio, the degree of isomerisation of the decene fraction can be measured. As shown in Table 3.3-9, the lowest degree of isomerisation was ensured using 4pic ligand. Surprisingly large differences were noted for three extremely similar borenium systems, again demonstrating how carbocationic oligomerisation is sensitive to each structural change in the catalyst.

In order to emulate continuous process with a batch reactor, the scheme in Figure 3.3-10 was adopted (Table 3.2-23). This allowed for the production of samples of sufficient size for fractionation and blending, which in turn allowed to assess how recycling changed the physical properties of the produced PAO samples.

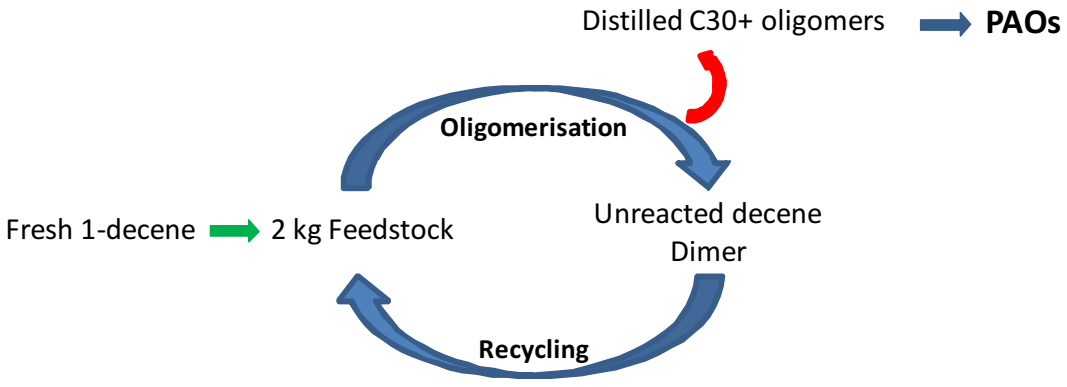

Figure 3.3-10: Reaction scheme for continous recycling experiments

To manufacture enough product to carry out a full sequence of fractionated distillation and blending, two reactions of 2 kg of feedstock (1-decene, recycled decene and dimer) were required. The reactions were performed at 80 °C, using $[BCl_2(4pic)][Al_2Cl_7]$ at 1 wt% as a

catalyst. Full mass balance for two cycles (4 reactions) is shown in Table 3.3-11. Conversions and product distributions obtained from each cycle are compared in Table 3.3-12.

Table 3.3-11: Mass balance for large-scale recycling reactions

Cycle 1							
Reaction 1				**Reaction 2**			
Reactant/ Reagent	**Mass in (g)**	**Product**	**Mass out (g)**	**Reactant/ Reagent**	**Mass in (g)**	**Product**	**Mass out (g)**
1-decene	2000	**Oligomers**	1757	**1-decene**	2000	**Oligomers**	1877
$[BCl_2(4pic)][Al_2Cl_7]$	20	**Red Oil**	17	**$[BCl_2(4pic)][Al_2Cl_7]$**	20	**Red Oil**	10
Water	1800	**Water**	1723	**Water**	2200	**Water**	2075
		Lost	323			**Lost**	258
Cycle 2							
Reaction 1				**Reaction 2**			
Reactant/ Reagent	**Mass in (g)**	**Product**	**Mass out (g)**	**Reactant/ Reagent**	**Mass in (g)**	**Product**	**Mass out (g)**
Recycled C_{10}	235	**Oligomers**	1585	**Recycled C_{10}**	238	**Oligomers**	1422
Recycled C_{20}	433	**Red Oil**	12	**Recycled C_{20}**	427	**Red Oil**	14
1-decene	1332	**Water**	1985	**1-decene**	1335	**Water**	1935
$[BCl_2(4pic)][Al_2Cl_7]$	20	**Lost**	438	**$[BCl_2(4pic)][Al_2Cl_7]$**	20	**Lost**	649
Water	2000			**Water**	2000		

Table 3.3-12: Oligomer distribution obtained by combination of two reactions per cycle.

Cycle	Conversion (± 3 %)	C_{20} (± 4 %)	C_{30} (± 3 %)	C_{40} (± 2 %)	C_{50} (± 2 %)	C_{60} (± 1 %)	C_{70+} (± 1 %)
Cycle 1	85.30	33.65	28.36	17.06	9.52	4.74	6.68
Cycle 2	87.66	33.87	24.13	15.00	10.08	6.37	10.54

Lower concentrations of linear 1-decene, with respect to isomerised 1-decene, were previously shown to result in lower conversions on the small scale (Table 3.2-20). However, the reaction in cycle 2, where recycled C_{10+C20} fraction was used, turned out to have a similar conversion to cycle 1, where fresh 1-decene was used. However, in cycle 2 there was a significant increase in both C_{60} and C_{70+} fractions, by 1.63 and 3.86%, respectively. The products were distilled and blended to form samples of both PAO 4 and PAO 6 (Table 3.3-13).

Table 3.3-13: Physical properties and product distribution of PAOs produced during cycle 1 and cycle 2

Catalyst (Cycle)	KV 100 (cSt)	KV40 (cSt)	VI	PP (°C)	C_{30} (%)	C_{40} (%)	C_{50+} (%)
$[BCl_2(4pic)][Al_2Cl_7]$ (1)	5.88	32.40	127	< -60	42	28	30
$[BCl_2(4pic)][Al_2Cl_7]$ (2)	5.62	31.00	121	< -60	82	17	1
$[BCl_2(4pic)][Al_2Cl_7]$ (1)	3.95	17.34	125	< -60	45	30	25
$[BCl_2(4pic)][Al_2Cl_7]$ (2)	3.96	17.77	120	< -60	80	19	1

Despite similar hydrocarbon distribution, there was a clear decrease in the VI of the PAOs produced with recycled feedstocks. For PAO 6 form cycle 2, the VI decreased by 6 units to 121, just above the threshold for marketable PAO samples (Table 3.1-1). Similarly, the VI for the PAO 4 sample decreased by 5 units to 120, exactly the minimum value for a marketable PAO. Considering these were only two cycles, it was deemed unfeasible to attempt subsequent recycling, as the operation was very time- and resource-consuming, and further decrease in the product quality could be clearly anticipated.

3.3.2.6 Recycling of Red Oil

In typical commercial operations, the BF_3 catalyst is not recycled. However, attempt to recycle this new ionic liquid catalyst was undertaken, aiming at minimisation the process OPEX. Nevertheless, from the very beginning it was more of an academic exercise than a viable option, due to two key problems. Firstly, borenium ionic liquids are Lewis acids and catalyse the oligomerisation of olefins by combining with protic impurities to form a Brønsted superacid (Chapter 3.1.3). It is this Brønsted superacidic species that would need to be recovered from the reaction mixture for the catalyst to be used again. Secondly, it is well known that acidic catalysts in the presence of unsaturated hydrocarbons form so-called red

oil, also known as conjunct polymers or acid soluble oils (ASO).[287] This red oil is a well-known problem for sulfuric acid alkylation units, where acid runaway can drastically lower the quality of the product produced.

Upon allowing a reaction to settle, without quenching with water, the expected red oil separated to the bottom of the reactor (Figure 3.3-11). This was seen when either borenium ionic liquid or LCC catalysts. This red oil was extracted using a gastight syringe, to prevent contact with atmospheric moisture, and analysed using multinuclear NMR spectroscopy (Figure 3.3-12, Figure 3.3-13).

Figure 3.3-11: Red oil separated from post-reaction mixture, oligomerisation of 1-decene using 1 wt% $[BCl_2(4pic)][Al_2Cl_7]$

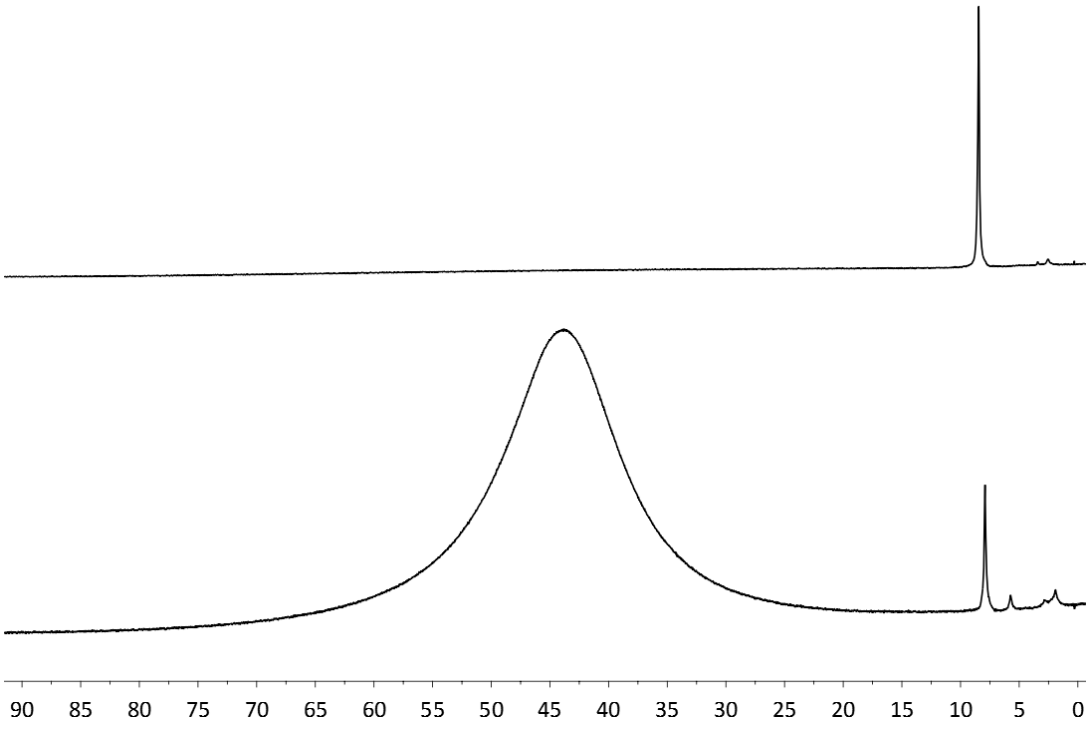

Figure 3.3-12: ^{11}B NMR spectra of a) $[BCl_2(py)][Al_2Cl_7]$ and b) red oil phase-separated from the post reaction mixture

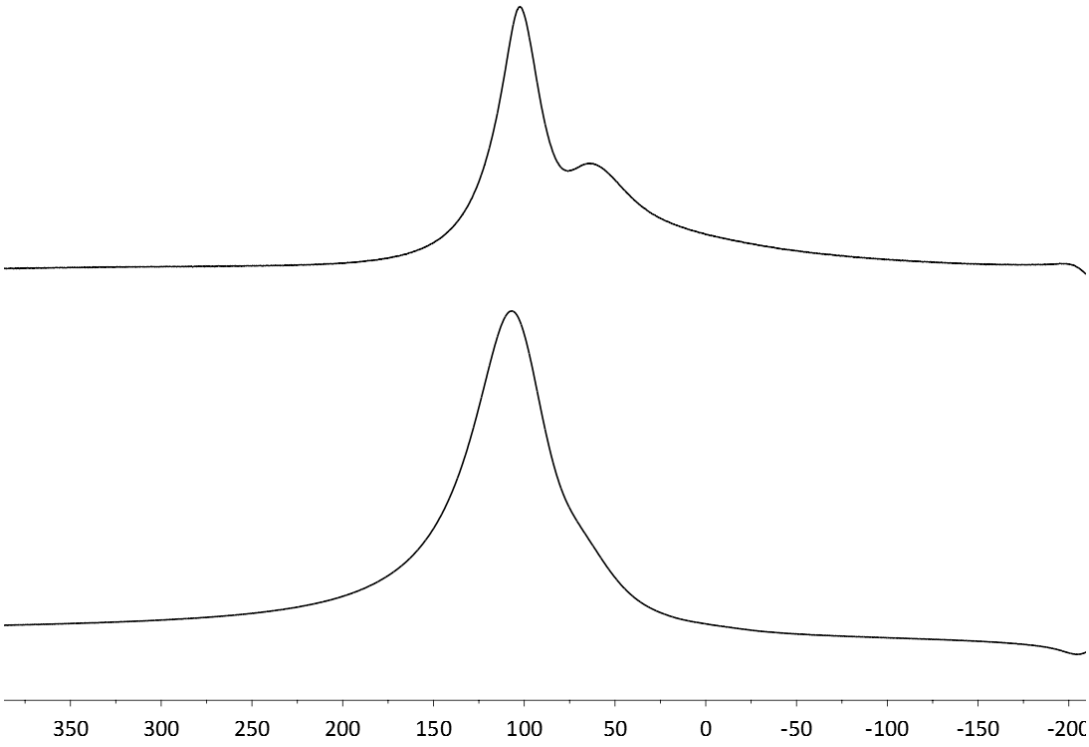

Figure 3.3-13: ^{27}Al NMR spectra of a) $[BCl_2(py)][Al_2Cl_7]$ and b) red oil phase-separated from the post reaction mixture

The broad peak at *ca*. 45 ppm is absent in the ^{11}B NMR spectrum of the red oil (Figure 3.3-12-b), which indicates that all remaining boron has quaternised (no Lewis acidic, tricoordinate borenium ions remain). From the ^{27}Al NMR spectrum (Figure 3.3-13-b) it can be seen that the aluminium peak has decreased in width, a possible indication of the shift from $[Al_2Cl_7]^-$ to $[AlCl_4]^-$. The sample is also highly diluted with organic materials, meaning the sample's signal: probe's signal ratio is smaller, meaning the probe can also be seen at ca. 70ppm.

Elemental analysis of red oil allowed measuring the ratio of aluminium to boron, which grew greatly in the red oil compared to the fresh catalyst (Table 3.2-15). This indicates that boron leaches to the organic phase, as was seen when neutralising reactions on the large scale. Furthermore, the ^{13}C NMR spectrum of the red oil was recorded, which showed strong peaks between 0 and 40 ppm, indicative of alkyl chains, and a broad highly deshielded peak at 247 ppm, which is assigned as belonging to a carbocation.[288] As such, the oil would appear to be a mix of hydrocarbons, including some carbocations accompanied by aluminium anions, and a trace of tetracoordinate boron complexes. This study gives an interesting insight into the reaction mechanism, and ensures the vital role of the ionic liquid anion, but does not promise an easy solution to the catalyst recycling.

Table 3.3-14: Metals analysis of fresh catalysts and red oil samples

	Fresh Catalyst			Red Oil		
Sample	**Mass Al (%)**	**Mass B (%)**	**Al : B**	**Mass Al (%)**	**Mass B (%)**	**Al : B**
$[BCl_2(py)][Al_2Cl_7]$	11.66	2.34	5 : 1	3.00	0.20	15 : 1
$[BCl_2(py)][Al_2Cl_7]$	11.66	2.34	5 : 1	3.90	0.30	13 : 1
$[BCl_2(4pic)][Al_2Cl_7]$	11.31	2.27	5 : 1	2.80	0.20	14: 1
$[BCl_2(4pic)][Al_2Cl_7]$	11.31	2.27	5 : 1	7.80	0.40	19.5 : 1

From the study of the red oil it is clear that the catalyst has deteriorated over the course of the reaction. To investigate remaining catalytic activity of the red oil, it was blended at varying proportions with fresh ionic liquid catalyst, before being used to oligomerise fresh 1-decene (Figure 3.3-14, Table 3.2-15)

The red oil itself had low catalytic activity in the oligomerisation of 1-decene, yielding a conversion of 27%. Mixing the red oil with fresh catalyst, in turn, resulted in increase in heavy oligomers forming, from 1.13 % C_{70}+ with the fresh catalyst, to 8.24% C_{70}+ with 10 % of the red oil and 90% of the fresh catalyst.

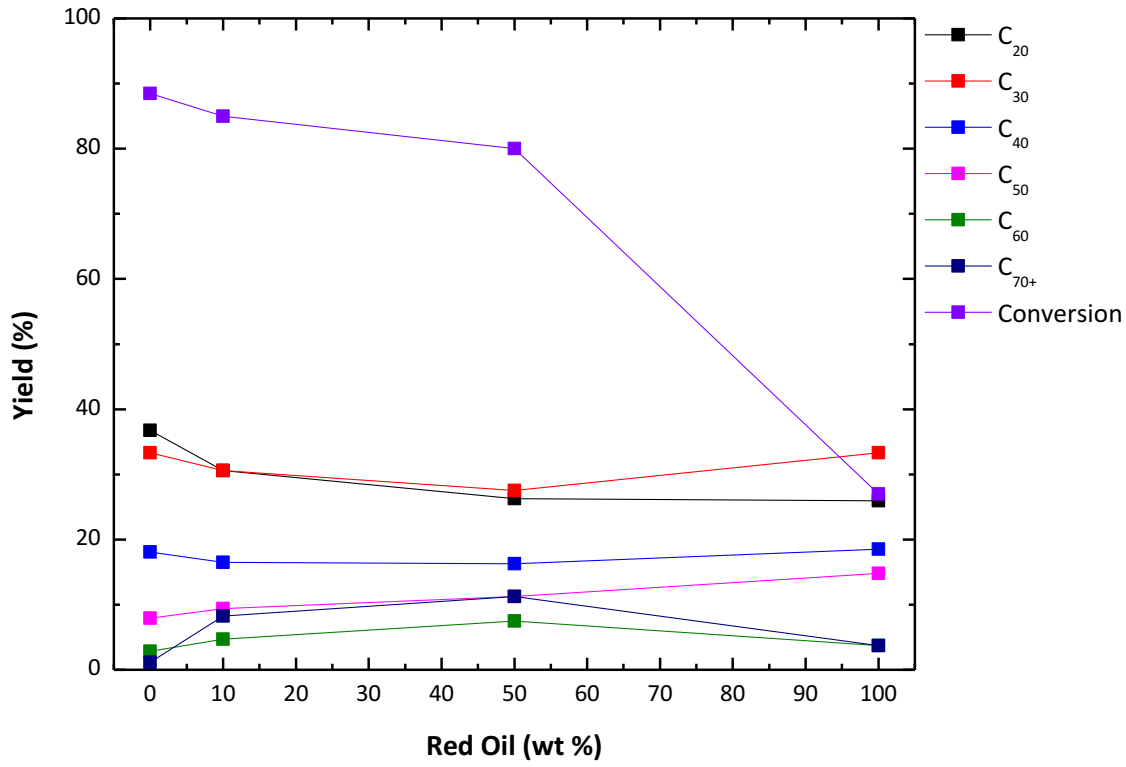

Figure 3.3-14: Product distributions in $[BCl_2 4Pic][Al_2Cl_7]$ catalysed oligomerisation, with partial replacement of the fresh catalyst by red oil, 1.24 mmol, 1 h, 100 °C

Table 3.3-15: Conversions and product distributions in $[BCl_2 4Pic][Al_2Cl_7]$ catalysed oligomerisation, with partial replacement of the fresh catalyst by red oil, 1.24 mmol, 1 h, 100 °C

Red Oil (%)	Conversion (± 3 %)	C_{20} (± 4 %)	C_{30} (± 3 %)	C_{40} (± 2 %)	C_{50} (± 2 %)	C_{60} (± 1 %)	C_{70+} (± 1 %)
0	88.50	36.73	33.33	18.08	7.91	2.82	1.13
10	85.00	30.59	30.59	16.47	9.41	4.71	8.24
50	80.00	26.25	27.50	16.25	11.25	7.50	11.25
100	27.00	25.93	33.33	18.52	14.81	3.70	3.70

A number of patents exist for the recovery of $AlCl_3$[289,290] or regenerating a chloroaluminate ionic liquid[291,292,293] from conjunct polymers. However, these tend to require the use of harsh conditions, such as high temperature hydrogenation to decrease the miscibility of the organic and inorganic species in the red oil, and were not tried. Attempts to directly sublime $AlCl_3$ from the conjunct polymers failed and yielded a black sludge. This concluded the attempt to recycle borenium catalyst in any form.

3.3.3 Conclusions

Borenium ionic liquids of the general formula $[BCl_2(L)][M_2Cl_7]$ (M = Ga, Al), were shown to be effective 1-decene oligomerisation catalysts. With the cation $[BCl_2(3pic)]^+$ the effect of the anion was measured. Oligomerisation was hampered by $[GaCl_4]^-$. $[AlCl_4]^-$ gave a slightly

heavier oligomeric distribution than $[Al_2Cl_7]^-$ and seemed to isomerise the oligomers less than $[Al_2Cl_7]^-$ possible in part due to a lower exotherm.

Following on from the experience and knowledge acquired in Chapter 3.2, the catalytic system $[BCl_2(L)][Al_2Cl_7]$ / H_2O was successfully employed on a 3 L scale to produce 1-decene oligomers which were fractionated and blended to give PAO 4 and PAO 6. Hydrogenation of a sample of PAO 6 was shown to increase the viscosity of the sample slightly, increase the pour point significantly, though the pour point was still below the minimum temperature specification, and did not affect the VI. Ligand choice was also found to have a large effect on the physical properties of the lubricant samples. Only when methypyridines were used as ligands did the catalyst yield PAO samples where VI > 120.

Distilled C_{10} and C_{20} were utilised in a recycling study, where C_{10} and C_{20} from the previous reaction were topped up with fresh 1-decene and oligomerised. After 1 cycle there was a noticeable drop in the VI of the produced lubricant samples. For further study it would be of interest to utilise the catalyst $[BCl_2(L)][AlCl_4]$ to assess the difference in physical properties of PAO samples produced by this catalyst and $[BCl_2(L)][Al_2Cl_7]$

3.4 Summary

Both liquid coordination complexes and borenium ionic liquids were shown to be potent catalysts for the oligomerisation of 1-decene, and in each case it was possible to produce marketable quality PAO 4 and PAO 6 grade lubricant base oils. For both liquid coordination complexes and borenium ionic liquids, the choice of ligand was found to have a significant effect on the reaction, with even small structural alteration leading to major changes in product distribution and physical properties. Further reaction conditions, in particular temperature, had to be carefully selected to minimise unwanted heavy oligomer product, as well as unwanted dimer product and to ensure the final product met the physical property specifications required.

In both cases, it was very challenging to meet economical demands of the project, especially to increase conversion and yield to the most valuable C_{30-50} fraction whilst maintaining good visometric properties. Unfortunately, recycling of unreacted 1-decene and the dimer decreased quality of PAOs produced.

The LCC catalysed oligomerisation study was published in *Green Chemistry*[294] and presented in poster format at *7th Green Solvents Conference, Dresden*, Oct – 2014. The oligomerisation

of 1-decene using borenium ionic liquids was patented[295] and present in poster format at *26th EUCHEM conference on molten salts and ionic liquids, Vienna*, July - 2016

4 Hydrogenation of toluene with LCC-SCILLs

4.1 Literature Review

4.1.1 Introduction to SILPs and SCILLs

Chlorometallate ionic liquids on solid support have been extensively studied in a range of catalytic applications, in particular by Wasserscheid and co-workers.[66,116,117,296] It was therefore extremely interesting to test the newly-developed LCCs in a similar supported arrangement, and benchmark them against well-known chloroaluminate systems. This project was carried out as part of the COST-STSM-CM1206 exchange program. The aim of this project was to assess LCCs as supported liquids for applications with gaseous reactants.

Using liquid Lewis acids has several advantages over solids, as outlined in Chapter 1.2. At the same time, recyclability and ease of handling make solid Lewis acid a popular choice, especially in large-scale industrial applications.[297] A popular method of minimising the use of ionic liquids, and of getting 'best of both worlds' in terms of advantages of liquid and solid catalysts, is to support ionic liquids on a solid material. An ionic liquid attached to a surface (whether covalently or by simple adsorption) is known as a Supported Ionic Liquid Phase or SILP (Figure 4.1-1). Typically, the ionic liquid will either be catalytically active itself or, as depicted in Figure 4.1-1, have a catalytic species dissolved in it. A more recent development is the approach of covering the catalytically active support material with ionic liquids, or using ionic liquids with a deposited solid catalyst (*e.g.* in the form of nanoparticles), which is known as a Solid Catalyst with an Ionic Liquid Layer or SCILL (Figure 4.1-1).[223] Here, the ionic liquid may enhance the catalytic process by modifying the surface of the catalyst, acting as a co-catalyst, or altering the solubility of the reactants.

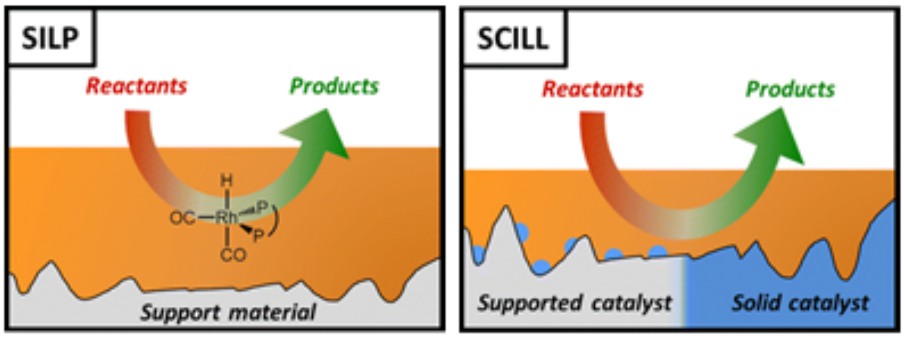

Figure 4.1-1: Pictorial representation of SILP and SCILL concepts[66]

4.1.2 Lewis acid-assisted hydrogenation

Hydrogenation reactions in ionic liquids have been widely studied.[298,299] Hydrogen has, in general, poor solubility in ionic liquids, though this does not always correlate with reduced reaction rates.[299] Typically, ionic liquids have been used to immobilise transition metal complexes by their dissolution in the ionic liquid phase (to ease separation from the product),[300] as well as to stabilise metal nanoparticles.[301]

In their recent *Angew. Chem*. publication, Song *et al.* reported the hydrogenation of aromatics using Pd/C under mild conditions (24 h, ambient temperature, 1 bar H_2), which was enhanced by the addition of 0.25 to 1 mole equivalent of the ionic liquid, $[C_4C_1im][Al_2Cl_7]$.[128] It was reasoned that the acceleration was due to activation of the aromatic ring by the Lewis acid. Conversely, when $AlCl_3$ powder was used as a Lewis acid, side reactions were observed. An equimolar mixture of anthracene and $[C_4C_1im][Al_2Cl_7]$ was analysed by ^1H and ^{13}C NMR spectroscopy and revealed the presence of the anthracenium salt (Figure 4.1-2), which was stable over the course of several weeks. In contrast, when the equimolar anthracene and $AlCl_3$ mixture was prepared, oligomerisation of the anthracene was observed after a short time. Computational studies showed stabilisation of the activated ring by coordination of the ionic liquid anion and cation to the ring (Figure 4.1-3). With $AlCl_3$ there is no stabilisation of the intermediate, hence the differing reaction outcomes.

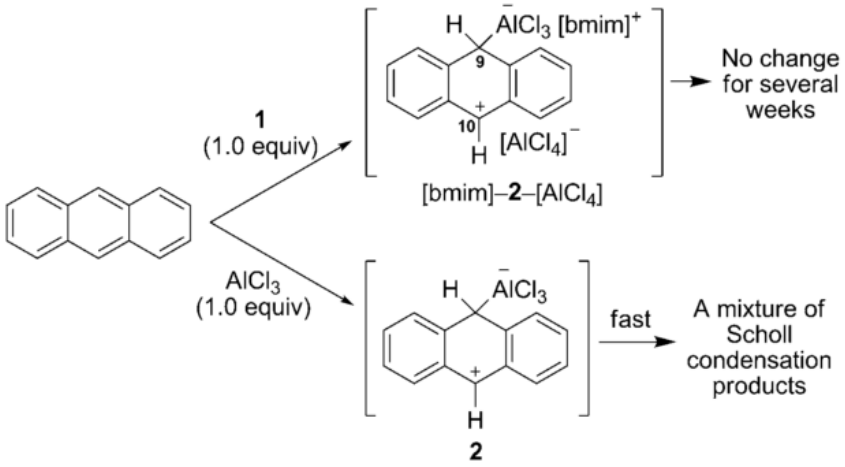

Figure 4.1-2: Anthracenium salts produced by addition of $[C_4C_1im][Al_2Cl_7]$ (top) and $AlCl_3$ (bottom)[128]

Han *et al.* used solid $AlCl_3$ to activate aromatic rings in the presence of supported Pd. Side reactions were observed when the palladium was supported on carbon.[302] When the support was changed from carbon to a hydroxyl group-containing support, *i.e.* silica or alumina, no

side reactions were seen. The combinations of Pd/SiO_2 and Pd/Al_2O_3 with $AlCl_3$ were both shown to catalyse the hydrogenation of benzene under mild conditions using low catalyst loadings and without unwanted side reactions (30 °C, 10 bar H_2, 1 mol % Pd, 2 mol % $AlCl_3$, and ≥ 3 h). Computational calculations supported the view that the ring is activated by $AlCl_3$ and the intermediate is stabilised by hydroxyl groups of the support, thus preventing side relations (Figure 4.1-3).

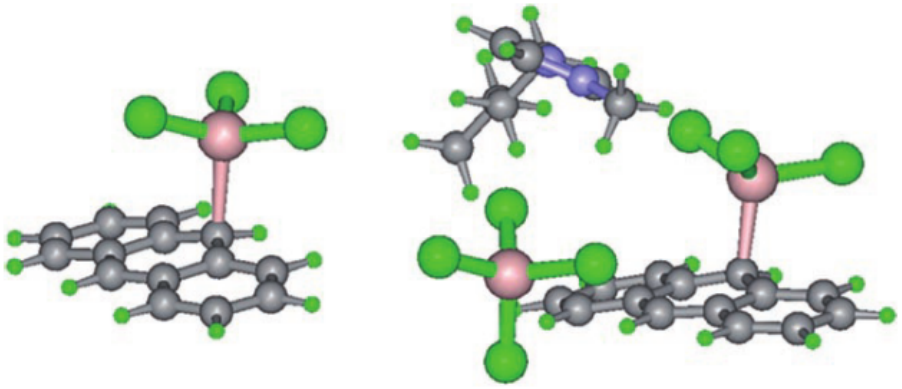

Figure 4.1-3: Calculated structure of anthracene activated by: $AlCl_3$ (left) and $[C_4C_1im][Al_2Cl_7]$ (right)[128]

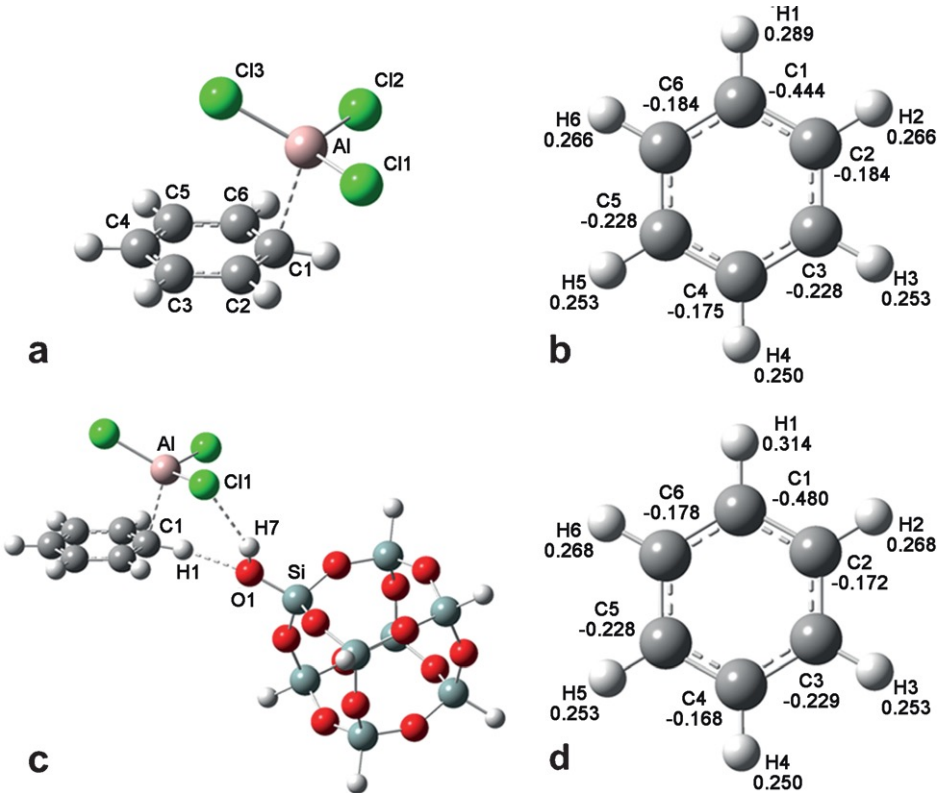

Figure 4.1-4: Calculated structure of activated benzene: in the absence of SiO_2 support (above) and in the precedence of SiO2 support (below)[302]

The Lewis acid and supported palladium combination has been shown to selectively hydrogenate phenol to cyclohexanone.[303] Addition of the Lewis acids, $AlCl_3$, $InCl_3$, $ZnCl_2$ or $SnCl_2$, to the reaction mixture of phenol, Pd/C and H_2 resulted in near-complete conversion of phenol at low temperature and low H_2 pressure. At low temperatures (≤ 50 °C) near complete conversion (>99.9) with high selectivity (≥ 99%) was seen, although long reaction times were required (≥ 7 h). At higher temperatures (100 °C) or above-ambient pressures higher conversions were achieved, albeit at the cost of a decrease in selectivity (95 – 99 %). The addition of a Lewis acid increased rates of conversion and selectivity compared to neat Pd (12.6 % after 12 h at 30 °C), irrespective of the support used.

Lee *et al.* took the concept a step further, going directly from phenol to ε-caprolactam in a one pot synthesis.[304] The use of scandium(III) triflate as a Lewis acid in the presence of palladium on carbon and hydrogen (1 bar) resulted in a rapid conversion of phenol to cyclohexaone, with high selectivity. Subsequently, hydroxylamine hydrochloride was added to form the ε-caprolactam. Utilising $[C_4C_1im][PF_6]$ as a solvent, the yield of ε-caprolactam from phenol was 67 %.

4.2 Experimental

4.2.1 Materials and methods

All chemicals were purchased from Sigma Aldrich unless otherwise stated. 1-Butyl-3-methylimazolium chloride (99.5 %), was dried under reduced pressure (80 °C, < 1 mbar, 48 h) before use. Pallidum on activated charcoal (10 wt% Pd) was dried (100 °C, 24 h) and stored in a glovebox before use. Toluene (99%), dichloromethane, decalin (99%) and cyclohexane (99%) were dried over activated 3 Å molecular sieves (≥ 24 h) before use. Hydrogen and argon (both 99.9999 % purity) were provided by Linde and were used as received.

4.2.2 Catalyst preparation

LCCs were prepared in a portable glovebox, which was purged by positive pressure of argon, without a circulator purifier or H_2O/O_2 monitoring. LCC preparation was otherwise the same as described in Chapter 2.2.

To prepare the supported catalyst, a desired amount of LCC (the mass equivalent to 0.65 mmol of metal chloride) was weighed into a round-bottomed flask with Pd/C (1.065 g, 1 mmol Pd), and cyclohexane (7 cm^3) was added. The solution was stirred for 1 h, before gently

removing the solvent under carefully-controlled reduced pressure (80 °C, 600 mbar) and subsequently drying overnight (100 °C, 12 h, < 1 mbar).

4.2.2.1 Hydrogenation experiments

Cyclohexane (78 g, 100 cm^3), toluene (2.3 g, 24.962 mmol) and decalin (0.59 g, 4.267 mmol) were added to a corrosion resistant, stainless steel reactor vessel, which was purged by positive pressure of argon. The supported catalyst was added to the vessel, which was then sealed and purged again by positive pressure of argon. The reactor was heated to the desired temperature, with stirring (40 - 90 °C, 1000 rpm). Then, the stirring was stopped, the reactor was pressurised with H_2 (5 – 25 bar) and the stirring was restarted. The reaction was carried out for typically 1 h, as measured from when the stirring speed reached 1000 rpm. Samples were taken at regular intervals and analysed by gas chromatography using GC Varian 3900, equipped with GC column Varian CP_Sil PONA CB. Conversion was calculated based on toluene peak decrease, and verified by methylcyclohexane increase, using decalin as an internal standard. No side reactions were observed by GC, *i.e*. toluene peak area decrease was matched by methylcyclohexane peak area increase.

4.3 LCC-SCILL hydrogenation of toluene

4.3.1 $GaCl_3$-LCC-SCILLs

A series of $GaCl_3$-LCCs were synthesised and supported for use in the hydrogenation of toluene to methylcyclohexane. Due to the complicated equilibria present in each LCC, it was rationalised that the best method for comparison was to ensure that a constant amount of metal chloride was used in each reaction. The amount of metal chloride was set at 0.65 mmol.

Early experiments revealed that the catalysts based on $GaCl_3$-LCCs were ineffective (Figure 4.3-1). In comparison to the uncoated Pd/C catalysts, the $GaCl_3$-LCCs gave lower conversions (≤ 2.2%) under the same conditions, typically stalling the reaction completely (Table 4.3-1) With $GaCl_3$-LCC coated Pd/C, conversions of less than 5 % were recorded after an hour, regardless of the ligand used. For comparison, the untreated Pd/C reached a conversion of 30.23% under the same conditions. It was also noted that, when using thiourea as a ligand, there was a noticeable sulphurous odour indicating decomposition of the LCC.

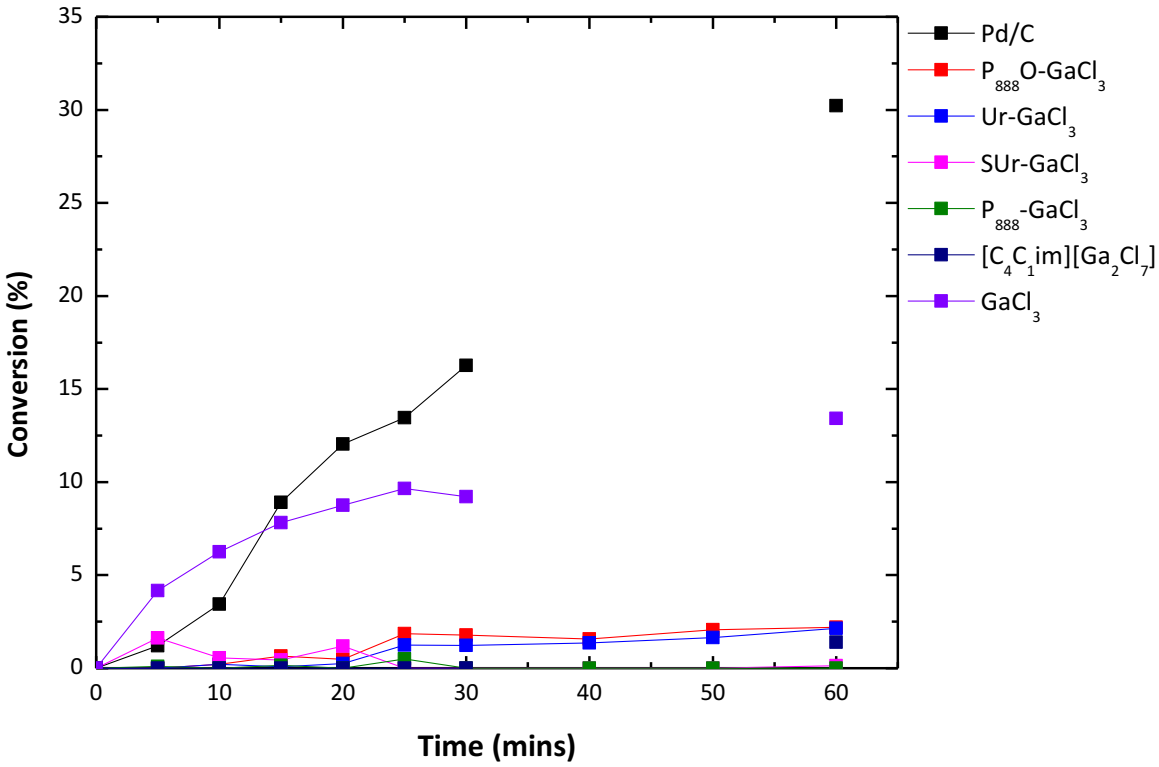

Figure 4.3-1: Conversion of toluene to methylcyclohexane *vs.* time with $GaCl_3$ co-catalysts. 60 °C, 15 bar H_2 24.962 mmol toluene, 100 ml cyclohexane, 4.267 mmol decalin, 1 mmol Pd, 0.65 mmol $GaCl_3$ eq.

To test whether this was LCCs-specific effect, or was this associated with gallium Lewis acid as such, the ionic liquid $[C_4C_1im][Ga_2Cl_7]$ and $GaCl_3$ powder were used as co-catalysts for hydrogenation with Pd/C . This ionic liquid was also found to decrease the reaction rate, giving a conversion of 1.39 % after 1 h. $GaCl_3$ powder promoted rapid conversion rate in the first ten minutes, but then decreased in performance, giving conversion of 13.42% after 1 h. In conclusion, Ga-based Lewis acids were deemed unsuitable for this process.

Table 4.3-1: Conversion of toluene to methylcyclohexane *vs.* time with $GaCl_3$ co-catalysts, 60 °C, 15 bar H_2 24.962 mmol toluene, 100 ml cyclohexane, 4.267 mmol decalin, 1 mmol Pd, 0.65 mmol $GaCl_3$ eq

Catalyst Supported	**Conversion after x minutes (%)**								
	5	10	15	20	25	30	40	50	60
None	1.20	3.44	8.90	12.04	13.46	16.27	-	-	30.23
$P_{888}O$-$GaCl_3$	0.00	0.21	0.65	0.48	1.85	1.78	1.57	2.06	2.20
Ur-$GaCl_3$	0.00	0.21	0.08	0.24	1.25	1.23	1.35	1.65	2.14
SUr-$GaCl_3$	1.63	0.56	0.44	1.18	0.00	0.00	0.00	0.00	0.13
P_{888}-$GaCl_3$	0.10	0.00	0.15	0.00	0.50	0.00	0.00	0.00	0.00
$[C_4C_1im][Ga_2Cl_7]$	0.00	0.00	0.00	0.00	0.00	0.00	-	-	1.39
$GaCl_3$	4.16	6.26	7.82	8.75	9.66	9.22	-	-	13.42

4.3.2 $AlCl_3$-LCC-SCILLs

A series of $AlCl_3$ based LCCs were supported on Pd/C. Because thiourea was suspected to degrade when used as a ligand under reducing conditions, SUr-$AlCl_3$ χ_{AlCl3} = 0.60 was not used.

In contrast to $GaCl_3$-LCCs, here the rate of conversion was noted to depend heavily upon the ligand used (Table 4.3-2, Figure 4.3-2).

When P_{888}-$AlCl_3$ χ_{AlCl3} = 0.60, was used the samples taken took on a yellow hue, which may be indicative of Pd or LCC leeching. The carbon support will be tested by inductively coupled plasma mass spectrometry (ICP-MS) to test this hypothesis. Conversion in this case was extremely low, 1.01 % after 1 h.

$P_{888}O$-$AlCl_3$ χ_{AlCl3} = 0.60 showed a *ca.* 6-fold improvement in conversion, up to 13.87 % after 1 h, over $P_{888}O$-$GaCl_3$ χ_{GaCl3} = 0.60, though was still well below the untreated Pd/C catalyst. Similarly DMA-$AlCl_3$ χ_{AlCl3} = 0.60 was superior to $GaCl_3$ based LCC coated catalysts, with 13.74 % conversion after 1 h, but still below the uncoated catalyst. AcA-$AlCl_3$ χ_{AlCl3} = 0.60 showed comparable conversion to the uncoated catalyst: 32.09% *vs*. 30.23% conversion after 1 h, respectively. Finally, conversion achieved with Ur-$AlCl_3$ χ_{AlCl3} = 0.60 was comparable to that obtained using $[C_4C_1im][Al_2Cl_7]$: 47.48% *vs*. 45.70% conversion after 1 h, respectively. Both results were a significant improvement over the uncoated catalyst.

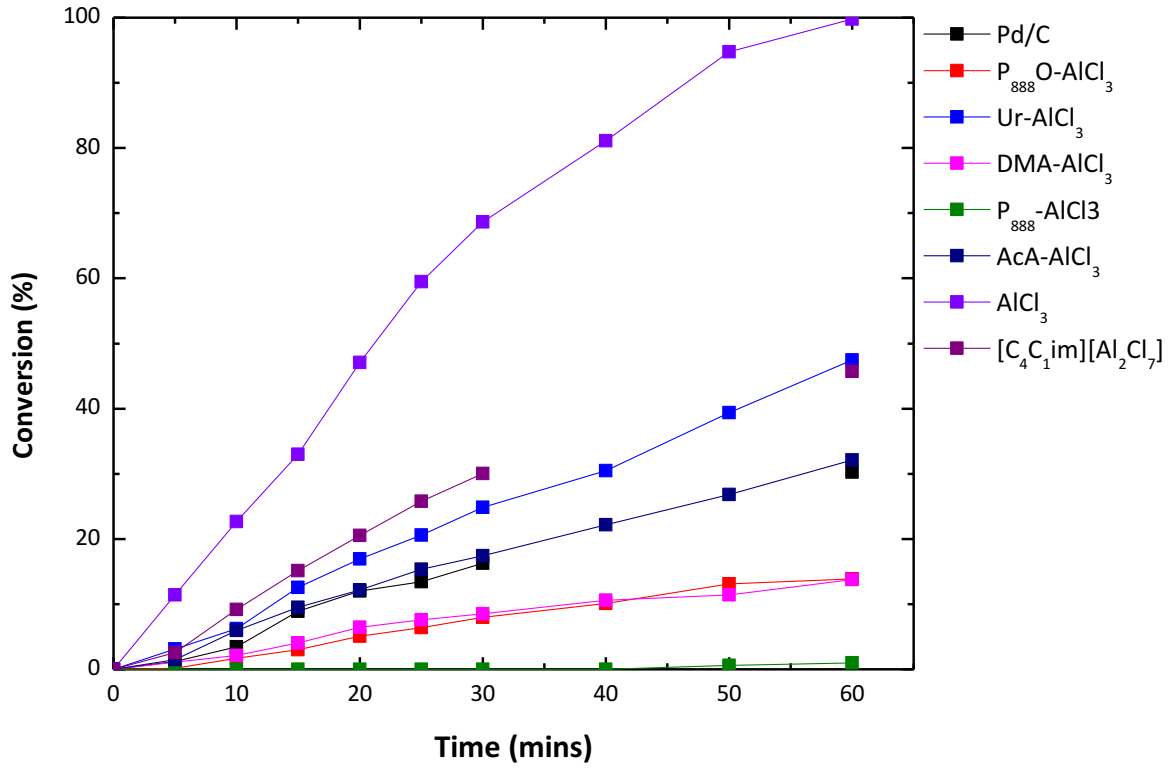

Figure 4.3-2: Conversion of toluene to methylcyclohexane *vs.* time with $AlCl_3$ catalysts. 60 °C, 15 bar H_2 24.962 mmol toluene, 100 ml cyclohexane, 4.267 mmol decalin, 1 mmol Pd, 0.65 mmol $AlCl_3$ eq

Table 4.3-2: Conversion of toluene to methylcyclohexane *vs.* time with $AlCl_3$ co-catalysts. 60 °C, 15 bar H_2 24.962 mmol toluene, 100 ml cyclohexane, 4.267 mmol decalin, 1 mmol Pd, 0.65 mmol $AlCl_3$ eq

Catalyst Supported	Conversion after x minutes (%)								
	5	10	15	20	25	30	40	50	60
None	1.20	3.44	8.90	12.04	13.46	16.27	-	-	30.23
$P_{888}O$-$AlCl_3$	0.14	1.69	3.01	5.06	6.39	8.00	10.13	13.12	13.87
Ur-$AlCl_3$	3.13	6.21	12.54	16.91	20.61	24.85	30.45	39.38	47.48
DMA-$AlCl_3$	1.10	2.12	4.06	6.43	7.58	8.54	10.60	11.44	13.74
P_{888}-$AlCl_3$	0.00	0.00	0.00	0.00	0.00	0.00	0.00	0.61	1.01
AcA-$AlCl_3$	1.50	5.96	9.53	12.18	15.33	17.44	22.19	26.84	32.09
$AlCl_3$	11.42	22.67	32.99	47.08	59.46	68.66	81.09	94.77	99.79
$[C_4C_1im][Al_2Cl_7]$	2.59	9.18	15.13	20.51	25.77	30.02	-	-	45.70

The reaction with Ur-$AlCl_3$ χ_{AlCl3} = 0.60 was repeated to ensure reproducibility of the results. Three runs were performed, which consistently gave greater conversion rate than that of the uncoated catalyst. Interestingly, the choice of solvent used to support the catalyst determined its effectiveness. When dichloromethane was used, a significant drop in activity was seen, which lowered the conversion after 1 h to below that of the untreated Pd/C (Figure 4.3-3, Table 4.3-3). This was observed for both LCCs and $[C_4C_1im][Al_2Cl_7]$, but as of now remains unexplained. In contrast, when cyclohexane was used to support the catalyst, the results were favourable as shown in Table 4.3-3.

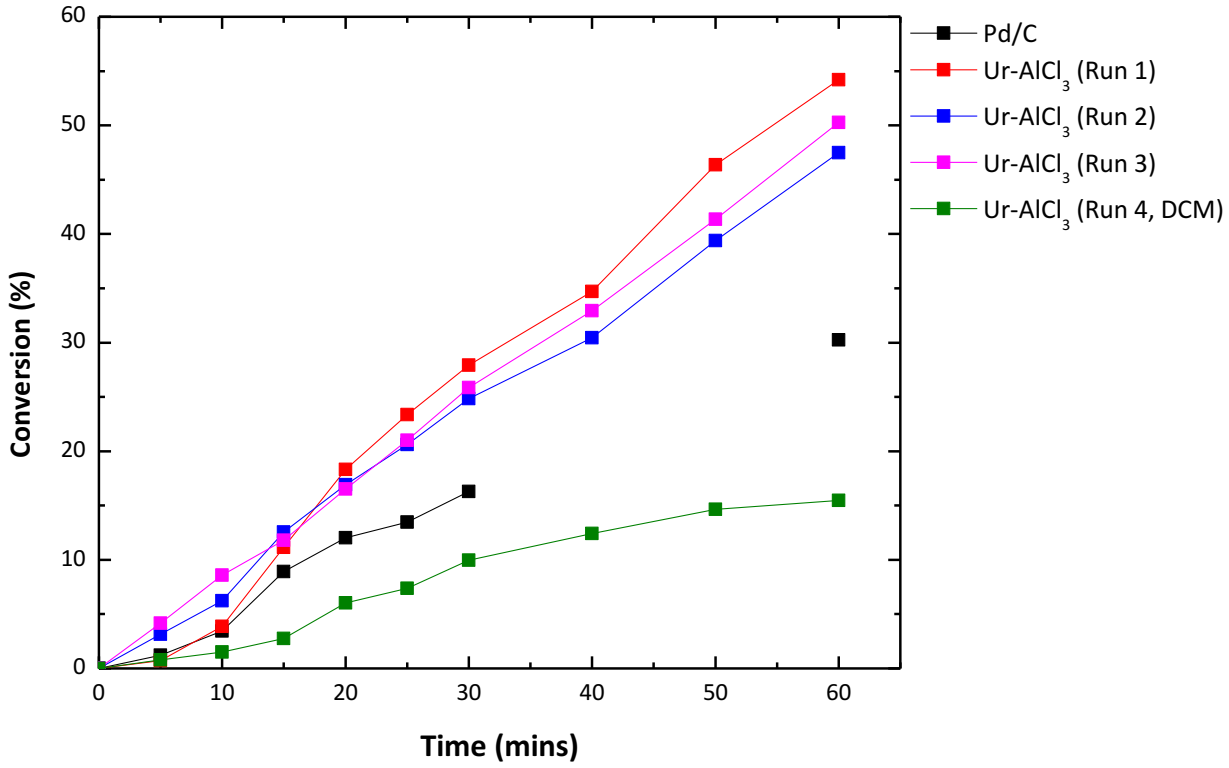

Figure 4.3-3: Conversion of toluene to methylcyclohexane *vs.* time with Ur-$AlCl_3$ χ_{AlCl3} = 0.60 co-catalyst. 60 °C, 15 bar H_2 24.962 mmol toluene, 100 ml cyclohexane, 4.267 mmol decalin, 1 mmol Pd, 0.65 mmol $AlCl_3$

Table 4.3-3: Conversion of toluene to methylcyclohexane *vs.* time with Ur-$AlCl_3$ χ_{AlCl3} = 0.60 co-catalyst. 60 °C, 15 bar H_2 24.962 mmol toluene, 100 ml cyclohexane, 4.267 mmol decalin, 1 mmol Pd, 0.65 mmol $AlCl_3$

Catalyst Supported (Run, Solvent)	Conversion after x minutes (%)								
	5	10	15	20	25	30	40	50	60
None	1.20	3.44	8.90	12.04	13.46	16.27	-	-	30.23
Ur-$AlCl_3$ (Run 1, CHex)	0.73	3.88	11.14	18.32	23.37	27.93	34.70	46.37	54.20
Ur-$AlCl_3$ (Run 2, CHex)	3.13	6.21	12.54	16.91	20.61	24.85	30.45	39.38	47.48
Ur-$AlCl_3$ (Run 3, CHex)	4.15	8.57	11.81	16.53	21.02	25.87	32.92	41.34	50.28
St Dev: Ur-$AlCl_3$	1.76	2.35	0.70	0.94	1.49	1.57	2.14	3.60	3.37
Ur-$AlCl_3$ (Run 4, DCM)	0.80	1.52	2.75	6.03	7.37	9.97	12.43	14.66	15.47

The catalyst was also tested for leeching. LCC-SCILL containing Ur-$AlCl_3$ χ_{AlCl3} = 0.60 was prepared and divided into two samples. The first sample was washed with cyclohexane and stored. The second sample was used in the reaction as per usual. At the end of the first cycle the reactor was drained and purged of H_2 using argon gas. The reactor was opened and a new charge of cyclohexane, toluene and decalin were added. The reactor was immediately sealed, heated, and the subsequent reaction started as soon as possible. This was repeated for 4 runs. The catalyst sample was submitted for ICP-MS analysis to determine if leeching of the LCC layer or the Pd metal has occurred, but the results are unknown at the time of submission of this work.

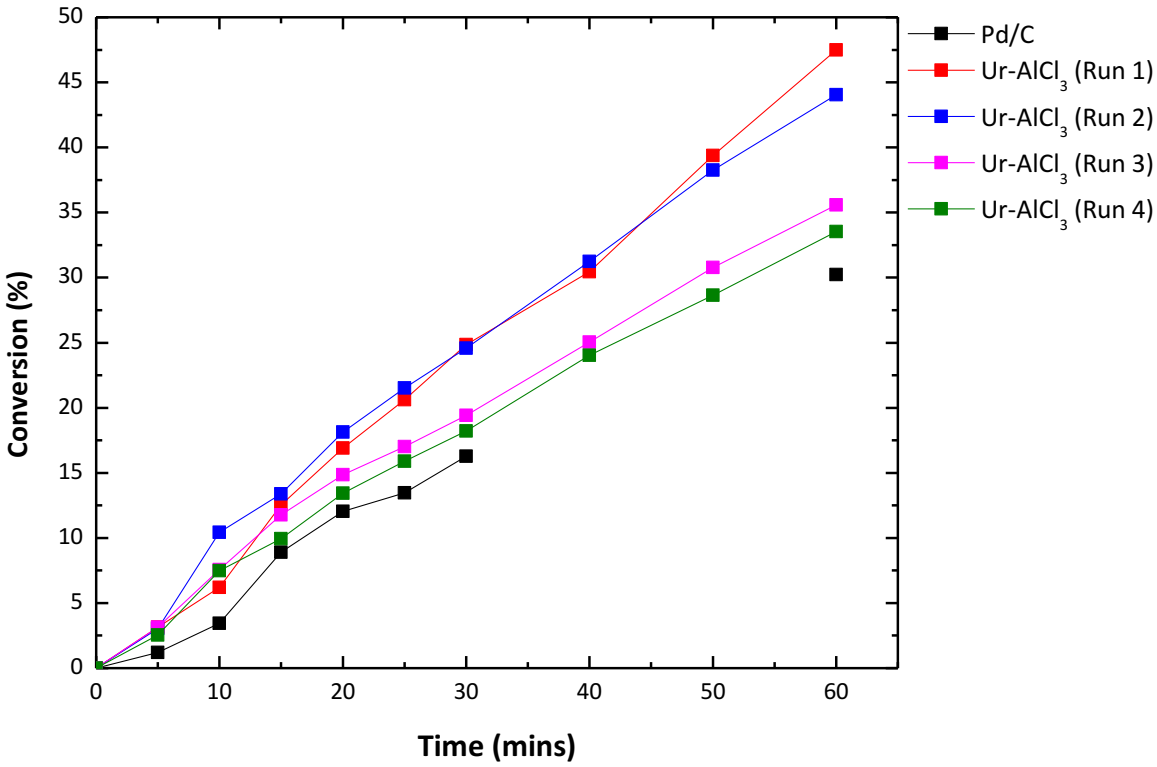

Figure 4.3-4: Conversion of toluene to methylcyclohexane *vs.* time with Ur-$AlCl_3$ χ_{AlCl3} = 0.60 co-catalyst used repeatedly. 60 °C, 15 bar H_2 24.962 mmol toluene, 100 ml cyclohexane, 4.267 mmol decalin, 1 mmol Pd, 0.65 mmol $AlCl_3$

A steady loss of activity was seen for each consecutive run, though the conversion was still slightly greater after the 4th run, when compared to the uncoated catalyst (Table 4.3-4). This loss of activity was expected, as with the reactor set-up it was impossible to exclude atmospheric moisture between catalytic runs. When ICP measurements are completed, it will be elucidated whether this loss of conversion is due to hydrolysis of the Lewis acid or due to leeching.

Table 4.3-4: Conversion of toluene to methylcyclohexane *vs.* time with Ur-$AlCl_3$ χ_{AlCl3} = 0.60 co-catalyst used repeatedly. 60 °C, 15 bar H_2 24.962 mmol toluene, 100 ml cyclohexane, 4.267 mmol decalin, 1 mmol Pd, 0.65 mmol $AlCl_3$

Catalyst Supported	Conversion after x minutes (%)								
	5	10	15	20	25	30	40	50	60
None	1.20	3.44	8.90	12.04	13.46	16.27	-	-	30.23
Ur-$AlCl_3$ (Run 1)	3.13	6.21	12.54	16.91	20.61	24.85	30.45	39.38	47.48
Ur-$AlCl_3$ (Run 2)	3.03	10.43	13.38	18.14	21.52	24.58	31.25	38.25	44.06
Ur-$AlCl_3$ (Run 3)	3.13	7.57	11.76	14.85	17.02	19.42	25.03	30.77	35.59
Ur-$AlCl_3$ (Run 4)	2.53	7.49	9.93	13.43	15.88	18.21	24.03	28.64	33.52

Finally, the catalyst was tested against variable temperature (Table 4.3-5, Figure 4.3-5) and H_2 pressure conditions (Table 4.3-8, Figure 4.3-7). Temperature was found to greatly affect the rate of hydrogenation, with full conversions achieved in 50 min at 80 °C. At the same temperature, for both $[C_4C_1im][Al_2Cl_7]$ and the uncoated catalyst, full conversion was not observed in 1 h. Conversely, the reaction rate was seen to decrease significantly as the temperature was decreased below 60 °C. Conversion at 1 h was 11.25 % at 40 °C for the LCC catalyst, compared to 13.81 % and 6.15 % for $[C_4C_1im][Al_2Cl_7]$ and Pd/C, respectively.

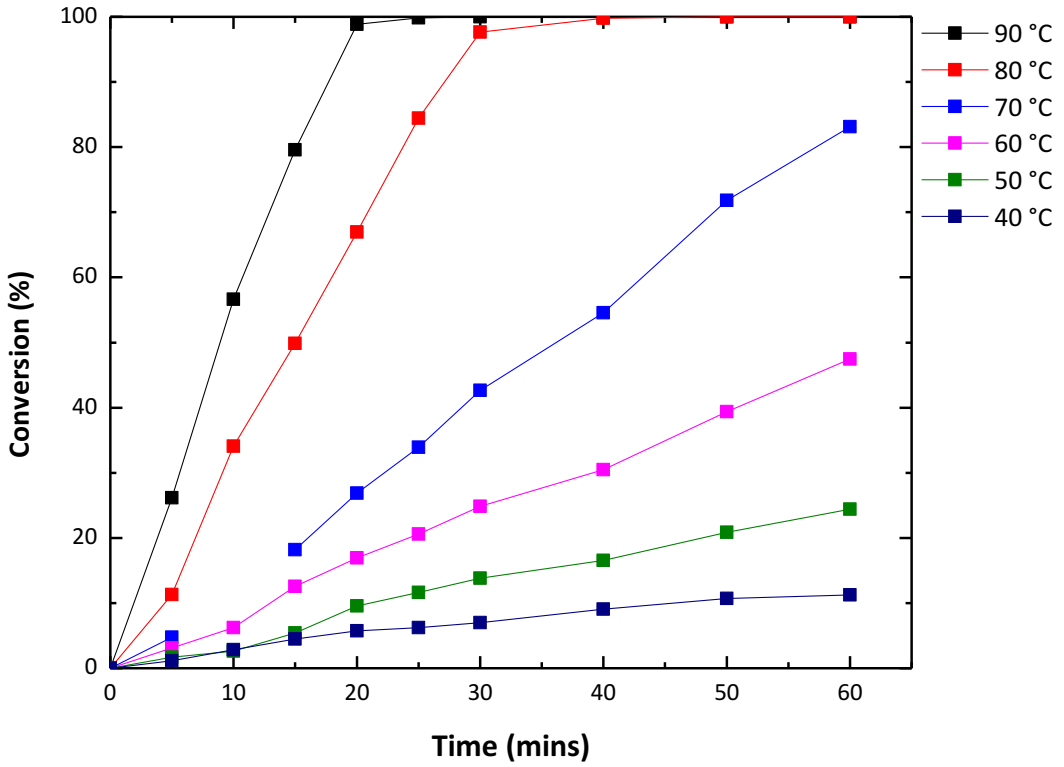

Figure 4.3-5: Conversion of toluene to methylcyclohexane *vs.* time with Ur-$AlCl_3$ χ_{AlCl3} = 0.60 co-catalyst at various temperatures. 15 bar H_2 24.962 mmol Toluene, 100 ml cyclohexane, 4.267 mmol decalin, 1 mmol Pd, 0.65 mmol $AlCl_3$

Table 4.3-5: Conversion of toluene to methylcyclohexane *vs.* time with Ur-$AlCl_3$ χ_{AlCl3} = 0.60 co-catalyst at various temperatures. 15 bar H_2 24.962 mmol Toluene, 100 ml cyclohexane, 4.267 mmol decalin, 1 mmol Pd, 0.65 mmol $AlCl_3$

Temperature	Conversion after x minutes (%)								
(°C)	5	10	15	20	25	30	40	50	60
90	26.16	56.64	79.56	98.88	99.86	100.00	100.00	100.00	100.00
80	11.32	34.09	49.89	66.94	84.43	97.66	99.79	100.00	100.00
70	4.75	-	18.18	26.88	33.89	42.65	54.57	71.84	83.12
60	3.13	6.21	12.54	16.91	20.61	24.85	30.45	39.38	47.48
50	1.68	2.62	5.40	9.55	11.65	13.84	16.54	20.88	24.41
40	1.16	2.82	4.47	5.75	6.23	6.99	9.04	10.69	11.25

Such a drastic change is could be due changes in LCC speciation with temperature.[135] It was shown that at higher temperatures the relative area of ^{27}Al NMR peaks changes. For DMA-$AlCl_3$ χ_{AlCl3} = 0.60 system, a shift is seen from upfield peaks to downfield peaks indicating an increase in charged species.

At all temperatures, the conversion appears to be linear (R^2 values for conversion *vs.* time are > 0.96) with time, as such it would appear that the reaction proceeds with a zero order dependency on the concentration of toluene. As such a plot of concentration *vs.* time should yield the effective rate of the reaction as its gradient (Figure 4.3-6, Table 4.3-6).

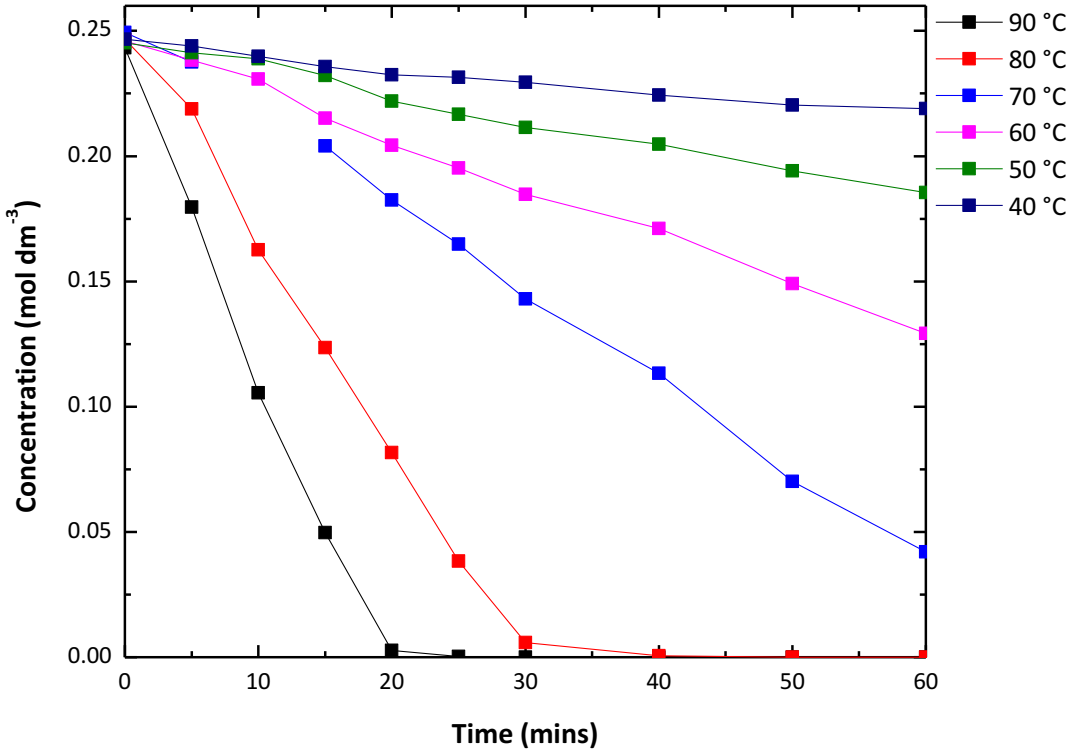

Figure 4.3-6: Toluene concentration *vs.* time with Ur-$AlCl_3$ χ_{AlCl3} = 0.60 co-catalyst at various temperatures. 15 bar H_2 24.962 mmol Toluene, 100 ml cyclohexane, 4.267 mmol decalin, 1 mmol Pd, 0.65 mmol $AlCl_3$

Table 4.3-6 Toluene concentration *vs.* time with Ur-$AlCl_3$ χ_{AlCl3} = 0.60 co-catalyst at various temperatures. 15 bar H_2 24.962 mmol Toluene, 100 ml cyclohexane, 4.267 mmol decalin, 1 mmol Pd, 0.65 mmol $AlCl_3$

Temp	Concentration of toluene after x minutes (mol dm^{-3})									
(°C)	0	5	10	15	20	25	30	40	50	60
90	0.2432	0.1796	0.1055	0.0497	0.0027	0.0003	0	0	0	0
80	0.2467	0.2188	0.1626	0.1236	0.0816	0.0384	0.0058	0.0005	0	0
70	0.2494	0.2376	-	0.2041	0.1824	0.1649	0.143	0.1133	0.0702	0.0421
60	0.246	0.2383	0.2307	0.2151	0.2044	0.1953	0.1848	0.1711	0.1491	0.1292
50	0.2453	0.2412	0.2389	0.2321	0.2219	0.2167	0.2114	0.2048	0.1941	0.1854
40	0.2467	0.2439	0.2398	0.2357	0.2325	0.2314	0.2295	0.2244	0.2204	0.219

The effective rate constant are summarised in Table 4.3-7 below. The reaction rate can be seen to vary from 8 x 10^{-6} mols dm^{-3} at 40 °C increasing by 2 orders of magnitude to 2 x 10^{-4} mol dm^{-3} at 90 °C. Plotting the natural logarithm of the rate against inverse temperature yields the activation energy of the reaction as 61.4 kJ mol^{-1}.

Table 4.3-7: Effective rate constant observed at varying temperature

Temperature (°C)	Rate Constant (mol dm^{-3} s^{-1})
40	0.9 x 10^{-5}
50	1.7 x 10^{-5}
60	3.3 x 10^{-5}
70	5.8 x 10^{-5}
80	1.4 x 10^{-4}
90	2.2 x 10^{-4}

The rate of reaction was also to found to depend upon the H_2 pressure. Here the behaviour of the LCC catalyst was similar to that $[C_4C_1im][Al_2Cl_7]$ (Figure 4.3-7). Though Ur-$AlCl_3$ χ_{AlCl3} = 0.60 consistently had a greater conversion than the untreated catalyst at the same pressures, it was also consistently below the chloroaluminate(III) ionic liquids.

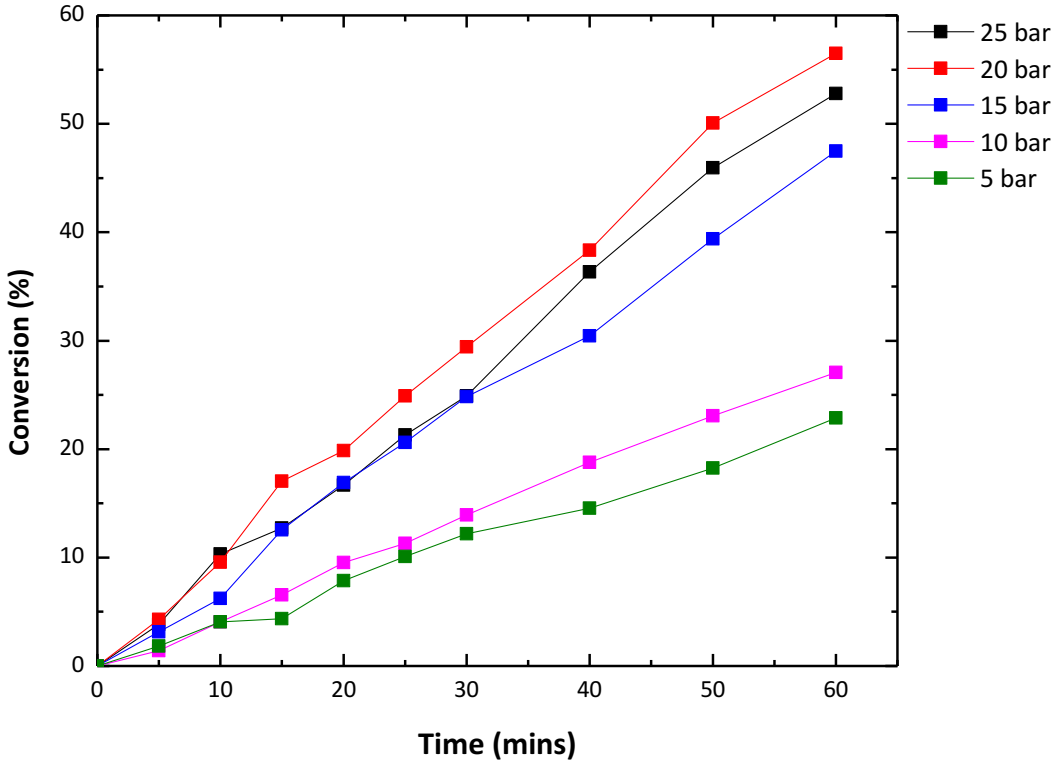

Figure 4.3-7: Conversion of toluene to methylcyclohexane *vs.* time with Ur-$AlCl_3$ χ_{AlCl3} = 0.60 co-catalyst at various pressures. 60 °C, 24.962 mmol Toluene, 100 ml cyclohexane, 4.267 mmol decalin, 1 mmol Pd, 0.65 mmol $AlCl_3$

Table 4.3-8: Conversion of toluene to methylcyclohexane *vs.* time with Ur-$AlCl_3$ χ_{AlCl3} = 0.60 co-catalyst at various pressures. 60 °C, 24.962 mmol Toluene, 100 ml cyclohexane, 4.267 mmol decalin, 1 mmol Pd, 0.65 mmol $AlCl_3$

Pressure Of Reaction	Conversion after x minutes (%)								
	5	10	15	20	25	30	40	50	60
25 bar	3.83	10.31	12.71	16.69	21.31	24.89	36.34	45.94	52.80
20 bar	4.29	9.56	17.03	19.85	24.92	29.44	38.35	50.07	56.49
15 bar	3.13	6.21	12.54	16.91	20.61	24.85	30.45	39.38	47.48
10 bar	1.42	4.06	6.56	9.54	11.30	13.94	18.78	23.06	27.06
5 bar	1.82	4.06	4.35	7.86	10.10	12.19	14.56	18.25	22.88

4.4 Conclusions

The use of LCCs as co-catalysts supported on Pd/C for the hydrogenation of toluene to methylcyclohexane was achieved with mixed success. LCCs of the formula L-$GaCl_3$ χ_{GaCl3} = 0.60 were found to completely stall the reaction as did the ionic liquid $[C_4C_1im][Ga_2Cl_7]$.

Furthermore addition of powdered $GaCl_3$ to the reaction mixture resulted in very low conversion.

When L-$AlCl_3$ χ_{AlCl3} = 0.60 was used the reaction was found to be highly ligand dependent. Of the catalysts tried AcA-$AlCl_3$ χ_{AlCl3} = 0.60 resulted in a minor conversion increase (1.86%) over the uncoated catalyst and Ur-$AlCl_3$ χ_{AlCl3} = 0.60 resulted in an appreciable conversion increase over the uncoated catalyst (17.25%). This increase was magnified with increasing temperature, with the Ur-$AlCl_3$ χ_{AlCl3} = 0.60 coated catalyst reaching full conversion by 30 and 50 min at 90 and 80 °C respectively. Higher pressures of H_2 also resulted increasing conversion. Compared to the ionic liquid $[C_4C_1im][Al_2Cl_7]$ coated catalyst, the Ur-$AlCl_3$ χ_{AlCl3} = 0.60 coated catalyst had lower conversions at lower temp but significantly higher conversions at higher temperatures. This rapid change in conversion with temperature may also indicate that other LCCs would be catalytically active at elevated temperatures.

Results from this chapter have been compiled with complementary work performed at FAU-Erlangan-Nuremberg, where $[C_4C_1im][Al_2Cl_7]$ was supported on Pd/C as the co-catalyst for toluene hydrogenation, and was published in *RSC Advances*.

5 Summary and conclusions

Liquid Lewis acids based on boron(III), Aluminium(III), Gallium(III), and antimony (III) chlorides were all synthesised and characterised, with those utilising B, Al and Ga being applied to the oligomerisation of 1-decene to produced PAO lubricants and Al and Ga Lewis acids being assessed as co-catalysts in aromatic hydrogenation. It has been seen repeatedly in this thesis, results from the catalytic applications often correlated and could be explained in terms of the speciation of the Lewis acids. If there is anything to take away from this thesis let it be that a good understanding of speciation, leads to a better understanding of chemistry. The speciation of LCCs was found to be dependent on the ligand, with harder donors promoting ionic products, and soft promoting molecular adducts.

The mixtures of C_7CN-$AlCl_3$ were, after spectroscopy study, found to be ionic liquids with a triply charged cation, rather than the LCCs they had been assumed to be when a liquid was seen upon mixing the two reagents. This potentially offers a way to synthesis chloroaluminate ionic liquids simply using simple organic donors. Further analysis of these systems under a wide compositional range is underway, with the aim of elucidating speciation and physio-chemical properties. It would be of interest to measure vapour pressure to see if this key property of ionic liquids is replicated in these new systems.

Borenium ionic liquids, and liquid coordination complexes both were shown to be highly acidic, and could potentially be utilised much like chloroaluminate ionic liquids, which have received much attention for their acidic catalytic abilities. Compared to chloroaluminate ionic liquids, they are quick and easy to synthesise due to the elimination of the lengthy alkylation step. However borenium ionic liquids suffer from a small degree of ligand exchange with the Lewis acidic anions, releasing BCl_3, which would limit catalyst life time. The use of non-coordinating, non-Lewis acidic anions could counteract these issues. Liquid coordination complexes have begun to be explored for electrochemical applications and Lewis acid catalysis. There is a third area that could be explored, inorganic synthesis, as their chlorometallate ionic liquid progenators have found widespread use in this area.

The strategy used to synthesise borenium ionic liquids was successfully applied to $SbCl_3$ as well. This represents a softer Lewis acid, which would be useful for catalysing different reactions, though the examples here have some drawbacks due to redox instability and/or high viscosity. Furthermore, spectroscopic studies of both liquid and solutions of $SbCl_3(P_{888}S)_n$

(n = 1, 2) showed that these can be complimentary to solid state characterisation, which is the mainstay of main group chemistry.

The successful synthesis of commercial quality lubricants by 1-decene oligomerisation was achieved using both Ur-$AlCl_3$ χ_{AlCl3} = 0.60 and $[BCl_2(L)][Al_2Cl_7]$ (where L = 2pic or 4pic). These catalysts represent safer, "greener" alternatives to the currently used BF_3 catalyst. They also represent cheaper alternatives to imidazolium cation based chloroaluminate ionic liquids, which have been widely patented for use as oligomerisation catalysts. Furthermore as they are not corrosive gases, they would result in a reduced CAPEX when building a new plant, compared to the BF_3 process. As they are synthesised from relatively cheap, readily available bulk chemicals they could be economically viable for a number of acid catalysed processes.

Work with LCCs supported on Pd/C showed that they could not always be simply interchangeable with chloroaluminate ionic liquids. Only the Ur-$AlCl_3$ χ_{AlCl3} = 0.60 showed comparable activity to $[C_4C_1im][Al_2Cl_7]$ as a co-catalyst in the Pd/C catalysed hydrogenation of toluene at low temperatures. Though at higher temperatures Ur-$AlCl_3$ χ_{AlCl3} = 0.60 proved to be a much more effective co catalyst than $[C_4C_1im][Al_2Cl_7]$.

6 References

1 C. Laurence and J.-F. Gal, *Lewis Basicity and Affinity Scales*, John Wiley & Sons, Ltd, Chichester, UK, 2009.

2 H. L. Finston and A. C. Rychtman, *A New View of Current Acid-Base-Theories*, John Wiley & Sons Inc, New York, 1982.

3 W. B. Jensen, *The Lewis Acid-Base Concepts: An Overview*, John Wiley & Sons Inc, New York, 1980.

4 A. L. Lavoisier, *Elements of chemistry, in a new systematic order containing all the modern discoveries.*, Dover Publications, 1965.

5 E. C. Franklin, *J. Am. Chem. Soc.*, 1905, **27**, 820–851.

6 E. C. Franklin, *J. Am. Chem. Soc.*, 1924, **46**, 2137–2151.

7 A. F. O. Germann, *J. Am. Chem. Soc.*, 1925, **47**, 2461–2468.

8 J. N. Bronsted, *J. Phys. Chem.*, 1925, **30**, 777–790.

9 G. N. Lewis, *Chem. Cat. Co.*, 1923.

10 G. N. Lewis, *J. Franklin Inst.*, 1938, **226**, 293–313.

11 M. Nič, J. Jirát, B. Košata, A. Jenkins and A. McNaught, Eds., *IUPAC Compendium of Chemical Terminology*, IUPAC, Research Triagle Park, NC, 2009.

12 R. G. Pearson, *J. Am. Chem. Soc.*, 1963, **85**, 3533–3539.

13 G. Klopman, *J. Am. Chem. Soc.*, 1968, **90**, 223–234.

14 R. G. Parr and R. G. Pearson, *J. Am. Chem. Soc.*, 1983, **105**, 7512–7516.

15 P. Geerlings, F. De Proft and W. Langenaeker, *Chem. Rev.*, 2003, **103**, 1793–1874.

16 E. Fernández and A. Whiting, *Synthesis and Application of Organoboron Compounds*, Springer International Publishing, Cham, 2015, vol. 49.

17 E. R. Clark, A. Del Grosso and M. J. Ingleson, *Chemistry*, 2013, **19**, 2462–6.

18 V. Gutmann, *Electrochim. Acta*, 1976, **21**, 661–670.

19 C. Reichardt, *Solvents and solvent effects in organic chemistry*, Wiley-VCH Verlag GmbH & Co. KGaA, Weinheim, Germany, 3rd Editio., 2003.

20 U. Mayer, V. Gutmann and W. Gerger, *Monatshefte fur Chemie*, 1975, **106**, 1235–

1257.

21 J. A. McCune, P. He, M. Petkovic, F. Coleman, J. Estager, J. D. Holbrey, K. R. Seddon and M. Swadźba-Kwaśny, *Phys. Chem. Chem. Phys.*, 2014, **16**, 23233–23243.

22 I. B. Sivaev and V. I. Bregadze, *Coord. Chem. Rev.*, 2014, **270**–**271**, 75–88.

23 R. A. Mantz, P. C. Trulove, R. T. Carlin, T. L. Theim and R. A. Osteryoung, *Inorg. Chem.*, 1997, **36**, 1227–1232.

24 T. A. Zawodzinski Jr. and R. A. Osteryoung, *Inorg. Chem.*, 1989, **28**, 1710–1715.

25 J. Estager, A. A. Oliferenko, K. R. Seddon and M. Swadźba-Kwaśny, *Dalt. Trans.*, 2010, **39**, 11375–82.

26 J. Estager, P. Nockemann, K. R. Seddon, M. Swadźba-Kwaśny and S. Tyrrell, *Inorg. Chem.*, 2011, **50**, 5258–5271.

27 M. Holthausen, M. Mehta and D. Stephan, *Angew. Chemie*, 2014, **53**, 6538–6541.

28 M. A. Beckett, G. C. Strickland, J. R. Holland and K. S. Varma, *Polymer* , 1996, **37**, 4629–4631.

29 R. F. Childs, D. L. Mulholland and A. Nixon, *Can. J. Chem.*, 1982, **60**, 801–808.

30 G. Hilt and A. Nödling, *European J. Org. Chem.*, 2011, **2011**, 7071–7075.

31 G. Hilt, F. Pünner, J. Möbus, V. Naseri and M. A. Bohn, *European J. Org. Chem.*, 2011, **2011**, 5962–5966.

32 C. S. Branch, S. G. Bott and A. R. Barron, *J. Organomet. Chem.*, 2003, **666**, 23–34.

33 L. O. Müller, D. Himmel, J. Stauffer, G. Steinfeld, J. Slattery, G. Santiso-Quiñones, V. Brecht and I. Krossing, *Angew. Chemie - Int. Ed.*, 2008, **47**, 7659–7663.

34 H. Böhrer, N. Trapp, D. Himmel, M. Schleep and I. Krossing, *Dalton Trans.*, 2015, **44**, 7489–7499.

35 E. R. Clark and M. J. Ingleson, *Organometallics*, 2013, **32**, 6712–6717.

36 C. Morterra, G. Cerrato, V. Bolis, S. Di Ciero and M. Signoretto, *J. Chem. Soc. Faraday Trans.*, 1997, **93**, 1179–1184.

37 Y.-L. Yang and Y. Kou, *Chem. Commun.*, 2004, 226–227.

38 T. M. Lowry, *J. Soc. Chem. Ind.*, 1923, **42**, 43–47.

39 G. A. Olah, G. K. S. Prakash and J. Sommer, *Science* , 1979, **206**, 13–20.

40 C. H. Rochester, *Acidity Functions*, Academic Press, New York, London, 1970.

41 L. P. Hammett and A. J. Deyrup, *J. Am. Chem. Soc.*, 1932, **54**, 2721–2739.

42 F. A. Long and M. A. Paul, *Chem. Rev.*, 1957, **57**, 935–1010.

43 M. J. Jorgenson and D. R. Hartter, *J. Am. Chem. Soc.*, 1963, **85**, 878–883.

44 M. A. Paul and F. A. Long, *Chem. Rev.*, 1957, **57**, 1–45.

45 J. L. E. Campbell and K. E. Johnson, *J. Am. Chem. Soc.*, 1995, **117**, 7791–7800.

46 R. D. Howells and J. D. Mc Cown, *Chem. Rev.*, 1977, **77**, 69–92.

47 D. Himmel, S. K. Goll, I. Leito and I. Krossing, *Angew. Chem. Int. Ed.*, 2010, **49**, 6885–6888.

48 G. A. Olah, *J. Org. Chem.*, 2005, **70**, 2413–2429.

49 G. Olah and R. Schlosberg, *J. Am. Chem. Soc.*, 1968, **90**, 2726–2727.

50 G. Olah, *J Am Chem Soc*, 1972, **94**, 808–820.

51 F. Scholz, D. Himmel, L. Eisele, W. Unkrig and I. Krossing, *Angew. Chem. Int. Ed.* , 2014, **53**, 1689–92.

52 S. Coffie, J. M. Hogg, L. Cailler, A. Ferrer-Ugalde, R. W. Murphy, J. D. Holbrey, F. Coleman and M. Swadźba-Kwaśny, *Angew. Chem. Int. Ed.* , 2015, **54**, 14970–14973.

53 J.-F. Gal, C. Iacobucci, I. Monfardini, L. Massi, E. Duñach and S. Olivero, *J. Phys. Org. Chem.*, 2013, **26**, 87–97.

54 J. Kennedy and E. Maréchal, *Carbocationic polymerization*, John Wiley & Sons Inc, New York, 1982.

55 John Wiley & Sons Inc, Ed., *Kirk-Othmer Encyclopedia of Chemical Technology*, John Wiley & Sons, Inc., Hoboken, NJ, USA, 2000.

56 *Ullmann's Encyclopedia of Industrial Chemistry*, Wiley-VCH Verlag GmbH & Co. KGaA, Weinheim, Germany, 2000.

57 N. G. Connelly and W. E. Geiger, *Chem. Rev.*, 1996, **96**, 877–910.

58 H. Yamamoto, *Lewis Acids in Organic Synthesis*, Wiley-VCH Verlag GmbH, Weinheim, Germany, 2000.

59 P. Espinet and A. M. Echavarren, *Angew. Chem. Int. Ed.*, 2004, **43**, 4704–4734.

60 T. Mukaiyama, K. Narasaka and K. Banno, *Chem. Lett.*, 1973, **2**, 1011–1014.

61 G. Coates, *Chem. Rev.*, 2000, **100**, 1223.

62 W. Kaminsky, *Macromolecules*, 2012, **45**, 3289–3297.

63 S. S. Chitnis, N. Burford, R. McDonald and M. J. Ferguson, *Inorg. Chem.*, 2014, **53**, 5359–5372.

64 T. Welton, *Chem. Rev.*, 1999, **99**, 2071–2083.

65 J. Estager, J. D. Holbrey and M. Swadźba-Kwaśny, *Chem. Soc. Rev.*, 2014, **43**, 847–86.

66 H.-P. Steinrück and P. Wasserscheid, *Catal. Letters*, 2015, **145**, 380–397.

67 J. S. Wilkes, *Green Chem.*, 2002, **4**, 73–80.

68 US Patent Office, 19111222, 1933.

69 US Patent Office, 2446331, 1948.

70 J. S. Wilkes, J. A. Levisky, R. A. Wilson and C. L. Hussey, *Inorg. Chem.*, 1982, **21**, 1263–1264.

71 N. V Plechkova and K. R. Seddon, *Chem. Soc. Rev.*, 2008, **37**, 123–50.

72 Z. Liu, R. Zhang, C. Xu and R. Xia, *Oil gas J.*, 2006, **104**, 52.

73 http://www.ogj.com/articles/2016/10/chevron-s-salt-lake-city-refinery-plans-alkylation-unit-revamp.html - Accessed 28/11/16

74 F. H. Hurley and T. P. Wier, *J. Electrochem. Soc.*, 1951, **98**, 203.

75 R. J. Gale and R. A. Osteryoung, *Inorg. Chem.*, 1979, **18**, 1603–1605.

76 R. Gale, B. Gilbert and R. Osteryoung, *Inorg. Chem.*, 1978, **17**, 2728–2729.

77 H. L. Chum, V. R. Koch, L. L. Miller and R. A. Osteryoung, *J. Am. Chem. Soc.*, 1975, **97**, 3264–3265.

78 V. R. Koch, L. L. Miller and R. A. Osteryoung, *J. Am. Chem. Soc.*, 1976, **98**, 5277–5284.

79 J. S. Wilkes, J. A. Levisky, J. L. Pflug, C. L. Hussey and T. B. Scheffler, *Anal. Chem.*, 1982, **54**, 2378–2379.

80 J. S. Wilkes, J. S. Frye and G. Fredric Reynolds, *Inorg. Chem.*, 1983, **22**, 3870–3872.

81 A. A. Fannin, L. a. King, J. a. Levisky and J. S. Wilkes, *J. Phys. Chem.*, 1984, **88**, 2609–2614.

82 A. a. Fannin, D. a. Floreani, L. A. King, J. S. Landers, B. J. Piersma, D. J. Stech, R. L. Vaughn, J. S. Wilkes and J. L. Williams, *J. Phys. Chem.*, 1984, **88**, 2614–2621.

83 S. Takahashi, M. Saboungi, R. Kilnger, J. Rathke and M. Chen, *J. Chem. Soc. Faraday*

Trans., 1993, **89**, 3591–3595.

84 C. J. Dymek, J. S. Wilkes, M.-A. Einarsrud and H. A. Øye, *Polyhedron*, 1988, **7**, 1139–1145.

85 H. Oye, M. Jagtoyen, T. Oksefjell and J. S. Wilkes, *Mater. Sci. Forum*, 1991, **73**, 183–189.

86 S. P. Wicelinski, R. J. Gale, S. D. Williams and G. Mamantov, *Spectrochim. Acta Part A Mol. Spectrosc.*, 1989, **45**, 759–762.

87 C. Hardacre, R. W. Murphy, K. R. Seddon, G. Srinivasan and M. Swadźba-Kwa(ś)ny, *Aust. J. Chem.*, 2010, **63**, 845.

88 D. C. Apperley, C. Hardacre, P. Licence, R. W. Murphy, N. V Plechkova, K. R. Seddon, G. Srinivasan, M. Swadźba-Kwaśny and I. J. Villar-Garcia, *Dalt. Trans.*, 2010, **39**, 8679–8687.

89 S. Tait and R. A. Osteryoung, *Inorg. Chem.*, 1984, **23**, 4352–4360.

90 T. A. Zawodzinski and R. A. Osteryoung, *Inorg. Chem.*, 1987, **26**, 2920–2922.

91 M. A. M. Noel, P. C. Trulove and R. A. Osteryoung, *Anal. Chem.*, 1991, **63**, 2892–2896.

92 T. A. Zawodzinski and R. A. Osteryoung, *Inorg. Chem.*, 1990, **29**, 2842–2847.

93 T. A. Zawodzinski and R. A. Osteryoung, *Inorg. Chem.*, 1988, **27**, 4383–4384.

94 C. Sikorska, S. Freza and P. Skurski, *J. Phys. Chem. A*, 2010, **114**, 2235–2239.

95 M. A. M. Noel, P. C. Truelove and R. A. Osteryoung, *Anal. Chem.*, 1987, **63**, 2892.

96 P. C. Trulove and R. A. Osteryoung, *Inorg. Chem.*, 1992, **31**, 3980–3985.

97 L. F. Albright and K. W. Li, *Ind. Eng. Chem. Process Des. Dev.*, 1970, **9**, 447–454.

98 Y. Chauvin, A. Hirschauer and H. Olivier, *J. Mol. Catal.*, 1994, **92**, 155–165.

99 T. L. T. Bui, W. Korth, S. Aschauer and A. Jess, *Green Chem.*, 2009, **11**, 1961.

100 S. Aschauer, L. Schilder, W. Korth, S. Fritschi and A. Jess, *Catal. Letters*, 2011, **141**, 1405–1419.

101 T. L. T. Bui, W. Korth and A. Jess, *Catal. Commun.*, 2012, **25**, 118–124.

102 S. J. Aschauer and A. Jess, *Ind. Eng. Chem. Res.*, 2012, **51**, 16288–16298.

103 F. Pöhlmann, L. Schilder, W. Korth and A. Jess, *Chempluschem*, 2013, **78**, 570–577.

104 L. Schilder, S. Maaß and A. Jess, *Ind. Eng. Chem. Res.*, 2013, **52**, 1877–1885.

105 K. Yoo, V. V. Namboodiri, R. S. Varma and P. G. Smirniotis, *J. Catal.*, 2004, **222**, 511–519.

106 J. Zhang, C. Huang, B. Chen, P. Ren and M. Pu, *J. Catal.*, 2007, **249**, 261–268.

107 C.-P. Huang, Z.-C. Liu, C.-M. Xu, B.-H. Chen and Y.-F. Liu, *Appl. Catal. A Gen.*, 2004, **277**, 41–43.

108 Y. Liu, R. Hu, C. Xu and H. Su, *Appl. Catal. A Gen.*, 2008, **346**, 189–193.

109 L. F. Albright, M. a. Spalding, C. G. Kopser and R. E. Eckert, *Ind. Eng. Chem. Res.*, 1988, **27**, 386–391.

110 H. Ma, R. Zhang, X. Meng, Z. Liu, H. Liu, C. Xu, R. Chen, P. A. A. Klusener and J. De With, *Energy and Fuels*, 2014, **28**, 5389–5395.

111 J. Cui, J. de With, P. a. a. Klusener, X. Su, X. Meng, R. Zhang, Z. Liu, C. Xu and H. Liu, *J. Catal.*, 2014, **320**, 26–32.

112 https://www.uop.com/?press_release=honeywell-uop-introduces-ionic-liquids Accessed 24/10/16

113 L. F. Albright, *Oil Gas J.*, 1990, **88**, 70.

114 https://www.uop.com/processing-solutions/refining/gasoline/#alkylation Accessed 24/10/16

115 T. M. Jyothi, M. L. Kaliya and M. V. Landau, *Angew. Chem. Int. Ed.*, 2001, **40**, 2881–2884.

116 J. Joni, M. Haumann and P. Wasserscheid, *Adv. Synth. Catal.*, 2009, **351**, 423.

117 J. Joni, M. Haumann and P. Wasserscheid, *Appl. Catal. A Gen.*, 2010, **372**, 8–15.

118 J. Joni, D. Schmitt, P. S. Schulz, T. J. Lotz and P. Wasserscheid, *J. Catal.*, 2008, **258**, 401–409.

119 G. W. Parshall, *J. Am. Chem. Soc.*, 1972, **94**, 8716–8719.

120 P. Wasserscheid and H. Waffenschmidt, *J. Mol. Catal. A Chem.*, 2000, **164**, 61–67.

121 J. D. Holbrey and K. R. Seddon, *Clean Prod. Process.*, 1999, 223–236.

122 P. T. Anastas, Ed., *Green Catalysis Vol 1: Homogeneous Catalysis*, Wiley-VCH Verlag GmbH, Weinheim, Germany, 2009.

123 Y. Chauvin, B. Gilbert and I. Guibard, *J. Chem. Soc. Chem. Commun.*, 1990, 1715.

124 B. Gilbert, H. Olivier-Bourbigou and F. Favre, *Oil Gas Sci. Technol. - Rev. l'IFP*, 2007, **62**, 745–759.

125 R. T. Carlin and J. S. Wilkes, *J. Mol. Catal.*, 1990, **63**, 125–129.

126 J. J. Eisch, A. M. Piotrowski, S. K. Brownstein, E. J. Gabe and F. L. Lee, *J. Am. Chem. Soc.*, 1985, **107**, 7219.

127 O. Stenzel, R. Brüll, U. M. Wahner, R. D. Sanderson and H. G. Raubenheimer, *J. Mol. Catal. A Chem.*, 2003, **192**, 217–222.

128 R. R. Deshmukh, J. W. Lee, U. S. Shin, J. Y. Lee and C. E. Song, *Angew. Chemie - Int. Ed.*, 2008, **47**, 8615–8617.

129 C. W. Lee, *Tetrahedron Lett.*, 1999, **40**, 2461–2464.

130 K. Matuszek, A. Chrobok, P. Latos, M. Markiton, K. Szymańska, A. Jarzębski and M. Swadźba-Kwaśny, *Catal. Sci. Technol.*, 2016, **6**, 8129–8137.

131 A. P. Abbott, G. Capper, D. L. Davies, R. K. Rasheed and V. Tambyrajah, *Green Chem.*, 2002, **4**, 24–26.

132 D. Yin, C. Li, B. Li, L. Tao and D. Yin, *Adv. Synth. Catal.*, 2005, **347**, 137–142.

133 M. . Valkenberg, C. DeCastro and W. . Hölderich, *Appl. Catal. A Gen.*, 2001, **215**, 185–190.

134 P. Wasserscheid and T. Welton, *Ionic liquids in Synthesis*, Wiley-VCH Verlag GmbH & Co. KGaA, Weinheim, Germany, 2002, vol. 7.

135 F. Coleman, G. Srinivasan and M. Swadźba-Kwaśny, *Angew. Chem. Int. Ed.* , 2013, **52**, 12582–6.

136 A. G. Suárez, *Tetrahedron Lett.*, 1999, **40**, 3523–3526.

137 E. G. Mata and A. G. Suárez, *Synth. Commun.*, 1997, **27**, 1291–1300.

138 J. Derouault and M. T. Forel, *Inorg. Chem.*, 1977, **16**, 3207–3213.

139 J. Derouault, P. Granger and M. T. Forel, *Inorg. Chem.*, 1977, **16**, 3214–3218.

140 A. H. Cowley, M. C. Cushner, R. E. Davis and P. E. Riley, *Inorg. Chem.*, 1981, **20**, 1179–1181.

141 M. Dalibart, J. Derouault and P. Granger, *Inorg. Chem.*, 1981, **20**, 3975–3978.

142 M. Dalibart, J. Derouault and P. Granger, *Inorg. Chem.*, 1982, **21**, 2241–2246.

143 M. Dalibart, J. Derouault, P. Granger and S. Chapelle, *Inorg. Chem.*, 1982, **21**, 1040–

1046.

144 N. C. Means, C. M. Means, S. G. Bott and J. L. Atwood, *Inorg. Chem.*, 1987, **26**, 1466–1468.

145 J. Mason, Ed., *Multinuclear NMR*, Plenum Press, New York, 1987.

146 O. H. Han and E. Oldfield, *Inorg. Chem.*, 1990, **29**, 3666–3669.

147 M. Dalibart, M. Fouassier and M. T. Forel, *J. Mol. Struct.*, 1977, **36**, 7–23.

148 D. A. Atwood, *Coord. Chem. Rev.*, 1998, **176**, 407–430.

149 A. P. Abbott, J. C. Barron, K. S. Ryder and D. Wilson, *Chem. - A Eur. J.*, 2007, **13**, 6495–6501.

150 H. M. a Abood, A. P. Abbott, A. D. Ballantyne and K. S. Ryder, *Chem. Commun.*, 2011, **47**, 3523–5.

151 R. Harris and B. Mann, *NMR and the Periodic Table*, Academic Press Inc, New York, 1978.

152 T. A. Engesser, M. R. Lichtenthaler, M. Schleep and I. Krossing, *Chem. Soc. Rev.*, 2016, **45**, 789–899.

153 H. Lian, S. Hong, A. Carranza, J. D. Mota-Morales and J. A. Pojman, *RSC Adv.*, 2015, **5**, 28778–28785.

154 P. Hu, R. Zhang, X. Meng, H. Liu, C. Xu and Z. Liu, *Inorg. Chem.*, 2016, **55**, 2374–2380.

155 Y. Fang, K. Yoshii, X. Jiang, X. G. Sun, T. Tsuda, N. Mehio and S. Dai, *Electrochim. Acta*, 2015, **160**, 82–88.

156 Y. Fang, X. Jiang, X.-G. Sun and S. Dai, *Chem. Commun.*, 2015, **51**, 13286–13289.

157 P. Hu, Y. Wang, X. Meng, R. Zhang, H. Liu, C. Xu and Z. Liu, *Fuel*, 2017, **189**, 203–209.

158 K. Matuszek, A. Chrobok, J. Hogg, F. Coleman and M. Swadźba-Kwaśny, *Green Chem.*, 2015, **17**, 4255–4262.

159 G. Pulletikurthi, B. Bödecker, A. Borodin, B. Weidenfeller and F. Endres, *Prog. Nat. Sci. Mater. Int.*, 2015, **25**, 603–611.

160 R. a Sheldon, *Chem. Commun.*, 2008, 3352–3365.

161 A. Taguchi and F. Schüth, *Microporous Mesoporous Mater.*, 2005, **77**, 1–45.

162 K. Tanabe and W. F. Hölderich, *Appl. Catal. A Gen.*, 1999, **181**, 399–434.

163 M. Li, B. Gao, C. Liu, W. Chen, Z. Shi, X. Hu and Z. Wang, *Electrochim. Acta*, 2015,

180, 811–814.

164 K. George, M. Jura, W. Levason, M. E. Light and G. Reid, *Dalton Trans.*, 2014, **43**, 3637–48.

165 F. Coleman, *Angew. Chem. Int. Ed.* , 2013, **52**, 12582.

166 N. Burford, B. W. Royan, R. E. v. H. Spence and R. D. Rogers, *J. Chem. Soc., Dalt. Trans.*, 1990, 2111–2117.

167 X. Chen, X. Bao, J.-C. Zhao and S. G. Shore, *J. Am. Chem. Soc.*, 2011, **133**, 14172–14175.

168 A. El-Hellani, J. Monot, R. Guillot, C. Bour and V. Gandon, *Inorg. Chem.*, 2013, **52**, 506–514.

169 D. G. Gusev, *Organometallics*, 2009, **28**, 6458–6461.

170 A. Fürstner, M. Alcarazo, R. Goddard and C. W. Lehmann, *Angew. Chem. Int. Ed.*, 2008, **47**, 3210–3214.

171 C. D. Tables, .

172 D. R. MacFarlane, M. Forsyth, E. I. Izgorodina, A. P. Abbott, G. Annat and K. Fraser, *Phys. Chem. Chem. Phys.*, 2009, **11**, 4962.

173 O. Fandiño, A. S. Pensado, L. Lugo, M. J. P. Comuñas and J. Fernández, *J. Chem. Eng. Data*, 2005, **50**, 939–946.

174 Y. A. Sanmamed, D. González-Salgado, J. Troncoso, C. A. Cerdeiriña and L. Romaní, *Fluid Phase Equilib.*, 2007, **252**, 96–102.

175 O. Fandiño, A. S. Pensado, L. Lugo, M. J. P. Comuñas and J. Fernández, *J. Chem. Eng. Data*, 2006, **51**, 2274–2274.

176 B. Kirchner, Ed., *Ionic Liquids*, Springer Berlin Heidelberg, Berlin, Heidelberg, 2010.

177 A. A. Fannin, D. A. Floreani, L. A. King, J. S. Landers, B. J. Piersma, D. J. Stech, R. L. Vaughn and J. S. Wilkes, *J. Phys. Chem.*, 1984, **88**, 2614–2621.

178 M. Blesic, M. Swadźba-Kwaśny, T. Belhocine, H. Q. N. Gunaratne, J. N. C. Lopes, M. F. C. Gomes, A. A. H. Pádua, K. R. Seddon and L. P. N. Rebelo, *Phys. Chem. Chem. Phys.*, 2009, **11**, 8939.

179 J. Jacquemin, P. Husson, A. A. H. Padua and V. Majer, *Green Chem.*, 2006, **8**, 172–180.

180 C. A. Angell, *Science*, 1995, **267**, 1924–1935.

181 J. Robinson and R. a Osteryoung, *J. Am. Chem. Soc.*, 1979, **101**, 323–327.

182 C. Maton, N. De Vos and C. V Stevens, *Chem. Soc. Rev.*, 2013, **42**, 5963.

183 P. P. Power, *Nature*, 2010, **463**, 171–177.

184 W. E. Piers, S. C. Bourke and K. D. Conroy, *Angew. Chem. Int. Ed.* , 2005, **44**, 5016–36.

185 W. Schneider, C. Narula, H. Nöth and B. Bursten, *Inorg. Chem.*, 1991, **30**, 3919–3927.

186 P. Kölle and H. Nöth, *Chem. Rev.*, 1985, **85**, 399–418.

187 T. S. De Vries, A. Prokofjevs and E. Vedejs, *Chem. Rev.*, 2012, **112**, 4246–4282.

188 J. Wiggans and G. Ryschkewitsch, *J. Am. Chem. Soc.*, 1970, **92**, 1790–1791.

189 M. K. Uddin, Y. Nagano, R. Fujiyama, S. Kiyooka, M. Fujio and Y. Tsuno, *Tetrahedron Lett.*, 2005, **46**, 627–630.

190 C. W. Chin and F. P. Gabbaï, *Organometallics*, 2008, **27**, 1657–1659.

191 H. Noth, S. Weber, B. Rasthofer, C. Narula and A. Konstantinov, *Pure Appl. Chem.*, 1983, **55**, 1453–1461.

192 E. J. Corey, T. Shibata and T. W. Lee, *J. Am. Chem. Soc.*, 2002, **124**, 3808–3809.

193 D. H. Ryu and E. J. Corey, *J. Am. Chem. Soc.*, 2003, **125**, 6388–6390.

194 G. Olah, *Friedel-Crafts Chemistry*, John Wiley & Sons Inc, New York, 1973.

195 D. W. Stephan, *Dalt. Trans.*, 2009, **9226**, 3129.

196 D. W. Stephan and G. Erker, *Angew. Chem. Int. Ed.* , 2010, **49**, 46–76.

197 G. C. Welch, R. R. S. Juan, J. D. Masuda and D. W. Stephan, *Science* , 2006, **314**, 1124–1126.

198 C. M. Momming, E. Otten, G. Kehr, R. Frohlich, S. Grimme, D. W. Stephan and G. Erker, *Angew. Chemie - Int. Ed.*, 2009, **48**, 6643–6646.

199 J. M. Farrell, J. A. Hatnean and D. W. Stephan, *J. Am. Chem. Soc.*, 2012, **134**, 15728–15731.

200 D. Prat, J. Hayler and A. Wells, *Green Chem.*, 2014, **16**, 4546–4551.

201 B. W. Benton and J. M. Miller, *Can. J. Chem.*, 1974, **52**, 2866–2872.

202 M. J. Bula, J. S. Hartman and C. V. Raman, *J. Chem. Soc. Dalt. Trans.*, 1974, 725.

203 T. Stahl, H. F. T. Klare and M. Oestreich, *ACS Catal.*, 2013, 3, 1578–1587.

204 A. Del Grosso, E. R. Clark, N. Montoute and M. J. Ingleson, *Chem. Commun.*, 2012, **48**, 7589–91.

205 J. R. Lawson, E. R. Clark, I. a Cade, S. a Solomon and M. J. Ingleson, *Angew. Chem. Int. Ed.* , 2013, **52**, 7518–22.

206 C. B. Caputo, L. J. Hounjet, R. Dobrovetsky and D. W. Stephan, *Science*, 2013, **341**, 1374–7.

207 A. P. M. Robertson, S. S. Chitnis, H. A. Jenkins, R. McDonald, M. J. Ferguson and N. Burford, *Chem. - A Eur. J.*, 2015, **21**, 7902–13.

208 A. P. M. Robertson, N. Burford, R. McDonald and M. J. Ferguson, *Angew. Chem. Int. Ed.*, 2014, **53**, 3480–3483.

209 M. Hirai, M. Myahkostupov, F. N. Castellano and F. P. Gabbaï, *Organometallics*, 2016, **35**, 1854–1860.

210 S. K. Porter and R. A. Jacobson, *Chem. Commun.*, 1967, **1**, 1244.

211 S. Porter and R. Jacobson, *J. Chem. Soc. A*, 1970, 1356–1359.

212 M. Bujak and J. Zaleski, *J. Mol. Struct.*, 2003, **647**, 121–128.

213 Z.-P. Wang, J.-Y. Wang, J.-R. Li, M.-L. Feng, G.-D. Zou and X.-Y. Huang, *Chem. Commun.*, 2015, **51**, 3094–3097.

214 A. R. J. Genge, N. J. Hill, W. Levason and G. Reid, *J. Chem. Soc. Dalt. Trans.*, 2001, 1007–1012.

215 K. L. Bamford, A. P. M. Robertson, H. A. Jenkins, B. O. Patrick and N. Burford, *Can. J. Chem.*, 2015, **93**, 375–379.

216 S. S. Chitnis, B. Peters, E. Conrad, N. Burford, R. McDonald and M. J. Ferguson, *Chem. Commun.*, 2011, **47**, 12331–3.

217 S. S. Chitnis, N. Burford, J. J. Weigand and R. McDonald, *Angew. Chem. Int. Ed.* , 2015, **54**, 7828–32.

218 S. M. Corcoran, W. Levason, R. Patel and G. Reid, *Inorganica Chim. Acta*, 2005, **358**, 1263–1268.

219 N. Bricklebank and S. Godfrey, *J. Chem. Soc., Dalt. Trans*, 1995, 1593.

220 R. M. Denton, J. An, B. Adeniran, A. J. Blake, W. Lewis and A. M. Poulton, *J. Org.*

Chem., 2011, **76**, 6749–6767.

221 A. P. M. Robertson, S. S. Chitnis, S. Chhina, H. J. Cortes S., B. O. Patrick, H. A. Jenkins and N. Burford, *Can. J. Chem.*, 2016, **94**, 424–429.

222 J. Burt, W. Levason, M. E. Light and G. Reid, *Dalton Trans.*, 2014, **43**, 14600–11.

223 R. Fehrmann, M. Haumann, A. Riisager and M. Haumann, *Supported Ionic Liquids: Fundamentals and Applications*, Wiley-VCH Verlag GmbH & Co, Weinheim, Germany, 2014.

224 S. E. Johnson and C. B. Knobler, *Organometallics*, 1992, **11**, 3684–3690.

225 E. MacDonald, L. Doyle, S. S. Chitnis, U. Werner-Zwanziger, N. Burford and A. Decken, *Chem. Commun.*, 2012, **48**, 7922–4.

226 W. McFarlane and N. H. Rees, *Polyhedron*, 1989, **8**, 2047–2050.

227 R. Colton, D. Dakternieks and C.-A. Harvey, *Inorganica Chim. Acta*, 1982, **61**, 1–7.

228 R. Mortier, S. Orszulik and M. Fox, *Chemistry and Technology of Lubricants*, Springer Netherlands, Dordrecht, 3rd edn., 1992.

229 M. Torbacke, Å. K. Å. Rudolphi and E. Kassfeldt, *Lubricants: Introduction to Properties and Performance*, John Wiley & Sons Ltd, Chichester, UK, 2014.

230 S. Q. A. Rizvi, *A Comprehensive Review of Lubricant Chemistry, Technology, Selection, and Design*, ASTM International, Baltimore, 2009.

231 *Kirk Orthmer Encyclopedia of Chemical Technology*, John Wiley and Sons, Inc.

232 L. Rudnick, *Synthetics, mineral oils, and bio-based lubricants: chemistry and technology*, CRC Press, Boca Raton, 2006.

233 R. Shubkin, M. Baylerian and A. Maler, *Ind. Eng. Chem. Prod. Res. Dev.*, 1980, **19**, 15–19.

234 L. I. Kioupis and E. J. Maginn, *J. Phys. Chem. B*, 1999, **103**, 10781–10790.

235 S. S. Scheuermann, S. Eibl and P. Bartl, *Lubr. Sci.*, 2011, **23**, 221–232.

236 M. Torbacke, Å. Rudolphi and E. Kassfeldt, *Ch2*, 2014.

237 R. Benda, J. Bullen and A. Plomer, *J. Synth. Lubr.*, 1996, **13**, 44–57.

238 http://www.cpchem.com/bl/pao/en-us/pages/lowviscositypao.aspx Accessed 19/06/16

239 S. Ray, P. P. V. C. P. Rao and N. V. N. Choudary, *Lubr. Sci.*, 2012, **24**, 23–44.

240 US Patent Office, 3382291, 1968.

241 US Patent Office, 2007/0225533 A1, 2007.

242 US Patent Office, 5196635, 1993.

243 US Patent Office, 3763244, 1973.

244 US Patent Office, 3780128, 1973.

245 US Patent Office, 3997621, 1976.

246 US Patent Office, 4032591, 1977.

247 US Patent Office, 4045507, 1977.

248 US Patent Office, 4376222, 1983.

249 US Patent Office, 4409415, 1983.

250 US Patent Office, 4587368, 1986.

251 US Patent Office, 6646174, 2003.

252 US Patent Office, 7592497, 2009.

253 US Patent Office, 8455416, 2013.

254 G. D. Yadav and N. S. Doshi, *Green Chem.*, 2002, **4**, 528–540.

255 Q. Huang, L. Chen, L. Ma, Z. Fu and W. Yang, *Eur. Polym. J.*, 2005, **41**, 2909–2915.

256 Q. Huang, L. Chen, Y. Sheng, L. Ma, Z. Fu and W. Yang, *J. Appl. Polym. Sci.*, 2006, **101**, 584–590.

257 P. Wasserscheid, S. Grimm, R. D. Köhn and M. Haufe, *Adv. Synth. Catal.*, 2001, **343**, 814–818.

258 H. Ding, B. Y. Zhang and J. Liu, *Pet. Sci. Technol.*, 2009, **27**, 1919–1925.

259 M. P. Atkins, K. R. Seddon and M. Swadźba-Kwaśny, *Pure Appl. Chem.*, 2011, **83**, 1391–1406.

260 G. Olah, *Friedel-Crafts and Related Reactions*, John Wiley & Sons Inc, New York, 1964.

261 A. Evans and M. Polanyi, *J. Chem. Soc.*, 1947, 252–256.

262 F. S. Dainton and G. B. B. M. Sutherland, *J. Polym. Sci.*, 1949, **4**, 37–43.

263 L. Balogh, L. Wang and R. Faust, *Macromolecules*, 1994, **27**, 3453–3458.

264 L. Balogh, Z. Fodor, T. Kelen and R. Faust, *Macromolecules*, 1994, **27**, 4648–4651.

265 P. J. Flory, *Principles of Polymer Chemistry*, Cornell University Press, Ithaca, 5th edn., 1966.

266 F. Eirich, *Science and Technology of Rubber*, Academic Press Inc, New York, 1978.

267 T. Hjgashimura, *J. Polym. Sci. Polym. Symp.*, 1976, **56**, 71–78.

268 M. Sawamoto and T. Higashimura, *Macromolecules*, 1978, **11**, 328–332.

269 M. Sawamoto and T. Higashimura, *Macromolecules*, 1978, **11**, 501–504.

270 V. Ipatieff and B. Corson, *Ind. Eng. Chem.*, 1935, **27**, 1067–1071.

271 S. R. Bethea and J. H. Karchmer, *Ind. Eng. Chem.*, 1956, **48**, 370–377.

272 A. Onopchenko, B. L. Cupples and A. N. Kresge, *Ind. Eng. Chem. Prod. Res. Dev.*, 1983, **22**, 182–191.

273 R. Ghosh, A. R. Bandyopadhyay, R. Jasra and M. M. Gagjibhai, *Ind. Eng. Chem. Res.*, 2014, **53**, 7622–7628.

274 J. P. Kennedy, *J. Polym. Sci. Part A Polym. Chem.*, 1999, **37**, 2285–2293.

275 J. Robinson and A. Osteryoung, *J. Am. Chem. Soc.*, 1979, **101**, 323–327.

276 Standard Test Method for Distillation of Heavy Hydrocarbon Mixtures (Vacuum Potstill Method) ASTM International, West Conshohocken, PA, 2015, www.astm.org, DOI: 10.1520/D5236-13

277 Standard Test Method for Kinematic Viscosity of Transparent and Opaque Liquids (and Calculation of Dynamic Viscosity) ASTM International, West Conshohocken, PA, 2015, www.astm.org, DOI: 10.1520/D0445-15A

278 Standard Practice for Calculating Viscosity Index from Kinematic Viscosity at 40 °C and 100 °C ASTM International, West Conshohocken, PA, 2015, www.astm.org, DOI: 10.1520/D2270-10R16

279 Standard Test Method for Pour Point of Petroleum Products ASTM International, West Conshohocken, PA, 2015, www.astm.org, 10.1520/D0097-16

280 ASTM D6352-15, Standard Test Method for Boiling Range Distribution of Petroleum Distillates in Boiling Range from 174 °C to 700 °C by Gas Chromatography, ASTM International, West Conshohocken, PA, 2015, www.astm.org, DOI: 10.1520/D6352-15

281 Standard Test Method for Distillation of Crude Petroleum (15-Theoretical Plate

Column), ASTM International, West Conshohocken, PA, 2015, www.astm.org, DOI: 10.1520/D2892-15

282 D. C. Villalanti, J. C. Raia and J. B. Maynard, in *Encyclopedia of Analytical Chemistry*, ed. R. A. Meyers, John Wiley & Sons Inc, Chichester, 2000, pp. 6726–6741.

283 D. B. G. Williams and M. Lawton, *J. Org. Chem.*, 2010, **75**, 8351–8354.

284 F. Favre, H. Olivier-Bourbigou, D. Commereuc and L. Saussine, *Chem. Commun.*, 2001, **2**, 1360–1361.

285 Y. V. Kissin and F. C. Schwab, *J. Appl. Polym. Sci.*, 2009, **111**, 273–280.

286 L. Green, L. Schmauch and J. Worman, *Anal. Chem.*, 1964, **36**, 1512.

287 G. Busca, *Chem. Rev.*, 2007, **107**, 5366–5410.

288 G. a Olah, *J. Org. Chem.*, 2001, **66**, 5943–5957.

289 US Patent Office, 6004519, 1999.

290 US Patent Office, 8541683, 2013.

291 US Patent Office, 7732364, 2010.

292 US Patent Office, 7955999, 2011.

293 US Patent Office, 8088338, 2012.

294 J. M. Hogg, F. Coleman, A. Ferrer-Ugalde, M. P. Atkins and M. Swadźba-Kwaśny, *Green Chem.*, 2015, **17**, 1831–1841.

295 World Intellectual Property Organisation, WO/2016/005769, 2016.

296 A. Riisager, R. Fehrmann, M. Haumann and P. Wasserscheid, *Eur. J. Inorg. Chem.*, 2006, **2006**, 695–706.

297 A. Corma and H. García, *Chem. Rev.*, 2003, **103**, 4307–4366.

298 J. P. Hallett and T. Welton, *Chem. Rev.*, 2011, **111**, 3508–3576.

299 V. I. Pârvulescu and C. Hardacre, *Chem. Rev.*, 2007, **107**, 2615–2665.

300 P. J. Dyson, D. J. Ellis, T. Welton and D. G. Parker, *Chem. Commun.*, 1999, 25–26.

301 Y. Gu and G. Li, *Adv. Synth. Catal.*, 2009, **351**, 817–847.

302 P. Zhang, T. Wu, M. Hou, J. Ma, H. Liu, T. Jiang, W. Wang, C. Wu and B. Han, *ChemCatChem*, 2014, **6**, 3323–3327.

303 H. Liu, T. Jiang, B. Han, S. Liang and Y. Zhou, *Science* , 2009, **326**, 1250–1252.

304 J. Y. Shin, D. J. Jung and S. G. Lee, *ACS Catal.*, 2013, **3**, 525–528.

7 Appendix

7.1 LCC synthesis

7.1.1 Synthesis of AcA-$AlCl_3$ χ_{AlCl3} = 0.60

To fine acetamide crystals (0.4560 g, 7.72 mmol) in a predied glass vial with a PTFE magnetic stirrer, aluminium chloride (1.5440 g, 11.57 mmol) was added in small aliquots (*ca.* 0.1 g) with rapid stirring. The reaction was highly exothermic and the vial was allowed to cool to the touch before addition of further aliquots of $AlCl_3$. Upon complete addition of the $AlCl_3$ the vial was heated to 60 °C and stirred for 1 hour yielding a clear, yellow liquid.

7.1.2 Synthesis of DMA-$AlCl_3$ χ_{AlCl3} = 0.60

To liquid dimethylacetamide (0.6069 g, 6.97 mmol) in a predied glass vial with a PTFE magnetic stirrer, aluminium chloride (1.3931 g, 10.45 mmol) was added in small aliquots (*ca.* 0.1 g) with rapid stirring. The reaction was highly exothermic and the vial was allowed to cool to the touch before addition of further aliquots of $AlCl_3$. Upon complete addition of the $AlCl_3$ the vial was heated to 60 °C and stirred for 1 hour yielding a clear, yellow liquid.

7.1.3 Synthesis of Ur-$AlCl_3$ χ_{AlCl3} = 0.50

To urea beads (0.6211 g, 10.34 mmol) in a predied glass vial with a PTFE magnetic stirrer, aluminium chloride (1.3789 g, 10.34 mmol) was added in small aliquots (*ca.* 0.1 g) with rapid stirring. The reaction was highly exothermic and the vial was allowed to cool to the touch before addition of further aliquots of $AlCl_3$. Upon complete addition of the $AlCl_3$ the vial was heated to 60 °C and stirred for 1 hour yielding a clear, colourless liquid.

7.1.4 Synthesis of Ur-$AlCl_3$ χ_{AlCl3} = 0.60

To urea beads (0.4619 g, 7.69 mmol) in a predied glass vial with a PTFE magnetic stirrer, aluminium chloride (1.5381 g, 11.54 mmol) was added in small aliquots (*ca.* 0.1 g) with rapid stirring. The reaction was highly exothermic and the vial was allowed to cool to the touch before addition of further aliquots of $AlCl_3$. Upon complete addition of the $AlCl_3$ the vial was heated to 60 °C and stirred for 1 hour yielding a clear, colourless liquid.

7.1.5 Synthesis of SUr-$AlCl_3$ χ_{AlCl3} = 0.50

To thiourea beads (0.7268 g, 9.55 mmol) in a predied glass vial with a PTFE magnetic stirrer, aluminium chloride (1.2732 g, 9.55 mmol) was added in small aliquots (*ca.* 0.3 g) with rapid stirring. The reaction was midly exothermic and the vial was allowed to cool to the touch

before addition of further aliquots of $AlCl_3$. Upon complete addition of the $AlCl_3$ the vial was heated to 60 °C and stirred for 24 hours yielding a clear, colourless liquid.

7.1.6 Synthesis of SUr-$AlCl_3$ χ_{AlCl3} = 0.60

To thiourea beads (0.5514 g, 7.24 mmol) in a predied glass vial with a PTFE magnetic stirrer, aluminium chloride (1.4486 g, 10.86 mmol) was added in small aliquots (*ca.* 0.3 g) with rapid stirring. The reaction was mildly exothermic and the vial was allowed to cool to the touch before addition of further aliquots of $AlCl_3$. Upon complete addition of the $AlCl_3$ the vial was heated to 60 °C and stirred for 24 hours yielding a clear, colourless liquid.

7.1.7 Synthesis of N_{888}-$AlCl_3$ χ_{AlCl3} = 0.50

To liquid trioctylamine (1.4524 g, 4.11 mmol) in a predied glass vial with a PTFE magnetic stirrer, aluminium chloride (0.5476 g, 4.11 mmol) was added in small aliquots (*ca.* 0.1 g) with rapid stirring. The reaction was exothermic and the vial was allowed to cool to the touch before addition of further aliquots of $AlCl_3$. Upon complete addition of the $AlCl_3$ the vial was heated to 60 °C and stirred for 1 hour yielding a yellow liquid.

7.1.8 Synthesis of P_{888}-$AlCl_3$ χ_{AlCl3} = 0.50

To liquid trioctylphosphine (1.4709 g, 3.97 mmol) in a predied glass vial with a PTFE magnetic stirrer, aluminium chloride (0.5291 g, 3.97 mmol) was added in small aliquots (*ca.* 0.1 g) with rapid stirring. The reaction was exothermic and the vial was allowed to cool to the touch before addition of further aliquots of $AlCl_3$. Upon complete addition of the $AlCl_3$ the vial was heated to 60 °C and stirred for 1 hour yielding a yellow liquid.

7.1.9 Synthesis of P_{888}-$AlCl_3$ χ_{AlCl3} = 0.60

To liquid trioctylphosphine (1.4524 g, 4.11 mmol) in a predied glass vial with a PTFE magnetic stirrer, aluminium chloride (0.5476 g, 4.11 mmol) was added in small aliquots (*ca.* 0.1 g) with rapid stirring. The reaction was exothermic and the vial was allowed to cool to the touch before addition of further aliquots of $AlCl_3$. Upon complete addition of the $AlCl_3$ the vial was heated to 60 °C and stirred for 1 hour yielding a yellow liquid.

7.1.10 Synthesis of $P_{222}O$-$AlCl_3$ χ_{AlCl3} = 0.50

To fine triethylphosphine oxide crystals (1.0031 g, 7.48 mmol) in a predied glass vial with a PTFE magnetic stirrer, aluminium chloride (0.9969 g, 7.48 mmol) was added in small aliquots (*ca.* 0.1 g) with rapid stirring. The reaction was highly exothermic and the vial was allowed to

cool to the touch before addition of further aliquots of $AlCl_3$. Upon complete addition of the $AlCl_3$ the vial was heated to 60 °C and stirred for 1 hour yielding a yellow liquid.

7.1.11 Synthesis of $P_{222}O$-$AlCl_3$ $\chi_{AlCl3} = 0.60$

To fine triethylphosphine oxide crystals (0.8030 g, 5.99 mmol) in a predied glass vial with a PTFE magnetic stirrer, aluminium chloride (1.1970 g, 8.98 mmol) was added in small aliquots (*ca.* 0.1 g) with rapid stirring. The reaction was highly exothermic and the vial was allowed to cool to the touch before addition of further aliquots of $AlCl_3$. Upon complete addition of the $AlCl_3$ the vial was heated to 60 °C and stirred for 1 hour yielding a yellow liquid.

7.1.12 Synthesis of $P_{888}O$-$AlCl_3$ $\chi_{AlCl3} = 0.50$

To powdered trioctylphosphine oxide (1.4871 g, 3.85 mmol) in a predied glass vial with a PTFE magnetic stirrer, aluminium chloride (0.5129 g, 3.85 mmol) was added in small aliquots (*ca.* 0.1 g) with rapid stirring. The reaction was highly exothermic and the vial was allowed to cool to the touch before addition of further aliquots of $AlCl_3$. Upon complete addition of the $AlCl_3$ the vial was heated to 60 °C and stirred for 1 hour yielding a yellow liquid.

7.1.13 Synthesis of $P_{888}O$-$AlCl_3$ $\chi_{AlCl3} = 0.60$

To powdered trioctylphosphine oxide (1.3181 g, 3.41 mmol) in a predied glass vial with a PTFE magnetic stirrer, aluminium chloride (0.6819 g, 5.11 mmol) was added in small aliquots (*ca.* 0.1 g) with rapid stirring. The reaction was highly exothermic and the vial was allowed to cool to the touch before addition of further aliquots of $AlCl_3$. Upon complete addition of the $AlCl_3$ the vial was heated to 60 °C and stirred for 1 hour yielding a yellow liquid.

7.1.14 Synthesis of $P_{888}S$-$AlCl_3$ $\chi_{AlCl3} = 0.50$

To liquid trioctylphosphine sulphide (1.5025 g, 3.73 mmol) in a predied glass vial with a PTFE magnetic stirrer, aluminium chloride (0.4975 g, 3.73 mmol) was added with rapid stirring. The reaction was mildly exothermic and the vial was allowed to cool to the touch before addition of further aliquots of $AlCl_3$. Upon complete addition of the $AlCl_3$ the vial was heated to 60 °C and stirred for 24 hour yielding a yellow liquid.

7.1.15 Synthesis of $P_{888}S$-$AlCl_3$ $\chi_{AlCl3} = 0.60$

To liquid trioctylphosphine sulphide (1.3363 g, 3.32 mmol) in a predied glass vial with a PTFE magnetic stirrer, aluminium chloride (0.6637 g, 4.98 mmol) was added with rapid stirring. The reaction was mildly exothermic and the vial was allowed to cool to the touch before

addition of further aliquots of $AlCl_3$. Upon complete addition of the $AlCl_3$ the vial was heated to 60 °C and stirred for 24 hour yielding a yellow liquid.

7.1.16 Synthesis of $P_{888}Se\text{-}AlCl_3$ $\chi_{AlCl3} = 0.50$

To liquid trioctylphosphine selenide (1.5426 g, 3.43 mmol) in a predied glass vial with a PTFE magnetic stirrer, aluminium chloride was added (0.4574 g, 3.43 mmol) with rapid stirring. The reaction was mildly exothermic. Upon complete addition of the $AlCl_3$ the vial was heated to 60 °C and stirred for 24 hour yielding a yellow liquid.

7.1.17 Synthesis of $P_{888}Se\text{-}AlCl_3$ $\chi_{AlCl3} = 0.60$

To liquid trioctylphosphine selenide (1.3363 g, 3.32 mmol) in a predied glass vial with a PTFE magnetic stirrer, aluminium chloride was added (0.6637 g, 4.98 mmol) with rapid stirring. The reaction was mildly exothermic. Upon complete addition of the $AlCl_3$ the vial was heated to 60 °C and stirred for 24 hour yielding a yellow liquid.

7.1.18 Synthesis of $C_7CN\text{-}AlCl_3$ $\chi_{AlCl3} = 0.50$

To liquid heptylcyanide (1.5426 g, 3.43 mmol) in a predied glass vial with a PTFE magnetic stirrer, aluminium chloride (0.4574 g, 3.43 mmol) was added in small aliquots (*ca.* 0.1 g) with rapid stirring. The reaction was exothermic and the vial was allowed to cool to the touch before addition of further aliquots of $AlCl_3$. Upon complete addition of the $AlCl_3$ the vial was heated to 60 °C and stirred for 1 hour yielding a yellow liquid.

7.1.19 Synthesis of $C_7CN\text{-}AlCl_3$ $\chi_{AlCl3} = 0.60$

To liquid heptylcyanide (1.3363 g, 3.32 mmol) in a predied glass vial with a PTFE magnetic stirrer, aluminium chloride (0.6637 g, 4.98 mmol) was added in small aliquots (*ca.* 0.1 g) with rapid stirring. The reaction was exothermic and the vial was allowed to cool to the touch before addition of further aliquots of $AlCl_3$. Upon complete addition of the $AlCl_3$ the vial was heated to 60 °C and stirred for 1 hour yielding a yellow liquid.

7.1.20 Synthesis of $PPh_3S\text{-}AlCl_3$ $\chi_{AlCl3} = 0.60$

To powdered triphenylphosphine sulphide (1.1909 g, 4.05 mmol) in a predied glass vial with a PTFE magnetic stirrer, aluminium chloride (0.8091 g, 6.07 mmol) was added with rapid stirring. Upon complete addition of the $AlCl_3$ the vial was heated to 60 °C and stirred for 24 hour yielding a yellow liquid.

7.1.21 Synthesis of AcA-$GaCl_3$ χ_{GaCl3} = 0.67

To fine acetamide crystals (0.2836 g, 4.80 mmol) in a predied glass vial with a PTFE magnetic stirrer, gallium chloride (1.7164 g, 9.75 mmol) was added in small aliquots (*ca.* 0.1 g) with rapid stirring. The reaction was highly exothermic and the vial was allowed to cool to the touch before addition of further aliquots of $GaCl_3$. Upon complete addition of the $GaCl_3$ the vial was heated to 60 °C and stirred for 1 hour yielding a clear, yellow liquid.

7.1.22 Synthesis of DMA-$GaCl_3$ χ_{GaCl3} = 0.50

To liquid dimethylacetamide (0.6620 g, 7.60 mmol) in a predied glass vial with a PTFE magnetic stirrer, gallium chloride (1.3380 g, 7.60 mmol) was added in small aliquots (*ca.* 0.1 g) with rapid stirring. The reaction was highly exothermic and the vial was allowed to cool to the touch before addition of further aliquots of $GaCl_3$. Upon complete addition of the $GaCl_3$ the vial was heated to 60 °C and stirred for 1 hour yielding a clear, purple liquid, which solidified when contatcted with a glass pipette.

7.1.23 Synthesis of DMA-$GaCl_3$ χ_{GaCl3} = 0.60

To liquid dimethylacetamide (0.4961 g, 5.69 mmol) in a predied glass vial with a PTFE magnetic stirrer, gallium chloride (1.5039 g, 8.54 mmol) was added in small aliquots (*ca.* 0.1 g) with rapid stirring. The reaction was highly exothermic and the vial was allowed to cool to the touch before addition of further aliquots of $GaCl_3$. Upon complete addition of the $GaCl_3$ the vial was heated to 60 °C and stirred for 1 hour yielding a clear, yellow liquid.

7.1.24 Synthesis of DMA-$GaCl_3$ χ_{GaCl3} = 0.67

To liquid dimethylacetamide (0.3919 g, 4.50 mmol) in a predied glass vial with a PTFE magnetic stirrer, gallium chloride (1.6081 g, 9.13 mmol) was added in small aliquots (*ca.* 0.1 g) with rapid stirring. The reaction was highly exothermic and the vial was allowed to cool to the touch before addition of further aliquots of $GaCl_3$. Upon complete addition of the $GaCl_3$ the vial was heated to 60 °C and stirred for 1 hour yielding a clear, yellow liquid.

7.1.25 Synthesis of DMA-$GaCl_3$ χ_{GaCl3} = 0.75

To liquid dimethylacetamide (0.2832 g, 3.25 mmol) in a predied glass vial with a PTFE magnetic stirrer, gallium chloride (1.7168 g, 9.75 mmol) was added in small aliquots (*ca.* 0.1 g) with rapid stirring. The reaction was highly exothermic and the vial was allowed to cool to the touch before addition of further aliquots of $GaCl_3$. Upon complete addition of the $GaCl_3$ the vial was heated to 60 °C and stirred for 1 hour yielding a clear, yellow liquid.

7.1.26 Synthesis of Ur-$GaCl_3$ χ_{GaCl3} = 0.60

To urea beads (0.3705 g, 6.17 mmol) in a predied glass vial with a PTFE magnetic stirrer, gallium chloride (1.6295 g, 9.25 mmol) was added in small aliquots (*ca.* 0.1 g) with rapid stirring. The reaction was highly exothermic and the vial was allowed to cool to the touch before addition of further aliquots of $GaCl_3$. Upon complete addition of the $GaCl_3$ the vial was heated to 60 °C and stirred for 1 hour yielding a clear, yellow liquid.

7.1.27 Synthesis of Ur-$GaCl_3$ χ_{GaCl3} = 0.67

To urea beads (0.2914 g, 4.85 mmol) in a predied glass vial with a PTFE magnetic stirrer, gallium chloride (1.7086 g, 9.70 mmol) was added in small aliquots (*ca.* 0.1 g) with rapid stirring. The reaction was highly exothermic and the vial was allowed to cool to the touch before addition of further aliquots of $GaCl_3$. Upon complete addition of the $GaCl_3$ the vial was heated to 60 °C and stirred for 1 hour yielding a clear, yellow liquid.

7.1.28 Synthesis of Ur-$GaCl_3$ χ_{GaCl3} = 0.75

To urea beads (0.2042 g, 3.40 mmol) in a predied glass vial with a PTFE magnetic stirrer, gallium chloride (1.7985 g, 10.20 mmol) was added in small aliquots (*ca.* 0.1 g) with rapid stirring. The reaction was highly exothermic and the vial was allowed to cool to the touch before addition of further aliquots of $GaCl_3$. Upon complete addition of the $GaCl_3$ the vial was heated to 60 °C and stirred for 1 hour yielding a clear, yellow liquid.

7.1.29 Synthesis of SUr-$GaCl_3$ χ_{GaCl3} = 0.67

To thiourea beads (0.3511 g, 4.61 mmol) in a predied glass vial with a PTFE magnetic stirrer, gallium chloride (1.6489 g, 9.36 mmol) was added in small aliquots (*ca.* 0.3 g) with rapid stirring. The reaction was midly exothermic and the vial was allowed to cool to the touch before addition of further aliquots of $GaCl_3$. Upon complete addition of the $GaCl_3$ the vial was heated to 60 °C and stirred for 1 hour yielding a clear, yellow liquid.

7.1.30 Synthesis of P_{888}-$GaCl_3$ χ_{GaCl3} = 0.67

To liquid trioctylphosphine (1.0694 g, 2.75 mmol) in a predied glass vial with a PTFE magnetic stirrer, gallium chloride (0.9819 g, 5.58 mmol) was added in small aliquots (*ca.* 0.3 g) with rapid stirring. The reaction was midly exothermic and the vial was allowed to cool to the touch before addition of further aliquots of $GaCl_3$. Upon complete addition of the $GaCl_3$ the vial was heated to 60 °C and stirred for 1 hour yielding a clear, yellow liquid.

7.1.31 Synthesis of $P_{888}O$-$GaCl_3$ χ_{GaCl3} = 0.50

To powdered trioctylphosphine oxide (1.3742 g, 3.55 mmol) in a predied glass vial with a PTFE magnetic stirrer, gallium chloride (0.6258 g, 3.55 mmol) was added in small aliquots (*ca.* 0.3 g) with rapid stirring. The reaction was exothermic and the vial was allowed to cool to the touch before addition of further aliquots of $GaCl_3$. Upon complete addition of the $GaCl_3$ the vial was heated to 60 °C and stirred for 1 hour yielding a clear, yellow liquid.

7.1.32 Synthesis of $P_{888}O$-$GaCl_3$ χ_{GaCl3} = 0.60

To powdered trioctylphosphine oxide (1.1883 g, 3.07 mmol) in a predied glass vial with a PTFE magnetic stirrer, gallium chloride (0.8117 g, 4.61 mmol) was added in small aliquots (*ca.* 0.3 g) with rapid stirring. The reaction was exothermic and the vial was allowed to cool to the touch before addition of further aliquots of $GaCl_3$. Upon complete addition of the $GaCl_3$ the vial was heated to 60 °C and stirred for 1 hour yielding a clear, yellow liquid.

7.1.33 Synthesis of $P_{888}O$-$GaCl_3$ χ_{GaCl3} = 0.67

To powdered trioctylphosphine oxide (1.0392 g, 2.69 mmol) in a predied glass vial with a PTFE magnetic stirrer, gallium chloride (0.9608 g, 5.46 mmol) was added in small aliquots (*ca.* 0.3 g) with rapid stirring. The reaction was exothermic and the vial was allowed to cool to the touch before addition of further aliquots of $GaCl_3$. Upon complete addition of the $GaCl_3$ the vial was heated to 60 °C and stirred for 1 hour yielding a clear, yellow liquid.

7.1.34 Synthesis of $P_{888}O$-$GaCl_3$ χ_{GaCl3} = 0.67

To powdered trioctylphosphine oxide (0.8452 g, 2.19 mmol) in a predied glass vial with a PTFE magnetic stirrer, gallium chloride (1.1548 g, 6.56 mmol) was added in small aliquots (*ca.* 0.3 g) with rapid stirring. The reaction was exothermic and the vial was allowed to cool to the touch before addition of further aliquots of $GaCl_3$. Upon complete addition of the $GaCl_3$ the vial was heated to 60 °C and stirred for 1 hour yielding a clear, yellow liquid.

7.1.35 Synthesis of C_7CN-$GaCl_3$ χ_{GaCl3} = 0.50

To liquid heptyl cyanide (0.8312 g, 6.64 mmol) in a predied glass vial with a PTFE magnetic stirrer, gallium chloride (1.1688 g, 6.64 mmol) was added in small aliquots (*ca.* 0.3 g) with rapid stirring. The reaction was exothermic and the vial was allowed to cool to the touch before addition of further aliquots of $GaCl_3$. Upon complete addition of the $GaCl_3$ the vial was heated to 60 °C and stirred for 1 hour yielding a clear, yellow liquid.

7.1.36 Synthesis of $C_7CN\text{-}GaCl_3$ $\chi_{GaCl3} = 0.60$

To liquid heptyl cyanide (0.6432 g, 5.14 mmol) in a predied glass vial with a PTFE magnetic stirrer, gallium chloride (1.3568 g, 7.71 mmol) was added in small aliquots (*ca.* 0.3 g) with rapid stirring. The reaction was exothermic and the vial was allowed to cool to the touch before addition of further aliquots of $GaCl_3$. Upon complete addition of the $GaCl_3$ the vial was heated to 60 °C and stirred for 1 hour yielding a clear, yellow liquid.

7.1.37 Synthesis of $C_7CN\text{-}GaCl_3$ $\chi_{GaCl3} = 0.67$

To liquid heptyl cyanide (0.5188 g, 4.14 mmol) in a predied glass vial with a PTFE magnetic stirrer, gallium chloride (1.4812 g, 8.41 mmol) was added in small aliquots (*ca.* 0.3 g) with rapid stirring. The reaction was exothermic and the vial was allowed to cool to the touch before addition of further aliquots of $GaCl_3$. Upon complete addition of the $GaCl_3$ the vial was heated to 60 °C and stirred for 1 hour yielding a clear, yellow liquid.

7.1.38 Synthesis of $C_7CN\text{-}GaCl_3$ $\chi_{GaCl3} = 0.75$

To liquid heptyl cyanide (0.3833 g, 3.06 mmol) in a predied glass vial with a PTFE magnetic stirrer, gallium chloride (1.6167 g, 9.18 mmol) was added in small aliquots (*ca.* 0.3 g) with rapid stirring. The reaction was exothermic and the vial was allowed to cool to the touch before addition of further aliquots of $GaCl_3$. Upon complete addition of the $GaCl_3$ the vial was heated to 60 °C and stirred for 1 hour yielding a clear, yellow liquid.